Acta Universitatis Agriculturae Sueciae

Doctoral Thesis No. 2022:60
Faculty of Natural Resources and Agricultural Sciences

Living through hard times: Dispose of or sequester?

Plant subcellular strategies for stress resilience

Pernilla Helena Elander

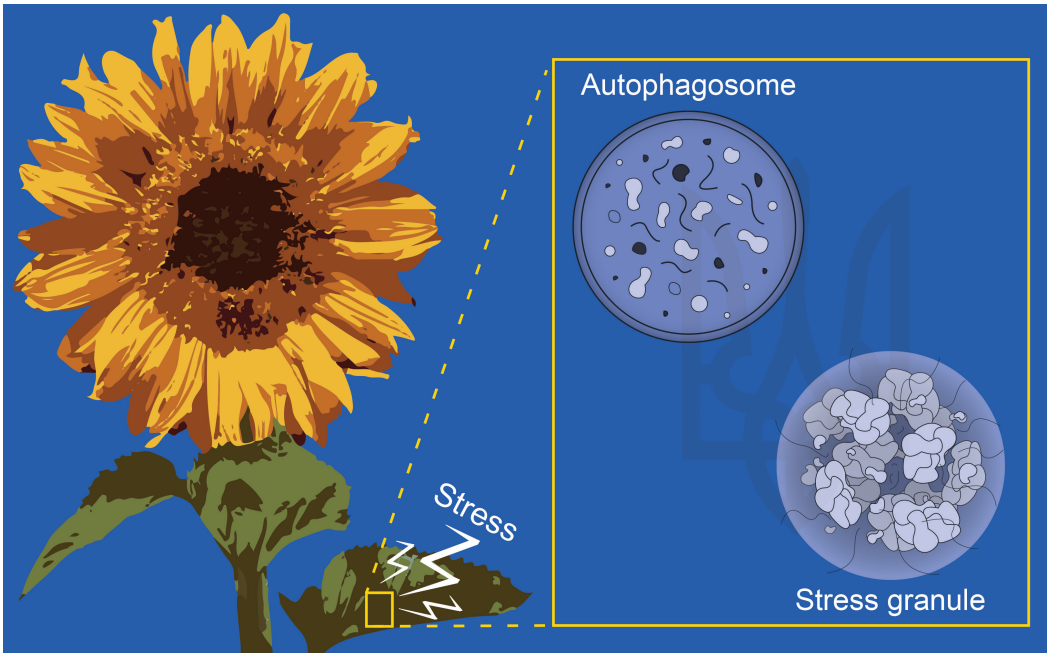

Living through hard times: Dispose of or sequester?

Plant subcellular strategies for stress resilience

Pernilla Helena Elander
Fakulteten för Naturresurser och Jordbruksvetenskap
Molekylära vetenskaper
Uppsala

SLU
SWEDISH UNIVERSITY OF AGRICULTURAL SCIENCES

DOCTORAL THESIS
Uppsala 2022

Acta Universitatis Agriculturae Sueciae
2022:60

Cover: Autophagy and Stress Granules in plant defense
(Image by Pernilla Elander and Adrian Dauphinee)

ISSN 1652-6880
ISBN (print version) 978-91-7760-995-7
ISBN (electronic version) 978-91-7760-996-4
© 2022 Pernilla Helena Elander, Swedish University of Agricultural Sciences
Uppsala
Print: SLU Service/Repro, Uppsala 2022

Living through hard times: Dispose of or sequester?

Abstract

Extreme weather events have become the new normal due to climate change and global warming. This damages crop harvests, threatening global food production. One of the many measures to ensure food security is to develop stress-resilient plants, but to do that we need to understand how plants respond to stress factors. In this work, we studied two cellular mechanisms underlying plant resilience, autophagy and formation of stress granules (SGs). Autophagy is an evolutionarily conserved vesicle trafficking pathway which at the time of stress disposes of cellular constituents which might be superfluous, hazardous or dysfunctional by degrading them in the lysosome (animals) or vacuole (fungi and plants).

In our studies we have focused on autophagy-related proteins ATG5 and ATG7, the core components of the ATG8 and ATG5-12 conjugation systems. Overexpression of ATG5 or ATG7 led to increased lipidation of ATG8 and enhanced autophagic recycling without affecting the transcription level of other components of the conjugation systems, indicating that ATG5 and ATG7 are rate-limiting steps of the autophagy pathway. Plants with enhanced levels of either ATG5 or ATG7 showed improved fitness for a broad range of agronomically important traits, such as, increased vegetative biomass, delayed senescence and increased seed set. Surprisingly, these plants also displayed improved tolerance to necrotrophic pathogens and oxidative stress. Our findings can be used for growing resilient crops with improved productivity. A follow up study addressed the roles of ATG5 unrelated to autophagy, by isolating interactomes of the wild-type ATG5 and its point mutant which does not conjugate to ATG12. LC-MS/MS analysis yielded 104 interactor hits for the wild-type ATG5, 78 for the mutant and 97 hits shared by the wild-type and the mutant. Further functional studies are required to understand the roles of ATG5 and its interactors of autophagy-unrelated pathways in plants.

SGs are membraneless protein-mRNA biomolecular condensates formed via phase separation under stress, which selectively sequester or concentrate proteins and mRNAs. The sequestration of proteins can result in activation or suppression of biochemical pathways. We investigated the interactome of the Tudor staphylococcal nuclease (TSN) protein. TSN is a multifunctional and evolutionary conserved regulator of gene expression, previously shown to stably associate with SGs under heat stress. We found that TSN functions as a docking platform for SG components and its localization to SGs is essential for the activation of a major regulator of energy homeostasis in the cell, SnRK1 (a homolog of AMPK/SNF1). Our work provides a proteome-wide resource of SG components and sheds light on the signalling role of stress granules in plant physiology.

Keywords: Recycling, degradation, stress response, biomolecular condensates, autophagy, stress granules, plant resilience, plant stress, climate change

Author's address: Pernilla Helena Elander, Swedish University of Agricultural Sciences, Department of Molecular Sciences, Uppsala, Sweden

Att överleva svåra förhållanden: Bortskaffa eller isolera?

Sammanfattning

Extremväder på grund av klimatförändringar och global uppvärmning har blivit allt vanligare vilket förstör skördar och hotar den globala matproduktionen. En utav flera tillvägagångssätt för att säkra en tryggad livsmedelsförsörjning är att utveckla motståndskraftiga grödor. För att vi ska kunna göra det behöver vi öka vår förståelse för växters motståndskraft. Vi har studerat två grundläggande cellulära mekanismer i växters stressrespons, autofagi och bildningen utav stressgranuler. Autofagi är en evolutionärt bevarad reaktionsväg för vesikeltransport som i situationer av stress bryter ner cellmaterial som är överflödiga, skadliga eller dysfunktionella i lysosomen (djur) eller vakuolen (svamp och växter).

I vår forskning har vi fokuserat på autofagi-proteinerna ATG5 och ATG7, kärnkomponenter i två konjugerade system, ATG8 och ATG5-12. Överuttryck av ATG5 eller ATG7 resulterade i ökad lipidering av ATG8 och ökad autofagi, men utan att förändra uttrycket av de andra proteinerna i de två konjugerade systemen, vilket indikerar att ATG5 och ATG7 är hastighetsbegränsande steg i autofagi. Växter med högre nivåer av ATG5 eller ATG7 visade på bättre fitness i flertalet värdefulla egenskaper såsom mer biomassa, längre levnadstid, och ökad avkastning Överraskande nog var också dessa växter mer motståndskraftiga till nekrotrofiska patogener och oxidativ stress. De här resultaten kan användas för att förbättra grödors motståndskraft och avkastning. Våra fortsatta studier berör funktionen av ATG5, orelaterat till autofagi, genom att isolera interaktom av vildtyps ATG5 och en muterad variant som inte konjugerar till ATG12. LC-MS/MS analys gav 104 träffar för vildtyps-ATG5, 78 för mutanten och 97 gemensamma träffar. Fortsatta funktionella studier krävs för att kunna förstå funktionen av ATG5 och proteinerna ATG5 interagerar med, i autofagi och andra biokemiska reaktionsvägar i växter.

Stressgranuler är membranlösa protein-mRNA organeller eller biomolekylära kondensat som bildas genom fasseparation under stress, vilket möjliggör avskiljning och koncentration av proteiner och mRNA. Kondensatet kan medföra både aktiviering och inhibering av biokemiska reaktionsvägar. Vi undersökte interaktomet utav den multifunktionella och det evolutionärt bevarade regulatorn av genuttryck, proteinet Tudor staphylococcal nuclease (TSN) vilket tidigare visat sig stabilt associera till stressgranuler under värmestress. Vi fann att TSN fungerar som en dockningsstation för andra molekyler tillhörande stressgranuler och lokaliseringen av TSN till stressgranuler är nödvändig för aktiveringen utav SnRK1 (homolog till AMPK/SNF1), en betydande regulator till cellens energihomeostas. Våra upptäckter tillhandahåller en resurs av stressgranulers proteom och belyser stressgranulers roll inom cellsignalering i växtfysiologi.

Keywords: Återvinning, nedbrytning, stressrespons, biomolekylära kondensat, autofagi, stressgranuler, växters motståndskraft, växtstress, klimatförändringar

Author's address: Pernilla Helena Elander, Swedish University of Agricultural Sciences, Department of Molecular Sciences, Uppsala, Sweden

Dedication

To my beloved husband for a never ceasing support of my endeavours

~We only know what we are capable of when we test our limits~

Violet, Downton Abbey

Contents

List of publications

This thesis is based on research presented in the following papers, referred to by Roman numerals in the text:

I. Elena A. Minina, Panagiotis N. Moschou*, Ramesh R. Vetukuri*, Victoria Sanchez-Vera*, Catarina Cardoso*, Qinsong Liu*, **Pernilla H. Elander**, Kerstin Dalman, Mirela Beganovic, Jenny Lindberg Yilmaz, Sofia Marmon, Lana Shabala, Maria F. Suarez, Karin Ljung, Ondřej Novák, Sergey Shabala, Sten Stymne, Daniel Hofius and Peter V. Bozhkov (2018). Transcriptional stimulation of rate-limiting components of the autophagic pathway improves plant fitness. Journal of Experimental Botany, Vol. 69, No. 6 pp. 1415–1432.
* These authors contributed equally.

II. **Pernilla H. Elander***, Sanjana Holla*, Emilio Gutierrez-Beltran, Patrick Willems, Peter V. Bozhkov and Elena A. Minina. Exploring Arabidopsis ATG5 functions beyond autophagy.
* These authors contributed equally.

III. **Pernilla H. Elander**, Elena A. Minina and Peter V. Bozhkov (2018). Review: Autophagy in turnover of lipid stores: trans-kingdom comparison. Journal of Experimental Botany, Vol. 69, No. 6 pp. 1301–1311.

IV. Emilio Gutierrez-Beltran, **Pernilla H. Elander**, Kerstin Dalman, Guy W. Dayhoff II, Panagiotis N. Moschou, Vladimir N. Uversky, Jose L. Crespo & Peter V. Bozhkov (2021). Tudor staphylococcal nuclease is a docking platform for stress granule components and is essential for SnRK1 activation in *Arabidopsis.* The EMBO Journal Vol. 40, No. 17 pp. e105043.

The contribution of Pernilla Helena Elander to the papers included in this thesis was as follows:

I. Plant phenotyping, genotyping and sampling as well as figure editing.

II. Project planning, molecular work, method optimization, major contributor to manuscript writing and figure design.

III. Planning of outline, major contributor to manuscript writing and figure design.

IV. Molecular work and method optimization.

Publications not included in the thesis:

I. Jonas A Ohlsson, Jia Xuan Leong, **Pernilla H. Elander**, Adrian N. Dauphinee, Florentine Ballhaus, Johan Johansson, Mark Lommel, Gero Hofmann, Staffan Betnér, Mats Sandgren, Karin Schumacher, Peter V. Bozhkov and Elena A Minina. (preprint 2021). SPIRO – The automated Petri plate imaging platform designed by biologists, for biologists. BioRxiv.

II. Tamar Avin-Wittenberg , Frantisek Baluška , Peter V Bozhkov, **Pernilla H Elander**, Alisdair R Fernie , Gad Galili, Ammar Hassan, Daniel Hofius, Erika Isono, Romain Le Bars, Céline Masclaux-Daubresse, Elena A Minina, Hadas Peled-Zehavi, Núria S Coll, Luisa M Sandalio, Béatrice Satiat-Jeunemaitre, Agnieszka Sirko , Pilar S Testillano, Henri Batoko (2018). Review: Autophagy-related approaches for improving nutrient use efficiency and crop yield protection. Journal of Experimental Botany, Vol. 69, No. 6 pp. 1335–1353.

III. Elena A. Minina, Salim Hossain Reza, Emilio Gutierrez-Beltran, **Pernilla H. Elander**, Peter V. Bozhkov, Panagiotis N. Moschou (2017). The *Arabidopsis* homolog of Scc4/MAU2 is essential for embryogenesis. Journal of Cell Science, Vol. 130, No. 6 pp. 1051–1063.

List of figures

Abbreviations

ATG	Autophagy related
AIM	ATG8 Interacting Motif
bZIP	Basic Leucine Zipper
CML38	Calmodulin-Like 38
eIF	Eukaryote Translation Initiation Factor
ESCRT	Endosomal Sorting Complex Required for Transport
GFP	Green Fluorescent Protein
IDP	Intrinsic Disordered Proteins
IDR	Intrinsically Disordered Regions
IRE	Inositol-Requiring Enzyme
LD	Lipid Droplet
MVB	Multi Vesicular Body
NBR1	Neighbor of BRCA1 gene 1
PE	Phosphatidylethanolamine
PI3K	Phosphoinositide 3-kinase
PI3P	Phosphatidylinositol 3-phosphate
RBP	RNA-Binding Protein
SG	Stress Granule

SGS3	Supressor of Gene Silencing 3
SH3P2	SH3 domain-containing Protein 2
SNARE	Soluble N-ethylmaleimide-sensitive factor Activating protein Receptors
TAG	Triacylglycerols
TOR	Target Of Rapamycin
TSN	Tudor Staphylococcal Nuclease
Ubl	Ubiquitin-like
VPS	Vacuolar Protein Sorting

1. Introduction
Plant stress and its agricultural relevance

Plants have evolved on earth in the course of 700 million years, yet only recently have humans begun to cultivate plants for human needs. Around the year 9000 BCE in the geographic area that is now Iraq, humans initiated agriculture, domesticating plants for the purpose of food supply. Over the next millennia, farmers worldwide started collecting seeds from well-performing individuals for sowing the coming year. Varieties that would become our corn and rice started to be bred. With the progress of agricultural practices, food became more accessible and over the millennia the world population increased, from an estimated 4 million in 9000 BCE to 7.9 billion today.

During the course of evolution, plants have overcome both biotic and abiotic stressors in order to survive. Then, humankind started to select a small subset of all plants on earth, which in our hands, now 11 000 years later, have become a even smaller subset. Plant breeding has focused on a yet even smaller subset of desirable traits, such as high yield, synchronized ripening, fast growth and good flavour. None of these traits is an advantage in the wild. The selection has favoured uniformity; from farmer to consumer, we have certain expectations of the produce. The farmers want the crop quality to be even over the field, and we as consumers want to know that the type of sweet corn we usually buy looks and tastes the same as the sweet corn we bought last week. The breeding and preference for uniformity have brought about a loss of other traits, evidently those of plant immunity. This has left our crops vulnerable to a number of diseases that their wild relatives or ancestors might

have had resistance to (National Research council, 1993). An additional factor is the trend of growing the same type of crop in large areas at the same time, upon which a pathogenic attack has the potential to affect large quantities (National Research council, 1993). An example of this is Fusarium wilt (Panama disease) in banana cultivars. *Fusarium oxysporum* f. sp. *cubense (Foc)* infects banana plants and ultimately kills them, leaving devastating yield losses. During the first half of the 20th century, one banana cultivar, "Gros Michel" dominated the global export trade. It is highly susceptible to Fusarium wilt and an epidemic of said Fusarium caused the closure and relocation of large plantations to new non-cultivated land. After several decades of relocating, the more resistant "Cavendish" subgroup was introduced to the market and to this day is the most exported banana. For decades, Cavendish was resistant to *Foc,* until *Foc* mutated and sidestepped the resistance. Outbreaks of the new variant of *Foc,* TR4 now poses a threat to global banana production (Ploetz 2015).

Throughout history, failure to overcome stress factors in crop cultivation has led to food shortages, famine, population migrations and conflicts. These effects are also highly relevant today, especially with more extreme weather events, such as storms, heavy rainfall, drought, cold- and heat- spells. With the challenges of securing crop harvest as well as feeding a growing population, we have constantly been trying to improve agricultural practices. A major breakthrough in this area came to be named the "Green Revolution", a series of inventions and improvements of agriculture practices worldwide in the 1960s and 1970s. The effects of the Green Revolution resulted in a 100% increase in cereal production between 1969 and 2004, reduced food prices and improved food supply in developing countries (Pingali 2012). Central was the establishment and distribution of new high-yielding varieties of wheat, rice and maize (Pingali 2012), a threefold increase in the use of chemical fertilizer and a doubling of irrigated areas which improved crop yields (FAO 2004). The world has definitely reached milestones in the challenge of feeding its population in the last 50 years. The proportion of undernourished people has fallen significantly, despite the doubling of the world population, and access to micronutrient-rich food has increased (Pingali 2012). Now, however, we are facing additional challenges with extreme weather phenomena due to climate change.

Climate change is now ever-present and poses new obstacles to plant breeding and agriculture (Pais *et al.* 2020; Zandalinas *et al.* 2021). The following are a few examples that shed light upon the issue. In 2017, Sweden experienced a very wet autumn, which resulted in reduced acreage of winter crops by 17%, varieties that in general are more drought resistant than spring varieties (Fig. 1). The following summer was very dry and hot, resulting in a 43% harvest reduction, the worst harvest in Sweden since 1959 (Gustafsson 2019). Last year (2021), Brazil experienced an initially dry spring which was subsequently followed by several rounds of frost in June and July, decimating the coffee harvest by approximately 25%, damage that will take years to overcome (Wallengren 2021). Following the drought and warmth of 2018, the Norway spruce population in Sweden was stressed and more susceptible to the European Spruce bark beetle; an invasion followed which in 4 years has damaged three times more trees than in the previous 60 years (Skogsindustrierna 2021). Sweden and Brazil are two countries that have sufficient economical means to handle a crisis, which is not the case for East and Central African countries currently experiencing severe drought and locust invasion, placing an estimated 30 million people on the brink of starvation (Oxfam International 2022).

To ensure food security (when all people at all times have access to safe and nutritious food in sufficient amounts), the world needs a new "green revolution" and it is not far-fetched that plant stress resilience will be the game-changer. In the Swedish Board of Agriculture report on the 2018 drought, Gustafsson (2019) emphasizes the need for higher stress endurance in future crops. To reach this breeding goal, we need an extensive understanding of plant stress.

In this thesis, I have sought to better understand plant stress by studying two major molecular pathways, Autophagy and Stress Granules: two action mechanisms that plants execute to protect their most essential functions, all in order to survive.

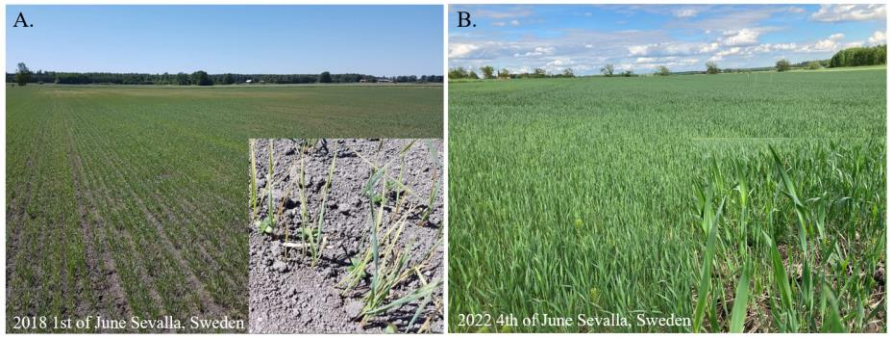

Figure 1. **Development comparison between spring crop and winter crop**

The wet autumn of 2017 unabled sowing of winter crops. The coming summer of 2018 was unusally hot and dry resulting in 43% harvest reduction. The spring crops depicted in **A**, displayed symtoms of drought stress in beginning of June (enlarged picture). In coparison the winter crop sown in 2021, depicted in **B**, had much more time for development and would likely have been more drought resilient than A.

2. Background

The cellular stress response: recycling versus condensation

It is the summer of 2018 in Sweden. May has already been unusually dry and hot in Svealand and Götaland, the parts of Sweden from which 90% of the food production is located (LRF, n.d.). June brings some rain, but still, at the end of the month, it is dryer and warmer than normal (SMHI 2018). In July the temperature is 3-5 degrees higher than normal, with days reaching temperatures of more than 30 degrees with subsequent tropical nights (night temperatures exceeding 20 degrees Celsius, SMHI 2018). What happened with our agricultural plants in these conditions, in general terms?

A number of physiological processes are affected by heat and drought, which ultimately reduces plant growth and impact reproduction (Zhao *et al.* 2021). Plants become smaller, set fewer leaves, and produce fewer seeds (Gray & Brady 2016). There are several ways for plants to overcome stress conditions like these to assure survival. In this chapter, I briefly introduce the plant cellular stress response. In the subsequent chapters I will guide you through the two coping mechanisms, intracellular recycling and intracellular condensation, with a focus on autophagy and stress granules, two different stress response pathways which aid the plant in overcoming stress, and also the focus of my thesis.

2.1 The endomembrane system during stress

Intracellular transport of cargo e.g. proteins, lipids, polysaccharides and other molecules is generally enabled by the endomembrane trafficking system. The system shuttles vesicles with cargo between the cellular compartments, such as proteins which are synthesized on ribosomes on the rough Endoplasmic reticulum (ER). The proteins are folded to their proper three-dimensional structure in the ER lumen and normally transported via COPII vesicles to the Golgi apparatus (Golgi) where they are matured and transported to their cellular destinations (Phillips *et al.* 2020). The endomembrane system constitutes of the nuclear envelope, smooth and rough ER, the Golgi, trans-Golgi network (TGN), the vacuole and different types of vesicles such as multivesicular bodies (MVBs), endosomes and autophagosomes. The endomembrane system comprises two major transport routes: the endocytic pathway and the secretory pathway. In the endocytic pathway molecules, mainly proteins, are taken up by the cell by invaginations of the plasma membrane. In the secretory pathway, proteins are transported out of the cell or to the vacuole.

As mentioned in the above paragraph, proteins are folded in the ER. Even in the best possible conditions, there will be a small occurrence of misfolding of proteins in the ER. Misfolded proteins can be harmful to the cell since their proper function is disabled. To assess this issue there is a system in place called the ER quality control (ERQC). ERQC can detect misfolded proteins and retain them for re-folding (Araki & Nagata 2011). If the folding attempts fail the misfolded proteins are degraded by another set of proteins in a process called ER-associated degradation (ERAD, Ruggiano *et al.* 2014). During stress conditions, for example heat-stress, ERQC and ERAD are not sufficient to handle the abundance of misfolded and unfolded proteins. This leads to a condition called ER stress (Bao & Howell, 2017). ER stress activates the unfolded protein response (UPR) which in turn upregulates the expression of stress response genes for protein folding and chaperones. ER stress is communicated to the nucleus via the UPR signalling pathway (Bao & Howell, 2017). Unsurprisingly, dysfunctional UPR response leads to impaired stress tolerance whereas upregulated UPR increases stress tolerance. For example, lacking UPR proteins Inositol-requiring enzyme (IRE) 1a and IRE1b display male sterility already at

moderately elevated temperatures (Deng *et al.* 2016). An additional study found that overexpression of UPR chaperone binding protein increased drought tolerance in soybean and tobacco (Valente *et al.* 2009).

2.2 Subcellular degradation and recycling

In order to maintain cellular homeostasis under stress conditions cells need to manage increased numbers of harmful molecules, like unfolded proteins, and simultaneously sustain the cell with energy. Part of this is achieved by three major degradation pathways in plants. These are the ubiquitin-proteasome pathway (UPP), MVB and autophagy pathway. While UPP and MVBs primarily target proteins tagged with ubiquitin, autophagy has a broader application, targeting various intracellular materials, ranging from proteins to organelles. Cellular content passing through these pathways is degraded to components that can be reused by the cell, for example, peptides from a degraded protein are utilized to build new proteins.

2.2.1 The ubiquitin-proteasome pathway

UPP or ubiquitin-proteasome system (UPS) is a protein degradation pathway part of the ERAD (Ruggiano *et al.* 2014) which takes place in the cytoplasm. It affects a range of cellular processes, such as signal transduction, stress and immune responses (Hershko 2005). The UPS includes a large number of proteins of which the main players are the families of ubiquitin-activating enzymes (E1), ubiquitin-conjugating enzymes (E2) and ubiquitin ligases (E3). The process of ubiquitination is initated by ubiquitin activation by E1, followed by a transfer of the activated ubiquitin by E2 to the E3 enzyme which ligates ubiquitin to the protein targeted for degradation. Different E3 enzymes recognize different substrates which are to be ubiquitinated (Stone & Callis, 2007). Ubiquitinated substrates are recognized by the multiprotein complex 26S proteasome which degrades the protein into peptides (Sahu & Glickman 2021).

2.2.2 Multivesicular bodies

MVBs or prevacuolar compartments (PVC) are single-membrane compartments containing intraluminal vesicles, mainly transporting proteins in the endocytic and secretory pathways under normal conditions in plants. They have also been suggested to partake in an interplay with autophagy (Wang *et al.* 2020). MVBs are a type of endosomes formed by inwards budding of the limiting membrane into its own lumen. During endocytosis, molecules from outside of the cell are taken up by the PM in endocytic vesicles. The endocytic vesicles are in turn taken up by early endosomes which mature into MVBs. With maturation, they gain the capability to fuse with the vacuole. In the secretory pathway proteins which have been synthesized in the ER are transported to the Golgi/TGN for further sorting and maturation. Proteins with a vacuolar sorting signal are transported to the vacuole by MVBs (Scheuring *et al.* 2011). MVBs have diverse roles in plant immunity, including degradation, recycling and re-localization of defense-related molecules. Additionally, several defense-related vesicles seem to be generated from MVBs (Li *et al.* 2018).

2.3 Autophagy

Autophagy (Greek for “self-eating”) is another intracellular degradation pathway that is currently known to be controlled by approximately 40 autophagy related (ATG) proteins involved in different stages of plant autophagy. Autophagy occurs in all eukaryotes under stress as well as on a basal level under normal conditions. This far there are two types of autophagy identified in plants, microautophagy and macroautophagy, where macroautophagy is further divided into bulk and selective autophagy. Microautophagy is a process whereupon cytoplasmic material is taken up by the vacuole directly and is degraded in the vacuolar lumen (Sieńko *et al.* 2020, fig. 2). In macroautophagy, material destined for degradation is enveloped by a growing double membrane (phagophore) which upon closure is called an autophagosome. The autophagosome is transferred to the vacuole where upon entering the vacuolar lumen is called autophagic body. The autophagic body with its content is degraded in the vacuole by hydrolases, active by the acidic pH of the vacuole (Parzych & Klionsky 2019). The degraded material is then reused by the cell.

In animals, chaperone-mediated autophagy has been added to the list of autophagy pathways, however, it is not identified in plants. This thesis has focused on macroautophagy which hereafter will be referred to as autophagy.

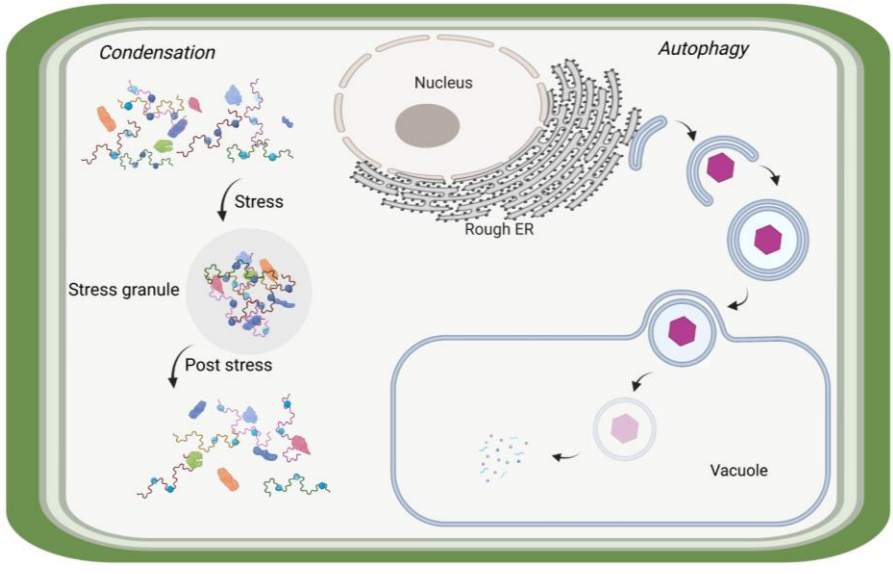

Figure 2. **Stress granule formation and autophagy pathway in plant cell**

Stress results in an abundance of RNA and RBPs in the cytoplasm which is condensated into stress granules. Post stress the material is released into the cytoplasm. Autophagosome formation occur on a basal level in cells, however the pathway is upregulated under stress. The autophagosome is mainly derived from the ER and grows around its targeted cargo. When sealed it is transferred to the vacuole where it fuses to the tonoplast and its material and inner membrane is degraded in the vacuolar lumen by hydrolases.

2.3.1 Autophagy activation

During stress, the plant cannot sustain energy homeostasis which leads to starvation. Starvation upregulates autophagy, mainly via Target Of Rapamycin (TOR). TOR is an evolutionary conserved serine/threonine protein kinase that under favorable conditions coordinates cellular metabolic processes and inhibits autophagy (Mugume *et al.* 2020). During stress, TOR is inhibited which activates autophagy (Liu *et al.* 2010). Autophagy activation can bypass TOR, called the TOR-independent pathway, this is the case with ER stress and oxidative stress. How this pathway functions in detail

is still unclear (Pu *et al.* 2017). There are several regulators of TOR, for example, sucrose non-fermented 1-related kinase (SnRK1, Fig. 3a). SnRK1 is a kinase complex and a major regulator of energy homeostasis in the cell and is activated upon starvation (Wurzinger *et al.* 2018). In Arabidopsis SnRK1 contains two catalytic domain isoforms, KIN10 and KIN11. The KIN10 domain of SnRK1 is responsible for the activation of autophagy via TOR (Soto-Burgos & Bassham, 2017).

In plants, TOR forms a complex called TOR complex 1 (TORC1, Mahfouz *et al.* 2006), together with a regulatory subunit Lethal with Sec Thirteen 8 (LST8) and the Regulatory-Associated Protein of TOR (RAPTOR) which acts as a target recognition cofactor (Anderson, *et al.* 2005; Deprost *et al.* 2005). Under normal conditions, TORC1 reversibly phosphorylates ATG1a (still to be proven in plants) and ATG13a, inhibiting their function (Fig. 3a). When the nutritional state of the cell is compromised TORC1 is inhibited and autophagy activated by dephosphorylation of ATG13a (Suttangkakul *et al.* 2011) and phosphorylation of ATG1a by SnRK1 catalytic subunit KIN10 (Chen *et al.* 2017). ATG13a and ATG1a form an active complex together with ATG11 and ATG101 which orchestrates several downstream steps in the autophagy pathway, probably by further phosphorylation events (Suttangkakul *et al.* 2011; Li and Vierstra 2014, Fig. 3a).

2.3.2 Autophagosome formation and delivery to the vacuole

The autophagosomal membrane origin is unique in that it is not budded off from a preexisting membrane but assembled in a fine-tuned interplay of proteins and lipids. In plants, the autophagosomal membrane mainly originates from the ER (Le Bars *et al.* 2014; Soto-Burgos *et al.* 2018) at a position called the phagophore assembly site (PAS) (Graef *et al.* 2013). ATG9 vesicles derived from the Golgi are recruited to PAS where ATG9 oligomerizes and forms the initiation of the autophagosome membrane (Yamamoto *et al.* 2012; Zhuang *et al.* 2017; Lai *et al.* 2020, fig. 3a).

Subsequent growth of the membrane is orchestrated by SH3 Domain-Containing Protein 2 (SH3P2) and Phosphoinositide 3-kinase (PI3K) complex consisting of Vacuolar Protein Sorting (VPS) 15 VPS34, VPS38 and ATG6. The PI3K complex is recruited to PAS via the ATG9-ATG18

complex (Fig. 3b, Suzuki *et al.* 2015). SH3P2 in coordination with PI3K enables the binding of the phospholipid phosphatidylinositol 3-phosphate (PI3P), one of the building blocks of the growing membrane (Zhuang *et al.* 2013, 2018 Fig. 3b). In order to sequester the cytosolic material bound for degradation the phagophore expands and closes. This is coordinated by two ubiquitin-like conjugation systems (detailed function in chapter 2.3.4), ATG8 and ATG5-ATG12. ATG8 is conjugated to the membrane lipid phosphatidylethanolamine (PE) in a series of reactions involving the ATG5-ATG12 conjugation system. ATG8-PE coats the double membrane which is subsequently sealed.

The delivery of the autophagosome to the vacuole is generally mediated by the Endosomal Sorting Complex Required for Transport (ESCRT) machinery (Gao *et al.* 2015a). Upon fusion of the autophagosome to the tonoplast, the outer membrane of the autophagosome is fused with the tonoplast while the inner membrane, with the autophagic cargo, is released into the lumen of the vacuole. Tethering of the autophagosome to the tonoplast is mediated by the Homotypic fusion and vacuole Protein Sorting (HOPS) complex which is recruited during autophagosome transport to the vacuole (Zhao *et al.* 2021). HOPS binds to the vacuolar membrane and interacts with Soluble N-ethylmaleimide-sensitive factor-Activating protein Receptors (SNARE) proteins, (Brillada *et al.* 2018). SNARE proteins are respectively localized on the acceptor membrane (tonoplast) and donor membrane (autophagosome, Bas *et al.* 2018). Upon proximity enabled by HOPS, the SNAREs form a complex which pulls the membranes into fusion (Wickner 2010). Plants have several identified SNARE proteins (Fujiwara *et al.* 2014) however their function in plant autophagy are still being investigated.

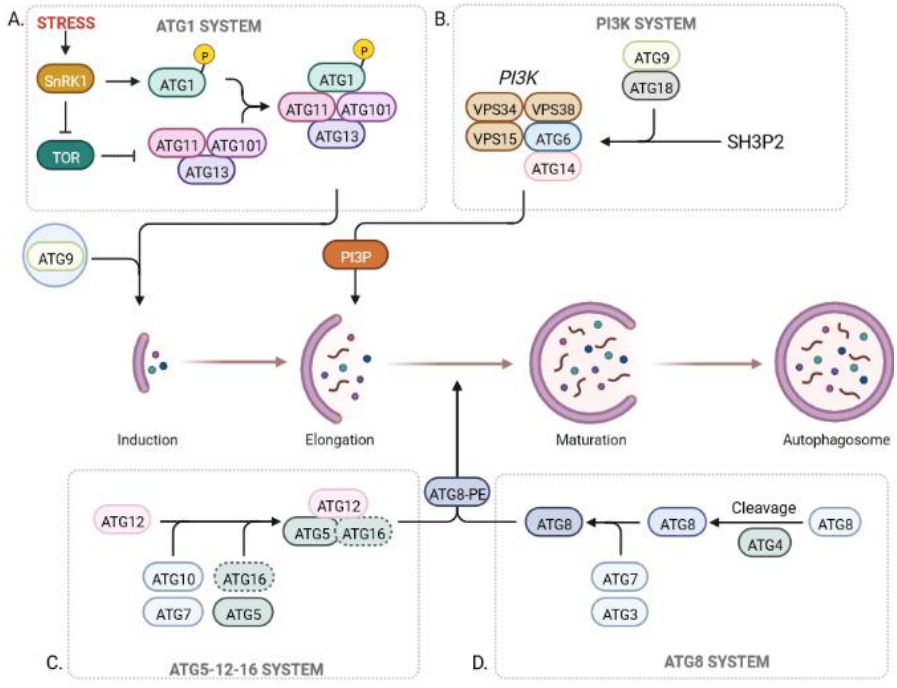

Figure 3. **Autophagosome formation**

Scheme of the different ATG-proteins, divided into four systems which are partaking in autophagosome induction, elongation and maturation. **A.** The ATG1 system or ATG1 kinase complex mediates autophagy initiation. **B.** PI3K system, also called PI3K complex, synthesises the lipid PI3P, a constituent of the autophagosomal membrane. **C.** The formation of ATG5-12-16 system required for ATG8 lipidation. **D.** The ATG8 system activates ATG8 to enable lipidation by ATG5-12-16.

2.3.3 Autophagy cargo recognition

For a long time, autophagy was considered an indiscriminate degradation pathway. This has been shown to not be the case, however, in some situations, there is evidence for a “bulk” autophagy. Leaving that discussion aside I will say that for the most part autophagy is a tightly controlled pathway. The target cargo ranges from singular molecules to full organelles.

In chapter 2.2.1 the ubiquitin-proteasome pathway is described. In order for recognition of proteins to degradation by UPS, they need to be ubiquitinated by the protein family E3. The ubiquitinated protein is subsequently identified by the 26S proteasome and degraded. Ubiquitinated protein aggregates are

also recognized by the Neighbor of BRCA1 gene 1 (NBR1) receptor which can recruit ATG8 via its ATG8 interacting motif (AIM). This way NBR1 connects the ubiquitinated aggregates to ATG8, which is distributed on the phagophore membrane. The aggregate is engulfed by the autophagosome and subsequently degraded in the vacuole (Svenning *et al.* 2011; Jung *et al.* 2020). NBR1 is essential for aggrephagy, the degradation of protein aggregates (Zhou *et al.* 2013; Jung *et al.* 2020) and xenophagy, which removes invading pathogens (Hafrén & Hofius 2017). During nitrogen starvation, autophagy also targets the 26S proteasome, the process termed proteaphagy. This is facilitated via the 26S proteasome subunit RPN10 which has a binding motif to ATG8 (Marshall *et al.* 2015).

All organelles are potential substrates for the autophagy pathway. For example during severe ER-stress (chapter 2.1) the overload of unfolded proteins is too excessive for ERAD and UPR to cope with, instead autophagy degrades whole chunks of ER, a selective route of autophagy called ER-phagy (Bernales *et al.* 2006; Liu *et al.* 2012; Yang *et al.* 2021). Even-though a number of ER-phagy receptors have been characterized in animals and yeast (Yang *et al.* 2021), plant ER-phagy receptors remain largely unknown. However, the protein C53 has recently been demonstrated to be a conserved ER-phagy receptor that is recruited to phagophores upon ER-stress in animals and plants (Stephani *et al.* 2021).

2.3.4 ATG8 and ATG12 conjugation systems

The autophagy pathway encompasses two ubiquitin-like conjugation systems, consisting of the ubiquitin-like proteins ATG8 and ATG12 and their respective E-like proteins (Fig. 3c, d). The protein sequence of ATG8 and ATG12 share no similarities to ubiquitin. However, the protein topology and the mechanisms for conjugation to respective substrates, including the role of E-like enzymes, are analogous to ubiquitin and ubiquitination, respectively (Sugawara *et al.* 2004; Suzuki *et al.* 2005). Both ATG8 and ATG12 conjugation systems are necessary for ATG8-PE incorporation into the growing phagophore.

ATG5-12/16

The ATG5-12/16 hexameric E3-like ligase is required for the lipidation of ATG8 to PE on the growing phagophore (Fig. 3c). It is formed in a series of reactions catalyzed by ATG7 (E1) and ATG10 (E2) involving an ATG12 C-terminal glycine and an ATG5 lysine sidechain. It is initiated by an activation step of ATG12 by ATG7 in a reaction dependent on ATP (Mizushima *et al.* 1998). The activation is followed by a transfer of ATG12 to ATG10 (Shintani *et al.* 1999) enabling the conjugation to ATG5. Interestingly, the conjugate ATG5-12 is sufficient for the lipidation of yeast ATG8 *in vitro* however *in vivo* requires the addition of autophagy protein ATG16 (Fujita *et al.* 2008).

ATG16 is a well-conserved protein among eukaryotes. It consists of an ATG5 interacting motif, a coiled-coil region and a WD40 (tryptophan-aspartic acid) repeat domain which is a hub for protein-protein interactions. In the formation of the ATG5-12/16 E3-like ligase, ATG16 binds non-covalently to ATG5 of the ATG5-ATG12 conjugate, forming a hetero-tetrameric complex. Without ATG16, ATG5-ATG12 do not localize to the growing phagophore in yeast nor mammals, indicating a direct or indirect membrane tethering function of ATG16 (Suzuki *et al.* 2001; Fujita *et al.* 2008). In mammals, one binding partner between the membrane and ATG16L1 is FIP200 (Fujita *et al.* 2008). Likely the ATG5-12-16 complex also plays a role in autophagosome release from the ER membrane (Le Bars *et al.* 2014). The functional role of plant ATG16 remains unsolved.

ATG8-PE

ATG8 is the central regulator of phagophore growth, cargo recognition and autophagosome trafficking (Ketelaar *et al.* 2004; Nakatogawa *et al.* 2007). Nine isoforms of the ATG8 protein have been identified in Arabidopsis, however early-diverged plant lineages such as green algae possess only one isoform. It is believed that the divergence into several isoforms is connected with the diversity of selective autophagy in plants (Stephani & Dagdas 2020). Plant ATG8 genes are grouped into two clades, clade I is closely related to the fungal ATG8 and constitutes Arabidopsis ATG8a-g. Clade II is more similar to animal homologs and comprises of Arabidopsis ATG8h and ATG8i. The ATG8 proteins consist of an N-terminal helical domain and

a C-terminal ubiquitin domain. The C-terminal part is conserved among ATG8 family members and probably plays a role in the conjugation machinery (Shpilka *et al.* 2011). In contrast, the N-terminal part is highly divergent and interacts with ATG8-binding proteins, including cargo receptors (Marshall & Vierstra, 2018).

The lipidation of ATG8 with PE is central for phagophore growth and autophagy substrate recognition (Fig. 3). Loss of function of ATG8 in yeast leads to impairment of autophagosome formation (Kirisako *et al.* 1999). This has yet to be shown in plants, however, overexpression of ATG8 promotes autophagosome formation in Arabidopsis and rice (Chen *et al.* 2018; Yu *et al.* 2019).

The series of reactions that furnishes ATG8-PE conjugate (Fig. 3d) is initiated by the processing of ATG8. A small part of the C-terminus is cleaved off by the cysteine protease ATG4 which exposes a glycine residue (Yoshimoto *et al.* 2004). The C-terminally cleaved ATG8 is then transferred to the C-terminus of ATG7 (E1) where the glycine residue is activated under the consumption of ATP (Yamaguchi *et al.* 2018). The ATG7 N-terminus then binds to the catalytic cysteine of ATG3 (E2) and thereby promotes the transfer of ATG8 to ATG3. (Hong *et al.* 2011; Noda *et al.* 2011; Taherbhoy *et al.* 2011). ATG3 binds to ATG12 of the ATG5-12/16 complex which transfers ATG8 to PE and the ATG8-PE conjugate incorporates into the growing phagophore (Matsushita *et al.* 2007). Prior to autophagosome docking to the yeast tonoplast, ATG4 releases ATG8 from PE (Yu *et al.* 2012).

2.3.5 Interactors of ATG5 separate of the autophagy pathway

Autophagy proteins have been shown to have autophagy-unrelated functions. In animal cells, ATG8 proteins have for example been shown to play a part in intracellular trafficking and Golgi transport (Bu *et al.* 2020). In plants, ATG8 is reported to interact with ABNORMAL SHOOT3 (ABS3) to promote senescence and survival in *atg7-3* mutant seedlings (Jia *et al.* 2019). In human cells, a part of the ATG5 protein is an apoptotic effector (Codogno & Meijer, 2006), and plays a major role in cellular immunity to pathogens in mouse cells (Zhao *et al.* 2008).

The ATG5 protein is encoded by a single gene in mammals, yeast and plants. It is also essential for the formation of the autophagosome, which has made it one of the most popular targets for studies of the autophagy pathway. Yeast ATG5 comprises three domains, two ubiquitin-like (Ubl) domains and a helix-rich domain (Matsushita *et al.* 2007). The structure prediction by Alpha fold identifies the same regions in Arabidopsis ATG5 (Jumper *et al.* 2021; Varadi *et al.* 2022). Plants with overexpressed ATG5 (paper I**)** have superior growth and stress resilience compared with WT, bringing us to the question if these phenotypic traits are due to upregulation of the autophagy pathway or if ATG5 might have important autophagy-unrelated roles.

A recently published study presents the ATG5 interactome in mice, identified approximately 500 interactors of ATG5 and non-conjugating ATG5, where Lys130 is replaced by Arg (K130R) preventing conjugation to ATG12 (Baines *et al.* 2022). Among those, 127 were putative non-conjugate ATG5 interactors. WT ATG5 was shown to have a close association to the clathrin-trafficking machinery, proteins which were largely absent in the ATG5 (K130R) proteome. The clathrin-mediated trafficking machinery is a part of endocytosis. Two proteins of the clathrin-trafficking machinery were studied in depth, PIK3C2A (a phosphoinositide 3-kinase, a well-known player of the clathrin-mediated endocytosis) and HIP1R (a clathrin vesicle component). Null mutants of either of these two proteins altered autophagic flux in mouse fibroblast cells (Baines *et al.* 2022). Clathrin was mainly found in the WT interactome of ATG5, indicating that the ATG5-ATG12 conjugate has a role in the clathrin-associated endocytic machinery.

The common grounds of ATG5 and clathrin-trafficking, as well as the roles of non-conjugated ATG5, have previously not been studied in plants. In paper II we sought to investigate the autophagy-unrelated roles of ATG5.

2.3.6 Role of autophagy in lipid turnover

Lipids have a fundamental role in most organisms, both as energy storage and as constituents of cellular membranes. Storage lipids mainly comprise triacylglycerols (TAGs) contained by a unilayer of phospholipids and

membrane proteins into an organelle called a “lipid droplet” (LD; also termed lipid body or oil body). LDs are degraded through two pathways: lipolysis, during which ATP is produced by β-oxidation of fatty acids in peroxisomes and mitochondria, and lipophagy. Lipophagy is the degradation of LDs by the autophagy pathway, a process common in animals and fungi, whereas only a few cases are described in plants. In budding yeast, microlipohagy constitutes the main lipid degradation pathway (van Zutphen *et al.* 2014), whereas in animals macrolipophagy seems to be more prominent (Goodman 2021).

Autophagy plays dual roles in the turnover of lipid stores. Firstly it is essential for cell differentiation, for example from bone marrow (mesenchymal) stem cells into fat-storing cells (adipocytes, Baerga *et al.* 2009; Zhang *et al.* 2009). Similarly, a differentiation function has also been demonstrated in rice (*Oryza sativa*), where autophagy is essential for correct pollen development. The *osatg7* line lacks LDs in tapetal cells, has reduced TAG content in pollen grains, incomplete tapetal cell degradation as well as impaired phosphatidylcholine editing and lipid desaturation, causing pollen sterility (Kurusu *et al.* 2014). The second role of autophagy and lipid turnover is that of degradation, complementing the pathway of lipolysis (van Zutphen *et al.* 2014). An example is the rapid uptake of LDs into the vacuole upon nitrogen starvation in yeast (van Zutphen *et al.* 2014). Correspondingly, fasting induces rapid LD breakdown in the liver to ensure energy supply (Ward *et al.* 2016).

The role of lipophagy in plants is scarcely studied, however, it is an interesting subject in order to further decipher lipid biosynthesis and catabolism in oil-rich agricultural plants such as rapeseed (*Brassica napus)* as well as how plants might utilize lipid storage during stress conditions. Fan *et al.* (2019) have studied the catabolic role of autophagy in plant LD degradation and found that Arabidopsis plants overexpressing oleosin coupled with GFP are degraded in the vacuole in a microlipophagy-dependent manner. In paper III we reviewed the role of autophagy in the turnover of lipid stores in yeast, animals and plants.

2.4 Biomolecular condensates

Biomolecular condensates are membraneless components or organelles, including but not limited to nucleoli (Pederson 2011), cajal bodies (Morris 2008), processing bodies (P-bodies; (Parker & Sheth 2007) and stress granules (SGs; Anderson & Kedersha 2009). The condensates are formed by a spontaneous or driven liquid-liquid phase separation (LLPS; Brangwynne *et al.* 2009). Specific macromolecules exhibiting multivalency (i.e. molecules prone to engage in multiple intermolecular interactions) are thought to drive the process of LLPS. Due to this property, these molecules naturally assemble into larger oligomers decreasing the solubility of other molecules and in this way promoting phase separation (Banani *et al.* 2017). Apart from multivalent molecules, biomolecular condensates,-especially those that also concentrate RNA- for example SGs, are also enriched in proteins with intrinsically disordered regions (IDRs). These regions are unable to stably fold into a single structure, instead, their conformation constantly changes (Wright & Dyson 2015). This feature, often together with low sequence complexity and enrichment of a small number of distinct amino acids promotes interaction with many other molecules (Banani *et al.* 2017; Holehouse 2019). Of note here, which Holehouse (2019) points out in his concluding remarks, the field of biomolecular condensates is rapidly evolving. The current view is that rather than ultimately driving the process of LLPS, IDRs are more of a tuning factor.

Biomolecular condensates have been suggested to play multiple functions in cells, for example regulating the rate of biochemical reactions. The high local concentration of reactants enables both enhancement and inhibition of reactions. One example from plant biology is the condensation of carbon dioxide and ribulose bisphosphate carboxylase/oxygenase (Rubisco). The concentration of the two molecules enhances the otherwise slow and imprecise carbon fixation reaction by Rubisco (Freeman Rosenzweig *et al.* 2017; Wunder *et al.* 2018; Wang *et al.* 2019; Oltrogge *et al.* 2020; Lyon *et al.* 2021). In the same way as biomolecular condensate can concentrate certain molecules they can also sequester them to inhibit reactions in the surrounding, dilute phase. A typical example includes plant transcription factors Auxin Response Factors (ARF) 7 and 19 which modulate auxin response in plants. ARF7 and ARF19 have been shown to form condensates

in the cytoplasm, inhibiting their nuclear translocation and by that quenching the gene regulatory response to auxin (Powers *et al.* 2019). Additionally, LLPS has been shown to drive the organization of autophagy machinery at PAS in the primordial steps of autophagosome formation, likely enabling activation of ATG1, as well as recruitment of ATG9 vesicles to PAS (Fujioka *et al.* 2020).

We assessed the assembly and function of SGs in paper IV and will therefore introduce them in the following text.

2.5 Plant stress granule function and composition

During stress, a cell´s speed of response is crucial for damage control and survival. Ongoing processes, for example, those facilitating growth must cease and give way to processes facilitating energy saving and redirect the cellular machinery into a stressor-specific response. SGs are dynamic cytoplasmic membraneless organelles forming under stress and partaking in the stress response by concentrating or sequestering cytoplasmic components, foremost translationally stalled mRNA and RNA-binding proteins (RBPs, Campos-Melo *et al.* 2021; Marcelo *et al.* 2021; Fig. 2). SGs are closely associated with polysomes (a group of ribosomes on the same strand of mRNA) and P-bodies. Depending on the status of the cell, the stalled mRNA is either stored in SGs, released to resume translation on polysomes or degraded by P-bodies (Anderson & Kedersha 2008; Campos-Melo *et al.* 2021). A recent and scrutinizing review on the association of RNA and SGs emphasizes that there is dissent regarding the specificity of RNA recruitment to SGs (Glauninger *et al.* 2022). Upon stress relief, the SGs are typically disassembled and mRNA and proteins are released into the cytoplasm to resume the processes essential for growth and development. SGs are enriched in proteins with IDRs and prion-like domains, RNA-binding proteins (RBPs), and proteins with ATPase activity (Maruri-López *et al.* 2021). A study conducted by Jain *et al* (2016) using ultra-resolution microscopy revealed SG regions (cores) with higher concentrations of certain proteins. Those regions were surrounded by more diluted shells. Using Fluorescence Recovery After Photo bleaching (FRAP) they found that

SGs contain both mobile and immobile fractions, demonstrating core-shell SG structure.

2.5.1 SG core

The core contains proteins essential for SG assembly, primarily proteins with IDRs and RNA-binding domains, as well as proteins associated with protein translation. The SG core composition in mammals and yeast has been well researched and consists of a range of different proteins, for example, the 40S ribosome subunit, eukaryotic translation initiation factors and prion-related RNA-binding proteins. (Grouši *et al.* 2009; Kedersha *et al.* 2016; Fomicheva & Ross 2021). A comparative study of plant SG proteomes to that of yeast and mammals present a 28% similarity (Kosmacz *et al.* 2019). Of these, a few have this far been linked to the SG core in plants. Of note is the RNA-binding protein 47b (Rbp47b), the first known plant SG component (Weber *et al.* 2008). Rbp47b is an oligouridylate binding protein 1B (UBP1B) which displays similarity to mammal TIA-1, which mediates SG assembly in humans (Gilks *et al.* 2004). Animal studies of SGs have identified a pre-existing interaction network of SG core proteins present in unstressed cells (Markmiller *et al.* 2018). The same was shown for plants a year later (Kosmacz *et al.* 2019) using Rbp47b as bait.

2.5.2 TSN protein

Tudor Staphylococcal nuclease (TSN, also known as Tudor-SN, SND1 and p100) is another example of a SG core protein, identified as a SG constituent in mammals in 2010 (Gao *et al.* 2010). TSN is an evolutionarily conserved protein, found in all eukaryotic lineages, except for budding yeast (*Saccharomyces cerevisiae*). Two TSN isoforms have been identified in Arabidopsis, TSN1 and TSN2. In plants, TSN has been demonstrated to regulate the biosynthesis of gibberellin and co-localizes to RbP47b under salt stress (Yan *et al.* 2014). It has also been shown to stably associate with heat-induced SGs, the first direct evidence of TSN as a SG core protein (Gutierrez-Beltran *et al.* 2015). TSN is conserved in most eukaryotes suggesting an important physiological role. Indeed, human research has shown a diverse set of functions for TSN, including transcription, splicing, RISC complex nucleolytic component, regulation of non-coding RNAs,

RNA stabilization, stress response, programmed cell death and cancer (Gutierrez-Beltran *et al.* 2016). Its multifunctional behaviour is explained by its peculiar domain composition, comprising a tandem repeat of four staphylococcal nuclease (SN) domains at the N-terminus, a single Tudor domain and finally an additional SN-domain at the C-terminus. Its domain composition and linear tertiary structure enable interaction with nucleic acids, proteins and protein complexes (Gutierrez-Beltran *et al.* 2016). In article IV we investigated the molecular role of TSN and its interactors in SG formation and stress signalling.

2.5.3 SG shell

Once the core is established, the high local concentration of IDRs of the core proteins promotes LLPS allowing the growth of the shell phase. The SG shell is interconnected via weak and dynamic interactions allowing an exchange of molecules between the cytoplasm and SGs (Jain *et al.* 2016). Depending on environmental factors, cell-type and organism the SG shell is hypothesized to comprise unique arrangements of molecules (Jain *et al.* 2016). The shell fraction of SGs is to the most extent unexplored both in animals and plants.

2.5.4 SG formation

SG formation is triggered when mRNA translation is arrested and mRNA is disassociated from polysomes. mRNA passes several control checkpoints in order to be translated, and in mammals, the protein Eukaryote Translation Initiation Factor 2*a* (eIF2*a*) is one of them. During stress, eiF2*a* is phosphorylated and incapacitated to pass through any mRNA, which effectively hinders mRNA translation. One would think that mechanisms regulating translation in eukaryotes would be conserved, however, plants have a very different lifestyle compared to their more portable eukaryotic counterparts. Plant eIF2*a* does have an effect upon translation but only under certain stress conditions, and to a much smaller extent than observed in yeast and mammalian systems (Zhigailov *et al.* 2020).

Another central translation initiator in non-plant systems is the eukaryotic translation initiation factor 4F (eIF4F)-complex which binda to the mRNA

5´cap and is essential for recruitment of the 40S ribosomal unit in cap-dependent translation initiation. eIF4F is regulated by TOR complex via phosphorylation of eIF4E binding protein (4E-BP). Under stress conditions, phosphorylation of 4E-BP is repressed which blocks translation (Sonenberg & Hinnebusch 2009) initiating SG assembly. In plants, there is an eIF4F complex, but also an eIFiso4F complex. The two complexes have both overlapping and specialized roles (Castellano & Merchante, 2021), but their role in SG formation in plants is this far unknown. An additional translation initiation factor in plants with a plausible effect upon SG initiation is a novel eIF4E interacting protein called CERES (Toribio *et al.* 2019). Future research will hopefully shine light on the mechanisms of plant SG formation.

When the translation machinery is stalled, mRNA and RBPs accumulates in the cytoplasm. RBPs have a tendency of forming aggregates that initiate SG assembly (Bounedjah *et al.* 2014). The subsequent route of action is more unclear. Under normal conditions, molecules in the cytoplasm are homogeneously distributed. However, in a case where there is a sudden increase of multivalent molecules, LLPS will occur, and the process is likely to drive SG formation (Molliex *et al.* 2015). The multivalent molecules in SG formation are RBPs containing IDRs (Lin *et al.* 2015; Nott *et al.* 2015) and plausibly also RNA (Tauber *et al.* 2020). The first evidence of LLPS also being part of plant SG assembly has recently been published (Zhu *et al.* 2022). The authors studied two RBPs in Arabidopsis, RBGD2 and RBGD4 and found that they undergo LLPS *in vitro*. While the LLPS seems crucial for SG formation, this process should be tightly regulated and fine-tuned, implying additional players. Research in animal and yeast systems has identified several RBPs with a key role in SG assembly, however, their significance depends on the type of stress. One example is the paralogs G3BP1/2 which are important for SG assembly in mammals during oxidative stress (Tourrière *et al.* 2003), but not required for SG formation during osmotic stress (Kedersha *et al.* 2016). Two out of three Arabidopsis G3BP orthologs have been shown to complement the function of their human homolog (Reuper *et al.* 2021). However, we failed to detect any G3BP isoform among TSN interactors in our study (Gutierrez-Beltran *et al.* 2021, paper IV). To conclude, many regulators of SG formation might be specific for different types of stress.

2.5.5 Signalling role of SGs

Recruitment and accumulation of proteins and mRNA to SGs impact their normal function, enabling both enhancement and inhibition of biochemical reactions. A recent study investigated the potential of biomolecular condensates to enhance enzymatic reactions (Peeples & Rosen 2021). The authors engineered a model condensate based on an enzymatic cascade of SUMOylation (an essential post-translational modification; Celen & Sahin 2020), which activity has been suggested to be regulated by biomolecular condensates. It was shown that phase separation of the SUMOylation cascade can enhance the enzymatic reaction rate up to 36-fold within the condensate, compared to the surrounding solution. These data illustrate that depending on the recruited components of a biomolecular condensate it can impact rates of enzymatic reactions to ultimately favour specific pathways, as well as inhibit them (Peeples & Rosen 2021).

The vast outcome of the protein condensation in SGs has had literature describing them as "signalling hubs". Signalling proteins recruited to SGs are for example enzymes such as kinases, phosphatases, GTPases, helicases, and ribonucleases, as well as adaptor/scaffolding proteins (Kedersha *et al*. 2013). Some of these proteins also regulate SG assembly, therefore their reduced expression inhibits SG formation, granting them the ability to impact any signalling pathway whose components partition in SGs. An example of this is the DEAD-box RNA helicase 3 DDX3 in mammalian systems (Kedersha *et al.* 2013; Cui *et al.* 2020).

In the animal kingdom, there are several examples where sequestering of proteins to SGs leads to the inhibition of apoptotic cell death. Under certain types of stress such as hypoxia, the heat-shock Receptor of Activated protein C Kinase 1 (RACK1) is recruited to SGs. This results in the suppression of the RACK1-dependent inhibition of the Mitogen-Activated Protein Kinase (MAPK)-pathway, inhibiting apoptosis (Arimoto *et al.* 2008; Campos-Melo *et al.* 2021). TOR complex component RAPTOR has also been found to associate with SGs via the interaction with astrin, preventing TOR-hyperactivation-induced apoptosis in cancer cells (Thedieck *et al.* 2013). TORC1 complex is also found to be sequestered by SGs in yeast cells upon heat-stress (Takahara and Maeda 2012). This far there has been no identified

connection between SGs and TOR in plants. Additionally the recent mapping of plant SG composition (Kosmacz *et al.* 2019) identified signalling proteins MKK5 and MPK3, two components of the MAPK signalling cascade (Asai *et al.* 2002).

2.6 Cross-talk between autophagy and SG pathways

Being two essential pathways in stress response across kingdoms, the question arises as to whether autophagic and SG pathways somehow interact. The quick answer to that is yes, and here is what has been found this far. Autophagy has been linked to the clearance of protein aggregates in several human diseases, such as Parkinson´s disease, Huntington´s disease and ALS (Monahan *et al.* 2016). Likewise, autophagy has been found to target SGs in yeast cells (Buchan *et al.* 2013). The authors made a large screen of non-essential gene deletions in *S. cerevisiae* under favourable growth conditions in order to determine which deletions affect SGs and P-bodies. The yeast SG component PAB1 was coupled to GFP to study the increase or decrease of the SGs in the mutants. Mutants of the autophagy pathway, namely *atg8, atg11,* and *atg18* resulted in an increase of SGs. *atg15* mutant had SGs accumulated in an intravacuolar compartment, consistent with the fact that ATG15 is a vacuolar lipase that degrades the membranes of vesicles in the vacuole. In subsequent experiments, the authors observed co-localization between PAB1-mCh and ATG19-GFP. ATG19 facilitates the loading of cargo into the growing phagophore. Additionally, they showed that CDC48 (VCP/p97 in animals), a chaperone-like protein and component of ubiquitin-targeted degradation, enhances the targeting of SGs to autophagy. These results taken together show targeting of SGs by the autophagic pathway.

In animals there are several connections between autophagy components and SGs, for example, ULK1/2 (aka ATG1) interactome is enriched in SG proteins and promotes SG disassembly in mice by phosphorylation of VCP/p97 (Wang *et al.* 2019a). On the same note, senescent fibroblast cells are unable to form SGs under chronic oxidative stress likely due to a simultaneous upregulation of autophagy and Heat Shock Protein 70 which promotes SG disassembly (Omer *et al.* 2020). Additionally, inhibition of autophagy has been shown to impair SG formation (Seguin *et al.* 2014), the

authors speculate that proteostasis imbalance due to inhibited autophagy impacts SG formation. Indeed their data demonstrated that under autophagy-deficient conditions SGs accumulate non-canonical components which impair proper SG-formation (Seguin *et al.* 2014). Also Sindbis virus infection is promoted by ATG16L which phosphorylates eiF2a, triggering formation of perinuclear SG containing capsid (Jefferson *et al.* 2019).

The role of autophagy in targeting SG for degradation in plants is still vague. Recently Field and colleagues (2021) reported that a type of SGs is targeted to autophagosomes upon extended hypoxia, a process requiring Calmodulin-Like 38 (CML38) and CDC48/p97 remodeling. The CML38 is a calcium-sensor protein and has been suggested to serve as a calcium signalling target within hypoxia-induced SGs (Lokdarshi *et al.* 2016). CML38 binds to Suppressor of Gene Silencing 3 (SGS3, Field *et al.* 2021), a protein that is necessary for the production of siRNA (Yoshikawa *et al.* 2005) and part of the epigenetic silencing of transposons (Kim *et al.* 2021). The reason for autophagy targeting these SGs at extended hypoxia is suggested to be due to acute carbohydrate starvation and therefore a need to recycle cellular resources. Also, the authors suggest that the function could be a part of the RNA regulatory program during hypoxia.

Further research is needed to find additional points of cross-talk between these two major stress-response pathways in plants. This knowledge will support crop breeding programs for more multi-stress-resistant plants to cope with climate change.

3. Objectives and aims of this study

The main objective of this thesis was to enhance our comprehension of plant molecular stress responses involving autophagy and the formation of stress granules.

The following specific aims were addressed:

- Investigate the potential role of ATG5 and ATG7 as the rate-limiting components of plant autophagy pathway (**paper I).**
- Characterize the autophagy-unrelated interactome of Arabidopsis ATG5 (**paper II**).
- To provide a cross-kingdom comparison of the roles and mechanisms of autophagy in the turnover of lipid stores (**paper III**).
- Investigate the molecular roll of TSN during stress (**paper IV**).

4. Results and Discussion

The main objective of this thesis was to enhance our comprehension of plant molecular stress responses involving autophagy and the formation of stress granules. This knowledge will contribute to our understanding of how crops overcome stress factors and provide plausible targets for genetic and chemical approaches to improve crop productivity.

4.1 Transcriptional stimulation of rate-limiting components of the autophagic pathway improves plant fitness (**paper I**)

Previous work in our and other laboratories has shown that reduced autophagic flux correlates with impaired plant fitness and stress response (Liu *et al*. 2009; Yoshimoto *et al*. 2009a; Minina, *et al*. 2014). On the other hand, elevating the autophagic flux by moderately decreasing light intensity suppressed senescence and increased longevity (Minina *et al*. 2013). Work by Wang *et al*. (2017a, 2017b) showed that overexpression of apple (*Malus* domestica) *ATG3a* or *ATG3b* as well as *ATG7* increased stress resilience in Arabidopsis. In paper I we sought to find the mechanistic link between the expression of certain *ATG* genes and autophagic flux. We found that constitutive upregulation of *ATG5* or *ATG7* in Arabidopsis enhanced autophagic flux and improved plant growth and stress resilience.

4.1.1 ATG5 and ATG7 are rate-limiting components of autophagy whose enhanced expression increases autophagic flux

The ATG5 protein is a component of the ATG5-ATG12 ubiquitin-like conjugation system in autophagy, required for the lipidation of ATG8 with PE. ATG7 catalyzes the formation of both ATG5-ATG12 and ATG8-PE conjugates (Fig. 3c, d). Knock-out (KO) mutants of either gene are autophagy-deficient (Otomo *et al.* 2013). We generated homozygous transgenic lines constitutively overexpressing *ATG5* or *ATG7* in Arabidopsis. We found that ATG5-ATG12 and ATG8-PE conjugation was enhanced in the *ATG5* OE whereas *ATG7* OE only stimulated ATG8-PE conjugation (Fig. 4a, b; data not shown). Autophagic flux measurements revealed an increase of autophagic flux in the respective OE line (Fig. 4c-f). These results indicate that i) ATG5 and ATG7 are rate-limiting components of autophagy in Arabidopsis, ii) upregulation of either of the genes increases autophagic flux, iii) ATG7 is not a rate-limiting factor of ATG5-ATG12 conjugation. The above results raise new questions, what control elements act on ATG5 and ATG7 and what other *ATG*-genes are regulatory checkpoints?

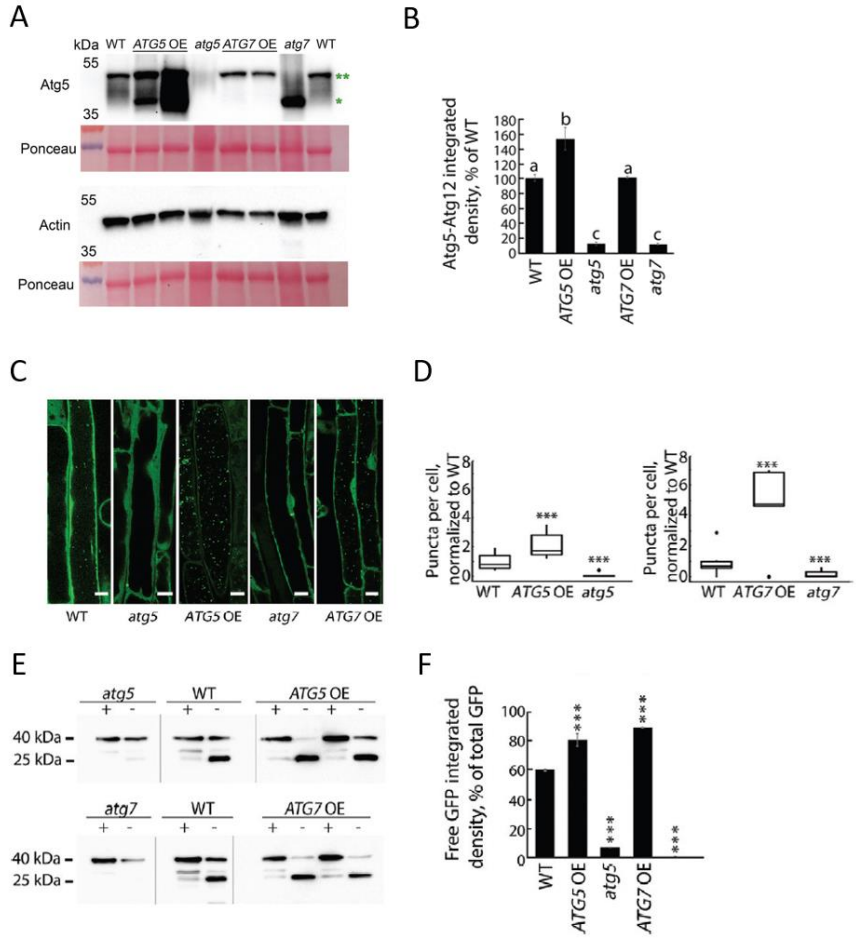

Figure 4 **Overexpression of *ATG5* or *ATG7* stimulates autophagic flux**

A. Western blot detection of Atg5 in Col-0 (WT), *ATG5* OE, *ATG7* OE, *atg5* and *atg7* mutants. *Atg5; **Atg12–Atg5 conjugate. **B.** Densitometry of the Atg5–Atg12 conjugate in A. **C.** Microscopy images of the epidermal root cells expressing GFP–Atg8a in WT, *ATG*-knockout, and *ATG*-overexpressing backgrounds. Seedlings were subjected to 0.5 µM ConA treatment for 16 h prior to imaging. Scale bars=10 µm. **D.** Number of the GFP-positive puncta in C. **E.** Western blot analysis with anti-GFP. The GFP–Atg8a fusion has a predicted molecular weight of ~40 kDa; free GFP has a predicted molecular weight of 27 kDa. **F.** Densitometry of the GFP–ATG8a cleavage assay in (E).

4.1.2 Overexpression of *ATG5* or *ATG7* improves plant fitness

Autophagy KO mutants display several phenotypic symptoms of impaired stress resistance, growth and longevity (Doelling *et al.* 2002; Yoshimoto *et al.* 2009b; Zhou *et al.* 2013). We phenotypically compared the plants with upregulated *ATG5* or *ATG7* versus their respective KO mutants and WT. OE plants were significantly larger than WT at 3 weeks, as well as when fully grown (Fig. 5a, b). Leaf biomass, as well as seed yield, were increased in OE-lines compared to WT whereas the opposite trends were observed in the *atg5* and *atg7* lines (Fig. 5c, d). OE plants also exhibited an extended duration of flowering and later onset of senescence (Fig. 5 e, f).

These results suggest that under non-stress conditions transcriptionally upregulated autophagy in Arabidopsis (i) stimulates cell division resulting in increased biomass, (ii) extends longevity and (iii) increases seed yield. This implies that autophagy impacts several pathways connected to plant fitness. Nitrogen availability is essential for plant growth and several studies have shown that autophagy is important for nitrogen remobilization in plants (Guiboileau *et al.* 2012; Wada *et al.* 2015; Ishida & Makino 2018; Cao *et al.* 2022). Additionally, a recent study in rice showed that overexpression of *ATG8b* improves seed yield under both normal and N-deficient conditions (Zhen *et al.* 2021). Likely increased autophagy improves plant nitrogen access which promotes growth and development. The delayed senescence phenotype could be linked to hormone signalling (Gou *et al.* 2019 for review). Particularly, autophagy has been shown to negatively regulate salicylic acid signalling leading to delayed senescence (Yoshimoto *et al.* 2009a).

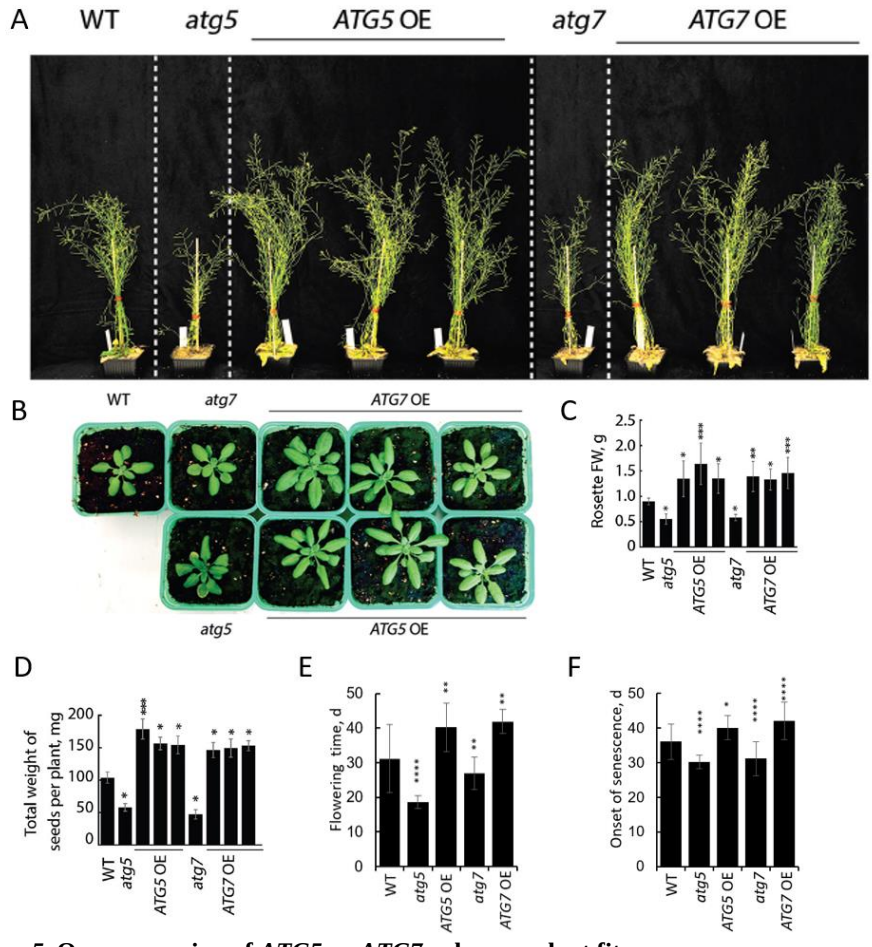

Figure 5. **Overexpression of *ATG5* or *ATG7* enhances plant fitness**

A, B. Representative phenotype of autophagy overexpressor lines and mutant lines at flowering stage (A) and 3 weeks (B). **C.** Fresh weight of rosettes. **D.** Seed yield. **E.** Flowering time (days). **F.** Onset of senescence (days after germination).

4.1.3 Autophagy improves resistance to necrotrophic pathogens and oxidative stress

The reallocation of resources between growth and stress resistance is central to the life cycle of plants (Chae *et al.* 2016). During stress, plant growth is inhibited to use the available resources to overcome the stress. In crop production, this generally means that a crop with high-stress resistance produces a smaller yield and vice versa (Karasov *et al.* 2017). Since we

observed significant growth and yield gain in our OE lines we further investigated if this was to the cost of stress resistance. Research by Lai *et al.* (2011) and Lenz *et al.* (2011) found that *atg* KO mutants display a higher sensitivity to necrotrophic pathogens. Thus, we subjected the *ATG5* or *ATG7* OE and KO lines to the necrotrophic fungus *Alternaria brassicicola.* Surprisingly, OE lines displayed a higher resistance than WT (Fig. 6a-c). We followed this up by conducting experiments on oxidative stress resistance. Oxidative stress is a result of the overproduction of Reactive Oxygen Species (ROS), one of the major components of necrotrophic pathogenicity (Choquer *et al.* 2007). The plants with enhanced autophagy displayed increased resistance to methyl viologen-induced oxidative stress (Fig. 6 d, e).

These results indicate that upregulation of autophagy bestows (i) a defense against necrotrophic pathogens and (ii) protection against oxidative stress. Necrotrophic fungi are a major challenge for crop production and storage world-wide, currently demanding enormous input of fungicides (Fones *et al.* 2020 for review). Autophagy has been previously shown to have a protective role against necrotrophic fungi via ATG18a and the transcription factor WRKY33 (Lai *et al.* 2011), which is required for necrotrophic pathogen resistance in plants (Zheng *et al.* 2006). The reason for the increased resistance to necrotrophic pathogens in plants with increased expression of ATG5 or ATG7, possibly lays in the inhibition of pathogen-induced cell death (Liu *et al.* 2005) and autophagy involvement in jasmonic- and salicylic acid signalling upon pathogen response (Lai *et al.* 2011). As for the role of autophagy in oxidative stress, it has been shown that autophagy counteracts the effect of oxidative stress by for example targeting oxidized proteins (Xiong *et al.* 2007), protein aggregates (Zhou *et al.* 2013; Jung *et al.* 2020) and damaged peroxisomes (Shibata *et al.* 2013; Yamauchi *et al.* 2019).

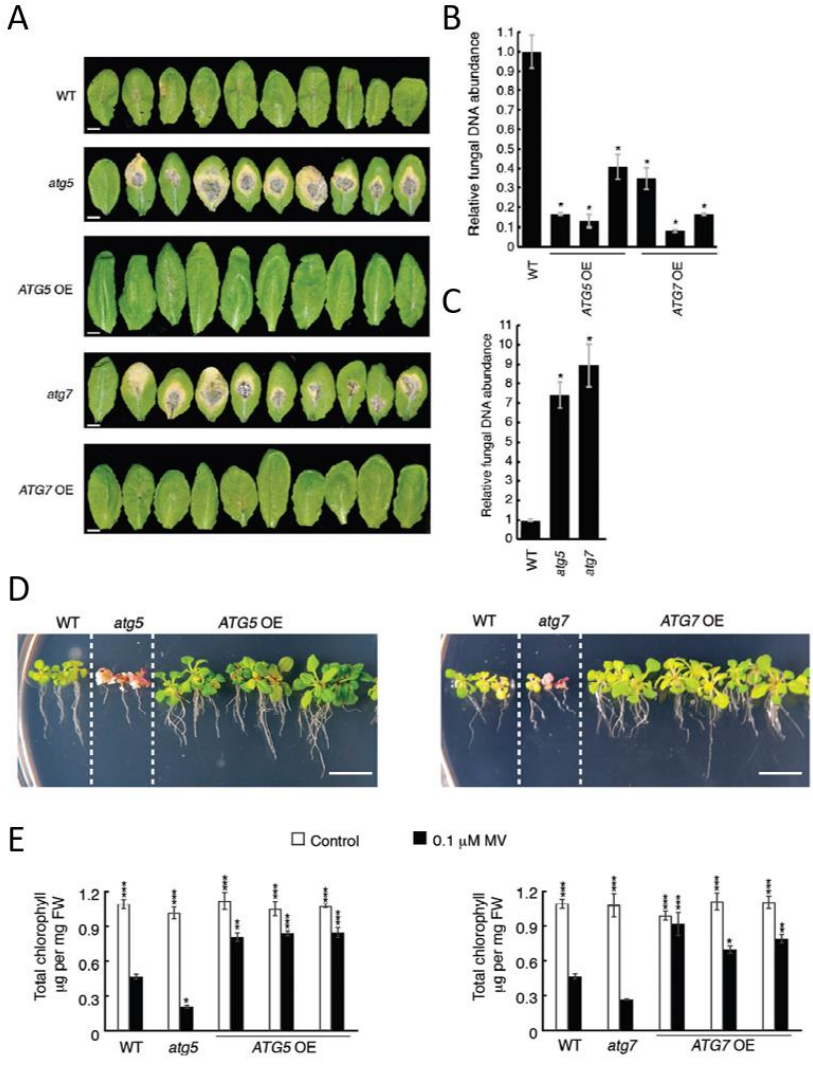

Figure 6. **Overexpression of *ATG5* or *ATG7* increases resistance to necrotrophic fungi and oxidative stress. A.** Three-week-old plants of the WT, *ATG*-knockout, and *ATG*-overexpressing lines inoculated with *Alternaria brassicicola*. Images display all rosette leaves from representative selected plants seven days post-inoculation. **B, C.** Fungal growth assessed by measuring fungal DNA using qRT-PCR to detect the fungal cutinase gene. Scale bars= 1cm. **D.** Phenpotype of 3 week-old seedlings of WT, *ATG*-knockout mutants, *ATG5*- and *ATG7*-overexpressing lines germinated on MS plates with or without addition of 0.1 µM methyl viologen (MV). **E**. Chlorophyll measurements to assess oxidative stress tolerance. Scale bars=1 cm.

4.2 Exploring Arabidopsis ATG5 functions beyond autophagy (**paper II**)

In our previous publication (Minina *et al.* 2018, chapter 4.1) we showed that OE-plants displayed improved fitness. Those results had as speculate if the superior phenotypes of the OE-plants were solely due to upregulated autophagy or additional autophagy-unrelated roles of ATG5 and ATG7. Here we aimed to investigate this by studying the interactome of wild-type ATG5, capable of forming a complete ATG5-ATG12-ATG16 complex and of the mutant ATG5^{K128R} that can form only the minimal ATG5-ATG16 complex.

4.2.1 Interactome of *Arabidopsis thaliana* ATG5

The point mutant ATG5^{K128R} is unable to conjugate to ATG12 (Fujioka *et al.* 2008) and therefore fails to sustain autophagy. We used this mutant and wild-type ATG5 expressed under constitutive promoter 2x35S as baits for alternative tandem affinity purification (Rubio *et al.* 2005) under favourable growth conditions in Arabidopsis. The respective proteomes were analyzed by LC-MS/MS. Hits were filtered by Log2 fold change >1.5 and a p-value <0.05. With these criteria, we obtained 104 hits for ATG5, 78 for ATG5^{K128R} and 97 hits shared by the two baits (Fig. 7a). String analysis displayed clusters mainly connected to the proteasome, ribosome, mitochondria, cellular transport and the chloroplast.

ATG proteins have evolved as an integral part of the endomembrane trafficking system, therefore their autophagy-unrelated functions might be intertwined with it. The potential roles in endomembrane trafficking and a recent study in mice demonstrating a connection with the ATG5 complete complex and clathrin mediated trafficking (Baines *et al.* 2022), made us direct our focus in the area of cellular trafficking. Among the LC-MS/MS hits we identified two proteins belonging to clathrin-mediated machinery: a TPLATE complex subunit (AT5G57460.1) in the ATG5 hits and SH3P2 (AT4G34660.1) in the proteome of shared hits. Within the ATG5^{K128R} hits, we found 4 proteins that have been annotated or been speculated to have roles in cellular transport.

Post-translational modifications (PTMs) are a rapid way of adjusting the cellular machinery during normal and stress conditions in cells (Friso and Van Wijk 2015; Han *et al.* 2022). ATG proteins are constitutively expressed and their activity is tightly controlled by PTMs, such as phosphorylation and dephosphorylation, ubiquitination, lipidation, S-sulfhydration, S-nitrosylation, sumoylation and acetylation (Suttangkakul *et al.* 2011, Chen *et al.* 2017, Qi *et al.* 2021). Additional filtering of the LC-MS/MS data enabled us to identify PTMs of our interactors. We found that PTMs were less prominent in the ATG5^{K128R} interactome than in the ATG5 interactome. 52% of the proteins of the ATG5^{K128R} interactome had no PTMs compared to 15% of the ATG5 interactome (Fig. 7b). The opposite was true for ATG5, where 43% of the proteins had PTMs compared to 16% and 14% in the ATG5^{K128R} and shared interactomes, respectively (Fig. 7b).

From the filtered hits we chose a subset for functional analysis (Fig. 7c). Of those, several have previously been annotated with functions connected to cellular trafficking, vesicular protein sorting, water transport, 20S proteasome and stress responses. The continuation of this study will allow us to expand our understanding of the autophagy related proteins beyond their role in autophagic pathway.

a.

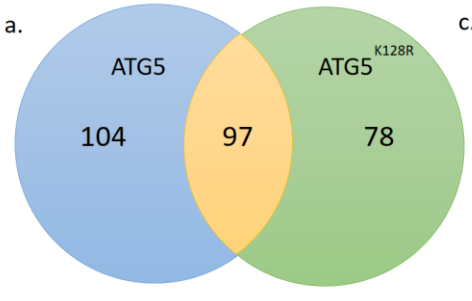

b.

Bait	PTM	noPTM	Both PTM and noPTM*
ATG5	45	16	43
ATG5^{K128R}	13	41	24
ATG5 and ATG5^{K128R}	15	40	42

c.

AGI code	Gene name
AT3G51260	PAD1
AT1G56450	PBG1
AT2G25950	PITH DOMAIN PROTEIN
AT1G13320	PP2A SUBUNIT A3
AT2G42500	PP2A3
AT4G34660.1	SH3P2
AT5G06140.1	SNX1
AT5G58440	SNX2A
AT3G01390.1	VACUOLAR MEMBRANE ATPASE 10
AT4G02620	MEMBER OF VTPASE FAMILY
AT5G54750.2	TRAPPC3
AT5G56030.2	HSP90.2
AT2G16600	ROTAMASE CYP 3
AT3G16240	DELTA-TIP 1
AT3G26520	GAMMA-TIP2
AT2G20990	SYNAPTOGAMIN A
AT1G22530	PATELLIN 2
AT1G35720	ANNEXIN 1

Figure 7. **The Arabidopsis ATG5 interactome**

a. Venn-diagram displaying number of potential interactors purified for complete and minimal ATG5 complexes. LC-MS/MS hits were filtered using MSqRob and LFQ values,log2FC>1.5, p-value <0.05.**b.** Summary table showing the number of potential

interactors identified using filtering for post-translational modifications (phosphorylation or acetylation) in the LC-MS/MS analysis. * Some peptides of the protein had PTMs whereas others had no PTM. **c.** List of potential protein interactors of complete and minimal complex and shared interactors.

4.3 Autophagy in turnover of lipid stores: trans-kingdom comparison (review, **paper III**)

Since the observed effects of upregulated autophagy in paper I also included elevated oil content we sought to investigate the plausible connections between autophagy and lipids further, by conducting a literature study focusing on autophagy and the lipid storage organelles lipid droplets (LDs). Following are the major points from the review paper with an up-to-date discussion encompassing articles that appeared after paper III was accepted for publication.

4.3.1 The role of autophagy in plant LD catabolism is still to be deciphered

Lipophagy, the targeting of lipids by the autophagosome and subsequent degradation in the vacuole or lysosome is an important pathway in animals and yeast systems (Ward *et al.* 2016; Zechner *et al.* 2017, Fig. 8). The green alga *Auxenochlorella protothecoides* displays a microlipophagy-like process in the remodeling required for the transition from heterotrophic to autotrophic growth (Zhao *et al.* 2014). Upon carbon starvation in the green alga *Micrasterias denticulate* LDs which under normal conditions reside in the chloroplast, move out to the cytoplasm where they are targeted by autophagosomes and degraded by the vacuole (Schwarz *et al.* 2017). In the beginning of 2018 when paper III was in preparation, no direct evidence for the occurrence of lipophagy in higher plants was available. Now, more than four years after the publishing of paper III, there has been some advancement in the field. For example further evidence that autophagy is important for proper male reproductive development in rice was presented (Hanamata *et al.* 2019, 2020). On the same note, a study in tobacco presented that pollen from *ATG* RNAi lines displayed an increased abundance of storage lipids such as TAGs, suggesting a role of autophagy in the degradation of storage lipids in pollen (Zhao *et al.* 2020). Arabidopsis leaves typically do not store

energy in the form of lipids, despite the high occurrence of TAG synthesis (Dahlqvist *et al.* 2000). One plausible reason for this is the high turnover of TAG by the lipase Sugar Dependent Protein 1 (SDP1, Eastmond 2006; Kelly *et al.* 2013). However during some stress conditions, e.g. extended dark stress, there is an accumulation of TAGs, (Fan *et al.* 2017). TAG levels initially increase in *sdp1* KO plants exposed to extended darkness, but then decrease, suggesting an alternative pathway of lipid degradation (Fan *et al.* 2017). In a follow-up study, Fan *et al.* (2019) established double *atg sdp1* mutants and found that initial TAG levels were higher than in *sdp1* mutants and also remained high upon 3 days of dark treatment. The authors suggested that this is due to decreased lipophagic activity. In the same study Fan *et al.* (2019) artificially introduced LDs into Arabidopsis leaves by either overexpressing oleosin or phospholipid:diacylglycerol acyltransferase (PDAT1) or by knocking out trigalactosyldiacylglycerol (tgd1) or glycerol-3-phosphate acyltransferase1 (act1). In these settings, they argue that autophagy has a degradative role upon LDs under dark starvation. However, a caveat of this study is the microscopic evidence for this claim, which is rather weak and requires additional experimental data to be conclusive.

4.3.2 Microlipophagy in higher plants is yet to be thoroughly investigated

Macrolipophagy constitutes the major pathway of lipophagy in animals. This is not the case in yeast, where instead microlipophagy is the major pathway (van Zutphen *et al.* 2014, Fig. 8). Studies in green algae have shown both macrolipophagy (*Micrasterias denticulate,* Schwarz *et al.* 2017 and *Chlamydomonas reinhardtii,* Kajikawa *et al.* 2019) and microlipophagy (*Auxenochlorella protothecoides,* Zhao *et al*. 2014). The question of to what extent lipophagy occurs in higher plants is yet to be thoroughly unraveled. Kurusu *et al,* (2014) showed that macroautophagy is essential for pollen development in rice. A more recent study of Arabidopsis pollen development demonstrated that microlipophagy takes place during the transition from bicellular to tricellular pollen stage, a process that is inhibited but not arrested in the *atg2* mutant (Akita *et al.* 2021). Fan *et al.* (2019) suggest that LDs are incorporated into the vacuole by microlipophagy. Thus far it is unknown what proteins take part in microlipophagy in plants. Fan *et al.* (2019)

observed increased TAG content in *atg sdp1* double mutants and concluded that microplipophagy is dependent on core *ATG*-genes which is in line with what van Zutphen *et al.* (2014) and Seo *et al.* (2017) have reported in yeast. On the contrary, other studies in yeast have suggested that core *ATG*-genes are non-essential and instead propose that ESCRT components are required for microlipophagy (Vevea *et al.* 2015; Oku *et al.* 2017). In conclusion, some evidence for both macrolipophagy and microlipophagy has been found in higher plants. Future research will decipher whether the occurrence of macro- versus microlipophagy is different for monocots and dicots, and whether it is organ-specific, developmental stage-specific and/or condition-specific.

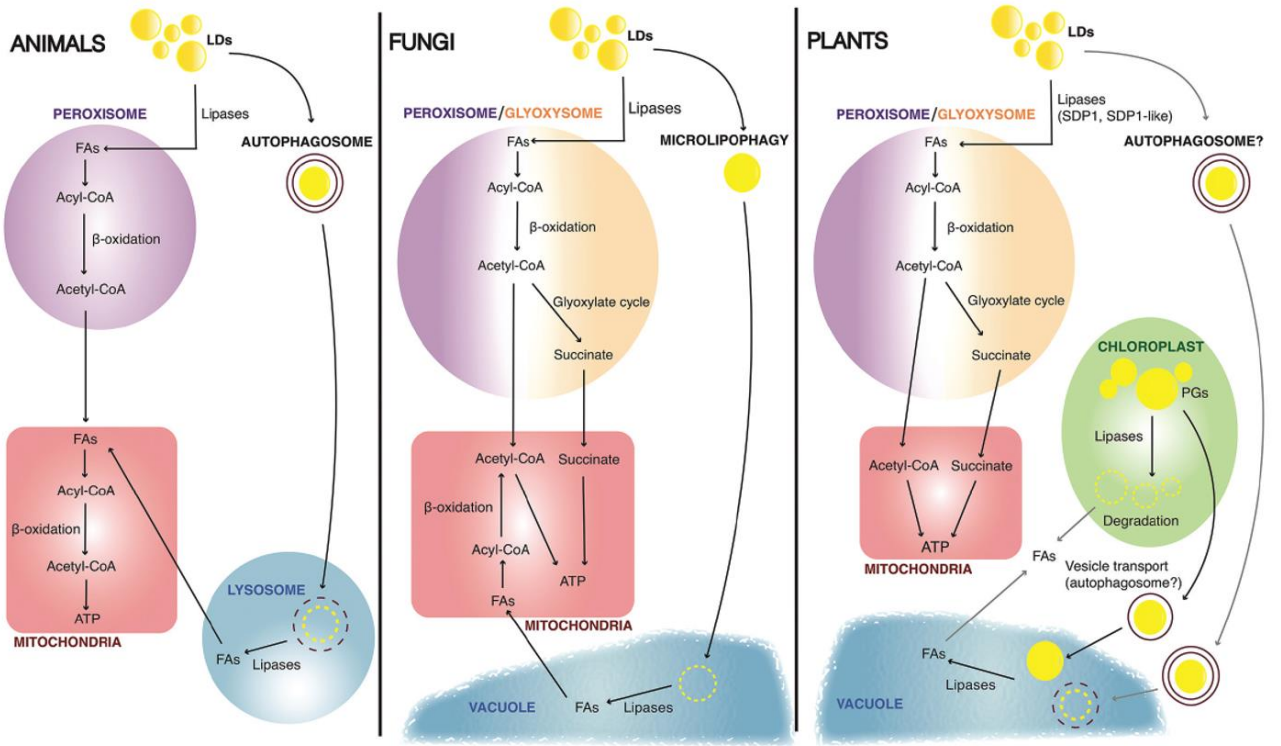

Figure 8. **Cross-kingdom comparison of LD degradation pathways.**
A schematic description of lipid degradation in animals, fungi and plants. Black arrows indicate known pathways whereas grey arrows indicate hypothetical pathways.

4.4 Tudor staphylococcal nuclease is a docking platform for stress granule components and is essential for SnRK1 activation in *Arabidopsis* (**paper IV**)

The formation and function of SGs in response to stress conditions have just started to be unraveled in plants. In 2019 Kosmacz *et al.* advanced the field by publishing the proteome and metabolome of plant SGs in heat-stressed and unstressed Arabidopsis seedlings. Overexpressed Rbp47b was used as bait and SGs were isolated by combining differential centrifugation and affinity purification. The authors found that approximately 1/3 of the identified proteins have known homologs in yeast or human cells, and are central to SG assembly and dynamics, displaying an evolutionarily conserved process. Of note is their finding that instead of SGs being completely disassembled under normal conditions they exist as a protein interaction network (Kosmacz *et al.* 2019). Tudor Staphylococcal Nuclease (TSN) is a known constituent of SGs in animals and plants (Zhu *et al.* 2013; Yan *et al.* 2014; Gao *et al.* 2015b; Gutierrez-Beltran *et al.* 2015) and the double ko mutant *tsn1 tsn2* displays hypersensitivity to salt and heat-stress in Arabidopsis (dit Frey *et al.* 2010) and ectopic cell death in heat-treated Arabidopsis roots (Gutierrez-Beltran *et al.* 2015). In a previous study we showed that TSN is stably associated with SGs and is indispensable for their integrity and function (Gutierrez-Beltran *et al.* 2015). In this work we aimed to increase our understanding of SG regulation and molecular function in plants by isolating TSN-interacting proteins and studying the role of TSN in heat-stress signalling.

4.4.1 Interactome of Arabidopsis TSN2 protein

Using the tandem affinity purification method (TAP, Rubio *et al.* 2005) with TSN2 as bait and GFP as a negative control we investigated the TSN2 interactome under heat-stress (HS) and no-stress (NS) conditions. The purified proteins were analyzed using a spectrometry-based label-free quantitative approach. After filtering we had 276 hits for NS and 148 interactors for HS with an overlap between the conditions of 31 (Fig. 9a). Twenty percent of the full interactome are known components of human or yeast SGs (Jain *et al.* 2016), enriched in RNA-binding proteins (RBPs),

proteins with predicted prion-like domains and ATPase activity proteins (Fig. 9b). With publicly available data of direct protein-protein interactions (PPI) we found that both TSN_NS and TSN_HS protein pools formed a dense network of PPIs. TSN2_NS was the most prominent of the two, with 239 nodes (proteins) and 1059 edges (interactions) in comparison with 120 nodes and 177 edges for TSN2_HS. The average number of interactions per protein in the TSN_NS was 8.86 and 2.95 for TSN2_HS.
These results suggest that (i) there is a pre-existing steady-state network of PPIs under NS-conditions in Arabidopsis and (ii) TSN could act as a protein assembly platform.

From the TSN2 interactome, we selected 16 of the most interesting proteins for further studies. These included homologs of well-known yeast and animal SG components, eIF4E5, PAB4, and RPS11, as well as some potential plant-specific SG-proteins with essential roles in eukaryotic pathways, e.g SKP1, MCA-Ia, TCTP, and the SnRK1α1 and SnRK1α2 isoforms. 10 out of 16 proteins were confirmed TSN interactors.

4.4.2 Role of TSN as a SG docking platform

Of the proteins which arrange into molecular condensates such as SGs, a small fraction is important for condensate formation called scaffolding proteins. Deletion of scaffold-proteins has a pronounced effect on the condensate composition (Ditlev *et al.* 2018 for review). In our previous study of TSN (Gutierrez-Beltran *et al.* 2015) we observed that TSN does not exchange between the cytoplasm and SG foci, suggesting a possible function as a SG scaffolding protein. In this study, we aimed to test this hypthesis by comparing the interactome of the well-known SG core protein RBP47 with that of TSN2 under NS and HS. We found that NS and HS interactomes shared 54 and 4 proteins respectively. Notably, TSN2 was identified in both RBP47_NS and HS interactomes. We further investigated the role of TSN in the RBP47 interactome by knocking out both TSN1 and TSN2. In absence of stress, the deletion of TSN increased the RBP47 interactome 10-fold. Also, the RBP47 protein interactome was almost completely altered in the *tsn1 tsn2* background compared to WT (Fig 9c).

These data demonstrate that (i) RBP47 interactome is extensively reorganized by TSN deficiency (ii) RBP47 is a constitutive interactor of TSN and (iii) TSN plays a role as a scaffold protein during SG formation.

It has been shown that SG scaffolding proteins exhibit enrichment of IDRs which regulate SG assembly via LLPS (Molliex *et al.* 2015; Guillén-Boixet *et al.* 2020; Yang *et al.* 2020). On average TSN2 is expected to have 11 disordered regions in the SN domains whereas the Tudor domain is ordered. Studies of the individual domains and four of the identified protein interactors established that the SN region is the essential TSN component for PPI.

Thus far we showed that TSN has an important scaffolding role in SG formation, where TSN deficiency strongly affects the protein composition of SGs. TSN interacts with a wide range of SG components via its N-terminal tandem repeat of four SN domains which are IDR-rich regions.

A model commonly used to explain the composition of diverse molecules in molecular condensates such as SGs is a scaffold-client model (Banani *et al.* 2016), where the scaffold is a high-valence molecule essential for the structural integrity of the condensate and the clients are dispensable and only reside with the SG under certain conditions. Also, the IDRs of scaffold proteins have been reported to be essential for SG formation in several studies (Gilks *et al.* 2004; Yang *et al.* 2020b; Fomicheva & Ross 2021). These properties are in line with what we show for TSN in our present and previous studies (Gutierrez-Beltran *et al.* 2015).

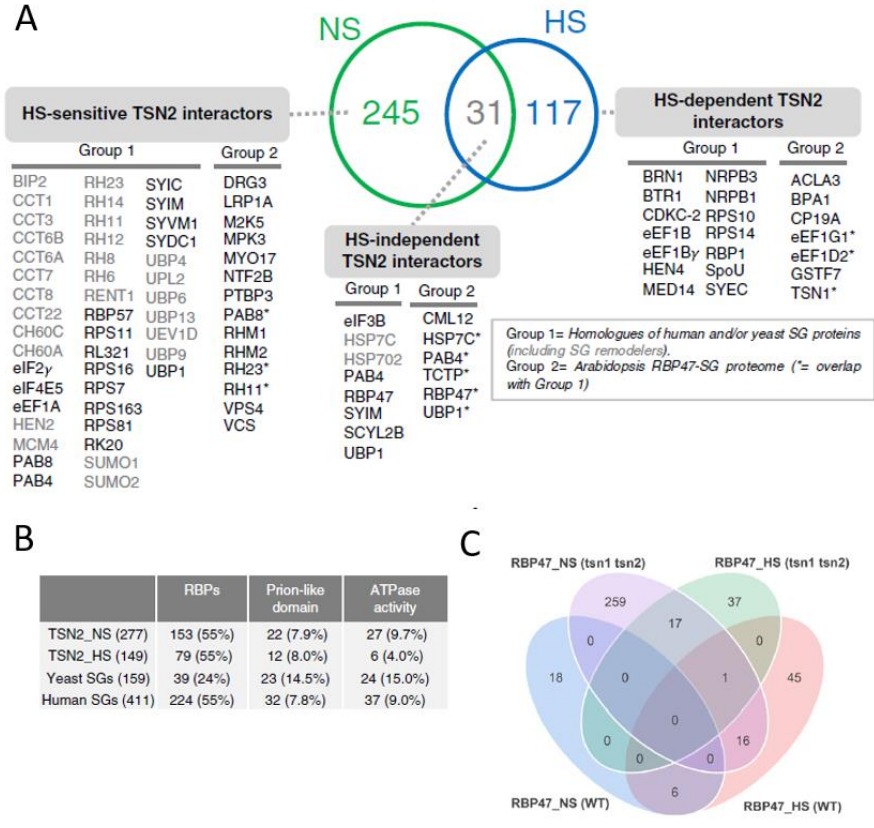

	RBPs	Prion-like domain	ATPase activity
TSN2_NS (277)	153 (55%)	22 (7.9%)	27 (9.7%)
TSN2_HS (149)	79 (55%)	12 (8.0%)	6 (4.0%)
Yeast SGs (159)	39 (24%)	23 (14.5%)	24 (15.0%)
Human SGs (411)	224 (55%)	32 (7.8%)	37 (9.0%)

Figure 9. **Characterization of the Arabidopsis TSN2-interacting proteins**
A. Venn diagram showing the comparison between TSN2_NS and TSN2_HS protein pools. **B**. Frequency of RBPs and proteins with prion-like domains or ATPase activity found in TSN2_NS and TSN2_HS protein pools in comparison with yeast and human SG proteomes (Jain *et al*, 2016). **C.** Venn diagram showing the comparison between RBP47_NS and RBP47_HS protein pools isolated from WT and *tsn1 tsn2* plants.

4.4.3 Role of TSN in the activation of SnRK1

SnRK1 is an evolutionarily conserved kinase that is a central modulator of stress signalling, known as AMPK in animals and Snf1 in yeast (Wurzinger *et al.* 2018 for review). We identified SnRK1α1 and SnRK1α2 as TSN-interactors in SGs upon HS and found that SnRK1α1 is bound to TSN in absence of stress, in agreement with our proteomic data. Upon HS treatment we observed a direct interaction between both SnRK1α1 and SnRK1α2 to

TSN. Since SGs are dynamic structures with many proteins exchanging continuously with a surrounding dilute phase (Mahboubi & Stochaj 2017), we investigated if TSN would affect the mobility of SnRK1α. Using Fluorescence recovery after photobleaching (FRAP) assay we found that in absence of TSN, mobility of SnRK1α1 was compromised (Fig. 10a, b).
This data indicates that (i) TSN2 interacts with both isoforms of SnRK1α under HS and normal conditions, (ii) TSN is important for the full mobility of SnRK1α1.

To link SnRK1 localization to SGs with its regulation under HS we subjected *Arabidopsis* seedlings to HS and measured the level of T175 phosphorylation, a post-translational modification demonstrating SnRK1 activation (Jossier *et al.* 2009). It revealed that both SnRK1 isoforms were rapidly activated under HS (fig 10c, d). Additionally, upon inhibition of SG formation by application of CHX (Kedersha *et al.* 2000) the T175 phosphorylation was abolished (Fig. 10e, f). To correlate this with actual SG localization we carried out a time-course analysis of SnRK1 localization, using confocal microscopy. Both SnRK1 isoforms became visibly associated with SGs after 40 min of HS and increased by 60 min, matching the immunoblot data (Fig. 10g, h). An investigation of SnRK1 activation under HS in the absence of TSN displayed decreased phosphorylation, which was reverted by complementation with TSN2 (Fig. 10i).

Finally, we sought to confirm that the reduced phosphorylation of SnRK1 in TSN-deficient plants also affects the SnRK1-dependent signalling pathway. We performed RT-qPCR of two known targets of the pathway, *DARK INDUCABLE 2 (DIN2)* and *DIN6* (Baena-González *et al.* 2007; Rodrigues *et al.* 2013; Belda-Palazón *et al.* 2020). The expression of both genes was enhanced in the WT under HS but reduced in the mutant lines.
Collectively, our data demonstrate that upon heat-stress: (i) formation of SGs is required for activation of SnRK1, (ii) TSN confers SnRK1 activation and downstream signalling.
Our finding that SnRK1 is an interactor of TSN further establishes the role of TSN as an important factor in plant stress. We show decreased phosphorylation of SnRK1 when SG formation is inhibited as well as in the

tsn1 tsn2 mutant, indicating that the catalytic activity of SnRK1 is regulated by TSN and localization to SGs. SnRK1-signalling is promoted when overexpressing the catalytic domain SnRK1α (Ramon *et al.* 2019). Plausibly its localization to SGs is a mechanism for increasing the concentration of both SnRK1 and its substrates by condensation to ensure enhanced SnRK1 signalling during stress (Lyon *et al.* 2021; Zhang *et al. 2021*. Even though SnRK1 is a well-studied protein across kingdoms, there has been no previous evidence connecting SGs to the activity of SnRK1 homologs. However, another central regulator mTOR has been demonstrated to translocate to SGs under stress in mammals, leading to its inactivation (Heberle *et al.* 2015). In plants mTOR and SnRK1 play antagonistic roles in stress and energy signalling (Baena-González *et al.* 2007; Belda-Palazón *et al.* 2020). During stress, SnRK1 signalling is activated whereas mTOR, which promotes growth and biosynthesis, is inhibited (Baena-González & Hanson 2017; Carroll & Dunlop 2017; Van Leene *et al.* 2019). Since SnRK1 is one of the key regulators of mTOR (Shaw 2009) we speculate as to whether SGs and TSN might regulate the SnRK1-mTOR signalling module, however further studies are required to decipher this relation.

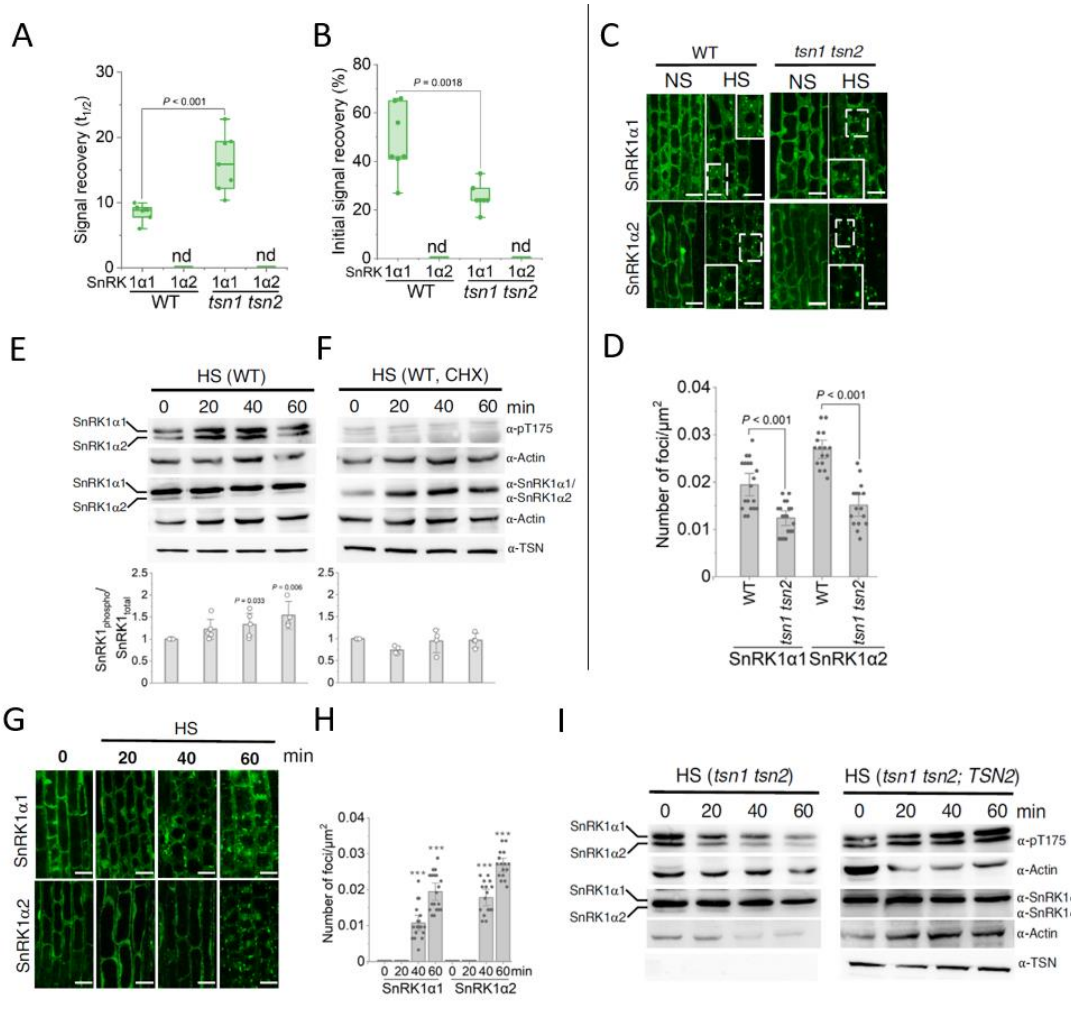

Figure 10. **TSN and SGs are essential for the movement and activation of SnRK1**

A, B. Signal recovery rate ($t_{1/2}$; **A**) and proportion of the initial signal recovered (%; **B**) of GFP-tagged isoforms of SnRK1α of WT and *tsn1 tsn2* HS (60 min at 39°C). nd, not detected. Upper and lower box boundaries represent the first and third quantiles, respectively; horizontal lines mark the median, and whiskers mark the highest and lowest values. **C.** Localization of GFP-SnRK1α1 and GFP-SnRK1α2 in root cells of 5-day-old *Arabidopsis* WT and *tsn1 tsn2* seedlings grown in NS or subjected to 60 min HS. Insets show enlarged areas inside dashed rectangles. Scale bars = 10 μm. **D.** Number of SnRK1α1- and SnRK1α2-foci in root tip cells of WT and *tsn1 tsn2* seedlings after HS. **E, F.** Immunoblot analysis with indicated antibodies of protein extracts of WT heat-

stressed seedlings. 0, 20, 40 and 60 min after the onset of HS. For CHX treatment in **F**, the seedlings were pre-treated with 200 ng/µl CHX for 30 min before HS. The charts show SnRK1 activity, expressed as the ratio of phosphorylated to total SnRK1 protein. **G.** Localization of GFP-SnRK1α1 and GFP-SnRK1α2 in root cells of *Arabidopsis* WT. Scale bars = 10 µm. **H.** Quantification of GFP-SnRK1α1 and GFP-SnRK1α2 foci in the experiment shown in G. **I.** Immunoblot analysis with indicated antibodies of protein extracts from *Arabidopsis tsn1 tsn2* or *tsn1 tsn2* expressing *ProTSN2:GFP-TSN2* in HS seedlings 0, 20, 40 and 60 min after the onset of HS.

5. Conclusions and future perspectives

Autophagy has great potential to improve the resilience of future crops.What is important to note, however, is that the majority of research regarding autophagy have been conducted in a model plant system, *Arabidopsis thaliana.* Fortunately, during the last 10 years, autophagy research in crops has gained more attention (Tang & Bassham 2018). This is important, because even though both crops and Arabidopsis are plants there are many differences, Arabidopsis have for example not been subjected to decades of selection and breeding. This ultimately means that results acquired in Arabidopsis are not necessarily true for all crops. Studies of autophagy in different crop species display valuable effects for agriculture purposes as well as new functions not found in Arabidopsis (Cao *et al.* 2021). The road to agricultural application of autophagy modification is somewhat harder. For example, the use of genetically modified genes is still controversial in parts of the world, mainly Europe. In addition the upregulation of autophagy might also be hazardous to plants, as in the case of plant viruses hijacking the autophagic pathway to suppress the immune response (Kushwaha, *et al.* 2019). A way to circumvent this would be to upregulate autophagy in crops when needed, in a controlled manner.

The area of SGs is relatively new in plant research and there is still much regarding their function that we do not know. From an agricultural perspective, overexpression of proteins essential for SG formation have improved stress resilience, whereas the mutants of the same proteins led to higher stress susceptibility (Nguyen *et al.* 2016; Gutierrez-Beltran *et al.* 2021). Many questions remain, such as what are the implications of the vast functions of SGs? From concentration of RNA and RBP to avoid reactions

with other components of the cytoplasm, to regulation of translation, and as enhancers and inhibitors of enzymatic reactions (Campos-Melo *et al.* 2021; Peeples and Rosen 2021; Marcelo *et al.* 2021). Do different subtypes of SGs in the cytoplasm during a certain stress have different tasks enabled by different scaffolding proteins? What roles do the different scaffolding proteins have under different stress conditions? Additionally, SG research needs to be conducted in crop species along with the ongoing fundamental research in model plant systems to assess the full agricultural potential of upregulating proteins connected to SG formation.

Finally, extreme weather phenomena due to climate change and global warming call for more knowledge of plant stress resilience during multifactorial stress conditions (Zandalinas *et al.* 2021). Future research on autophagy and SGs will need to consider several stress-factors acting simultaneously.

References

Akita K, Takagi T, Kobayashi K *et al.* Ultrastructural characterization of microlipophagy induced by the interaction of vacuoles and lipid bodies around generative and sperm cells in Arabidopsis pollen. *Protoplasma* 2021;**258**:129–38.

Anderson GH, Veit B, Hanson MR. The Arabidopsis AtRaptor genes are essential for post-embryonic plant growth. *BMC Biol* 2005;**3**, DOI: 10.1186/1741-7007-3-12.

Anderson P, Kedersha N. Stress granules: the Tao of RNA triage. *Trends Biochem Sci* 2008;**33**:141–50.

Anderson P, Kedersha N. Stress granules. *Curr Biol* 2009;**19**:397–8.

Araki K, Nagata K. Protein folding and quality control in the ER. *Cold Spring Harb Perspect Biol* 2011;**3**, DOI: 10.1101/cshperspect.a007526.

Arimoto K, Fukuda H, Imajoh-Ohmi S *et al.* Formation of stress granules inhibits apoptosis by suppressing stress-responsive MAPK pathways. *Nat Cell Biol* 2008;**10**:1324–32.

Asai T, Tena G, Plotnikova J *et al.* Map kinase signalling cascade in Arabidopsis innate immunity. *Nature* 2002;**415**:977–83.

Baena-González E, Hanson J. Shaping plant development through the SnRK1–TOR metabolic regulators. *Curr Opin Plant Biol* 2017;**35**:152–7.

Baena-González E, Rolland F, Thevelein JM *et al.* A central integrator of transcription networks in plant stress and energy signalling. *Nature* 2007;**448**:938–42.

Baerga R, Zhang Y, Chen P-H *et al.* Targeted deletion of autophagy-related 5 (atg5) impairs adipogenesis in a cellular model and in mice. *Autophagy* 2009;**5**:1118–30.

Baines K, Yoshioka K, Takuwa Y *et al.* The ATG5 interactome links clathrin-mediated vesicular trafficking with the autophagosome assembly machinery. *Autophagy Reports* 2022;**1**:88–118.

Banani SF, Lee HO, Hyman AA *et al.* Biomolecular condensates: Organizers of cellular biochemistry. *Nat Rev Mol Cell Biol* 2017;**18**:285–98.
Banani SF, Rice AM, Peeples WB *et al.* Compositional Control of Phase-Separated Cellular Bodies. *Cell* 2016;**166**:651–63.
Bao Y, Howell SH. The unfolded protein response supports plant development and defense as well as responses to abiotic stress. *Front Plant Sci* 2017;**8**:344.
Le Bars R, Marion J, Le Borgne R *et al.* ATG5 defines a phagophore domain connected to the endoplasmic reticulum during autophagosome formation in plants. *Nat Commun* 2014;**5**:4121.
Bas L, Papinski D, Licheva M *et al.* Reconstitution reveals Ykt6 as the autophagosomal SNARE in autophagosome–vacuole fusion. *J Cell Biol* 2018;**217**:3656–69.
Belda-Palazón B, Adamo M, Valerio C *et al.* A dual function of SnRK2 kinases in the regulation of SnRK1 and plant growth. *Nat Plants* 2020;**6**:1345–53.
Bernales S, McDonald KL, Walter P. Autophagy Counterbalances Endoplasmic Reticulum Expansion during the Unfolded Protein Response. Ploegh H (ed.). *PLoS Biol* 2006;**4**:e423.
Bounedjah O, Desforges B, Wu T Di *et al.* Free mRNA in excess upon polysome dissociation is a scaffold for protein multimerization to form stress granules. *Nucleic Acids Res* 2014;**42**:8678.
Brangwynne CP, Eckmann CR, Courson DS *et al.* Germline P granules are liquid droplets that localize by controlled dissolution/condensation. *Science (80-)* 2009;**324**:1729–32.
Brillada C, Zheng J, Krüger F *et al.* Phosphoinositides control the localization of HOPS subunit VPS41, which together with VPS33 mediates vacuole fusion in plants. *Proc Natl Acad Sci U S A* 2018;**115**:E8305–14.
Bu F, Yang M, Guo X *et al.* Multiple Functions of ATG8 Family Proteins in Plant Autophagy. *Front Cell Dev Biol* 2020;**8**:466.
Buchan JR, Kolaitis RM, Taylor JP *et al.* Eukaryotic stress granules are cleared by autophagy and Cdc48/VCP function. *Cell* 2013;**153**:1461.
Campos-Melo D, Hawley ZCE, Droppelmann CA *et al.* The Integral Role of RNA in Stress Granule Formation and Function. *Front Cell Dev Biol* 2021;**9**:808.
Cao J, Zheng X, Xie D *et al.* Autophagic pathway contributes to low-nitrogen tolerance by optimizing nitrogen uptake and utilization in tomato. *Hortic Res* 2022;**9**, DOI: 10.1093/hr/uhac068.
Cao JJ, Liu CX, Shao SJ *et al.* Molecular Mechanisms of Autophagy Regulation in Plants and Their Applications in Agriculture. *Front Plant*

Sci 2021;**11**, DOI: 10.3389/fpls.2020.618944.
Carroll B, Dunlop EA. The lysosome: A crucial hub for AMPK and mTORC1 signalling. *Biochem J* 2017;**474**:1453–66.
Castellano MM, Merchante C. Peculiarities of the regulation of translation initiation in plants. *Curr Opin Plant Biol* 2021;**63**:102073.
Celen AB, Sahin U. Sumoylation on its 25th anniversary: mechanisms, pathology, and emerging concepts. *FEBS J* 2020;**287**:3110–40.
Chae E, Tran DTN, Weigel D. Cooperation and Conflict in the Plant Immune System. Zipfel C (ed.). *PLOS Pathog* 2016;**12**:e1005452.
Chantarachot T, Sorenson RS, Hummel M *et al.* DHH1/DDX6-like RNA helicases maintain ephemeral half-lives of stress-response mRNAs. *Nat Plants* 2020;**6**:675–85.
Chen L, Su ZZ, Huang L *et al.* The AMP-activated protein kinase kin10 is involved in the regulation of autophagy in arabidopsis. *Front Plant Sci* 2017;**8**:1201.
Chen Q, Soulay F, Saudemont B *et al.* Overexpression of *ATG8* in Arabidopsis stimulates autophagic activity and increases nitrogen remobilization efficiency and grain filling. *Plant Cell Physiol* 2018, DOI: 10.1093/pcp/pcy214.
Choquer M, Fournier E, Kunz C *et al. Botrytis cinerea* virulence factors: new insights into a necrotrophic and polyphageous pathogen. *FEMS Microbiol Lett* 2007;**277**:1–10.
Citation S. *Managing Global Genetic Resources.*, 1993.
Climate and food crisis in East and Central Africa | Oxfam International.
Codogno P, Meijer AJ. Atg5: more than an autophagy factor. *Nat Cell Biol 2006 810* 2006;**8**:1045–7.
Cui BC, Sikirzhytski V, Aksenova M *et al.* Pharmacological inhibition of DEAD-Box RNA Helicase 3 attenuates stress granule assembly. *Biochem Pharmacol* 2020;**182**, DOI: 10.1016/j.bcp.2020.114280.
Dahlqvist A, Ståhl U, Lenman M *et al.* Phospholipid:diacylglycerol acyltransferase: An enzyme that catalyzes the acyl-CoA-independent formation of triacylglycerol in yeast and plants. *Proc Natl Acad Sci U S A* 2000;**97**:6487–92.
Deng Y, Srivastava R, Quilichini TD *et al.* IRE1, a component of the unfolded protein response signaling pathway, protects pollen development in Arabidopsis from heat stress. *Plant J* 2016;**88**:193–204.
Deprost D, Truong HN, Robaglia C *et al.* An Arabidopsis homolog of RAPTOR/KOG1 is essential for early embryo development. *Biochem Biophys Res Commun* 2005;**326**:844–50.
dit Frey NF, Muller P, Jammes F *et al.* The RNA binding protein tudor-Sn is

essential for stress tolerance and stabilizes levels of stress-responsive mRNAs encoding secreted proteins in Arabidopsis. *Plant Cell* 2010;**22**:1575–91.
Ditlev JA, Case LB, Rosen MK. Who's In and Who's Out—Compositional Control of Biomolecular Condensates. *J Mol Biol* 2018;**430**:4666–84.
Doelling JH, Walker JM, Friedman EM *et al.* The APG8/12-activating enzyme APG7 is required for proper nutrient recycling and senescence in Arabidopsis thaliana. *J Biol Chem* 2002;**277**:33105–14.
Eastmond PJ. SUGAR-DEPENDENT1 encodes a patatin domain triacylglycerol lipase that initiates storage oil breakdown in germinating Arabidopsis seeds. *Plant Cell* 2006;**18**:665–75.
Fan J, Yu L, Xu C. A central role for triacylglycerol in membrane lipid breakdown, fatty acid β-oxidation, and plant survival under extended darkness. *Plant Physiol* 2017;**174**:1517–30.
Fan J, Yu L, Xu C. Dual role for autophagy in lipid metabolismin arabidopsis. *Plant Cell* 2019;**31**:1598–613.
FAO. *The State of Food and Agriculture: Meeting the Needs of the Poor?*, 2004.
Field S, Conner WC, Roberts DM. Arabidopsis CALMODULIN-LIKE 38 Regulates Hypoxia-Induced Autophagy of SUPPRESSOR OF GENE SILENCING 3 Bodies. *Front Plant Sci* 2021;**12**:1872.
Fomicheva A, Ross ED. From prions to stress granules: Defining the compositional features of prion-like domains that promote different types of assemblies. *Int J Mol Sci* 2021;**22**:1–19.
Fones HN, Bebber DP, Chaloner TM *et al.* Threats to global food security from emerging fungal and oomycete crop pathogens. *Nat Food* 2020;**1**:332–42.
Freeman Rosenzweig ES, Xu B, Kuhn Cuellar L *et al.* The Eukaryotic CO2-Concentrating Organelle Is Liquid-like and Exhibits Dynamic Reorganization. *Cell* 2017;**171**:148-162.e19.
Friso G, Van Wijk KJ. Posttranslational protein modifications in plant metabolism. *Plant Physiol* 2015;**169**:1469–87.
Fujioka Y, Alam JM, Noshiro D *et al.* Phase separation organizes the site of autophagosome formation. *Nature* 2020;**578**:301–5.
Fujioka Y, Noda NN, Fujii K *et al.* In vitro reconstitution of plant Atg8 and Atg12 conjugation systems essential for autophagy. *J Biol Chem* 2008;**283**:1921–8.
Fujita N, Itoh T, Omori H *et al.* The Atg16L complex specifies the site of LC3 lipidation for membrane biogenesis in autophagy. *Mol Biol Cell* 2008;**19**:2092–100.
Fujiwara M, Uemura T, Ebine K *et al.* Interactomics of Qa-SNARE in

Arabidopsis thaliana. *Plant Cell Physiol* 2014;**55**:781–9.
Gao C, Zhuang X, Cui Y *et al.* Dual roles of an Arabidopsis ESCRT component FREE1 in regulating vacuolar protein transport and autophagic degradation. *Proc Natl Acad Sci U S A* 2015a;**112**:1886–91.
Gao X, Fu X, Song J *et al.* Poly(A)+ mRNA-binding protein Tudor-SN regulates stress granules aggregation dynamics. *FEBS J* 2015b;**282**:874–90.
Gao X, Ge L, Shao J *et al.* Tudor-SN interacts with and co-localizes with G3BP in stress granules under stress conditions. *FEBS Lett* 2010;**584**:3525–32.
Gilks N, Kedersha N, Ayodele M *et al.* Stress granule assembly is mediated by prion-like aggregation of TIA-1. *Mol Biol Cell* 2004;**15**:5383–98.
Glauninger H, Wong Hickernell CJ, Bard JAM *et al.* Stressful steps: Progress and challenges in understanding stress-induced mRNA condensation and accumulation in stress granules. *Mol Cell* 2022;**82**:2544–56.
Goodman JM. The importance of microlipophagy in liver. *Proc Natl Acad Sci U S A* 2021;**118**:e2024058118.
Gou W, Li X, Guo S *et al.* Autophagy in plant: A new orchestrator in the regulation of the phytohormones homeostasis. *Int J Mol Sci* 2019;**20**, DOI: 10.3390/ijms20122900.
Graef M, Friedman JR, Graham C *et al.* ER exit sites are physical and functional core autophagosome biogenesis components. *Mol Biol Cell* 2013;**24**:2918–31.
Gray SB, Brady SM. Plant developmental responses to climate change. *Dev Biol* 2016;**419**:64–77.
Grouši T, Ivanov P, Frýdlová I *et al.* Robust heat shock induces eIF2α-phosphorylationin-dependent assembly of stress granules containing eIF3 and 40S ribosomal subunits in budding yeast, Saccharomyces cerevisiae. *J Cell Sci* 2009;**122**:2078–88.
Guiboileau A, Yoshimoto K, Soulay F *et al.* Autophagy machinery controls nitrogen remobilization at the whole-plant level under both limiting and ample nitrate conditions in Arabidopsis. *New Phytol* 2012;**194**:732–40.
Guillén-Boixet J, Kopach A, Holehouse AS *et al.* RNA-Induced Conformational Switching and Clustering of G3BP Drive Stress Granule Assembly by Condensation. *Cell* 2020;**181**:346-361.e17.
Gustafsson A. Enheten för handel och marknad. 2019.
Gutierrez-Beltran E, Denisenko T V., Zhivotovsky B *et al.* Tudor staphylococcal nuclease: Biochemistry and functions. *Cell Death Differ* 2016;**23**:1739–48.
Gutierrez-Beltran E, Moschou PN, Smertenko AP *et al.* Tudor

staphylococcal nuclease links formation of stress granules and processing bodies with mRNA catabolism in arabidopsis. *Plant Cell* 2015;**27**:926–43.
Gutierrez-Beltran E, Elander PH, Dalman K *et al.* Tudor staphylococcal nuclease is a docking platform for stress granule components and is essential for SnRK1 activation in Arabidopsis . *EMBO J* 2021;**40**, DOI: 10.15252/embj.2020105043.
Hafrén A, Hofius D. NBR1-mediated antiviral xenophagy in plant immunity. *Autophagy* 2017;**13**:2000–1.
Han D, Yu Z, Lai J *et al.* Post-translational modification: a strategic response to high temperature in plants. *aBIOTECH* 2022;**3**:49–64.
Hanamata S, Sawada J, Bunki T *et al.* Monitoring autophagy in rice tapetal cells during pollen maturation. *Plant Biotechnol* 2019;**36**:99–105.
Hanamata S, Sawada J, Ono S *et al.* Impact of Autophagy on Gene Expression and Tapetal Programmed Cell Death During Pollen Development in Rice. *Front Plant Sci* 2020;**11**, DOI: 10.3389/fpls.2020.00172.
Heberle AM, Prentzell MT, van Eunen K *et al.* Molecular mechanisms of mTOR regulation by stress. *Mol Cell Oncol* 2015;**2**, DOI: 10.4161/23723548.2014.970489.
Hershko A. The ubiquitin system for protein degradation and some of its roles in the control of the cell division cycle. *Cell Death Differ* 2005;**12**:1191–7.
Holehouse AS. IDPs and IDRs in biomolecular condensates. *Intrinsically Disordered Proteins*. Elsevier, 2019, 209–55.
Hong SB, Kim BW, Lee KE *et al.* Insights into noncanonical E1 enzyme activation from the structure of autophagic E1 Atg7 with Atg8. *Nat Struct Mol Biol* 2011;**18**:1323–30.
Ishida H, Makino A. Impacts of autophagy on nitrogen use efficiency in plants. *Soil Sci Plant Nutr* 2018;**64**:100–5.
Jain S, Wheeler JR, Walters RW *et al.* ATPase-Modulated Stress Granules Contain a Diverse Proteome and Substructure. *Cell* 2016;**164**:487–98.
Jefferson M, Bone B, Buck JL *et al.* The Autophagy Protein ATG16L1 Is Required for Sindbis Virus-Induced eIF2α Phosphorylation and Stress Granule Formation. *Viruses* 2019;**12**:39.
Jia M, Liu X, Xue H *et al.* Noncanonical ATG8-ABS3 interaction controls senescence in plants. *Nat plants* 2019;**5**:212–24.
Jossier M, Bouly JP, Meimoun P *et al.* SnRK1 (SNF1-related kinase 1) has a central role in sugar and ABA signalling in Arabidopsis thaliana. *Plant J* 2009;**59**:316–28.
Juli 2018 - Långvarig hetta och svåra skogsbränder | SMHI.

Jumper J, Evans R, Pritzel A *et al.* Highly accurate protein structure prediction with AlphaFold. *Nat 2021 5967873* 2021;**596**:583–9.
Jung H, Lee HN, Marshall RS *et al.* Arabidopsis cargo receptor NBR1 mediates selective autophagy of defective proteins. *J Exp Bot* 2020;**71**:73–89.
Juni 2018 - Svalt och regnigt kring midsommar | SMHI.
Kajikawa M, Yamauchi M, Shinkawa H *et al.* Isolation and Characterization of *Chlamydomonas* Autophagy-Related Mutants in Nutrient-Deficient Conditions. *Plant Cell Physiol* 2019;**60**:126–38.
Karasov TL, Chae E, Herman JJ *et al.* Mechanisms to mitigate the trade-off between growth and defense. *Plant Cell* 2017;**29**:666–80.
Kedersha N, Cho MR, Li W *et al.* Dynamic shuttling of TIA-1 accompanies the recruitment of mRNA to mammalian stress granules. *J Cell Biol* 2000;**151**:1257–68.
Kedersha N, Ivanov P, Anderson P. Stress granules and cell signaling: More than just a passing phase? *Trends Biochem Sci* 2013;**38**:494–506.
Kedersha N, Panas MD, Achorn CA *et al.* G3BP-Caprin1-USP10 complexes mediate stress granule condensation and associate with 40S subunits. *J Cell Biol* 2016;**212**:845–60.
Kelly AA, van Erp H V., Quettier AL *et al.* The SUGAR-DEPENDENT1 lipase limits triacylglycerol accumulation in vegetative tissues of Arabidopsis. *Plant Physiol* 2013;**162**:1282–9.
Ketelaar T, Voss C, Dimmock SA *et al.* Arabidopsis homologues of the autophagy protein Atg8 are a novel family of microtubule binding proteins. *FEBS Lett* 2004;**567**:302–6.
Kim EY, Wang L, Lei Z *et al.* Ribosome stalling and SGS3 phase separation prime the epigenetic silencing of transposons. *Nat Plants* 2021;**7**:303–9.
Kirisako T, Baba M, Ishihara N *et al.* Formation Process of Autophagosome Is Traced with Apg8/Aut7p in Yeast. *J Cell Biol* 1999;**147**:435.
Kosmacz M, Gorka M, Schmidt S *et al.* Protein and metabolite composition of Arabidopsis stress granules. *New Phytol* 2019;**222**:1420–33.
Kurusu T, Koyano T, Hanamata S *et al.* OsATG7 is required for autophagy-dependent lipid metabolism in rice postmeiotic anther development. *Autophagy* 2014;**10**:878–88.
Kushwaha NK, Hafrén A, Hofius D. Autophagy–virus interplay in plants: from antiviral recognition to proviral manipulation. *Mol Plant Pathol* 2019;**20**:1211–6.
Lai LTF, Yu C, Wong JSK *et al.* Subnanometer resolution cryo-EM structure of Arabidopsis thaliana ATG9. *Autophagy* 2020;**16**:575–83.
Lai Z, Wang F, Zheng Z *et al.* A critical role of autophagy in plant resistance

to necrotrophic fungal pathogens. *Plant J* 2011;**66**:953–68.
Van Leene J, Han C, Gadeyne A *et al.* Capturing the phosphorylation and protein interaction landscape of the plant TOR kinase. *Nat Plants* 2019;**5**:316–27.
Lenz HD, Haller E, Melzer E *et al.* Autophagy differentially controls plant basal immunity to biotrophic and necrotrophic pathogens. *Plant J* 2011;**66**:818–30.
Li F, Vierstra RD. Arabidopsis ATG11, a scaffold that links the ATG1-ATG13 kinase complex to general autophagy and selective mitophagy. *Autophagy* 2014;**10**:1466–7.
Li X, Bao H, Wang Z *et al.* Biogenesis and Function of Multivesicular Bodies in Plant Immunity. *Front Plant Sci* 2018;**9**:979.
Lin Y, Protter DSW, Rosen MK *et al.* Formation and Maturation of Phase-Separated Liquid Droplets by RNA-Binding Proteins. *Mol Cell* 2015;**60**:208–19.
Liu Y, Bassham DC, James M *et al.* TOR Is a Negative Regulator of Autophagy in Arabidopsis thaliana. Schumacher K (ed.). *PLoS One* 2010;**5**:e11883.
Liu Y, Burgos JS, Deng Y *et al.* Degradation of the endoplasmic reticulum by autophagy during endoplasmic reticulum stress in Arabidopsisc w. *Plant Cell* 2012;**24**:4635–51.
Liu Y, Schiff M, Czymmek K *et al.* Autophagy regulates programmed cell death during the plant innate immune response. *Cell* 2005;**121**:567–77.
Liu Y, Xiong Y, Bassham DC. Autophagy is required for tolerance of drought and salt stress in plants. *Autophagy* 2009;**5**:954–63.
Lokdarshi A, Craig Conner W, McClintock C *et al.* Arabidopsis CML38, a calcium sensor that localizes to ribonucleoprotein complexes under hypoxia stress. *Plant Physiol* 2016;**170**:1046–59.
Lyon AS, Peeples WB, Rosen MK. A framework for understanding the functions of biomolecular condensates across scales. *Nat Rev Mol Cell Biol* 2021;**22**:215–35.
Mahboubi H, Stochaj U. Cytoplasmic stress granules: Dynamic modulators of cell signaling and disease. *Biochim Biophys Acta - Mol Basis Dis* 2017;**1863**:884–95.
Mahfouz MM, Kim S, Delauney AJ *et al.* Arabidopsis TARGET of RAPAMYCIN interacts with RAPTOR, which regulates the activity of S6 kinase in response to osmotic stress signals. *Plant Cell* 2006;**18**:477–90.
Marcelo A, Koppenol R, de Almeida LP *et al.* Stress granules, RNA-binding proteins and polyglutamine diseases: too much aggregation? *Cell Death Dis* 2021;**12**:1–17.

Markmiller S, Soltanieh S, Server KL *et al.* Context-Dependent and Disease-Specific Diversity in Protein Interactions within Stress Granules. *Cell* 2018;**172**:590-604.e13.
Marshall RS, Li F, Gemperline DC *et al.* Autophagic Degradation of the 26S Proteasome Is Mediated by the Dual ATG8/Ubiquitin Receptor RPN10 in Arabidopsis. *Mol Cell* 2015;**58**:1053–66.
Marshall RS, Vierstra RD. Autophagy: The Master of Bulk and Selective Recycling. *Annu Rev Plant Biol* 2018;**69**:173–208.
Maruri-López I, Figueroa NE, Hernández-Sánchez IE *et al.* Plant Stress Granules: Trends and Beyond. *Front Plant Sci* 2021;**12**:1538.
Matsushita M, Suzuki NN, Obara K *et al.* Structure of Atg5.Atg16, a complex essential for autophagy. *J Biol Chem* 2007;**282**:6763–72.
Minina EA, Bozhkov P V., Hofius D. Autophagy as initiator or executioner of cell death. *Trends Plant Sci* 2014;**19**:692–7.
Minina EA, Moschou PN, Vetukuri RR *et al.* Transcriptional stimulation of rate-limiting components of the autophagic pathway improves plant fitness. *J Exp Bot* 2018;**69**, DOI: 10.1093/jxb/ery010.
Minina EA, Sanchez-Vera V, Moschou PN *et al.* Autophagy mediates caloric restriction-induced lifespan extension in *Arabidopsis*. *Aging Cell* 2013;**12**:327–9.
Mizushima N, Noda T, Yoshimori T *et al.* A protein conjugation system essential for autophagy. *Nature* 1998;**395**:395–8.
Molliex A, Temirov J, Lee J *et al.* Phase Separation by Low Complexity Domains Promotes Stress Granule Assembly and Drives Pathological Fibrillization. *Cell* 2015;**163**:123–33.
Monahan Z, Shewmaker F, Pandey UB. Stress granules at the intersection of autophagy and ALS. *Brain Res* 2016;**1649**:189–200.
Morris GE. The Cajal body. *Biochim Biophys Acta - Mol Cell Res* 2008;**1783**:2108–15.
Mugume Y, Kazibwe Z, Bassham DC. Target of rapamycin in control of autophagy: Puppet master and signal integrator. *Int J Mol Sci* 2020;**21**:1–29.
Nakatogawa H, Ichimura Y, Ohsumi Y. Atg8, a Ubiquitin-like Protein Required for Autophagosome Formation, Mediates Membrane Tethering and Hemifusion. *Cell* 2007;**130**:165–78.
Nguyen CC, Nakaminami K, Matsui A *et al.* Oligouridylate Binding Protein 1b Plays an Integral Role in Plant Heat Stress Tolerance. *Front Plant Sci* 2016;**7**:853.
Noda NN, Satoo K, Fujioka Y *et al.* Structural basis of Atg8 activation by a homodimeric E1, Atg7. *Mol Cell* 2011;**44**:462–75.
Nott TJ, Petsalaki E, Farber P *et al.* Phase Transition of a Disordered Nuage

Protein Generates Environmentally Responsive Membraneless Organelles. *Mol Cell* 2015;**57**:936–47.
Oku M, Maeda Y, Kagohashi Y *et al.* Evidence for ESC RT- and clathrin-dependent microautophagy. *J Cell Biol* 2017;**216**:3263–74.
Oltrogge LM, Chaijarasphong T, Chen AW *et al.* Multivalent interactions between CsoS2 and Rubisco mediate α-carboxysome formation. *Nat Struct Mol Biol* 2020;**27**:281–7.
Omer A, Patel D, Moran JL *et al.* Autophagy and heat-shock response impair stress granule assembly during cellular senescence. *Mech Ageing Dev* 2020;**192**:111382.
Otomo C, Metlagel Z, Takaesu G *et al.* Structure of the human ATG12~ATG5 conjugate required for LC3 lipidation in autophagy. *Nat Struct Mol Biol* 2013;**20**:59–66.
Pais IP, Reboredo FH, Ramalho JC *et al.* Potential impacts of climate change on agriculture-A review. *Emirates J Food Agric* 2020;**32**:397–407.
Parker R, Sheth U. P Bodies and the Control of mRNA Translation and Degradation. *Mol Cell* 2007;**25**:635–46.
Parzych KR, Klionsky DJ. Vacuolar hydrolysis and efflux: current knowledge and unanswered questions. *Autophagy* 2019;**15**:212–27.
Pederson T. The nucleolus. *Cold Spring Harb Perspect Biol* 2011;**3**:1–15.
Peeples W, Rosen MK. Mechanistic dissection of increased enzymatic rate in a phase-separated compartment. *Nat Chem Biol* 2021;**17**:693–702.
Phillips BP, Gomez-Navarro N, Miller EA. Protein quality control in the endoplasmic reticulum. *Curr Opin Cell Biol* 2020;**65**:96–102.
Pingali PL. Green revolution: Impacts, limits, andthe path ahead. *Proc Natl Acad Sci U S A* 2012;**109**:12302–8.
Ploetz RC. Management of Fusarium wilt of banana: A review with special reference to tropical race 4. *Crop Prot* 2015;**73**:7–15.
Powers SK, Holehouse AS, Korasick DA *et al.* Nucleo-cytoplasmic Partitioning of ARF Proteins Controls Auxin Responses in Arabidopsis thaliana. *Mol Cell* 2019;**76**:177-190.e5.
Pu Y, Luo X, Bassham DC. Tor-dependent and -independent pathways regulate autophagy in arabidopsis thaliana. *Front Plant Sci* 2017;**8**:1204.
Qi H, Xia F, Xiao S. Autophagy in plants: Physiological roles and post-translational regulation. *J Integr Plant Biol* 2021;**63**:161–79.
Ramon M, Dang TVT, Broeckx T *et al.* Default Activation and Nuclear Translocation of the Plant Cellular Energy Sensor SnRK1 Regulate Metabolic Stress Responses and Development. *Plant Cell* 2019;**31**:1614–32.
Reuper H, Götte B, Williams L *et al.* Arabidopsis thaliana G3BP Ortholog

Rescues Mammalian Stress Granule Phenotype across Kingdoms. *Int J Mol Sci* 2021;**22**:6287.

Rodrigues A, Adamo M, Crozet P *et al.* ABI1 and PP2CA phosphatases are negative regulators of Snf1-related protein kinase1 signaling in Arabidopsis. *Plant Cell* 2013;**25**:3871–84.

Rubio V, Shen Y, Saijo Y *et al.* An alternative tandem affinity purification strategy applied to Arabidopsis protein complex isolation. *Plant J* 2005;**41**:767–78.

Ruggiano A, Foresti O, Carvalho P. ER-associated degradation: Protein quality control and beyond. *J Cell Biol* 2014;**204**:869–79.

Sahu I, Glickman MH. Proteasome in action: Substrate degradation by the 26S proteasome. *Biochem Soc Trans* 2021;**49**:629–44.

Scheuring D, Viotti C, Krüger F *et al.* Multivesicular Bodies Mature from the *Trans* -Golgi Network/Early Endosome in *Arabidopsis* . *Plant Cell* 2011;**23**:3463–81.

Schwarz V, Andosch A, Geretschläger A *et al.* Carbon starvation induces lipid degradation via autophagy in the model alga Micrasterias. *J Plant Physiol* 2017;**208**:115–27.

Seguin SJ, Morelli FF, Vinet J *et al.* Inhibition of autophagy, lysosome and VCP function impairs stress granule assembly. *Cell Death Differ* 2014;**21**:1838–51.

Seo AY, Lau PW, Feliciano D *et al.* AMPK and vacuole-associated Atg14p orchestrate μ-lipophagy for energy production and long-term survival under glucose starvation. *Elife* 2017;**6**, DOI: 10.7554/eLife.21690.

Shaw RJ. LKB1 and AMP-activated protein kinase control of mTOR signalling and growth. *Acta Physiologica*. Vol 196. Acta Physiol (Oxf), 2009, 65–80.

Shibata M, Oikawa K, Yoshimoto K *et al.* Highly oxidized peroxisomes are selectively degraded via autophagy in Arabidopsis. *Plant Cell* 2013;**25**:4967–83.

Shintani T, Mizushima N, Ogawa Y *et al.* Apg10p, a novel protein-conjugating enzyme essential for autophagy in yeast. *EMBO J* 1999;**18**:5234–41.

Shpilka T, Weidberg H, Pietrokovski S *et al.* Atg8: an autophagy-related ubiquitin-like protein family. *Genome Biol* 2011;**12**:226.

Sieńko K, Poormassalehgoo A, Yamada K *et al.* Microautophagy in Plants: Consideration of Its Molecular Mechanism. *Cells* 2020;**9**, DOI: 10.3390/cells9040887.

Skogsindustrierna. Fortsatt stora mängder granbarkborrar väntas . 2021.

Sonenberg N, Hinnebusch AG. Regulation of Translation Initiation in Eukaryotes: Mechanisms and Biological Targets. *Cell* 2009;**136**:731–

45.
Soto-Burgos J, Bassham DC. SnRK1 activates autophagy via the TOR signaling pathway in Arabidopsis thaliana. *PLoS One* 2017;**12**, DOI: 10.1371/journal.pone.0182591.
Soto-Burgos J, Zhuang X, Jiang L *et al.* Dynamics of Autophagosome Formation. *Plant Physiol* 2018;**176**:219–29.
Stephani M, Dagdas Y. Plant Selective Autophagy—Still an Uncharted Territory With a Lot of Hidden Gems. *J Mol Biol* 2020;**432**:63–79.
Stephani M, Picchianti L, Dagdas Y. C53 is a cross-kingdom conserved reticulophagy receptor that bridges the gap betweenselective autophagy and ribosome stalling at the endoplasmic reticulum. *Autophagy* 2021;**17**:586–7.
Stone SL, Callis J. Ubiquitin ligases mediate growth and development by promoting protein death. *Curr Opin Plant Biol* 2007;**10**:624–32.
Sugawara K, Suzuki NN, Fujioka Y *et al.* The crystal structure of microtubule-associated protein light chain 3, a mammalian homologue of Saccharomyces cerevisiae Atg8. *Genes Cells* 2004;**9**:611–8.
Suttangkakul A, Li F, Chung T *et al.* The ATG1/ATG13 protein kinase complex is both a regulator and a target of autophagic recycling in Arabidopsis. *Plant Cell* 2011;**23**:3761–79.
Suzuki K, Kirisako T, Kamada Y *et al.* The pre-autophagosomal structure organized by concerted functions of APG genes is essential for autophagosome formation. *EMBO J* 2001;**20**:5971–81.
Suzuki NN, Yoshimoto K, Fujioka Y *et al.* The crystal structure of plant ATG12 and its biological implication in autophagy. *Autophagy* 2005;**1**:119–26.
Suzuki SW, Yamamoto H, Oikawa Y *et al.* Atg13 HORMA domain recruits Atg9 vesicles during autophagosome formation. *Proc Natl Acad Sci U S A* 2015;**112**:3350–5.
Svenning S, Lamark T, Krause K *et al.* Plant NBR1 is a selective autophagy substrate and a functional hybrid of the mammalian autophagic adapters NBR1 and p62/SQSTM1. *Autophagy* 2011;**7**:993.
Sveriges matberedskap - LRF.
Taherbhoy AM, Tait SW, Kaiser SE *et al.* Atg8 transfer from Atg7 to Atg3: a distinctive E1-E2 architecture and mechanism in the autophagy pathway. *Mol Cell* 2011;**44**:451–61.
Takahara T, Maeda T. Transient sequestration of TORC1 into stress granules during heat stress. *Mol Cell* 2012;**47**:242–52.
Tang J, Bassham DC. Autophagy in crop plants: What's new beyond Arabidopsis? *Open Biol* 2018;**8**, DOI: 10.1098/rsob.180162.
Tauber D, Tauber G, Parker R. Mechanisms and Regulation of RNA

Condensation in RNP Granule Formation. *Trends Biochem Sci* 2020;**45**:764–78.

Thedieck K, Holzwarth B, Prentzell MT *et al.* Inhibition of mTORC1 by astrin and stress granules prevents apoptosis in cancer cells. *Cell* 2013;**154**:859–74.

Toribio R, Muñoz A, Castro-Sanz AB *et al.* A novel eIF4E-interacting protein that forms non-canonical translation initiation complexes. *Nat Plants* 2019;**5**:1283–96.

Tourrière H, Chebli K, Zekri L *et al.* The RasGAP-associated endoribonuclease G3BP assembles stress granules. *J Cell Biol* 2003;**160**:823–31.

Valente MAS, Faria JAQA, Soares-Ramos JRL *et al.* The ER luminal binding protein (BiP) mediates an increase in drought tolerance in soybean and delays drought-induced leaf senescence in soybean and tobacco. *J Exp Bot* 2009;**60**:533–46.

Varadi M, Anyango S, Deshpande M *et al.* AlphaFold Protein Structure Database: massively expanding the structural coverage of protein-sequence space with high-accuracy models. *Nucleic Acids Res* 2022;**50**:D439–44.

Vevea JD, Garcia EJ, Chan RB *et al.* Role for Lipid Droplet Biogenesis and Microlipophagy in Adaptation to Lipid Imbalance in Yeast. *Dev Cell* 2015;**35**:584–99.

Wada S, Hayashida Y, Izumi M *et al.* Autophagy Supports Biomass Production and Nitrogen Use Efficiency at the Vegetative Stage in Rice. *Plant Physiol* 2015;**168**:60–73.

Wallengren M. The Big Brazil Frost - Global Coffee Report. 2021.

Wang B, Maxwell BA, Joo JH *et al.* ULK1 and ULK2 Regulate Stress Granule Disassembly Through Phosphorylation and Activation of VCP/p97. *Mol Cell* 2019a;**74**:742-757.e8.

Wang H, Yan X, Aigner H *et al.* Rubisco condensate formation by CcmM in β-carboxysome biogenesis. *Nature* 2019b;**566**:131–5.

Wang M, Li X, Luo S *et al.* Coordination and Crosstalk between Autophagosome and Multivesicular Body Pathways in Plant Stress Responses. *Cells* 2020;**9**:119.

Wang P, Sun X, Jia X *et al.* Apple autophagy-related protein MdATG3s afford tolerance to multiple abiotic stresses. *Plant Sci* 2017a;**256**:53–64.

Wang P, Sun X, Wang N *et al.* Ectopic expression of an autophagy-associated MdATG7b gene from apple alters growth and tolerance to nutrient stress in Arabidopsis thaliana. *Plant Cell Tissue Organ Cult* 2017b;**128**:9–23.

Ward C, Martinez-Lopez N, Otten EG *et al.* Autophagy, lipophagy and lysosomal lipid storage disorders. *Biochim Biophys Acta - Mol Cell Biol Lipids* 2016;**1861**:269–84.
Weber C, Nover L, Fauth M. Plant stress granules and mRNA processing bodies are distinct from heat stress granules. *Plant J* 2008;**56**:517–30.
Wickner W. Membrane Fusion: Five Lipids, Four SNAREs, Three Chaperones, Two Nucleotides, and a Rab, All Dancing in a Ring on Yeast Vacuoles. *Annu Rev Cell Dev Biol* 2010;**26**:115–36.
Wright PE, Dyson HJ. Intrinsically disordered proteins in cellular signalling and regulation. *Nat Rev Mol Cell Biol* 2015;**16**:18–29.
Wunder T, Cheng SLH, Lai SK *et al.* The phase separation underlying the pyrenoid-based microalgal Rubisco supercharger. *Nat Commun* 2018;**9**, DOI: 10.1038/s41467-018-07624-w.
Wurzinger B, Nukarinen E, Nägele T *et al.* The snrk1 kinase as central mediator of energy signaling between different organelles. *Plant Physiol* 2018;**176**:1085–94.
Xiong Y, Contento AL, Nguyen PQ *et al.* Degradation of oxidized proteins by autophagy during oxidative stress in arabidopsis. *Plant Physiol* 2007;**143**:291–9.
Yamaguchi M, Satoo K, Suzuki H *et al.* Atg7 Activates an Autophagy-Essential Ubiquitin-like Protein Atg8 through Multi-Step Recognition. *J Mol Biol* 2018;**430**:249–57.
Yamamoto H, Kakuta S, Watanabe TM *et al.* Atg9 vesicles are an important membrane source during early steps of autophagosome formation. *J Cell Biol* 2012;**198**:219.
Yamauchi S, Mano S, Oikawa K *et al.* Autophagy controls reactive oxygen species homeostasis in guard cells that is essential for stomatal opening. *Proc Natl Acad Sci U S A* 2019;**116**:19187–92.
Yan C, Yan Z, Wang Y *et al.* Tudor-SN, a component of stress granules, regulates growth under salt stress by modulating GA20ox3 mRNA levels in Arabidopsis. *J Exp Bot* 2014;**65**:5933–44.
Yang M, Luo S, Wang X *et al.* ER-Phagy: A New Regulator of ER Homeostasis. *Front Cell Dev Biol* 2021;**9**:1692.
Yang P, Mathieu C, Kolaitis RM *et al.* G3BP1 Is a Tunable Switch that Triggers Phase Separation to Assemble Stress Granules. *Cell* 2020;**181**:325-345.e28.
Yoshikawa M, Peragine A, Mee YP *et al.* A pathway for the biogenesis of trans-acting siRNAs in Arabidopsis. *Genes Dev* 2005;**19**:2164–75.
Yoshimoto K, Hanaoka H, Sato S *et al.* Processing of ATG8s, Ubiquitin-Like Proteins, and Their Deconjugation by ATG4s Are Essential for Plant Autophagy. *Plant Cell* 2004;**16**:2967–83.

Yoshimoto K, Jikumaru Y, Kamiya Y *et al.* Autophagy Negatively Regulates Cell Death by Controlling NPR1-Dependent Salicylic Acid Signaling during Senescence and the Innate Immune Response in Arabidopsis. *Plant Cell Online* 2009a;**21**.

Yoshimoto K, Jikumaru Y, Kamiya Y *et al.* Senescence and the Innate Immune Response in Arabidopsis. *Plant Cell Online* 2009b;**21**.

Yu J, Zhen X, Li X *et al.* Increased autophagy of rice can increase yield and nitrogen use efficiency (NUE). *Front Plant Sci* 2019;**10**:584.

Yu ZQ, Ni T, Hong B *et al.* Dual roles of Atg8 - PE deconjugation by Atg4 in autophagy. *Autophagy* 2012;**8**:883–92.

Zandalinas SI, Fritschi FB, Mittler R. Global Warming, Climate Change, and Environmental Pollution: Recipe for a Multifactorial Stress Combination Disaster. *Trends Plant Sci* 2021;**26**:588–99.

Zechner R, Madeo F, Kratky D. Cytosolic lipolysis and lipophagy: two sides of the same coin. 2017, DOI: 10.1038/nrm.2017.76.

Zhang Y, Goldman S, Baerga R *et al.* Adipose-specific deletion of autophagy-related gene 7 (atg7) in mice reveals a role in adipogenesis. *Proc Natl Acad Sci* 2009;**106**:19860–5.

Zhang Y, Narlikar GJ, Kutateladze TG. Enzymatic Reactions inside Biological Condensates. *J Mol Biol* 2021;**433**:166624.

Zhao J, Lu Z, Wang L *et al.* Plant responses to heat stress: Physiology, transcription, noncoding rnas, and epigenetics. *Int J Mol Sci* 2021;**22**:1–14.

Zhao L, Dai J, Wu Q. Autophagy-like processes are involved in lipid droplet degradation in Auxenochlorella protothecoides during the heterotrophy-autotrophy transition. *Front Plant Sci* 2014;**5**:400.

Zhao P, Zhou XM, Zhao LL *et al.* Autophagy-mediated compartmental cytoplasmic deletion is essential for tobacco pollen germination and male fertility. *Autophagy* 2020;**16**:2180–92.

Zhao YG, Codogno P, Zhang H. Machinery, regulation and pathophysiological implications of autophagosome maturation. *Nat Rev Mol Cell Biol* 2021;**22**:733–50.

Zhao Z, Fux B, Goodwin M *et al.* Autophagosome-Independent Essential Function for the Autophagy Protein Atg5 in Cellular Immunity to Intracellular Pathogens. *Cell Host Microbe* 2008;**4**:458–69.

Zhen X, Zheng N, Yu J *et al.* Autophagy mediates grain yield and nitrogen stress resistance by modulating nitrogen remobilization in rice. Shi H (ed.). *PLoS One* 2021;**16**:e0244996.

Zheng Z, Qamar SA, Chen Z *et al.* Arabidopsis WRKY33 transcription factor is required for resistance to necrotrophic fungal pathogens. *Plant J* 2006;**48**:592–605.

Zhigailov A V., Alexandrova AM, Nizkorodova AS *et al.* Evidence That Phosphorylation of the α-Subunit of eIF2 Does Not Essentially Inhibit mRNA Translation in Wheat Germ Cell-Free System. *Front Plant Sci* 2020;**11**:936.

Zhou J, Wang J, Cheng Y *et al.* NBR1-Mediated Selective Autophagy Targets Insoluble Ubiquitinated Protein Aggregates in Plant Stress Responses. Gassmann W (ed.). *PLoS Genet* 2013;**9**:e1003196.

Zhu L, Tatsuke T, Mon H *et al.* Characterization of tudor-sn-containing granules in the silkworm, bombyx mori. *Insect Biochem Mol Biol* 2013;**43**:664–74.

Zhu S, Gu J, Yao J *et al.* Liquid-liquid phase separation of RBGD2/4 is required for heat stress resistance in Arabidopsis. *Dev Cell* 2022;**57**:583-597.e6.

Zhuang X, Chung KP, Cui Y *et al.* ATG9 regulates autophagosome progression from the endoplasmic reticulum in Arabidopsis. *Proc Natl Acad Sci U S A* 2017;**114**:E426–35.

Zhuang X, Chung KP, Luo M *et al.* Autophagosome Biogenesis and the Endoplasmic Reticulum: A Plant Perspective. *Trends Plant Sci* 2018;**23**:677–92.

Zhuang X, Wang H, Lam SK *et al.* A BAR-domain protein SH3P2, which binds to phosphatidylinositol 3-phosphate and ATG8, regulates autophagosome formation in Arabidopsis. *Plant Cell* 2013;**25**:4596–615.

van Zutphen T, Todde V, de Boer R *et al.* Lipid droplet autophagy in the yeast Saccharomyces cerevisiae. *Mol Biol Cell* 2014;**25**:290–301.

Populärvetenskaplig sammanfattning

Växter kan bli stressade, inte för att de måste passa en deadline eller se till att komma i tid för en flygresa, utan för att de är utsatta för en miljöfaktorer som inte är optimala för deras överlevnad. Värme, kyla, insekter, virus, för lite vatten eller alldeles för mycket är bara ett fåtal exempel på faktorer som kan få växter att bli stressade. Det här skulle inte betyda särskilt mycket för oss om det inte vore för att vi är beroende av dem. Vi förlitar oss på dem för mat till oss själva och våra djur, använder dem som byggnadsmaterial och bränsle för att värma våra bostäder. Under de årtusenden som mänskligheten förlitat sig på växter har vi också bevittnat konsekvenserna av växtstress. Förstörda skördar på grund av dåliga väder- och miljö-förhållanden som leder till matbrist, högre matpriser, konflikter, och i värsta fall; svält, sjukdom och död. Beklagligt nog har sådana konsekvenser blivit vanligare och vanligare på grund av klimatförändringar. Växterna vi förlitar oss på, oavsett om det är spannmål eller träd, har blivit förädlade för att passa vissa regionala skillnader i miljöfaktorer. Som exempel är havre som odlas i norra Sverige bättre anpassad för att klara av midnattssol än de sorter som odlas i södra Sverige. Miljöfaktorerna vi har nu till följd av klimatförändringar är däremot långt mycket mer extrema än de regionala skillnader vi haft historiskt sett. Extremväder som plötslig hög värme följt av kraftiga skyfall är exempel på faktorer som våra förädlade växter här i Sverige har liten eller väldigt dålig motståndskraft mot. Därför är det av yttersta vikt att hitta tillvägagångssätt för att förbättra växterna vi odlar för att säkra vår globala matförsörjning.

Växtceller har flertalet strategier för att överleva stress. Till exempel nedbrytning och återvinning via *autofagi* och bildandet av *stressgranuler* som är en ihop-klumpning av molekyler som möjliggör en snabb anpassning

för stress i cellen. Autofagi är till största del, en kontrollerad reaktionsväg som bryter ner cellens beståndsdelar, allt från små molekyler till hela organeller. Materialet som är kvar efter nedbrytning används av cellen för energi eller byggnadsmaterial. När en växt är stressad och behöver göra sig av med delar som hindrar stressresponsen eller behöver material för att bygga nya delar, kan de använda sig utav autofagi. I vår forskning om autofagi har vi sett att mer autofagi resulterar i förbättrad tillväxt och motståndskraft i växter. Växterna sätter fler blad, blommor och frön, lever längre och har bättre immunförsvar mot den nekrotiska svampen *Alternaria brassicicola* som infekterar kålväxter. Efter de här upptäckterna har vi fortsatt att forska på autofagi för att förbättra vår förståelse för reaktionsvägen och studera hur vi kan använda den för att förbättra växters stresstålighet. Ur ett växtförädlingsperspektiv skulle våra upptäckter kunna användas för att förbättra grödors avkastning och stresstålighet.

Stressgranuler är den andra mekanismen i växtcellens stressrespons som berörs i den här avhandlingen En situation av stress får växtceller att ackumulera en hel del material som kan vara skadliga för cellens stressrespons. För att ta hand om det klumpas materialet ihop i en mer eller mindre kontrollerad process. Klumparna kallas stressgranuler. Stressgranulerna ser inte bara till att hålla undan potentiellt skadligt material utan har också kapacitet att möjliggöra reaktioner som annars inte skulle kunna ske. Vår forskning har fokuserat på ett specifikt protein som kallas TSN och dess roll som beståndsdel i stressgranuler. Vi fann att TSN interagerar med ett stort antal andra proteiner som en dockningsstation. När TSN inte existerar i cellen förändras kompostionen av stressgranulen och växtens stressrespons försämras En särskilt intressant observation är att TSNs inverkar på ett utav cellens mest centrala stressproteiner, SnRK1, som reglerar cellens energibalans under stress. När vi utsatte växterna för värme var bildandet av stressgranuler och närvaro av TSN avgörande för aktivering och korrekt funktion av SnRK1. Vi har fortsatt mycket att lära om stressgranuler i växter för att kunna använda dem för att förbättra växters stresstålighet. Däremot har våra upptäckter tillsammans med andra nya framsteg börjat nysta upp den här vitala mekanismen av växters stressrespons. De här kunskaperna har stor betydelse för hur vi ska kunna anpassa växter till att snabbt hantera förändrade miljöbetingelser på grund av klimatförändringar.

Popular science summary

Plants can get stressed, not because they want to fit a deadline or make sure to be in time for a flight, but because they are exposed to a surrounding environment that is not optimal for their lifecycle. Heat, cold, insects, viruses, too little water, and too much water are just a few examples of conditions that induce plant stress. This would be of little interest to us if we were not dependent on them. We rely on plants to feed ourselves, our livestock, use them as building material, and to heat our homes. Since we are dependent on plants, their welfare is also of great importance to us. Historically and now we see the consequences of plant stress, failed harvests leading to food shortages, increased prices, and ultimately starvation and death. Regrettably, such conditions have become more abundant due to climate change. The plants we depend on -being it crops or trees- have been bred to fit the regional diversities of their surroundings. For example, oat varieties in northern Sweden are better at managing the excess light during the summer months compared to varieties grown in southern Sweden. However, what we see now due to climate change is often extreme to the point that our plants have little to no resilience. Therefore it is of utmost importance to find ways for our plants to become more resilient to these conditions, in order to improve our food security. A viable strategy toward this aim is to better understand adaptive stress responses in plants.

Plants have several strategies to survive stress, I will bring you through two of the strategies which take place in a general plant cell. These are degradation or recycling via *autophagy* (self-eating) and how plant cells manage to quickly adapt to stress and change their protein production and activity by forming *stress granules*.

Autophagy is a cellular recycling pathway, which can target all cellular constituents and deliver it for degradation. The degraded material can then be used by the cell. When a plant is stressed and in need to dispose of material that hinders the stress response or in need of building material it can utilize autophagy. In our studies of autophagy, we have found that more autophagy results in better growth and improved stress resilience in plants. The plants set more leaves, flowers, and seeds, lives longer, and are more resistant to the necrotrophic pathogen *Alternaria brassicicola*, a fungus that infects cabbage species. In terms of crop production, autophagy presents a new and exciting target that warrants further investigation. We have since then continued our research in plant autophagy to improve our understanding of the pathway. Our results could be used to improve crop productivity and immunity.

Stress granules are the second stress resilience mechanism which is part of this thesis. A stress event in the cell results in an excess of certain materials which might be harmful to the cellular stress response. To assess that, the material is isolated into a clump called stress granules in a partly controlled manner. The isolation not only keeps material away but also has the capacity to enhance processes within the stress granules which otherwise would rarely occur. We studied a specific protein, called TSN, and its roles as a constituent of stress granules. We found that TSN interacts with a large number of other proteins as a docking platform. When TSN is absent it changes the stress granule arrangement and also the stress response. An interesting find was the impact of TSN on one of the central stress proteins SnRK1, which regulates energy balance in the cell upon stress. In conditions of heat-stress, stress granule formation and the presence of TSN were essential for the activation of SnRK1. We still have a lot to learn about stress granules in plants to utilize them to improve the stress tolerance of crops. However, our findings together with other recent advances in the field have started to unravel this vital plant stress response. This knowledge is of great importance to be able to enhance our plants stress resilience to cope with rapidly changing conditions due to climate change.

Acknowledgements

Doing a PhD has been a very exciting but challenging experience. Being able to engulf myself in science, trying to put the bits and pieces together to understand how mechanisms in plant biology work is amazing. BUT it is also extremely frustrating. For someone who has never run any biology experiments, I can explain it like this: Biology is a bitch. Anything that works one day will probably not work the same way the next day. Sometimes it feels like my PhD has been constant method optimization! To cope with these situations you need to have supporting group members and colleagues around who can share your frustration, joke about it and help you. I have been fortunate to have all of this.

Foremost I would like to thank my main supervisor *Peter* who has supported me and allowed me to venture out from the lab bench to do outreach activities. I found a calling in talking to the general public about science and it made me more curious about science. You also met me with understanding when I told you I needed a break and was going to spend that break in the Swedish Armed Forces, it must have been weird. Thank you for that!

Thanks to my supervisor *Alyona* for sharing your amazing expertise in plant science, your curiosity and determination to understand is inspiring. You have challenged me by questioning my ideas and taught me to foresee consequences and think at least one step ahead.

Thanks to current and previous lab members: *Sanjana* for being my fellow PhD student and friend whom I can confide in and discuss research with, you are an amazing person. *Adrian* for always being there to support, chat and help out in the lab (and special thanks for helping me with the amazing cover image for the thesis!). *Anna* and *Kerstin* for pep-talk, deep conversations and research discussions. *Florentine* and *Igor* for good chats over lunch and coffee as well as research inputs. *Glenn, Yong, Emilio* and *Panos* for helping

out and bringing new ideas to the table. *Jonas*, you haven´t been part of our group but in periods it really felt like it. Thanks for adding to the crazy ideas!

Thanks to the following colleagues for making my days brighter with conversations on day-to-day matters, TV-shows, politics, research and gossip: *Laura O, Mikolaj, Giselle, Ani, Yasha, Thomas E, Anja, Klara, Solja, Anis, Jerry, Johanna, Topi, Nils, Simon, Mathilde, Volkmar, Naike, Piera, Simon, Xue, Tomas L, Hernán, Hasi, Sabine, Mats, Robert, Frida W, Fredric, Hanna, Monika, Saeid, Chen* and *Su-Lin.*

Thanks to the following previous employees of plant biology department at SLU who inspired me to pursue a PhD: *Rita, Clément, Rocky, Duarte, Minerva and Matthew.*

Thanks also to all my other friends living in Sweden and the rest of the world, for your support and curious questions.

Finally, thanks to my family and relatives who have supported me even though you hardly understand what I have been doing research on ("something with molecular biology, or is it microbiology?").
Firstly and foremost my life partner, my beloved husband *Tomas*, you have loved and comforted me through my frustration and hardships and I am most grateful. Special thanks to my siblings *Elisabeth* and *Johan*, my loving parents *Per* and *Gunilla*, my grandmother *Evy* and my uncle *Tord*. The weekends and holidays spent having coffee, dinner, picking mushrooms, fishing, horseback riding, skiing and waterskiing is what I value most for recreation. My family have from time to time also been the harshest of critics, I cannot count how many times I have heard:
"BUT you are a BIOLOGIST you should know!"

I´m now expecting the following: "BUT you are a DOCTOR you should know"! <3

I

Journal of Experimental Botany, Vol. 69, No. 6 pp. 1415–1432, 2018
doi:10.1093/jxb/ery010 Advance Access publication 20 January 2018
This paper is available online free of all access charges (see http://jxb.oxfordjournals.org/open_access.html for further details)

RESEARCH PAPER

Transcriptional stimulation of rate-limiting components of the autophagic pathway improves plant fitness

Elena A. Minina[1,*], Panagiotis N. Moschou[2,†], Ramesh R. Vetukuri[2,3,†], Victoria Sanchez-Vera[2,†], Catarina Cardoso[1,†], Qinsong Liu[2,†], Pernilla H. Elander[1], Kerstin Dalman[1], Mirela Beganovic[4], Jenny Lindberg Yilmaz[5], Sofia Marmon[4], Lana Shabala[6], Maria F. Suarez[7], Karin Ljung[8], Ondřej Novák[9,10], Sergey Shabala[6], Sten Stymne[4], Daniel Hofius[2] and Peter V. Bozhkov[1,*]

[1] Department of Molecular Sciences, Uppsala BioCenter, Swedish University of Agricultural Sciences and Linnean Center for Plant Biology, PO Box 7015, SE-75007 Uppsala, Sweden
[2] Department of Plant Biology, Uppsala BioCenter, Swedish University of Agricultural Sciences and Linnean Center for Plant Biology, PO Box 7080, SE-75007 Uppsala, Sweden
[3] Department of Plant Protection Biology, Swedish University of Agricultural Sciences, PO Box 102, SE-230 53 Alnarp, Sweden
[4] Department of Plant Breeding, Swedish University of Agricultural Sciences, PO Box 101, SE-230 53 Alnarp, Sweden
[5] ScanBiRes AB, PO Box 158, SE-230 53 Alnarp, Sweden
[6] School of Land and Food, University of Tasmania, Private Bag 54, Hobart, TAS, 7001, Australia
[7] Departamento de Biologia Molecular y Bioquimica, Facultad de Ciencias, Universidad de Malaga, Campus de Teatinos, 290071 Malaga, Spain
[8] Umeå Plant Science Centre, Department of Forest Genetics and Plant Physiology, Swedish University of Agricultural Sciences, SE-901 83 Umea, Sweden
[9] Laboratory of Growth Regulators, Centre of the Region Haná for Biotechnological and Agricultural Research, Institute of Experimental Botany Academy of Sciences of the Czech Republic (AS CR), CZ-78371 Olomouc, Czech Republic
[10] Faculty of Science, Palacký University, CZ-78371 Olomouc, Czech Republic

[†] These authors contributed equally to this work.
* Correspondence: alena.minina@slu.se and peter.bozhkov@slu.se

Received 12 September 2017; Editorial decision 14 December 2017; Accepted 14 December 2017

Editor: Christine Raines, University of Essex, UK

Abstract

Autophagy is a major catabolic process whereby autophagosomes deliver cytoplasmic content to the lytic compartment for recycling. Autophagosome formation requires two ubiquitin-like systems conjugating Atg12 with Atg5, and Atg8 with lipid phosphatidylethanolamine (PE), respectively. Genetic suppression of these systems causes autophagy-deficient phenotypes with reduced fitness and longevity. We show that Atg5 and the E1-like enzyme, Atg7, are rate-limiting components of Atg8–PE conjugation in Arabidopsis. Overexpression of *ATG5* or *ATG7* stimulates Atg8 lipidation, autophagosome formation, and autophagic flux. It also induces transcriptional changes opposite to those observed in *atg5* and *atg7* mutants, favoring stress resistance and growth. As a result, *ATG5*- or *ATG7*-overexpressing plants exhibit increased resistance to necrotrophic pathogens and oxidative stress, delayed aging and enhanced growth, seed set, and seed oil content. This work provides an experimental paradigm and mechanistic insight into genetic stimulation of autophagy *in planta* and shows its efficiency for improving plant productivity.

Keywords: Aging, *ATG* genes, autophagy, autophagy-related ubiquitin-like conjugation systems, biomass, oil content, rate-limiting components of autophagic flux, seed yield, stress resistance, transcriptional regulation.

Abbreviations: ATG, autophagy-related gene; Atg, autophagy-related protein; ConA, concanamycin A; DAF, days after the first flower opened; DEG, differentially expressed gene; MV, methyl viologen; NBR1, neighbor of BRCA1; PAS, phagophore assembly site or pre-autophagosomal structure; PE, phosphatidylethanolamine; ROS, reactive oxygen species; WT, wild type.

© The Author(s) 2018. Published by Oxford University Press on behalf of the Society for Experimental Biology.
This is an Open Access article distributed under the terms of the Creative Commons Attribution License (http://creativecommons.org/licenses/by/4.0/), which permits unrestricted reuse, distribution, and reproduction in any medium, provided the original work is properly cited.

Introduction

Homeostasis of all biological systems relies on the continuous renewal of individual subunits. The turnover of cellular components ensures the replacement of old or damaged macromolecules and organelles by new ones. Autophagy is a major catabolic process in eukaryotic cells, able to degrade not only proteins and protein complexes but also entire organelles. Upon induction of autophagy, autophagic cargo is sequestered into double membrane vesicles, autophagosomes, and digested following fusion of autophagosomes with lysosomes or lytic vacuoles (Mizushima and Komatsu, 2011; Klionsky *et al.*, 2016). The dynamic process of autophagosome formation, delivery of autophagic cargo to the lysosome or vacuole, and degradation defines autophagic flux, which can be measured experimentally by a number of dedicated assays.

Autophagy plays a paramount role in eukaryotic life as a key process maintaining proteostasis, conferring stress tolerance, and suppressing aging (Levine *et al.*, 2011; Mizushima and Komatsu, 2011; Rubinsztein *et al.*, 2011). Under favorable conditions, a low level of autophagic flux serves housekeeping functions by clearing obsolete cytoplasmic content. During periods of stress or starvation, autophagic flux is enhanced to promote cell survival by recycling damaged proteins and organelles and thereby reallocate energy and building blocks for the biosynthetic processes (Rabinowitz and White, 2010; Mathew and White, 2011).

Autophagy-related (*ATG*) genes were first discovered in budding yeast and later shown to be conserved in almost all eukaryotes (Yang and Klionsky, 2010). To date, >35 *ATG* genes are functionally characterized in yeast, and most of them have close homologs in plants (Liu and Bassham, 2012; Shibutani and Yoshimori, 2014). Understanding the role of autophagy in plant biology was largely facilitated by the use of *ATG*-knockout (*atg*) mutants of *Arabidopsis thaliana*. At the cellular level, autophagy in plants participates in a whole array of vital processes, such as starch degradation (Wang *et al.*, 2013), chloroplast recycling (Xie *et al.*, 2015), elimination of oxidized proteins (Xiong *et al.*, 2007) and peroxisomes (Shibata *et al.*, 2013), salicylic acid signaling (Yoshimoto *et al.*, 2009), cytoprotection against necrosis (Minina *et al.*, 2013*a*), and both initiation and execution of programmed cell death (Minina *et al.*, 2014). At the whole-plant level, these cellular functions of autophagy jointly contribute to an efficient nutrient remobilization (Guiboileau *et al.*, 2012; Guiboileau *et al.*, 2013), stress tolerance (Zhou *et al.*, 2013, 2014), control of senescence (Yoshimoto *et al.*, 2009), disease resistance (Hofius *et al.*, 2009; Lai *et al.*, 2011), and longevity (Minina *et al.*, 2013*b*). Accordingly, decreased autophagic flux in Arabidopsis *atg* mutants correlates with the overall reduction in plant fitness, including reduced growth and fecundity, accelerated senescence, as well as high susceptibility to nutrient starvation, other types of abiotic stresses, and necrotrophic pathogens.

The above findings unequivocally illustrate the importance of preventing a decline in the autophagic flux to minimize the impact on growth and stress sensitivity. The question is whether one can achieve an opposite, invigorating effect on plants by increasing autophagic flux. We have previously shown that autophagy can be enhanced in wild-type (WT) Arabidopsis plants by moderately reducing light intensity, conditions that mimic an effect of caloric restriction in animals (Rubinsztein *et al.*, 2011), resulting in suppression of senescence and extension of life span (Minina *et al.*, 2013*b*). Recent studies using budding yeast and animal models have uncovered transcriptional and epigenetic regulation of *ATG* genes as essential mechanisms modulating the autophagic response and maintaining homeostasis necessary for stress tolerance and longevity (Feng *et al.*, 2015; Lapierre *et al.*, 2015). Notably, genes encoding the components of two ubiquitin-like conjugation systems (*ATG3*, *ATG5*, *ATG7*, *ATG8*, *ATG10*, *ATG12*, and *ATG16*) operating to form Atg12–Atg5 and Atg8–phosphatidylethanolamine (PE) conjugates (Fig. 1A; Chen and Klionsky, 2011) are among the most frequently found targets of transcription factors, miRNAs, and chromatin-modifying enzymes (Frankel and Lund, 2012; Füllgrabe *et al.*, 2016). Previous works, including the two most recent phenotypic studies, indicated that ectopic expression of the components of the two autophagy-related conjugation systems have beneficial effects on plant growth and stress tolerance (Slavikova *et al.*, 2008; Xia *et al.*, 2012; Wang *et al.*, 2016, 2017). Although these studies did not provide a mechanistic link between expression of certain *ATG* genes and the regulation of autophagic flux, they suggest that transcriptional activation of the components of the Atg12–Atg5 and Atg8–PE conjugation systems might be the 'bottleneck' during autophagy induction.

In the present work, we found that constitutive overexpression of *ATG5* or *ATG7* in Arabidopsis enhances the activity of the two conjugation systems, autophagosome formation and autophagic flux, leading to suppression of aging and strong stimulation of growth and stress resistance. To provide the first insight into the possible molecular mechanisms underlying the phenotypic differences of plants with enhanced and suppressed autophagy, we performed global gene expression analysis, which revealed key transcriptional trends associated with up-regulated or impaired autophagy.

Materials and methods

Plant material

We used the previously described T-DNA knockout lines *atg5-1* (Thompson *et al.*, 2005) and *atg7-2* (Hofius *et al.*, 2009) referred to here as *atg5* and *atg7*, respectively. For generation of overexpression lines, cDNA of *ATG5* and coding DNA sequence of *ATG7* were amplified using primers attB1-ATG5UTR-Fw/attB2-ATG5-Rev and FWatg7/RVatg7, respectively (see Supplementary Table S5 at *JXB* online). The PCR products were recombined under the control of the 35S promoter into the pGWB2 vector (Nakagawa *et al.*, 2007) (GenBank accession no. AB289765.1) using the Gateway cloning system (Invitrogen). pGWB2 constructs were used for transformation of *Agrobacterium tumefaciens* strain GV3101. WT Arabidopsis plants of the Col-0 ecotype were transformed using the floral dip method (Clough and Bent, 1998). Transgenic plants were selected on Murashige and Skoog (MS) medium containing 50 µg ml^{-1}

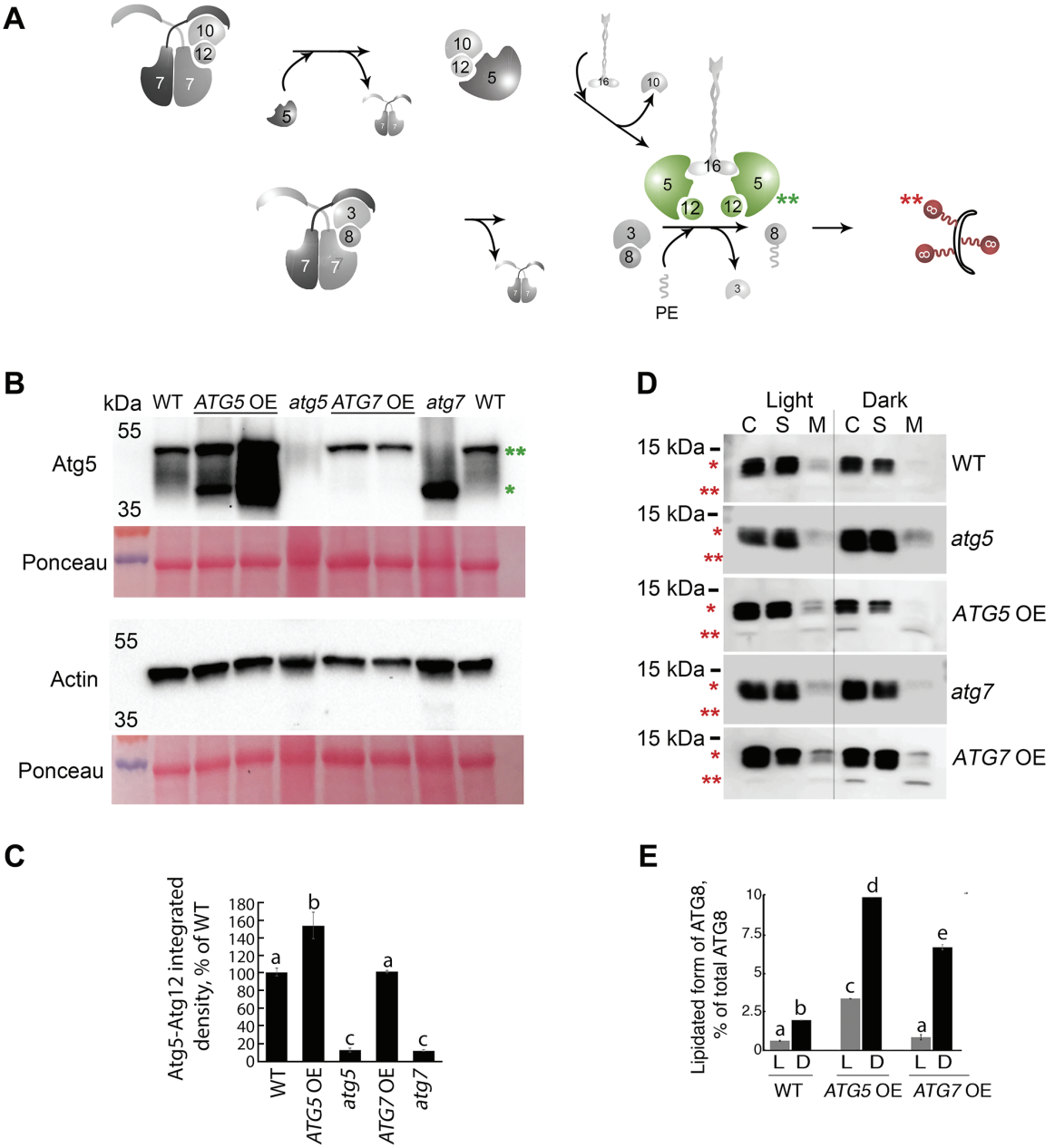

Fig. 1. Constitutive overexpression of *ATG5* or *ATG7* in Arabidopsis stimulates lipidation of Atg8. (A) A schematic representation of two autophagy-related ubiquitin-like conjugation systems (Nakatogawa, 2013). Atg7 acts as an E1-like ligase by stimulating conjugation of two substrate pairs: of a ubiquitin-like protein Atg12 with its E2-like ligase, Atg10, and of a ubiquitin-like protein Atg8 with its E2-like ligase, Atg3. Atg12 is further transferred from Atg10 onto Atg5 protein in an E3-ligase-independent manner. The Atg12–Atg5 conjugate forms a complex with Atg16 and gains an E3-like ligase activity. Atg12–Atg5–Atg16 E3-like ligase stimulates conjugation of Atg8 with a phosphatidylethanolamine (PE), followed by anchoring of Atg8–PE on a membrane of a growing phagophore. Double green and double red asterisks indicate Atg12–Atg5 and Atg8–PE conjugates, respectively, also shown on the western blots on (B) and (D). (B) Atg5, but not Atg7, is a limiting component in the Atg12–Atg5 conjugation pathway. Western blot detection of Atg5 in rosette leaves of Col-0 (WT), two individual *ATG5*- or *ATG7*-overexpressing lines (*ATG5* OE or *ATG7* OE, respectively), and *ATG5*- or *ATG7*-knockout (*atg5* or *atg7*, respectively) mutants. *Atg5; **Atg12–Atg5 conjugate. The experiment was repeated four times, using three individual lines of each overexpressor background. Western blot detection of actin and Ponceau staining were used as loading controls. (C) Densitometry of the Atg5–Atg12 conjugate in (B). Integrated density of bands corresponding to the Atg5–Atg12 conjugate were first normalized to the corresponding values for actin and then expressed as a percentage of the obtained value for the WT. Data represent means ±SE; n=6. Mean values denoted by the same letter do not differ significantly at P<0.001 (Student's t-test). (D) Up-regulation of either *ATG5* or *ATG7* stimulates lipidation of Atg8. Seven-day-old seedlings of Col-0 (WT), *atg5*, *ATG5* OE, *atg7*, and *ATG7* OE genotypes were incubated for 3 d under 150 μE m^{-2} s^{-1} light, 16 h photoperiod (Light) or in the darkness (Dark). Total proteins were fractionated by ultracentrifugation and used for western blot analysis to detect free (*) and lipidated (**) forms of Atg8. C, crude extract; S, supernatant of 100 000 *g* fraction; M, pellet of 100 000 *g* fraction, containing membranes. (E) Densitometry of the Atg8–PE conjugate in (D). Integrated density of bands corresponding to the Atg8–PE in the crude fraction was expressed as a percentage of the integrated density of the total amount of Atg8 in the corresponding sample. Data represent means ±SE; n=6. Mean values denoted by the same letter do not differ significantly at P<0.001 (Student's t-test). L, light; D, dark.

kanamycin. Seeds of the homozygous T_3 generation were used for further experiments.

WT, *ATG5*- or *ATG7*-overexpressing (*ATG5* OE or *ATG7* OE), *atg5*, and *atg7* plants were crossed with a green fluorescent protein (GFP)–Atg8a-expressing line kindly provided by R. Vierstra (Thompson *et al.*, 2005). Crosses were brought to the F_4 generation to establish homozygous knockout and *ATG*-overexpressing backgrounds, and checked with qPCR to ensure lack of somatic silencing.

The homozygous T_3 generation of *ATG5* OE and *ATG7* OE lines were reciprocally crossed to obtain *ATG5*/*ATG7* OE lines. The F_2 generation of the double overexpressors was used for further experiments. Individual plants were genotyped in each experiment to confirm the presence of both transgenes.

Plant growth conditions

Seeds were dried at 37 °C for 48 h, treated at –20 °C overnight, surface-sterilized in 10–15% bleach for 10–30 min, and rinsed in sterile deionized water. Sterilized seeds were placed on half-strength MS medium (M0222, Duchefa), supplemented with 1% (w/v) sucrose, 10 mM MES (pH 5.8), and 0.6% (w/v) plant agar (P1001, Duchefa), and vernalized at 4 °C for 48 h. Germination was carried out in growth rooms at 16 h/8 h light/dark cycles, light intensity 110 µE m^{-2} s^{-1}, and 22 °C/20 °C day/night temperature. Seedlings with four rosette leaves were transferred into individual 8 cm^3 pots filled with soil S-Jord (Hasselfors) and grown in controlled-environment cabinets (Percival AR- 41L2, CLF Plant Climatics) at 16 h/8 h light/dark cycles, at 65% relative humidity, 22 °C/20 °C day/night temperature, and light intensity 150 µE m^{-2} s^{-1} at the level of the leaf rosette. Plants were regularly watered with tap water.

Western blotting

Lipidation of Atg8 was assessed as previously described (Chung *et al.*, 2010). Atg8a was detected using an antibody kindly provided by Y. Ohsumi (Yoshimoto *et al.*, 2004). For NBR1 (neighbor of BRCA1) detection, 100 mg of the sampled plant material was mixed with 100 µl of urea extraction buffer (4 M urea, 100 mM DTT, 1% Triton X-100) and incubated on ice for 10 min. Samples were boiled in two vols of 2× Laemmli sample buffer (Laemmli, 1970) for 10 min and centrifuged in a table centrifuge at 13 000 rpm for 15 min. Equal amounts of supernatants were loaded on a pre-cast 4–20% polyacrylamide gel (Bio-Rad) and blotted onto a polyvinylidene difluoride (PVDF) membrane. Membranes were cut horizontally at the level corresponding to ~55 kDa. The top part of a membrane containing proteins with a mol. wt >55 kDa was used for blotting with anti-NBR1 1:2000 [kindly provided by T. Johansen (Svenning *et al.*, 2011)] and the lower part of the membrane containing proteins <55 kDa was blotted with anti-actin 1:2000 (AS13 2640, Agrisera). The reaction was developed using an ECL Prime kit (RPN2232, Amersham, GE Healthcare) and detected in Chemidoc XRS+ (Bio-Rad). Several exposures were selected for different samples to avoid quantification of saturated signal. Comparisons of absolute integrated density values for each line were made using the same exposure. First, for each exposure, corresponding background values were subtracted from integrated density values of the protein bands. Then the integrated density values for bands corresponding to NBR1 protein were normalized to the respective values of actin for the same sample. Finally, obtained values were expressed as relative values, namely as the percentage of 0 days after the first flower opened (DAF) for each line. For each line, normalized values for NBR1 protein at 0 DAF were assigned as 100% and values for 10 DAF were recalculated as a percentage of it. All images were quantified using ImageJ software.

For GFP–Atg8 cleavage assay, sterilized seeds were sown on 50 µm nylon mesh placed on the top of half-strength MS medium, supplemented with 1% (w/v) sucrose, 10 mM MES (pH 5.8), and 0.6% (w/v) plant agar, and vernalized at 4 °C for 48 h. All genotypes were represented on each plate; four plates were used in each experiment. Plates were incubated vertically in a growth cabinet (Sanyo) at 16 h/8 h light/dark cycles, light intensity 120 µE m^{-2} s^{-1}, and 21 °C/20 °C day/night temperature for 7 d. To induce starvation, meshes with seedlings from half of the plates were transferred to half-strength MS medium without sucrose, and plates were wrapped in metal foil and incubated under the same conditions for a further 4 d. Seedling of the same genotype grown under the same conditions were pooled together, ground in liquid nitrogen, boiled in 2 vols of 2× Laemmli sample buffer (Laemmli, 1970) for 10 min, and centrifuged in a table-top centrifuge at 13 000 rpm for 15 min. Equal amounts of supernatants were loaded on a pre-cast 4–20% polyacrylamide gel (Bio-Rad), blotted on a PVDF membrane, and stained with anti-GFP (632381, Clontech). The reaction was developed using the ECL Prime kit and detected using Chemidoc XRS+ (Bio-Rad). Several exposures were selected for different samples to avoid quantification of saturated signal. Comparisons of absolute integrated density values for each line were made using the same exposure. For each exposure, corresponding background values were subtracted from integrated density values, then integrated density values for bands corresponding to free GFP were expressed as relative values, namely as a percentage of total GFP present in the same sample. For each line, a sum of values for free GFP and GFP–ATG8a was assigned as 100% and values for free GFP were recalculated as a percentage of it. All images were quantified using ImageJ software.

For Atg5 detection, plant material was ground in liquid nitrogen, mixed with 2 vols of 2× Laemmli buffer, and boiled for 10 min. Debris was pelleted for 5 min at 17 000 *g*. Proteins were separated on a 10% polyacrylamide gel, transferred onto PVDF membranes, and blotted with anti-Atg5 1:1000 [kindly provided by R. Vierstra (Thompson *et al.*, 2005)] or anti-actin 1:2000 (AS13 2640, Agrisera). Detection of Atg5 and actin was performed on two separate membranes due to the similarity in molecular weight of the proteins of interest. The reaction was developed using the ECL Prime kit and detected using LAS-3000 (Fujifilm). All membranes were additionally stained in Ponceau to visualize the total protein concentration in the samples.

Plant growth analysis

Plant growth analysis was performed according to the previously described procedure (Minina *et al.*, 2013*b*). Values outside the range of ± double the SD were considered outliers and were excluded from the statistical analysis. Each growth trial included WT, *ATG5* OE or *ATG7* OE lines, *atg5* or *atg7* mutants, and sometimes the corresponding complementation lines, with 20–40 plants per genotype, and was repeated twice, every time in a different growth cabinet. Plants of different genotypes were randomly distributed in the growth cabinets. For estimating seed set, seeds were harvested from 6–11 individual plants per genotype using an ARACON device (Arasystem), sieved, and weighed on ultra-balances. For life span determination, plants were considered dead at the stage after rosettes underwent senescence and degradation, and new inflorescences, leaves, flowers, or flower buds were no longer emerging, indicating cessation of cell division in the shoot apical meristem.

Microscopy

Six-day-old seedlings grown on half-strength MS medium, supplemented with 1% (w/v) sucrose, 10 mM MES (pH 5.8), and 0.6% (w/v) plant agar were transferred into liquid half-strength MS medium containing 0.5 µM concanamycin A (ConA; C9705, Sigma), briefly vacuum infiltrated, and left under light for 16 h before imaging.

Root epidermal cells of the elongation zone were imaged using an LSM 780 confocal microscope (Carl Zeiss), 488 nm argon laser, and ×63 objective (NA1.2, water immersion). One to three cells per root and 4–7 roots per genotype were imaged for the analysis.

The images were processed using ImageJ 1.51g (Fiji) to measure the number and area of GFP puncta in the cell vacuoles. The mean number of GFP–Atg8 puncta per cell of each genotype was compared with that of Col-0 by performing a Dunnett's test and assuming a Poisson distribution of the data ('Multcomp' R package; Hothorn *et al.*, 2008). The mean areas of the puncta per genotype were compared using the Wilcoxon rank sum test with continuity correction in R.

Pathogen infections

For necrotrophic fungal infection, *Alternaria brassicicola* strain MUCL20297 was cultured on potato dextrose agar plates for 2 weeks at 22 °C. Spores were harvested in water and filtered through Miracloth (EM475855-1R, VWR) to remove hyphae. The spore suspension was adjusted to the final concentration of 5×10^5 spores ml^{-1} supplemented with 0.05% Tween-20. *Alternaria brassicicola* inoculation of 3-week-old plants was performed by adding 10 µl drops of spore suspension onto the upper leaf surface as described previously (Thomma *et al.*, 1998). Plants were maintained under saturating humidity for 1 d prior to pathogen inoculation and 2 d post-inoculation. Leaf samples for fungal quantification were collected 7 d post-inoculation, snap-frozen in liquid nitrogen, and stored at –70 °C prior to DNA extraction. Total DNA was extracted from frozen leaf samples using the GeneJET Plant Genomic DNA Purification Kit (K0791, Thermo Fisher Scientific) following the manufacturer's protocol. Fungal DNA quantification of three independent biological replicates was carried out by quantitative real-time (qRT)-PCR using the iQ5 qPCR System (Bio-Rad) to detect fungal *cutinase* (GI 416217) and Arabidopsis *UBQ5* (AT3G62250) and *PR2* (AT3G57260) genes with corresponding primer pairs listed in Supplementary Table S5.

Oxidative stress and chlorophyll measurement

Seeds were sown on half-strength MS medium as described above, with or without addition of 0.1 µM methyl viologen (MV; 856177, Sigma) and grown in vertically positioned plates. For each genotype, several seedlings were pooled into three groups representing biological replicates. Pooled seedlings were weighed and incubated in 80% acetone overnight at 4 °C in the darkness. A 150 µl aliquot of each chlorophyll extract was used to measure absorbance at 647 nm and 665 nm. Chlorophyll content was estimated as described previously (Inskeep and Bloom, 1985) and normalized to the fresh weight of the corresponding sample.

Rosette leaf number and cell size measurements

Seeds were dried at 37 °C for 48 h, treated at –20 °C overnight, surface-sterilized in 10–15% bleach for 10–30 min, and rinsed in sterile deionized water. Sterilized seeds were sown directly into soil and grown in controlled environment rooms at 16 h/8 h light/dark cycles, 22 °C/20 °C day/night temperature, and light intensity 150 µE m^{-2} s^{-1} at the level of the leaf rosette. Three individual lines overexpressing *ATG5* or *ATG7* were used for the analysis to exclude possible insert position effects. At least four biological replicates were used for each genotype. All genotypes were represented in each tray and placed at random positions. Plants were regularly watered with tap water and imaged every 2–3 d.

Most bottom rosette leaves were sampled at 20 DAF to ensure full expansion of the leaf blade. Leaf samples were treated as described previously (Wuyts *et al.*, 2010). Leaf blade areas closest to petioles were imaged from the abaxial side using Axioplan A1 (Carl Zeiss) and ZEN lite software. For area measurement, individual epidermal cells were selected using the freehand selection tool of ImageJ software and a touchscreen. Eight to 10 cells per image, at least three images per plant, and three plants per genotype were analyzed.

Transcriptome profiling

Plants were grown at 16 h/8 h light/dark cycles, 120 µE m^{-2} s^{-1} light intensity, and 22 °C in individual pots. All genotypes were represented in each tray and were placed at random positions. Complete rosettes were sampled at the budding stage and 10 DAF. Four biological replicates were pooled together for each genotype. The material was stored at –80 °C prior to RNA extraction.

RNA was extracted from the material ground in liquid nitrogen using a Spectrum Plant total RNA kit (STRN250, Sigma) and treated with Turbo DNase (AM2238, ThermoFisher). Quality and concentration of RNA were analyzed with NanoDrop and BioAnalyzer. Samples with an RNA integrity number (RIN) >6 were used for further analysis. The expression level of *ATG5* and *ATG7* was verified for all samples by qRT-PCR analysis (data not shown).

The gene expression assay was done on an Agilent 8 × 60 K ArrayXS, and primary normalization and quality control of data were performed at OakLabs, Germany (for more information, see Supplementary file S1). Common trends in changes of transcriptional profiles for both *ATG5* OE and *ATG7* OE lines were compared with WT and both knockout genotypes. Because *ATG5* OE and *ATG7* OE or knockout genotypes were pooled together for the analysis, a fold change >1.5 was considered as significant and a *P*-value <0.1 acceptable.

Venn diagrams were built in Venny 2.1.0 to see intersects between common differentially expressed genes (DEGs). The obtained lists of targets were used for gene ontology using Virtual Plant 1.3 (http://virtualplant.bio.nyu.edu/cgi-bin/vpweb/) and Classification SuperViewer Tool w/ Bootstrap (http://bar.utoronto.ca/ntools/cgi-bin/ntools_classification_superviewer.cgi).

Corresponding 3'-untranslated regions (UTRs) were not included in both constructs used for overexpression (pGWB2 35S::ATG5 and pGWB2 35S:ATG7). Microarray chip used for analysis carried the probe ZA7224578 (TCCTCAAAGGTGAAGTGTAAGGTTCTCTGCAGTTACAATCCATCTGTGAATTG) complementary primarily to the 3'-UTR of *ATG5* (AT5G17290); thus only endogenous *ATG5* expression levels were detected. ZA7248403 probe (TGATACTGATGATGACGATGTAGCTGTAGATCTTTAAAGACAGATTTAT) annealing mostly on the coding 3' part of *ATG7* (AT5G45900) allowed detection of both endogenous and exogenous *ATG7* transcripts. Microarray data also revealed low levels of *ATG5* and *ATG7* expression in the corresponding knockout lines, consistent with our previous observations obtained by qRT-PCR analysis. Although full-length mRNA of *ATG5* and *ATG7* could not be detected in the corresponding knockout lines, both 5' and 3' parts of the transcripts were detectable, indicating transcription of partial sequences driven from T-DNA insertion promoters.

Data analysis

Data were analyzed using the JMP 10.0.0 64-bit edition software, unless described differently. If not stated otherwise, Dunnett's test was used for comparing transgenic lines with the WT. Survival analysis of life span data was performed using the Kaplan–Meier method.

qRT-PCR and analysis of lipid content were performed as described in the Supplementary methods.

Results

Overexpression of ATG5 *or* ATG7 *stimulates ubiquitin-like conjugation systems and enhances autophagic flux in Arabidopsis*

We generated a panel of homozygous transgenic lines of Arabidopsis constitutively overexpressing either *ATG5* or *ATG7* under control of the 35S promoter (*ATG5* OE or

ATG7 OE, respectively), and showing 7- to 10-fold higher transcript levels of the corresponding genes compared with WT (Col-0) plants (Supplementary Fig. S1A). Additionally, we established lines expressing GFP–Atg8a in WT, *ATG5* OE, *ATG7* OE, *ATG5*-knockout (*atg5*), and *ATG7*-knockout (*atg7*) backgrounds (Supplementary Fig. S1B). In agreement with previous studies (Thompson *et al.*, 2005), homologous overexpression of *ATG8a* in Arabidopsis did not reveal any discernible phenotype.

First, we assessed the impact of *ATG5* or *ATG7* overexpression on the activity of the ubiquitin-like conjugations systems (Fig. 1A) by immunodetection of two conjugates generated by the systems: Atg12–Atg5 (Fig. 1B, C) and Atg8–PE (Fig. 1D, E). We found that overexpression of *ATG5* enhanced both Atg12–Atg5 and Atg8–PE conjugation, whereas overexpression of *ATG7* had stimulatory effect only on the lipidation of Atg8 and did not influence the efficacy of Atg12–Atg5 conjugation (Fig. 1B–E). Importantly, overexpression of either *ATG5* or *ATG7* did not affect expression levels of other components of the ubiquitin-like conjugation systems (Supplementary Fig. S2). Collectively, these results indicate that Atg5 and Atg7 are rate-limiting components of the Atg8 lipidation pathway. While Atg5 exerts its effect on Atg8 lipidation via directly controlling the rate of Atg12–Atg5 conjugation (Fig. 1A–C), Atg7 presumably acts via catalyzing formation of the Atg8–Atg3 conjugate (Fig. 1A, D, E).

We attempted to assess a possible impact of a simultaneous overexpression of *ATG5* and *ATG7* genes by crossing single overexpressors. Interestingly, the amount of Atg5–Atg12 conjugate in double overexpressors was similar to the level in the single *ATG5* OE (Supplementary Fig. S3A, B), corroborating the notion that Atg5 but not Atg7 is a rate-limiting component of this reaction. Unfortunately, expression levels of the two genes in double overexpressors were considerably lower than in single overexpressors (Supplementary Fig. S3C), impeding an accurate comparison of the respective phenotypes. Additionally, simultaneous overexpression of both *ATG* genes caused a significant transcriptional down-regulation of some components of the conjugation systems, including *ATG8* isoforms and *ATG12a* (Supplementary Fig. S3C). Although this phenomenon hampers further investigation of the simultaneous expression of *ATG5* and *ATG7*, it provides interesting evidence for a negative feedback loop connecting autophagic flux and transcription of plant *ATG* genes.

Next, we studied the effect of enhanced Atg8 lipidation in *ATG* OE lines on autophagic flux by analyzing the efficacy of autophagosome formation (Fig. 2A, B; Supplementary Fig. S4) and degradation of potential autophagosomal cargo (Fig. 2C–F). Plants were treated with ConA to block vacuolar lysis and to cause accumulation of undegraded GFP–Atg8a-labeled autophagic bodies in the vacuolar lumen. We found an increased number of GFP-positive puncta in *ATG5* OE and *ATG7* OE lines co-expressing the GFP–Atg8a marker (Fig. 2A, B). Interestingly, assessment of the area of GFP-positive puncta did not reveal any difference in their size in the overexpressing lines compared with the WT (Supplementary Fig. S4), indicating that overexpression of *ATG5* or *ATG7* increases only the number of autophagosomes, but not their size.

Degradation of the autophagic adaptor protein NBR1 (Svenning *et al.*, 2011; Minina *et al.*, 2013*b*; Klionsky *et al.*, 2016) as well as the accumulation of free GFP in GFP–Atg8-expressing cells (Nair *et al.*, 2011) are indicative of the completion of autophagic flux. Detection of NBR1 protein (Fig. 2C, D, top chart) was combined with the quantification of *NBR1* mRNA in the same leaf samples (Fig. 2D, bottom chart) to exclude the possibility that observed differences in NBR1 abundance were caused by variation at the transcriptional level. Analysis of GFP–Atg8a cleavage leading to accumulation of free GFP was performed on seedlings grown under normal conditions or subjected to starvation (Fig. 2E, F). The assay revealed increased autophagic flux in *ATG5* OE and *ATG7* OE lines. Therefore, we conclude that Arabidopsis lines overexpressing either *ATG5* or *ATG7* might represent a potent tool for studying the impact of enhanced autophagy on plant development and physiology.

Enhanced autophagy promotes plant growth and suppresses aging

Accelerated senescence of rosette leaves is a phenotypic hallmark of Arabidopsis *atg* mutants (Doelling *et al.*, 2002; Hanaoka *et al.*, 2002). Accordingly, we observed earlier onset and a more rapid progression of leaf senescence in the *atg5* and *atg7* backgrounds (Table 1). In contrast, plants from both *ATG5* OE and *ATG7* OE lines exhibited a significantly delayed onset (by 4–7 d) of leaf senescence, as compared with WT plants, albeit the duration of leaf senescence was not affected (Table 1). Notably, while the onset of flowering was independent of the level of autophagy, the duration of the flowering period correlated with autophagic flux, so that overexpressors of *ATG5* or *ATG7* flowered for ~10 d longer than WT plants (Table 2). As a result, plants of different overexpressor lines had on average a 10–20% longer life span compared with WT plants (Fig. 3A).

Apart from accelerated aging, autophagy-deficient plants exhibit reduced fecundity and suppressed vegetative growth, even when grown under nutrient-rich conditions (Hanaoka *et al.*, 2002; Bassham *et al.*, 2006; Guiboileau *et al.*, 2012, 2013). Accordingly, *atg5* and *atg7* plants grown under standard growth conditions showed an 50% reduction in both rosette fresh weight (Fig. 3B, C; Supplementary Fig. S5A) and the total weight of mature seeds per plant (Fig. 3E). In contrast, *ATG* overexpressors exhibited increased vegetative growth and seed yield (Fig. 3B, C, E; Supplementary Fig. S5A), although the weight of an individual seed was not affected (Supplementary Fig. S6). Therefore the observed variation in seed yield was caused by differences in fecundity, eventually reflecting a strong impact of the basal autophagy activity on flowering duration (Table 2). *ATG5*- or *ATG7*-overexpressing plants developed more and taller inflorescences than the respective knockout mutants and WT plants (Fig. 3D), flowered longer (Tables 1, 2), and thus produced more seeds per plant (Fig. 3E).

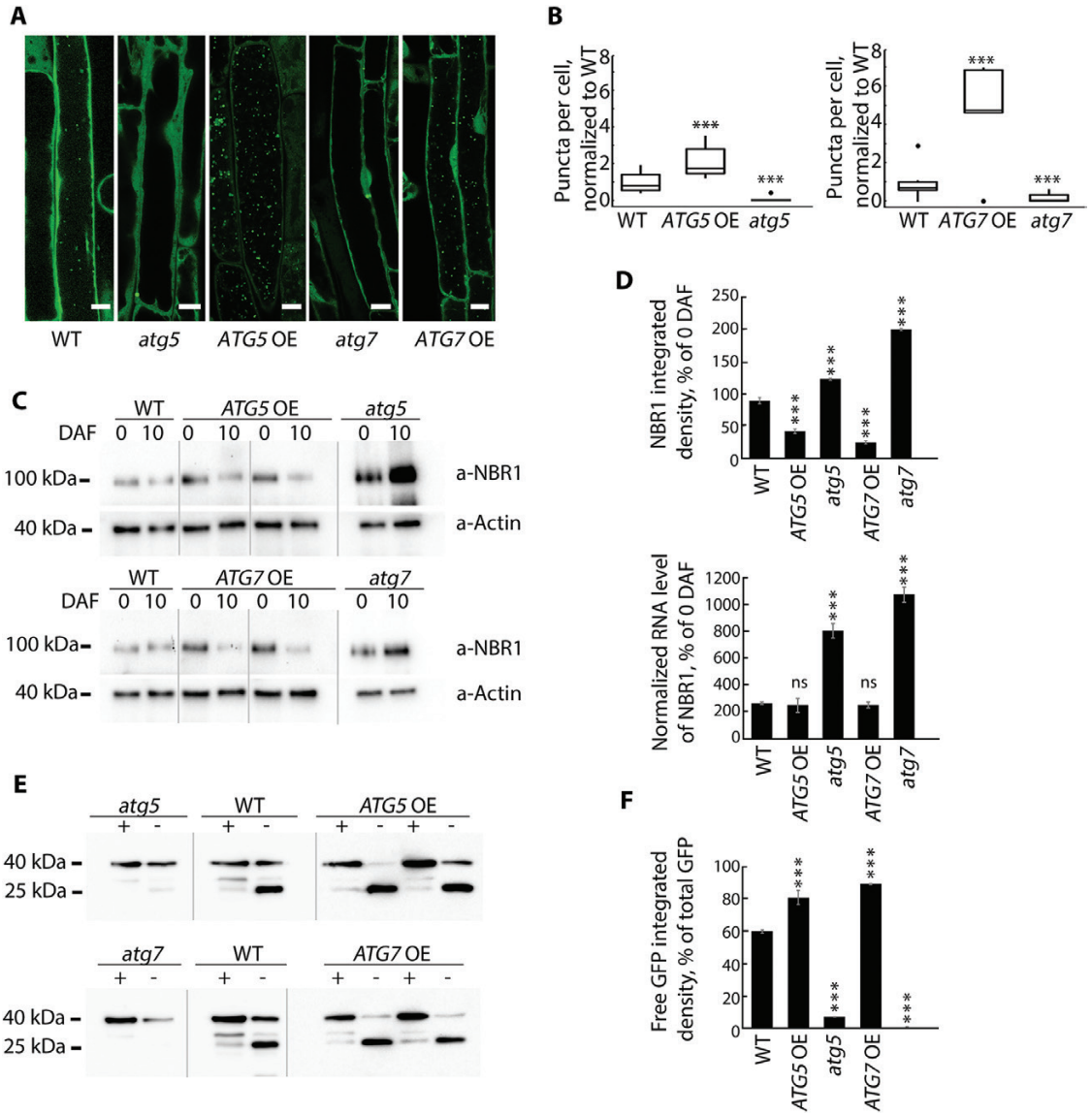

Fig. 2. Constitutive overexpression of *ATG5* or *ATG7* stimulates formation of autophagosomes and increases autophagic flux. (A) Representative confocal microscopy images of the epidermal root cells expressing GFP–Atg8a in WT, *ATG*-knockout, and *ATG*-overexpressing backgrounds. Seedlings were grown under 150 μE m^{-2} s^{-1} light, 16 h photoperiod for 6 d and subjected to 0.5 μM ConA treatment for 16 h prior to imaging. Scale bars=10 μm. (B) The box-plot diagram shows the number of the GFP-positive puncta in the epidermal root cells in (A). The average number of puncta for two or three cells belonging to the same root was considered as a single measurement. Four to seven roots were imaged per genotype. The means of each genotype were compared with the WT using Dunnett's test, assuming a Poisson distribution of the data. ***P<0.001; ·, outliers. (C) Increase of autophagic flux in *ATG5*- or *ATG7*-overexpressing plants confirmed by a higher rate of NBR1 degradation. Plants of the indicated genotypes were grown under 150 μE m^{-2} s^{-1}. Rosette leaves were sampled at the onset of flowering (0 days after flowering, DAF) and 10 d later (10 DAF). Total protein extracts from sampled leaves were used for western blot analysis to detect NBR1 and actin. (D) Densitometry of the NBR1 signal in (C) and expression level of *NBR1* in the same samples. Integrated density values for NBR1 were first normalized to actin and then expressed as a percentage of 0 DAF for the corresponding sample. Data represent means ±SE; n=6. The means of each genotype were compared with the WT using Dunnett's test, ***P<0.001. Detection of the *NBR1* transcript level in *ATG*-overexpressing plants confirmed that the decrease in NBR1 protein was caused by protein degradation and did not originate from transcriptional variation. qRT-PCR was performed on the same leaf material as in (C). Data represent means ±SE for each genotype, normalized to two reference genes (*PP2A* and *HEL*) and to 0 DAF; n=6. The means of each genotype were compared with the WT using Dunnett's test, ***P<0.001. (E) Increased autophagic flux in *ATG5*- or *ATG7*-overexpressing plants additionally confirmed by detection of free GFP accumulation in the seedlings expressing GFP–Atg8a in the indicated backgrounds. Seven-day-old seedlings grown under normal conditions (150 μE m^{-2} s^{-1} light, 16 h photoperiod) were either transferred onto sucrose-depleted MS medium and kept in the darkness (–) or left growing under normal conditions (+). Total protein extracts from the whole seedlings of each genotype were used for western blot analysis with anti-GFP. The GFP–Atg8a fusion has a predicted molecular weight of ~40 kDa; free GFP has a predicted molecular weight of 27 kDa. To avoid quantification of saturated pixels, several exposures were used for different samples. Comparisons of the absolute integrated density values for each line were made using the same exposure. For more information, see the Materials and methods. (F) Densitometry of the GFP–ATG8a cleavage assay in (E) confirms elevated autophagic flux in *ATG* OE backgrounds. The experiment was repeated twice; at least three western blot assays were performed for each experiment. The figure shows a representative example. Free GFP was expressed as a percentage of the total amount of GFP for each sample in (E). Data represent means ±SE of three individual measurements. The means of each genotype were compared with the WT using Dunnett's test, ***P<0.001.

Table 1. *Enhanced autophagy delays onset of leaf senescence*

Genotype	Onset of rosette senescence, DAG	Complete rosette senescence, DAG	Duration of rosette senescence, d
ATG5 trial			
WT	36.1 ± 3.74	55.6 ± 5.13	19.5 ± 5.08
atg5	30.2 ± 1.86****	44.5 ± 2.13****	14.3 ± 2.58****
ATG5 OE	40.1 ± 3.55**	58.6 ± 3.52*	18.5 ± 5.22 ns
ATG7 trial			
WT	35.1 ± 5.11	56.2 ± 5.00	21.1 ± 3.50
atg7	31.2 ± 4.91**	47.6 ± 5.39****	16.4 ± 4.03****
ATG7 OE	42.1 ± 5.38**	62.1 ± 2.53**	20.0 ± 5.10 ns

DAG, days after germination (radicle emergence); OE, overexpression.
All time data are shown as the mean ±SD, with 20 plants per genotype.
Each trial was repeated twice, every time with a different overexpression line. Although there was variation among replicate trials in the absolute mean values, they all showed the same effects. *P<0.05, **P<0.01, ***P<0.001, ****P<0.0001; ns, not significant versus the WT in the same trial; Dunnett's test.

Table 2. *Enhanced autophagy sustains flowering*

Genotype	First flower open, DAG	Cessation of flowering, DAG	Duration of flowering, d
ATG5 trial			
WT	27.5 ± 1.61	58.7 ± 9.61	31.2 ± 9.89
atg5	27.8 ± 1.75 ns	46.4 ± 1.72****	18.6 ± 1.93****
ATG5 OE	27.4 ± 1.37 ns	67.6 ± 5.99*	40.2 ± 7.05*
ATG7 trial			
WT	30.0 ± 4.36	62.5 ± 7.35	32.6 ± 6.19
atg7	28.5 ± 4.02 ns	55.3 ± 4.04****	26.9 ± 4.77****
ATG7 OE	32.4 ± 3.28 ns	74.3 ± 3.25****	41.9 ± 3.54****

DAG, days after germination (radicle emergence); OE, overexpression. All time data are shown as the mean ±SD, with 20 plants per genotype. Each trial was repeated twice, every time with a different overexpression line. Although there was variation among replicate trials in the absolute mean values, they all showed the same effects. *P<0.05, **P<0.01, ***P<0.001, ****P<0.0001; ns, not significant versus the WT in the same trial; Dunnett's test.

Importantly, the observed phenotypes were dependent on the growth conditions. The phenotypic differences between WT and *ATG*-overexpressing plants were not significant under autophagy-stimulating conditions, namely under light intensity level reduced to 100 µE m^{-2} s^{-1} (data not shown; Minina *et al.*, 2013*b*).

Interestingly, tracking of rosette development revealed a trend in *ATG*-overexpressing lines to develop more leaves compared with WT plants, whereas *ATG*-knockout plants developed a slightly lower number of leaves (Supplementary Fig. S5A). However, the observed differences in leaf number between WT and *ATG*-overexpressing plants were not statistically significant at any developmental stage and therefore did not influence the onset of flowering (Table 2).

The increased biomass (Fig. 3C) and larger size of leaf rosettes (Fig. 3B; Supplementary Fig. S5A) of *ATG*-overexpressing plants and opposite traits in the *ATG*-knockouts point to importance of autophagy in leaf cell expansion and/or division. Analysis of the cell size in fully expanded rosette leaf blades did not reveal any statistically significant difference between *ATG* overexpressors, WT, or *ATG*-knockouts (Supplementary Fig. S5B), suggesting that autophagy facilitates leaf cell division.

It was shown that autophagy can regulate fatty acid and lipid metabolism in animals through the recycling of lipid droplets in various cell types (in the process termed lipophagy; Singh *et al.*, 2009). Furthermore, autophagy mediates differentiation of white adipocytes, a cell type specialized in the storage of large unilocular lipid droplets (Zhang *et al.*, 2009).

Arabidopsis accumulates massive amounts of fatty acids in the form of triacylglycerols in seeds, making it a robust model for studying oil biosynthesis pathways and translating these findings to oil-seed crops (Bates *et al.*, 2013). We found that autophagy stimulates seed lipid accumulation, since knockout and overexpression of *ATG5* or *ATG7* led to a moderate decrease and increase of fatty acid content, respectively, compared with the WT (Fig. 3F). Since enhanced autophagy boosts seed set (Fig. 3E), the stimulatory effect of enhanced autophagy on seed oil yield per plant was much stronger, in the range of a 25–50% increase compared with the WT (Fig. 3G). Interestingly, the *atg5* and *atg7* knockouts had a significant change in seed fatty acid composition compared with the WT; the oleic acid (18:1) proportion was decreased with a corresponding increase in eicosa-13,16-dienoic acid (20:2) and erucic acid (22:1) (Supplementary Fig. S7), whereas *ATG*-overexpressing plants did not differ from the WT in this respect.

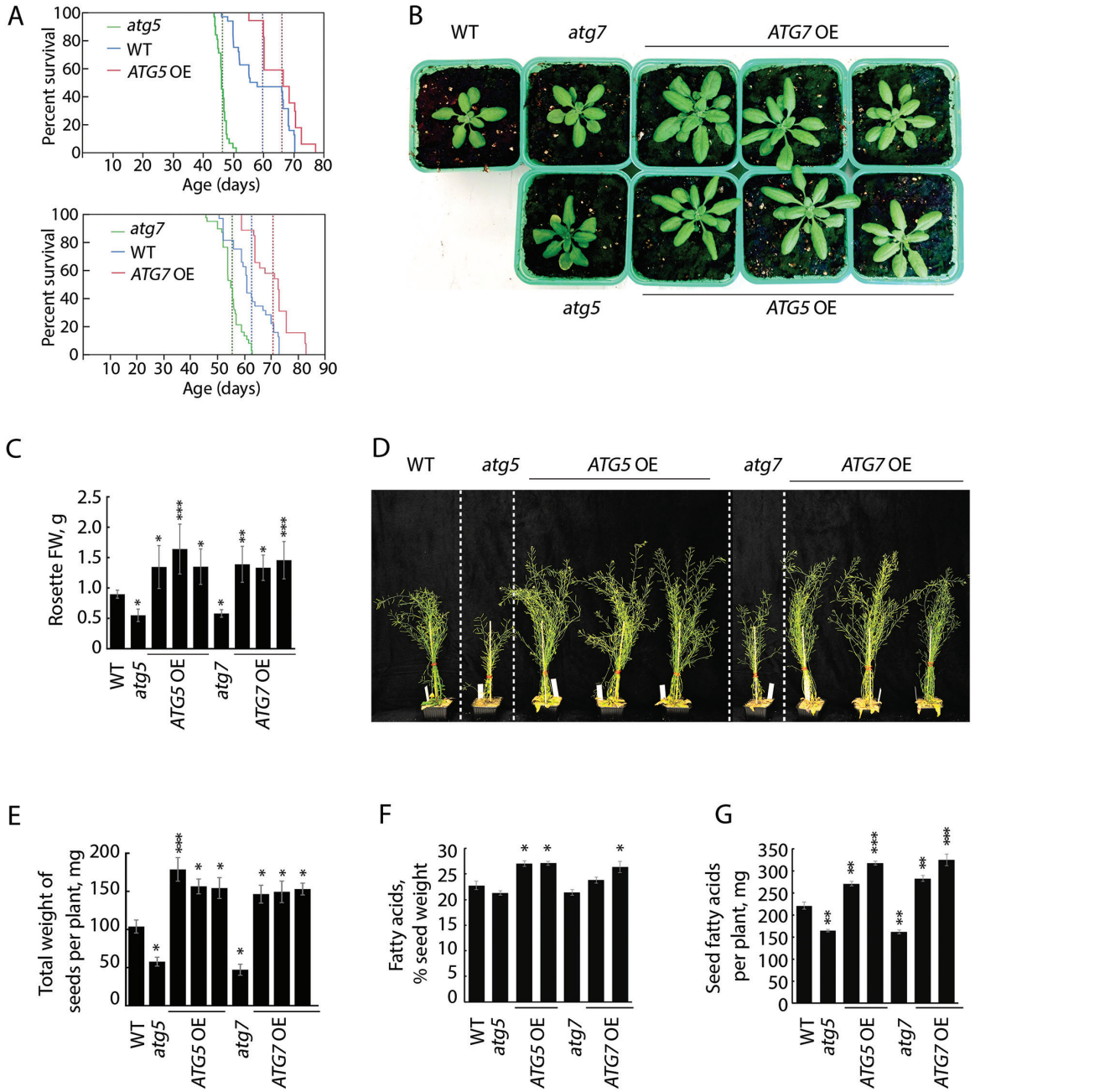

Fig. 3. Enhanced autophagy extends plant life span and promotes vegetative growth, seed production, and accumulation of seed oil. (A) Kaplan–Meier survival curves for the WT plants, *ATG*-knockout (*atg5* and *atg7*), and *ATG*-overexpressing lines (*ATG5* OE and *ATG7* OE) grown under normal conditions (150 μE m^{-2} s^{-1} light, 16 h photoperiod). The dashed lines show mean life spans for different genotypes. Each of the two trials was repeated twice, every time with a different *ATG5*- or *ATG7*-overexpressing line. The life span of an individual plant was measured as the time period from radicle emergence to complete senescence of the rosette and cessation of flowering. (B) Representative phenotype of 3-week-old plants of the WT, *ATG*-knockout mutants, and three individual *ATG5*- or *ATG7*-overexpressing lines grown under normal conditions. Planting pot size was 8 × 8 cm. (C) Fresh weight of rosettes. Data represent means ±SE, n=3–4. ***P<0.0001; **P<0.001; *P<0.05; versus control (WT), Dunnett's test. (D) Representative phenotype of plants of the same genotypes as in (B) at the flowering stage. Planting pot size was 8 × 8×8 cm. (E) The seed yield of WT, *ATG*-knockout, and *ATG*-overexpressing plants grown under normal conditions. Data represent means ±SE, n=6–11. ***P<0.0001; **P<0.001; *P<0.05; versus the WT, Dunnett's test. (F, G) Oil content of seeds expressed as a percentage of seed weight (F) and in mg per plant, normalized to the seed yield presented in E (G). Acyl groups were measured in mature seeds harvested from three plants per genotype grown under normal conditions. Data represent means ±SE, n=3. ***P<0.001; **P<0.01; *P<0.05; versus the WT, Dunnett's test.

Collectively, our data demonstrate that Arabidopsis plants with constitutively enhanced autophagic flux show an increased vigor: longevity, vegetative growth, and fecundity. Additionally, we show the positive effect of constitutively up-regulated autophagy on seed oil accumulation.

Enhanced autophagy confers increased resistance to necrotrophic pathogens and oxidative stress

Reallocation of resources from growth to stress resistance (and vice versa) determines the fitness costs, and their

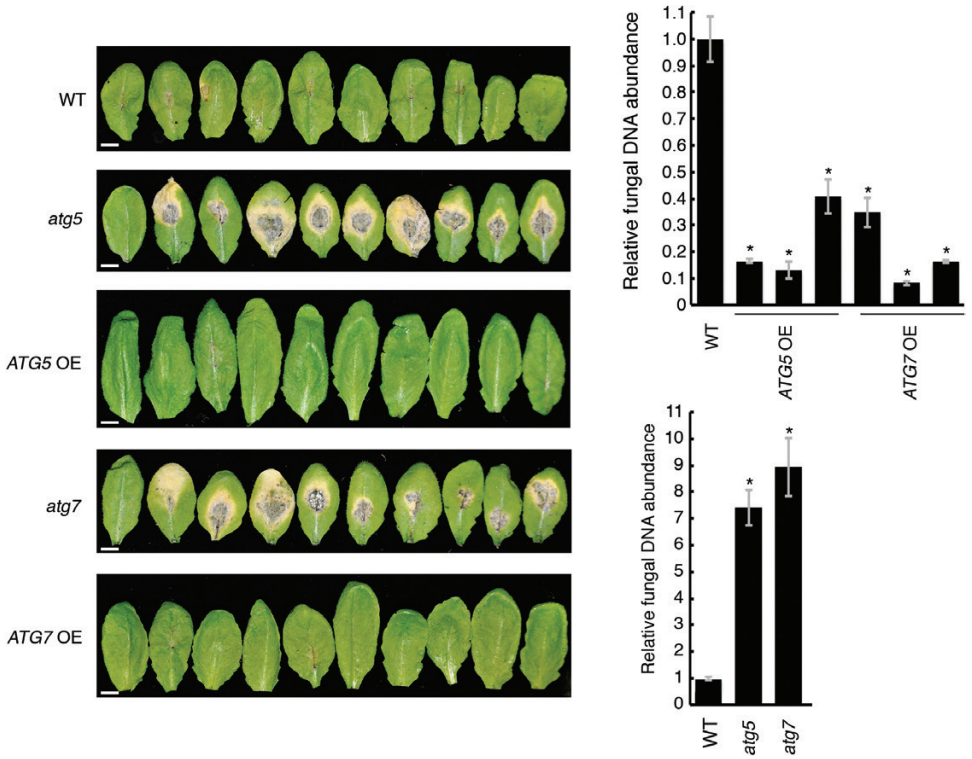

Fig. 4. Plants with enhanced autophagy are more resistant to necrotrophic phytopathogens. Three-week-old plants of the WT, *ATG*-knockout, and three individual *ATG*-overexpressing lines were inoculated with 10 µl of suspension containing 5×10^5 spores ml^{-1} of *Alternaria brassicicola*. Images display all rosette leaves from representative selected plants on the seventh day post-inoculation. Charts display fungal growth assessed by measuring fungal DNA using qRT-PCR to detect the fungal cutinase gene. Data represent means ±SE normalized to two reference genes (*UBQ5* and *PR2*), $n \geq 3$. *$P<0.0001$; versus the WT, Dunnett's test. Scale bars=1 cm.

cutbacks represent an important task in plant breeding and biotechnology (Brown, 2002; Cabello *et al.*, 2014). Since autophagy plays a pivotal role in energy reallocation and metabolism and, as shown in this study, plants with enhanced autophagy gain in growth fitness, we hypothesized that these plants might ultimately lose in stress resistance.

Previous observations revealed increased fungal growth in Arabidopsis *atg* mutants, indicating that autophagy is required for plant resistance to necrotrophic fungi (Lai *et al.*, 2011; Lenz *et al.*, 2011). In agreement with these studies, *atg5* and *atg7* plants developed unrestricted necrotic leaf lesions following inoculation with *A. brassicicola*, thereby greatly facilitating fungal growth (Fig. 4). In contrast, *ATG5*- or *ATG7*-overexpressing plants developed fewer necrotic lesions and showed suppressed fungal growth compared with WT plants (Fig. 4).

We reasoned that if enhanced autophagy plays a cytoprotective role during the necrotrophic infection, it might also aid in decreasing plant susceptibility to oxidative stress, which represents one of the major components of necrotrophic pathogenicity (AbuQamar *et al.*, 2006; Choquer *et al.*, 2007). In our experiments, *atg5* and *atg7* plants exhibited stronger growth suppression and chlorosis than WT plants when exposed to oxidative stress induced by MV treatment (Fig. 5). Correspondingly, *ATG*-overexpressing lines demonstrated enhanced resistance to MV, with their chlorophyll content levels slightly below the corresponding control (untreated plants) and much higher than those of MV-treated WT plants (Fig. 5).

Taken together, these data imply that elevated autophagy can improve plant resistance to both necrotrophic pathogens and oxidative stress.

Transcriptional profiling of plants with enhanced autophagy

To investigate further molecular mechanisms underlying improved growth and stress resistance phenotypes of the *ATG*-overexpressing plants, we performed transcriptome analyses of rosette leaves at two time points representing distinct developmental stages. For the first time point, complete rosettes were sampled at the budding stage, when no difference in phenotype of WT, *ATG*-knockout, and *ATG*-overexpressing plants was detectable. The second sampling was performed 10 DAF, when *ATG*-knockout plants showed early signs of senescence, and differences between WT and *ATG*-overexpressing plants became detectable at the molecular level (Fig. 2C, D).

Expression of each transcript at either time point was first normalized to the corresponding values in the WT. Next, transcripts were sorted to select only those that displayed common expression trends in both *atg5* and *atg7* mutants or in both *ATG5* OE and *ATG7* OE lines.

Our results confirm general transcriptional trends of Arabidopsis *atg* mutants reported previously (Masclaux-Daubresse *et al.*, 2014; Avin-Wittenberg *et al.*, 2015) and also indicate the presence of a complex signaling similar to the

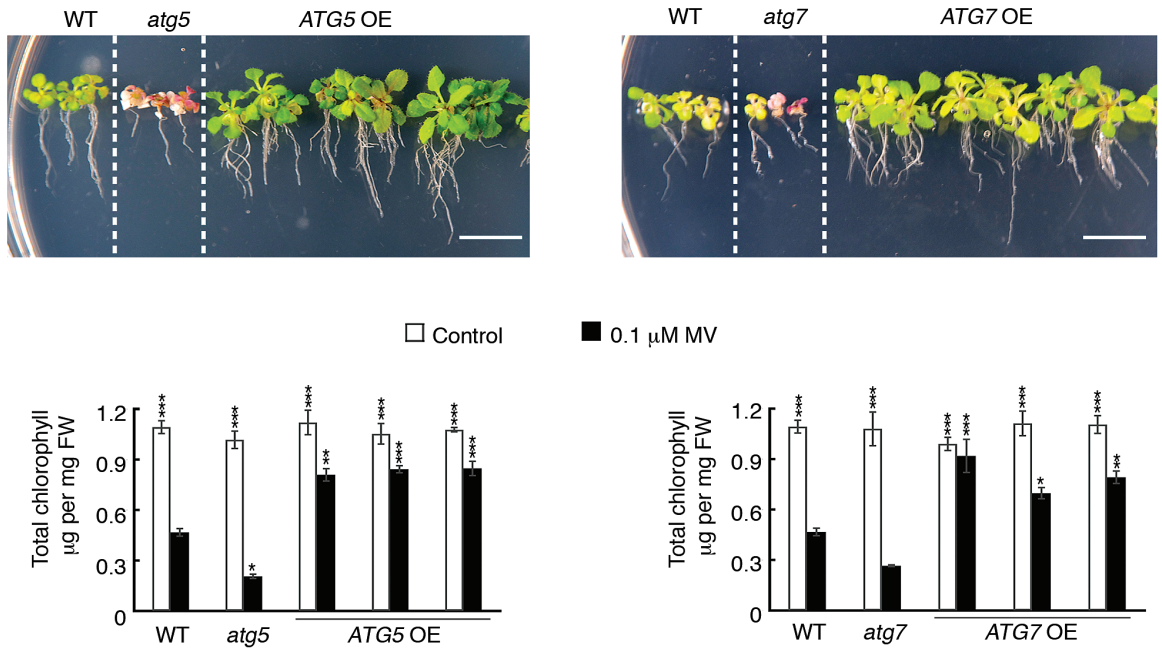

Fig. 5. Plants with enhanced autophagy are more resistant to oxidative stress. Seeds of the WT, *ATG*-knockout mutants, and three individual *ATG5*- and *ATG7*-overexpressing lines were germinated on MS plates with or without addition of 0.1 μM methyl viologen (MV). The phenotype was assessed after 3 weeks. The difference in the tolerance to oxidative stress between different genotypes was confirmed by measuring chlorophyll content. Untreated plants (control) of all genotypes exhibited no significant difference in the chlorophyll content. Upon treatment with MV, WT and *ATG*-knockout plants showed a dramatic decrease in the chlorophyll content, while *ATG*-overexpressing lines maintained high levels of chlorophyll. Data represent means ±SEM, n=3–7. ***P<0.0001; **P<0.001; *P<0.05; versus MV-treated WT, Dunnett's test. Scale bars=1 cm.

immune response, induction of pathways managing oxidative stress, and elevated response to salicylic acid (Supplementary Tables S2–S4). We did not observe the previously reported up-regulation of methionine and ethylene biosynthesis (Masclaux-Daubresse *et al.*, 2014) either in *atg5* or in *atg7* plants, which might be explained by the differences in sampling stages.

In agreement with the results of the phenotypic analysis, the number of differentially expressed genes at the first time point was relatively low (Fig. 6A; Supplementary Table S3). Nevertheless, already at this stage we could observe an increase in the expression of enzymes involved in lipid metabolism in *ATG*-overexpressing plants, while *atg* plants displayed up-regulation of stress- and starvation-related genes (Fig. 6B, C; Supplementary Table S3).

At the second time point, the number of DEGs significantly increased for both *atg* and *ATG*-overexpressing plants, and the opposite trends became readily identifiable (Fig. 7; Supplementary Tables S1, S4). In general, we could observe an increase in transcripts involved in proteolysis, lipid degradation, and salicylic acid signaling in *atg* plants and an opposite trend in *ATG*-overexpressing plants.

One of the causes of the early onset of senescence in *atg* plants was proposed to be their susceptibility to UV light and reactive oxygen species (ROS). This phenomenon has been linked to the decreased production of flavonoids and anthocyanin observed in *ATG*-deficient plants (Masclaux-Daubresse *et al.*, 2014). Interestingly, a large number of genes involved in flavonoid biosynthesis and anthocyanin production, as well as in oxidative stress response were up-regulated in *ATG*-overexpressing plants (Supplementary Tables S1, S4). Furthermore, at the developmental stages later than 10 DAF (second time point), *ATG*-overexpressing plants accumulated visibly higher amounts of anthocyanin than WT plants (data not shown), thus confirming the functionality of transcriptional up-regulation of the anthocyanin biosynthesis pathway. This observation is also in agreement with the recent reports proposing the link between elevated anthocyanin production and enhanced autophagy flux in plants overexpressing one of the apple orthologs of ATG18 (Sun *et al.*, 2017; Sun *et al.*, 2018).

It is noteworthy, that at the second time point, sugar transport genes were significantly down-regulated in *atg* plants and up-regulated in *ATG*-overexpressing plants when compared with the WT (Fig. 7; Tables S1, S2 and S4). Transport of sugars from rosette leaves to the inflorescence is essential for sustaining seed onset and development (Wingenter *et al.*, 2010). Thus, higher seed yield of *ATG*-overexpressing plants could be attributed to the combined effect of the long-lasting rosette and high efficacy of sugar transport towards the inflorescence.

Discussion

Transcriptional regulation of autophagy

Previous studies in animals and plants demonstrate that artificial manipulation of autophagy can drastically affect various aspects of organismal physiology related to growth, aging, and diseases (Fleming *et al.*, 2011; Rubinsztein *et al.*, 2011; Liu and Bassham, 2012). In plants, these studies were mainly conducted using *ATG*-knockout mutants and RNAi

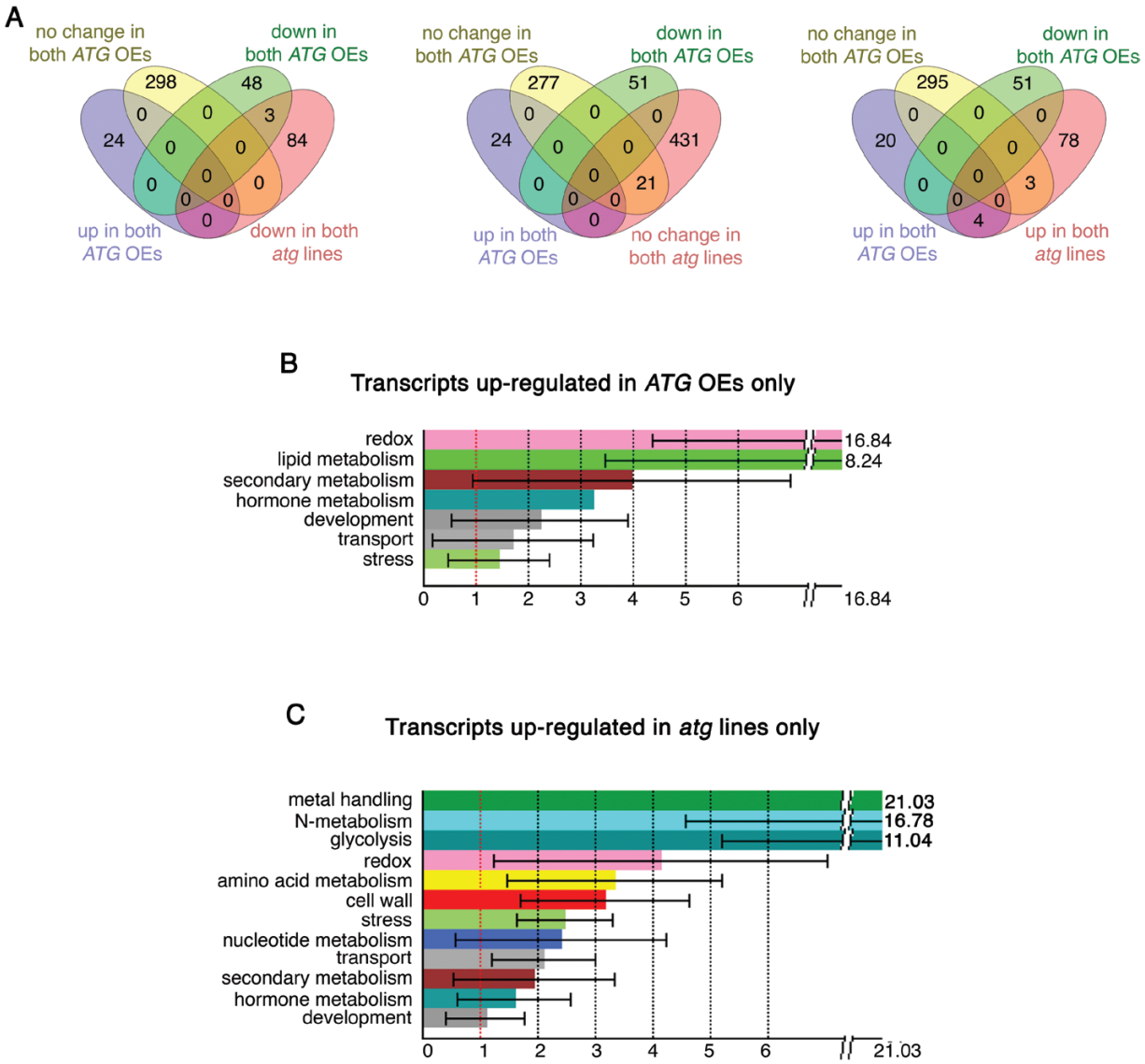

Fig. 6. Transcriptional trends characteristic for *ATG*-overexpressing and *ATG*-knockout lines at the bolting stage. Complete rosettes from four individual plants of each genotype were harvested at the bolting stage (0 DAF) and pooled together for RNA extraction followed by microarray analysis. Differentially expressed genes (DEGs) were selected by normalizing values obtained for transgenic backgrounds to the corresponding expression values obtained for the WT background. Only the genes showing common trends for both *ATG5*- and *ATG7*-overexpressing backgrounds (*ATG* OEs) or both *ATG5*- and *ATG7*-knockout backgrounds (*atg* lines) were used for further analysis. (A) Venn diagrams illustrating the number of DEGs (genes expressed differently from the WT at the bolting stage) in *ATG*-overexpressing and *ATG*-knockout plants. (B, C) Gene ontology analysis of DEGs specific for *ATG*-overexpressing (B) or *ATG*-knockout (C) plants.

lines, which allowed compromised growth and stress resistance coupled with accelerated aging as a consequence of suppressed autophagy to be revealed. Here we present evidence that constitutive overexpression of *ATG5* or *ATG7* in Arabidopsis is sufficient to enhance lipidation of Atg8, leading to the formation of a higher number of autophagosomes, enhanced autophagic flux, and improved plant fitness.

Regulation of autophagy is complex and includes transcriptional, post-transcriptional, and post-translational steps (Feng *et al.*, 2015). One of the post-translational modifications essential for the formation of autophagosomes is lipidation of Atg8 mediated by two ubiquitin-like conjugation systems (Fig. 8A). Here we demonstrate that Atg5 is a rate-limiting factor in the Atg12–Atg5 conjugation pathway, and accumulation of a higher amount of the Atg12–Atg5 conjugate upon overexpression of *ATG5* tightly correlates with the efficacy of Atg8–PE formation (Fig. 8B). Furthermore, we show that although overexpression of *ATG7* does not contribute to Atg12–Atg5 conjugation, it still boosts lipidation of Atg8, suggesting that higher efficacy of Atg8–Atg3 conjugation is beneficial for the Atg8 lipidation rate even at the 'normal' abundance of the Atg12–Atg5–Atg16 complex (Fig. 8C). Consequently, we suggest that Atg8 lipidation can be enhanced either by increasing amounts of the E3-like ligase (Atg12–Atg5–Atg16 complex) or by boosting Atg5-unrelated activity of Atg7, for example formation of the intermediate conjugate Atg8–Atg3. Whether artificial transcriptional up-regulation of other *ATG* genes can be instrumental in controlling the autophagic flux or will be just a bystander event (as in the case of Arabidopsis *ATG8a*) remains an open question.

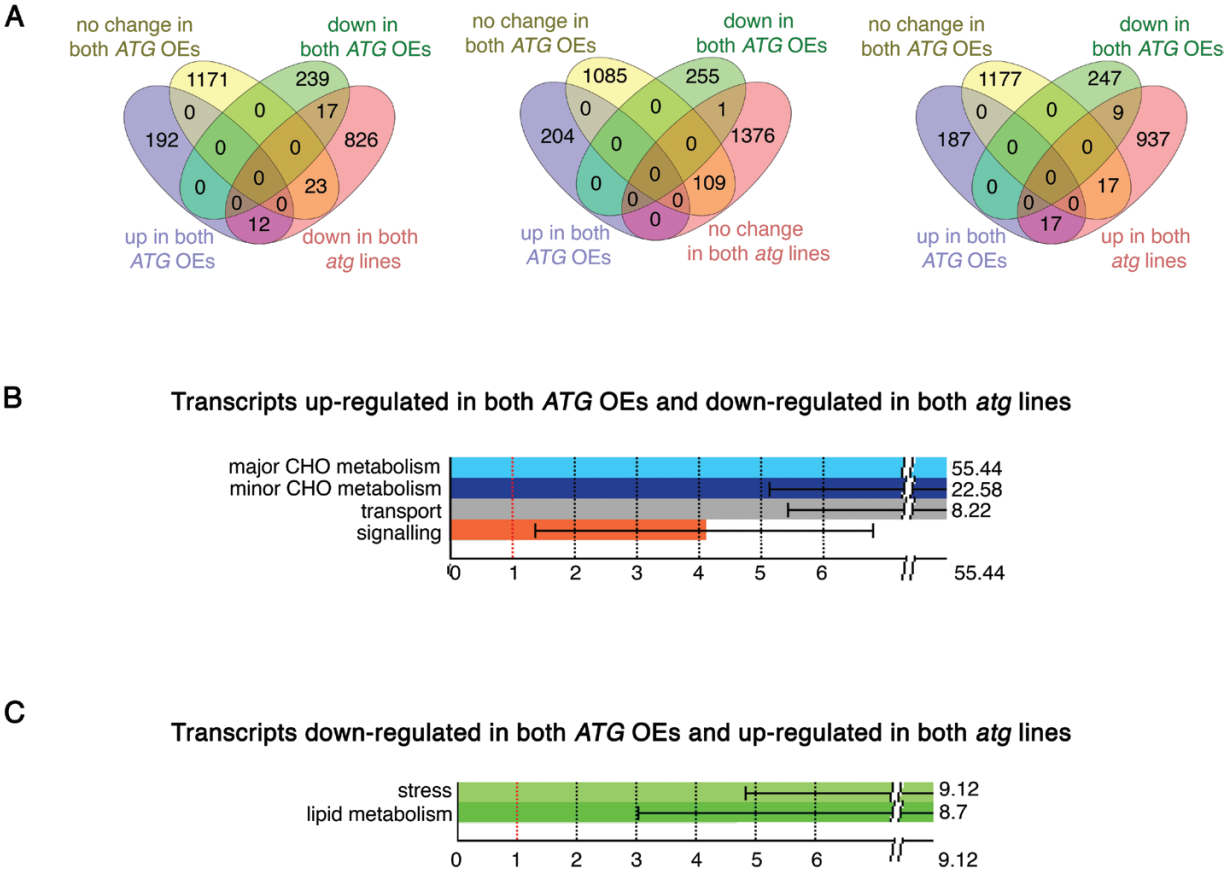

Fig. 7. Transcriptional trends characteristic for *ATG*-overexpressing and *ATG*-knockout lines at the 10 DAF stage. Complete rosettes from four individual plants of each genotype were harvested at 10 DAF and pooled together for RNA extraction followed by microarray analysis. Differentially expressed genes (DEGs) were selected by normalizing values obtained for transgenic backgrounds to the corresponding expression values obtained for the WT background. Only the genes showing common trends for both *ATG5*- and *ATG7*-overexpressing backgrounds (*ATG* OEs) or both *ATG5*- and *ATG7*-knockout backgrounds (*atg* lines) were used for further analysis. (A) Venn diagrams illustrating the number of DEGs (genes expressed differently from the WT at 10 DAF) in *ATG*-overexpressing and *ATG*-knockout plants. (B, C) Gene Ontology analysis of DEGs showing opposite expression trends in *ATG*-overexpressing and *ATG*-knockout plants.

Importantly, while overexpression of *ATG* genes in yeast does not significantly affect autophagic activity (Ma *et al.*, 2007), several studies, including this work, demonstrate that overexpression of some of these genes in plant and animal models has a stimulatory effect on autophagic flux (Scott *et al.*, 2007; Pyo *et al.*, 2013). A plausible explanation for these contrasting observations made in yeast and other organisms could be the differences between the number of phagophore assembly sites or pre-autophagosomal structures (PASs) at which the core Atg proteins function. While yeast cells possess only a single PAS, plant and animal cells do not seem to have any limitation in the potential number of PASs per cell (Parzych and Klionsky, 2014). Thus, overexpression of rate-limiting PAS components might increase the number of forming PASs and result in the higher frequency of autophagosome formation, as was indeed observed in this study.

In plants, transient overexpression of *ATG3* in *Nicotiana benthamiana* (Han *et al.*, 2015) or stable overexpression of either *ATG5* or *ATG7* in Arabidopsis (present study) is sufficient to stimulate autophagy. In contrat, overexpression of *ATG8* genes fused to a fluorescent protein, which is routinely used for live imaging of autophagosomes (Bassham, 2015; Klionsky *et al.*, 2016), has never been reported to enhance autophagy. An increased vegetative growth and seed production previously observed upon heterologous expression of soybean *ATG8c* in Arabidopsis (Xia *et al.*, 2012) might be caused by autophagy-independent functions of the Atg8c protein. A recent study of heterologous overexpression of apple *ATG7* in Arabidopsis plants (Wang *et al.*, 2016) reports some observations similar to those demonstrated in this study, such as enhanced biomass, but also some phenotypes not found in the Arabidopsis lines overexpressing Arabidopsis *ATG7*, such as accelerated bolting. This finding indicates that heterologous Atg proteins might bring some additional functions besides their participation in autophagy and/or different efficacy when compared with the native homologs.

Interestingly, while individual overexpression of either *ATG5* or *ATG7* did not influence expression of other components of the ubiquitin-like conjugation systems (Supplementary Figs S2, Fig. S3C), simultaneous overexpression of both genes led to a significant suppression of other *ATG* genes involved in the conjugation systems, showing trends opposite to expression profiles observed in the *ATG*-knockout plants (Fig. S3C). These results indicate the presence of a complex feedback loop controlling autophagic activity at the transcriptional level. While a number of transcription

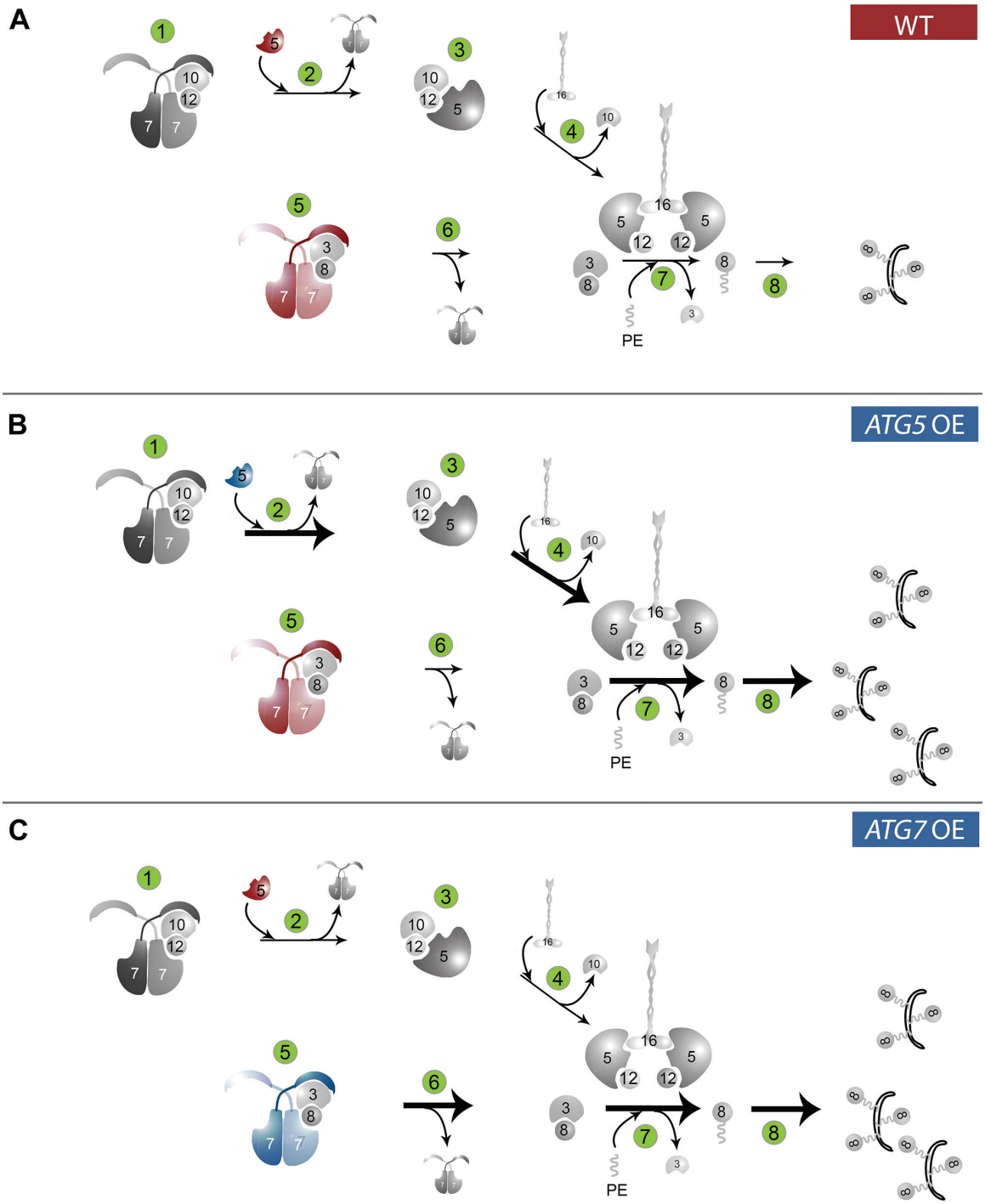

Fig. 8. A schematic representation of the proposed effects of *ATG5* or *ATG7* overexpression on the efficacy of Atg8 lipidation. (A) A schematic representation of two autophagy-related ubiquitin-like conjugation systems in the WT background. Atg7 acts as an E1-like ligase catalyzing formation of Atg12–Atg10 (step 1) and Atg8–Atg3 (step 5) conjugates. Atg12 is further transferred onto Atg5 and the resulting Atg12–Atg5 conjugate forms a complex with Atg16 (steps 2–4). The Atg12–Atg5–Atg16 complex serves as an E3-like ligase for conjugating Atg8 with a phosphatidylethanolamine (PE) (steps 6 and 7). Lipidated Atg8 contributes to elongation of a phagophore (step 8). Red color indicates pools of Atg5 and Atg7 that act as rate-limiting components of the corresponding reactions. (B) Atg5 is a limiting component of steps 2–4, 7, and 8. Constitutive overproduction of Atg5 (blue color) in the *ATG5 OE* background does not influence expression profiles of other components of the conjugation systems but is sufficient to stimulate conjugation of Atg12 with Atg5 and of Atg8 with PE, indicating enhanced efficacy of steps 2–4, 7, and 8 (bold arrows). (C) Atg7 is a limiting component of steps 5–8. Overexpression of *ATG7* (blue color) also does not change expression of other *ATG* genes involved in the ubiquitin-like conjugation systems. In agreement with the assumption that Atg5 is the limiting component of steps 2 and 3 of the pathway, the Atg12–Atg5 conjugate does not accumulate in *ATG7* OE plants. However, *ATG7* OE plants still have a higher amount of the Atg8–PE conjugate, suggesting enhanced efficacy of steps 7 and 8 (bold arrows). This indicates that the constitutively enhanced abundance of Atg7 (blue color) boosts steps 5 and 6 (bold arrow). Possibly, increased formation of the Atg8–Atg3 conjugate stimulates Atg8 lipidation without requiring more of the Atg12–Atg5–Atg16 complex. Enhanced lipidation of Atg8 in *ATG5* OE or *ATG7* OE plants does not lead to changes in the size of autophagosomes, but instead augments the frequency of phagophore formation, as illustrated in (B) and (C).

factors and other regulatory proteins directly targeting *ATG* genes have been identified in animal models (Lee *et al.*, 2014; Seok *et al.*, 2014; Feng *et al.*, 2015; Lapierre *et al.*, 2015), master transcription regulators of plant autophagy remain unknown.

Phenotypic expression of manipulated autophagy

Autophagy plays a multifaceted role in plant physiology by performing a broad array of cellular and organismal functions. Therefore, it is not surprising that enhancement of the autophagic flux in Arabidopsis by overexpressing *ATG5* or *ATG7* affected so many traits, ranging from longevity to lipid biosynthesis and stress resistance.

A potential reason for the delayed leaf senescence, as well as for increased vegetative growth of *ATG5*- or *ATG7*-overexpressing plants (Fig. 3B, C; Table 1; Supplementary Fig. S5) might be linked to the pathway of starch remobilization, which is reliant on the autophagy-dependent targeting of non-plastidial starch granule-like structures to the vacuoles for degradation (Wang *et al.*, 2013). Autophagy was also shown to be necessary for delaying senescence by suppressing salicylic acid signaling (Yoshimoto *et al.*, 2009), and our results indicate that this pathway might contribute to the longevity phenotype of the plants with constitutively up-regulated autophagy (Fig. 3A; Table 1; Supplementary Table S1). Additionally, autophagy participates in the recycling of chloroplastic proteins and whole chloroplasts in leaves (Ishida *et al.*, 2008; Wada *et al.*, 2009), thus supporting nitrogen remobilization and use efficiency (Guiboileau *et al.*, 2012, 2013; Ren *et al.*, 2014; Li *et al.*, 2015; Wada *et al.*, 2015). The more efficient flux of nitrogen from source to sink might result in a better support of apical shoot meristem and thus more flowers and increased seed set, both traits consistently observed in the transgenic plants with enhanced autophagy (Table 2; Fig. 3D, E).

Studies in animal systems revealed a complex cross-talk between lipids and autophagy. Not only are numerous lipids, free fatty acids, and enzymes of lipid metabolism involved in modulation (usually stimulation) of autophagy, but autophagy in return controls the lipid status of the cell, tissue, and whole organism through a process of selective recycling of lipid droplets (lipophagy) and by an as yet undefined molecular mechanism conferring differentiation of adipose tissues (Dall'Armi *et al.*, 2013; Liu and Czaja, 2013). It remains unknown whether a similar or distinct mechanistic connection between autophagy and lipid metabolism exists in plants (for a review, see Elander *et al*, 2018). Recent lipidomics analysis of *atg5* and *atg7* Arabidopsis seedlings subjected to carbon deprivation revealed increased accumulation of most classes of fatty acids in *atg5* mutants and most classes of lipids in both *atg5* and *atg7* mutants, indicating that autophagy is required for lipid catabolism during seedling growth under carbon-deprived conditions (Avin-Wittenberg *et al.*, 2015). It is not feasible to compare these results with results obtained in our study due to major differences in the experimental design, namely seedlings grown under starvation versus seeds maturing under nutrient-rich conditions. We observed a direct correlation between the level of autophagy and seed fatty acid content (Fig. 3F, G), suggesting that increased autophagic flux mediates deposition of seed lipids. Both *atg5* and *atg7* mutants had similar changes in seed fatty acid composition, with a decrease in oleic acid and an increase in very long chain fatty acids, whereas the *ATG* overexpressors had a WT-like fatty acid composition (Supplementary Fig. S7). Thus, functional autophagy not only regulates the accumulation of lipids but can, at least to some extent, also regulate the fatty acid composition of these lipids.

Autophagy is a major cytoprotective mechanism activated during various stress responses to remove or recycle toxic compounds, protein aggregates, and defective organelles (Liu and Bassham, 2012). These homeostatic functions were proposed to underlie altered cell death and resistance phenotypes of autophagy-deficient mutants in comparison with the WT during pathogen infection. While the response of autophagy-deficient mutants to biotrophic pathogens appears to be variable due to age-dependent changes in the salicylic acid content and downstream signaling (Patel and Dinesh-Kumar, 2008; Hofius *et al.*, 2009; Yoshimoto *et al.*, 2009; Lenz *et al.*, 2011; Minina *et al.*, 2014; Zhou *et al.*, 2014), their enhanced susceptibility towards different necrotrophic pathogens has been consistently observed (Lai *et al.*, 2011) (Fig. 4). Our finding that *ATG5* and *ATG7* OE lines are more resistant to *A. brassicicola* further suggests an important and direct role for autophagy in plant immunity to necrotrophs. Such a contribution might be related to the suppression of a disease-associated necrotic cell death through removal of plant- or pathogen-derived toxic cellular constituents. Alternatively, autophagy is known to modulate jasmonic acid-dependent signaling positively (Lai *et al.*, 2011), which is an essential component of the immune system against necrotrophic pathogens. The recent observation that the fungus *Sclerotinia sclerotiorum* enhances virulence via phytotoxin-mediated suppression of autophagy further highlights the importance of autophagic mechanisms in the host defense against necrotrophs (Kabbage *et al.*, 2013).

Plants with enhanced autophagy are also more resistant to oxidative stress (Fig. 5) and show an elevated level of expression of genes involved in UV and oxidative stress responses, and anthocyanin and flavonoid biosynthesis (Supplementary Tables S1, S2). These data are in good agreement with the previously reported roles of autophagy in suppressing oxidative damage through clearance of oxidized proteins (Xiong *et al.*, 2007), protein aggregates (Zhou *et al.*, 2014), and defective peroxisomes (Shibata *et al.*, 2013) and with the most recent report suggesting a link between elevated anthocyanin production, clearance of the oxidized proteins and, possibly, enhanced autophagy in the plants overexpressing an apple ortholog of ATG18 (Sun *et al.*, 2017). Further work is required to conclude how general is an improved disease and stress resistance of plants with an elevated level of basal autophagy by studying their responses to other types of pathogens and stresses.

It is important to emphasize that the observed plant phenotypes were highly dependent on growth conditions and were most prominent under standard conditions (16 h light, 150 µE m^{-2} s^{-1} light intensity, 22 °C, 75% humidity).

Phenotypic differences between WT and *ATG*-overexpressing plants greatly diminished under conditions previously shown to induce autophagy in WT plants, namely under light intensity reduced to 100 µE m^{-2} s^{-1} (Minina *et al.*, 2013*b*; unpublished data), suggesting the existence of a wide range within which autophagic activity can be tuned by changing growth conditions.

Concluding remarks

An important question is why do plants not have a constitutively up-regulated autophagy, considering its potential benefits. The high plasticity of autophagic activity and its condition-dependent tuning in WT plants indicate that under highly variable conditions constitutively up-regulated autophagy might be less beneficial than tunable autophagy. For instance, an extended life span might be a drawback in the field environment, exposing plants to suboptimal climate conditions and another set of pathogens. As of yet, we have not been able to identify any fitness costs of constitutively up-regulated autophagy. Further experiments in field conditions will allow us to discover the costs, if they exist.

In conclusion, our work revises an experimental paradigm of autophagy in plant biology by complementing data obtained using *atg* mutants with data obtained using plants with a constitutively elevated level of autophagy due to overexpression of *ATG5* or *ATG7*. In contrast to perturbed growth, decreased fecundity, and compromised stress resistance caused by the autophagy deficiency, elevated autophagy results in delayed aging, enhanced vegetative growth and seed production, increased accumulation of seed lipids, and improved resistance to necrotrophs and oxidative stress; that is, a significant improvement of a number of agronomically important traits. These results obtained in Arabidopsis are reminiscent of the reported anti-aging phenotype of *ATG5*-overexpressing mice, which displayed a longer life span, leanness, increased insulin sensitivity, improved motor function, and oxidative stress resistance (Pyo *et al.*, 2013). Taken together, these results demonstrate a cross-kingdom conservation of the pleiotropic invigorating effect of enhanced autophagy.

Supplementary data

Supplementary data are available at *JXB* online.

Fig. S1. qRT-PCR analysis of *ATG5* and *ATG7* transcripts in WT and *ATG*-overexpressing plants.

Fig. S2. Overexpression of either *ATG5* or *ATG7* does not influence transcription of other components of the ubiquitin-like conjugation systems.

Fig. S3. Simultaneous overexpression of *ATG5* and *ATG7* has the same effect on Atg5–Atg12 conjugation as overexpression of *ATG5* only and causes transcriptional suppression of other components of the two ubiquitin-like conjugation systems.

Fig. S4. Size of GFP-positive puncta measured in the WT, *ATG*-overexpressing, and *ATG*-knockout backgrounds expressing GFP–Atg8a.

Fig. S5. Overexpression of *ATG5* or *ATG7* does not influence the number of rosette leaves or cell size.

Fig. S6. Overexpression of *ATG5* or *ATG7* does not influence the weight of an individual seed.

Fig. S7. Knockout but not overexpression of *ATG5* or *ATG7* alters the composition of seed fatty acids.

Table S1. Selected differentially expressed genes.

Table S2. Developmental trends of gene expression common for both *atg5* and *atg7* mutants and both *ATG5* OE and *ATG7* OE lines.

Table S3. Expression profiles characteristic for both *atg5* and *atg7* mutants and both *ATG5* OE and *ATG7* OE lines at the first time point.

Table S4. Expression profiles characteristic for both *atg5* and *atg7* mutants and both *ATG5* OE and *ATG7* OE lines at the second time point

Table S5. List of primers used in this study

File S1. Guide to genome-wide gene expression analysis.

Methods S1.

Acknowledgements

This work was supported by grants from the Knut and Alice Wallenberg Foundation (to DH and PVB, 19679-006), the Swedish Research Council (to PVB, 20419-000), Pehrssons Fond (to PVB, 16406-000), the Swedish Foundation for Strategic Research (to StSt and PVB, 21236-000), Olle Engkvist Foundation (to PVB, 18510-000), Carl Tryggers Foundation (to EAM, 21196-000) and Trees and Crops for the Future Research Programme (to PVB). We would like to express our sincere gratitude to T. Johansen, Y. Ohsumi, and R. Vierstra for kindly providing us with the antibodies required for this study.

References

AbuQamar S, Chen X, Dhawan R, Bluhm B, Salmeron J, Lam S, Dietrich RA, Mengiste T. 2006. Expression profiling and mutant analysis reveals complex regulatory networks involved in Arabidopsis response to Botrytis infection. The Plant Journal **48,** 28–44.

Avin-Wittenberg T, Bajdzienko K, Wittenberg G, Alseekh S, Tohge T, Bock R, Giavalisco P, Fernie AR. 2015. Global analysis of the role of autophagy in cellular metabolism and energy homeostasis in Arabidopsis seedlings under carbon starvation. The Plant Cell **27,** 306–322.

Bassham DC. 2015. Methods for analysis of autophagy in plants. Methods **75,** 181–188.

Bassham DC, Laporte M, Marty F, Moriyasu Y, Ohsumi Y, Olsen LJ, Yoshimoto K. 2006. Autophagy in development and stress responses of plants. Autophagy **2,** 2–11.

Bates PD, Stymne S, Ohlrogge J. 2013. Biochemical pathways in seed oil synthesis. Current Opinion in Plant Biology **16,** 358–364.

Brown JK. 2002. Yield penalties of disease resistance in crops. Current Opinion in Plant Biology **5,** 339–344.

Cabello JV, Lodeyro AF, Zurbriggen MD. 2014. Novel perspectives for the engineering of abiotic stress tolerance in plants. Current Opinion in Biotechnology **26,** 62–70.

Chen Y, Klionsky DJ. 2011. The regulation of autophagy—unanswered questions. Journal of Cell Science **124,** 161–170.

Choquer M, Fournier E, Kunz C, Levis C, Pradier JM, Simon A, Viaud M. 2007. *Botrytis cinerea* virulence factors: new insights into a necrotrophic and polyphageous pathogen. FEMS Microbiology Letters **277,** 1–10.

Chung T, Phillips AR, Vierstra RD. 2010. ATG8 lipidation and ATG8-mediated autophagy in Arabidopsis require ATG12 expressed from the differentially controlled ATG12A and ATG12B loci. The Plant Journal **62,** 483–493.

Clough SJ, Bent AF. 1998. Floral dip: a simplified method for *Agrobacterium*-mediated transformation of *Arabidopsis thaliana*. The Plant Journal **16,** 735–743.

Dall'Armi C, Devereaux KA, Di Paolo G. 2013. The role of lipids in the control of autophagy. Current Biology **23,** R33–R45.

Doelling JH, Walker JM, Friedman EM, Thompson AR, Vierstra RD. 2002. The APG8/12-activating enzyme APG7 is required for proper nutrient recycling and senescence in *Arabidopsis thaliana*. Journal of Biological Chemistry **277,** 33105–33114.

Elander PH, Minina EA, Bozkov PV. 2018. Autophagy in turnover of lipid stores: trans-kingdom comparison. Journal of Experimental Botany **69,** doi:10.1093/jxb/erx433.

Feng Y, Yao Z, Klionsky DJ. 2015. How to control self-digestion: transcriptional, post-transcriptional, and post-translational regulation of autophagy. Trends in Cell Biology **25,** 354–363.

Fleming A, Noda T, Yoshimori T, Rubinsztein DC. 2011. Chemical modulators of autophagy as biological probes and potential therapeutics. Nature Chemical Biology **7,** 9–17.

Frankel LB, Lund AH. 2012. MicroRNA regulation of autophagy. Carcinogenesis **33,** 2018–2025.

Füllgrabe J, Ghislat G, Cho DH, Rubinsztein DC. 2016. Transcriptional regulation of mammalian autophagy at a glance. Journal of Cell Science **129,** 3059–3066.

Guiboileau A, Avila-Ospina L, Yoshimoto K, Soulay F, Azzopardi M, Marmagne A, Lothier J, Masclaux-Daubresse C. 2013. Physiological and metabolic consequences of autophagy deficiency for the management of nitrogen and protein resources in Arabidopsis leaves depending on nitrate availability. New Phytologist **199,** 683–694.

Guiboileau A, Yoshimoto K, Soulay F, Bataillé MP, Avice JC, Masclaux-Daubresse C. 2012. Autophagy machinery controls nitrogen remobilization at the whole-plant level under both limiting and ample nitrate conditions in Arabidopsis. New Phytologist **194,** 732–740.

Han S, Wang Y, Zheng X, Jia Q, Zhao J, Bai F, Hong Y, Liu Y. 2015. Cytoplastic glyceraldehyde-3-phosphate dehydrogenases interact with ATG3 to negatively regulate autophagy and immunity in *Nicotiana benthamiana*. The Plant Cell **27,** 1316–1331.

Hanaoka H, Noda T, Shirano Y, Kato T, Hayashi H, Shibata D, Tabata S, Ohsumi Y. 2002. Leaf senescence and starvation-induced chlorosis are accelerated by the disruption of an Arabidopsis autophagy gene. Plant Physiology **129,** 1181–1193.

Hofius D, Schultz-Larsen T, Joensen J, *et al*. 2009. Autophagic components contribute to hypersensitive cell death in Arabidopsis. Cell **137,** 773–783.

Hothorn T, Bretz F, Westfall P. 2008. Simultaneous inference in general parametric models. Biometrical Journal J **50,** 346–363.

Inskeep WP, Bloom PR. 1985. Extinction coefficients of chlorophyll a and b in N,N-dimethylformamide and 80% acetone. Plant Physiology **77,** 483–485.

Ishida H, Yoshimoto K, Izumi M, Reisen D, Yano Y, Makino A, Ohsumi Y, Hanson MR, Mae T. 2008. Mobilization of rubisco and stroma-localized fluorescent proteins of chloroplasts to the vacuole by an ATG gene-dependent autophagic process. Plant Physiology **148,** 142–155.

Kabbage M, Williams B, Dickman MB. 2013. Cell death control: the interplay of apoptosis and autophagy in the pathogenicity of *Sclerotinia sclerotiorum*. PLoS Pathogens **9,** e1003287.

Klionsky DJ, Abdelmohsen K, Abe A, *et al*. 2016. Guidelines for the use and interpretation of assays for monitoring autophagy (3rd edition). Autophagy **12,** 1–222.

Laemmli UK. 1970. Cleavage of structural proteins during the assembly of the head of bacteriophage T4. Nature **227,** 680–685.

Lai Z, Wang F, Zheng Z, Fan B, Chen Z. 2011. A critical role of autophagy in plant resistance to necrotrophic fungal pathogens. The Plant Journal **66,** 953–968.

Lapierre LR, Kumsta C, Sandri M, Ballabio A, Hansen M. 2015. Transcriptional and epigenetic regulation of autophagy in aging. Autophagy **11,** 867–880.

Lee JM, Wagner M, Xiao R, Kim KH, Feng D, Lazar MA, Moore DD. 2014. Nutrient-sensing nuclear receptors coordinate autophagy. Nature **516,** 112–115.

Lenz HD, Haller E, Melzer E, *et al*. 2011. Autophagy differentially controls plant basal immunity to biotrophic and necrotrophic pathogens. The Plant Journal **66,** 818–830.

Levine B, Mizushima N, Virgin HW. 2011. Autophagy in immunity and inflammation. Nature **469,** 323–335.

Li F, Chung T, Pennington JG, Federico ML, Kaeppler HF, Kaeppler SM, Otegui MS, Vierstra RD. 2015. Autophagic recycling plays a central role in maize nitrogen remobilization. The Plant Cell **27,** 1389–1408.

Liu K, Czaja MJ. 2013. Regulation of lipid stores and metabolism by lipophagy. Cell Death and Differentiation **20,** 3–11.

Liu Y, Bassham DC. 2012. Autophagy: pathways for self-eating in plant cells. Annual Review of Plant Biology **63,** 215–237.

Ma J, Jin R, Dobry CJ, Lawson SK, Kumar A. 2007. Overexpression of autophagy-related genes inhibits yeast filamentous growth. Autophagy **3,** 604–609.

Masclaux-Daubresse C, Clément G, Anne P, Routaboul JM, Guiboileau A, Soulay F, Shirasu K, Yoshimoto K. 2014. Stitching together the multiple dimensions of autophagy using metabolomics and transcriptomics reveals impacts on metabolism, development, and plant responses to the environment in Arabidopsis. The Plant Cell **26,** 1857–1877.

Mathew R, White E. 2011. Autophagy in tumorigenesis and energy metabolism: friend by day, foe by night. Current Opinion in Genetics and Development **21,** 113–119.

Minina EA, Bozhkov PV, Hofius D. 2014. Autophagy as initiator or executioner of cell death. Trends in Plant Science **19,** 692–697.

Minina EA, Filonova LH, Fukada K, *et al*. 2013*a*. Autophagy and metacaspase determine the mode of cell death in plants. Journal of Cell Biology **203,** 917–927.

Minina EA, Sanchez-Vera V, Moschou PN, Suarez MF, Sundberg E, Weih M, Bozhkov PV. 2013*b*. Autophagy mediates caloric restriction-induced lifespan extension in Arabidopsis. Aging Cell **12,** 327–329.

Mizushima N, Komatsu M. 2011. Autophagy: renovation of cells and tissues. Cell **147,** 728–741.

Nair U, Thumm M, Klionsky DJ, Krick R. 2011. GFP–Atg8 protease protection as a tool to monitor autophagosome biogenesis. Autophagy **7,** 1546–1550.

Nakagawa T, Kurose T, Hino T, *et al*. 2007. Development of series of gateway binary vectors, pGWBs, for realizing efficient construction of fusion genes for plant transformation. Journal of Bioscience and Bioengineering **104,** 34–41.

Nakatogawa H. 2013. Two ubiquitin-like conjugation systems that mediate membrane formation during autophagy. Essays in Biochemistry **55,** 39–50.

Parzych KR, Klionsky DJ. 2014. An overview of autophagy: morphology, mechanism, and regulation. Antioxidants and Redox Signaling **20,** 460–473.

Patel S, Dinesh-Kumar SP. 2008. Arabidopsis ATG6 is required to limit the pathogen-associated cell death response. Autophagy **4,** 20–27.

Pyo JO, Yoo SM, Ahn HH, Nah J, Hong SH, Kam TI, Jung S, Jung YK. 2013. Overexpression of Atg5 in mice activates autophagy and extends lifespan. Nature Communications **4,** 2300.

Rabinowitz JD, White E. 2010. Autophagy and metabolism. Science **330,** 1344–1348.

Ren C, Liu J, Gong Q. 2014. Functions of autophagy in plant carbon and nitrogen metabolism. Frontiers in Plant Science **5,** 301.

Rubinsztein DC, Mariño G, Kroemer G. 2011. Autophagy and aging. Cell **146,** 682–695.

Scott RC, Juhász G, Neufeld TP. 2007. Direct induction of autophagy by Atg1 inhibits cell growth and induces apoptotic cell death. Current Biology **17,** 1–11.

Seok S, Fu T, Choi SE, *et al*. 2014. Transcriptional regulation of autophagy by an FXR–CREB axis. Nature **516,** 108–111.

Shibata M, Oikawa K, Yoshimoto K, *et al*. 2013. Highly oxidized peroxisomes are selectively degraded via autophagy in Arabidopsis. The Plant Cell **25,** 4967–4983.

Shibutani ST, Yoshimori T. 2014. A current perspective of autophagosome biogenesis. Cell Research **24,** 58–68.

Singh R, Kaushik S, Wang Y, Xiang Y, Novak I, Komatsu M, Tanaka K, Cuervo AM, Czaja MJ. 2009. Autophagy regulates lipid metabolism. Nature **458,** 1131–1135.

Slavikova S, Ufaz S, Avin-Wittenberg T, Levanony H, Galili G. 2008. An autophagy-associated Atg8 protein is involved in the responses of Arabidopsis seedlings to hormonal controls and abiotic stresses. Journal of Experimental Botany **59,** 4029–4043.

Sun X, Wang P, Jia X, Huo L, Che R, Ma F. 2017. Improvement of drought tolerance by overexpressing MdATG18a is mediated by modified antioxidant system and activated autophagy in transgenic apple. Plant Biotechnology Journal. doi: 10.1111/pbi.12794

Sun X, Jia X, Huo L, Che R, Gong X, Wang P, Ma F. 2018. MdATG18a overexpression improves tolerance to nitrogen deficiency and regulates anthocyanin accumulation through increased autophagy in transgenic apple. Plant, Cell and Environment **41:** 469–480.

Svenning S, Lamark T, Krause K, Johansen T. 2011. Plant NBR1 is a selective autophagy substrate and a functional hybrid of the mammalian autophagic adapters NBR1 and p62/SQSTM1. Autophagy **7,** 993–1010.

Thomma BPHJ, Eggermont K, Penninckx IAMA, Mauch-Mani B, Vogelsang R, Cammue BPA, Broekaert WF. 1998. Separate jasmonate-dependent and salicylate-dependent defense-response pathways in Arabidopsis are essential for resistance to distinct microbial pathogens. Proceedings of the National Academy of Sciences, USA **95,** 15107–15111.

Thompson AR, Doelling JH, Suttangkakul A, Vierstra RD. 2005. Autophagic nutrient recycling in Arabidopsis directed by the ATG8 and ATG12 conjugation pathways. Plant Physiology **138,** 2097–2110.

Wada S, Hayashida Y, Izumi M, *et al*. 2015. Autophagy supports biomass production and nitrogen use efficiency at the vegetative stage in rice. Plant Physiology **168,** 60–73.

Wada S, Ishida H, Izumi M, Yoshimoto K, Ohsumi Y, Mae T, Makino A. 2009. Autophagy plays a role in chloroplast degradation during senescence in individually darkened leaves. Plant Physiology **149,** 885–893.

Wang P, Sun X, Jia X, Ma F. 2017. Apple autophagy-related protein MdATG3s afford tolerance to multiple abiotic stresses. Plant Science **256,** 53–64.

Wang P, Sun X, Wang N, Jia X, Ma F. 2016. Ectopic expression of an autophagy-associated MdATG7b gene from apple alters growth and tolerance to nutrient stress in *Arabidopsis thaliana*. Plant Cell, Tissue and Organ Culture 1–15.

Wang Y, Yu B, Zhao J, *et al*. 2013. Autophagy contributes to leaf starch degradation. The Plant Cell **25,** 1383–1399.

Wingenter K, Schulz A, Wormit A, *et al*. 2010. Increased activity of the vacuolar monosaccharide transporter TMT1 alters cellular sugar partitioning, sugar signaling, and seed yield in Arabidopsis. Plant Physiology **154,** 665–677.

Wuyts N, Palauqui JC, Conejero G, Verdeil JL, Granier C, Massonnet C. 2010. High-contrast three-dimensional imaging of the Arabidopsis leaf enables the analysis of cell dimensions in the epidermis and mesophyll. Plant Methods **6,** 17.

Xia T, Xiao D, Liu D, Chai W, Gong Q, Wang NN. 2012. Heterologous expression of ATG8c from soybean confers tolerance to nitrogen deficiency and increases yield in Arabidopsis. PLoS One **7,** e37217.

Xie Q, Michaeli S, Peled-Zehavi H, Galili G. 2015. Chloroplast degradation: one organelle, multiple degradation pathways. Trends in Plant Science **20,** 264–265.

Xiong Y, Contento AL, Nguyen PQ, Bassham DC. 2007. Degradation of oxidized proteins by autophagy during oxidative stress in Arabidopsis. Plant Physiology **143,** 291–299.

Yang Z, Klionsky DJ. 2010. Eaten alive: a history of macroautophagy. Nature Cell Biology **12,** 814–822.

Yoshimoto K, Hanaoka H, Sato S, Kato T, Tabata S, Noda T, Ohsumi Y. 2004. Processing of ATG8s, ubiquitin-like proteins, and their deconjugation by ATG4s are essential for plant autophagy. The Plant Cell **16,** 2967–2983.

Yoshimoto K, Jikumaru Y, Kamiya Y, Kusano M, Consonni C, Panstruga R, Ohsumi Y, Shirasu K. 2009. Autophagy negatively regulates cell death by controlling NPR1-dependent salicylic acid signaling during senescence and the innate immune response in Arabidopsis. The Plant Cell **21,** 2914–2927.

Zhang Y, Goldman S, Baerga R, Zhao Y, Komatsu M, Jin SK. 2009. Adipose-specific deletion of autophagy-related gene 7 (atg7) in mice reveals a role in adipogenesis. Proceedings of the National Academy of Sciences, USA **106,** 19860–19865.

Zhou J, Wang J, Cheng Y, Chi YJ, Fan B, Yu JQ, Chen Z. 2013. NBR1-mediated selective autophagy targets insoluble ubiquitinated protein aggregates in plant stress responses. PLoS Genetics **9,** e1003196.

Zhou J, Yu JQ, Chen Z. 2014. The perplexing role of autophagy in plant innate immune responses. Molecular Plant Pathology **15,** 637–645.

III

Journal of Experimental Botany, Vol. 69, No. 6 pp. 1301–1311, 2018
doi:10.1093/jxb/erx433 Advance Access publication 23 December 2017

REVIEW PAPER

Autophagy in turnover of lipid stores: trans-kingdom comparison

Pernilla H. Elander*, Elena A. Minina* and Peter V. Bozhkov*

Department of Molecular Sciences, Uppsala BioCenter, Swedish University of Agricultural Sciences and Linnean Center for Plant Biology, PO Box 7015, SE-75007 Uppsala, Sweden

* Correspondence: pernilla.elander@slu.se, alena.minina@slu.se, peter.bozhkov@slu.se

Dedicated to Professor Sten Stymne on the occasion of his retirement.

Received 8 September 2017; Editorial decision 14 November 2017; Accepted 14 November 2017

Editor: Christine Raines, University of Essex, UK

Abstract

Lipids and their cellular utilization are essential for life. Not only are lipids energy storage molecules, but their diverse structural and physical properties underlie various aspects of eukaryotic biology, such as membrane structure, signalling, and trafficking. In the ever-changing environment of cells, lipids, like other cellular components, are regularly recycled to uphold the housekeeping processes required for cell survival and organism longevity. The ways in which lipids are recycled, however, vary between different phyla. For example, animals and plants have evolved distinct lipid degradation pathways. The major cell recycling system, autophagy, has been shown to be instrumental for both differentiation of specialized fat storing-cells, adipocytes, and fat degradation in animals. Does plant autophagy play a similar role in storage and degradation of lipids? In this review, we discuss and compare implications of bulk autophagy and its selective route, lipophagy, in the turnover of lipid stores in animals, fungi, and plants.

Keywords: Autophagy, catabolism, fatty acids, lipases, lipid droplet, lipophagy, lipolysis, β-oxidation, plastoglobule, triacylglycerols.

Introduction

Most organisms use lipids as a source of energy at times when other energy supplies are scarce, one dramatic example being plant seed germination and early seedling growth (Murphy, 2001). Lipids are commonly stored as triacyglycerols (TAGs) in spherical organelles contained within a monolayer of phospholipids and membrane proteins. These organelles have several alternative names: lipid bodies, lipid droplets (LDs), and the more plant-specific names, oleosomes and oil bodies. For clarity, we will refer to these organelles as LDs throughout this review. LDs vary in size and amount depending on cell type and organism. While highly specialized fat-storing animal cells, adipocytes, have single LDs up to 100 µm in diameter, other mammalian cell types and also those from plants harbour much smaller LDs of ~0.5–2.5 µm in diameter. Cells of oil seeds can accumulate up to thousands of such small LDs per cell (Schmid and Ohlrogge, 2002; Jolivet *et al.*, 2004).

Recent research in mammalian systems revealed intricate relationships between the life cycle of LDs and autophagy, the major catabolic process in eukaryotic cells. Upon activation of autophagy, a portion of the cytoplasm is engulfed by a cup-shaped double membrane structure (phagophore) that grows around the cargo and closes on itself forming an autophagosome (Feng *et al.*, 2014). This double membrane

Abbreviations: ACSL, acyl-coenzyme A synthetase; AMPK, AMP-activated protein kinase; ATG, AuTophaGy-related proteins; ATGL, adipose triglyceride lipase; CIDE, cell death-inducing DNA fragmentation factor 45-like effector; DHAP, dihydroxyacetone phosphate; ER, endoplasmic reticulum; FA, fatty acid; FIT, fat storage-inducing transmembrane protein; LACS, long-chain acyl-coenzyme A synthetase; LD, lipid droplet; PCD, programmed cell death; PG, plastoglobule; PPARγ2, peroxisome proliferator-activated receptor; SDP1, sugar dependent protein1; SNARE, soluble *N*-ethylamide-sensitive factor attachment protein receptor; TAG, triacylglycerol.

© The Author(s) 2017. Published by Oxford University Press on behalf of the Society for Experimental Biology. All rights reserved.
For permissions, please email: journals.permissions@oup.com

vesicle delivers its cargo to the lysosome (in animals) or the lytic vacuole (in fungi and plants) where it is digested by hydrolytic enzymes. Autophagy is controlled by a specialized set of AuTophaGy-related, *ATG*, genes which are conserved in most eukaryotes (Ohsumi, 2014). Under normal conditions, basal autophagy functions as a housekeeping process clearing away damaged or surplus cell contents. During stress or starvation, the rate of autophagic degradation activity (autophagic flux) is enhanced. This promotes cell survival by removing damaged macromolecules and organelles and recycling cell content to 'feed' cells with breakdown products which can be used as a source of energy and for biosynthesis (Mizushima and Komatsu, 2011).

The same harsh conditions activate breakdown of LDs to generate free fatty acids (FAs) that fuel cellular rates of mitochondrial oxidation. It has been shown that apart from canonical lipolysis operating in the cytoplasm of mammalian cells, a form of selective autophagy named 'lipophagy' or 'macrolipophagy' also contributes to LD degradation (Singh *et al.*, 2009*a*; Liu and Czaja, 2013; Zechner *et al.*, 2017). In addition to the role of autophagy in clearing LDs, it is also required for the differentiation of specialized adipocyte cells containing giant LDs (Zhang *et al.*, 2013). Therefore, autophagy is implicated in both breakdown and accumulation of LDs in animals, representing the primary target to manipulate lipid metabolism *in vivo* and intervene in the development of lipid storage disorders, such as type 2 diabetes (Ducharme and Bickel, 2008).

Compared with animals, the knowledge about implications of autophagy for the turnover of LDs in plants has just begun to emerge. We anticipate that this field might soon start growing rapidly, especially considering the potential to enhance the productivity of oil crops by targeted manipulation of autophagy. This review provides timely synthesis and comparison of current knowledge about regulation of LD turnover in plants versus animals and fungi, with special reference to autophagy.

Formation of LDs

LD formation is an evolutionarily conserved process. Generally, LDs are derived from the endoplasmic reticulum (ER) by a process involving accumulation of neutral lipids, mainly TAGs, between the two leaflets of the ER membrane. TAGs within the bilayer exist in either solitary form or clustered in unstable structures called pre-droplets. The formation of LDs is divided into three major steps, namely nucleation, growth, and budding (for a detailed review, see Thiam and Forêt, 2016; Table 1).

Nucleation is the initial accumulation of TAGs when pre-droplets form stable nascent LDs. Whether this step is spontaneous, enzymatically controlled, or both is not yet completely clear. However, a spontaneous phase separation, also called demixing, is a well-understood phenomenon and is a plausible molecular event to occur between TAG and phospholipid molecules in the bilayer leaflet. For spontaneous demixing to take place, two primary conditions have to be fulfilled (Thiam and Forêt, 2016). First, the energy cost of the interaction between different types of molecules must be higher than the cost between molecules of the same type. In this case, TAG molecules interacting with each other rather than with phospholipid molecules represent the less energetically costly state. Secondly, the concentration of TAG molecules must exceed a certain threshold level (Barrat and Hansen, 2003). These conditions taken together are referred to as the nucleation barrier which, as the word implies, needs to be overcome for nascent LDs to form.

The composition of the ER membrane is not uniform, and this opens up the possibility that some parts of the membrane can be less energetically costly for demixing, which would reduce the nucleation barrier. Such membrane-impacting factors could, for example, be protrusion tips, which are highly bent parts of the ER, a result of phospholipid packing defects. Also TAG synthesis sites, and the presence of curvature-inducing proteins could be sites of LD nucleation. Proteins shown or proposed to regulate LD nucleation in animals (Table 1) are fat storage-inducing transmembrane (FIT) proteins (Gross *et al.*, 2011), perilipins perilipin 1/PLIN1 (Kimmel *et al.*, 2010; Yang *et al.*, 2012), adipophilin/PLIN2 (Robenek *et al.*, 2006; Kimmel *et al.*, 2010), and TIP47/PLIN3 (Bulankina *et al.*, 2009; Kimmel *et al.*, 2010), as well as acyl-CoA synthetases (ACSLs; Fujimoto *et al.*, 2007), seipins (Cartwright *et al.*, 2015), and lipins (Sembongi *et al.*, 2013). Also other proteins and lipids favouring TAG interaction might have a role in LD nucleation (Thiam and Forêt, 2016).

Fungi also express FIT proteins but they have not, in contrast to animals, been found to function in LD nucleation (Moir *et al.*, 2012). Although perilipins were thought not to exist in fungi, Gao *et al.*, (2017) have recently proposed the LD-localized Pet10p to be the first yeast perilipin essential for the early steps of LD assembly. The seipin Fld1p (Szymanski *et al.*, 2007) and lipin Pah1p (Adeyo *et al.*, 2011) are also components of the fungal LD nucleation machinery. Although plants lack direct homologues of both FIT and perilipin family proteins, ectopically expressed murine FIT2 protein is functional and is able to increase LD accumulation and oil content in *Arabidopsis thaliana* (Cai *et al.*, 2017). There are nine ACSL enzymes in Arabidopsis, named long-chain acyl-coenzyme A synthetases (LACSs). While the mechanistic role of LACSs in plants is not completely understood, LACS1 and 9 have been demonstrated to contribute to TAG biosynthesis (Zhao *et al.*, 2010). Plants have three or more seipin proteins, in contrast to the single seipin in animals and fungi. Together with caleosins, they have been proposed to take part in LD nucleation (Shen *et al.*, 2014; Cai *et al.*, 2015; Table1).

The growth of LDs can occur in different ways. If the flow of TAG molecules to different nascent LDs is equal, the nascent LDs will not influence each other. However, if there is a difference in the flow of TAGs to the nascent LDs, there will be a change in Laplace pressure, which will in turn induce a flux of TAGs from smaller nascent LDs to larger ones. In adipocytes, this process is mediated by the LD–LD contact site cell death-inducing DNA fragmentation factor 45-like effector (CIDE) protein Fsp27 which mediates lipid exchange between LDs (Gong *et al.*, 2011). CIDE proteins do not have direct homologues in plants or fungi. Fusion between two nascent droplets is another possible mechanism

Table 1. *Trans-kingdom comparison of proteins regulating LD formation*

Step of LD formation	Regulators	Animals	Fungi	Plants
Nucleation	**FIT proteins**	Yes (Kadereit *et al.*, 2008)	No such function (Moir *et al.*, 2012)	Possibly[a] (Cai *et al.*, 2017)
	Perilipins	Possibly[a] (PLIN1/Perilipin 1; Yang *et al.*, 2012) Yes (PLIN2/Adipophilin; Robenek *et al.*, 2006) Yes (PLIN3/TIP47; Bulankina *et al.*, 2009) Possibly[a] (PLIN4; Itabe *et al.*, 2017) Possibly[a] (PLIN5; Beller *et al.*, 2010)	Yes (Pet10p; Gao *et al.*, 2017)	Absent
	ACSLs	Yes (Fujimoto *et al.*, 2007) Yes (ACSL3; Kassan *et al.*, 2013)	No data available	Yes (LACS1, LACS9; Zhao *et al.*, 2010)
	Caleosins	Absent	No data available	Possibly[a] (Shen *et al.*, 2014)
	Seipins	Yes (Cartwright *et al.*, 2015)	Yes (Fld1p; Szymanski *et al.*, 2007)	Possibly[a] (seipin1; Cai *et al.*, 2015)
	Lipins	Yes (Sembongi *et al.*, 2013)	Yes (Pah1p; Adeyo *et al.*, 2011)	No data available
Growth	**FIT proteins**	Possibly[a] (Gross *et al.*, 2011)	No such function (Moir *et al.*, 2012)	Possibly[a] (Cai *et al.*, 2017)
	CIDE proteins	Yes (Fsp27; Gong *et al.*, 2011)	Absent	Absent
	SNAREs	Possibly[a] (Boström *et al.*, 2007)	No data available	No data available
	ACSLs	Yes (ACSL3; Kassan *et al.*, 2013)	No data available	Possibly[a] (LACS1, LACS9; Zhao *et al.*, 2010)
	Seipins	Yes (Salo *et al.*, 2016)	Yes (Fld1p; Fei *et al.*, 2008)	Yes (Cai *et al.*, 2015)
	Caleosins	Absent	Possibly[a] (Bbcal1; Fan *et al.*, 2015)	Possibly[a] (Shen *et al.*, 2014)
	Caveolins	Possibly[a] (Blouin *et al.*, 2010)	Absent	Absent
	Oleosins	Absent	Absent	Possibly[a] (Frandsen *et al.*, 2001)
Budding	**FIT proteins**	Yes (Choudhary *et al.*, 2015)	Yes (Choudhary *et al.*, 2015)	Possibly[a] (Cai *et al.*, 2017)
	Perilipins	Possibly[a] (Thiam *et al.*, 2013)	No data available	Absent
	Seipins	No data available	Yes (Cartwright *et al.*, 2015)	No data available
	Caleosins	Absent	Possibly[a] (Bbcal1; Fan *et al.*, 2015)	No data available
	Oleosins	Absent	Absent	Possibly[a] (Frandsen *et al.*, 2001)
LD release to the cytoplasm	**Oleosins**	Absent	Absent	Yes (Huang and Huang, 2017)

[a]Proposed role with no direct experimental evidence.

of LD growth. This occurs when two pre-droplets or nascent LDs laterally approach each other and coalesce when they are close enough. In addition to CIDE protein Fsp27 (Gong *et al.*, 2011), ACSL3 (Kassan *et al.*, 2013) and seipin have been shown to regulate LD growth and fusion in animals. Seipin is associated with ER–LD contact sites in human cells where it is suggested to facilitate the transfer of protein and lipid cargo to the growing LDs (Salo *et al.*, 2016). Seipin is also found to regulate LD growth in plants and fungi. Individual expression of Arabidopsis seipins 1, 2, and 3 in leaves of *Nicotiana benthamiana* revealed that seipin 1 promotes accumulation of large-sized LDs, while seipins 2 and 3 promote accumulation of small LDs (Cai *et al.*, 2015; Table 1). Furthermore, reduced expression of seipin 1 in Arabidopsis resulted in reduced seed size and amount of TAGs per seed (Cai *et al.*, 2015).

Seipin-deficient *fld1p Saccharomyces cerevisiae* cells display overgrown LDs, suggesting that Fld1p modulates LD fusion by an alteration of the physical property of the LD surface (Fei *et al.*, 2008). ACSLs have thus far not been shown to function in fungal LD nucleation or growth, but LACS1 and LACS9 might have a role in LD growth in plants (Zhao *et al.*, 2010; Table 1).

For the LD to bud off from the ER, it needs to form a nearly spherical droplet. Several proteins, as well as the surface interplay of ER, LD, and cytoplasm, can mediate this process. The LD's position between the ER and cytoplasm can be envisaged as three different phases with different surface tension. This tension plays the major role when the LD buds off and is released into the cytoplasm. The corresponding phenomenon is called dewetting, and is the opposite of wetting where a liquid spreads evenly on a surface resulting in a film. Dewetting is hence the formation of a droplet from a film. The surface tension of the ER–cytosolic monolayer and ER–lumen monolayer is probably similar, so it is a shift in the tension that will initiate the formation of an LD bud. This shift can be facilitated by the activity of phospholipid-modifying proteins (Cartwright *et al.*, 2015), membrane-bound proiteins (Kassan *et al.*, 2013), and transmembrane proteins (Choudhary *et al.*, 2015). In mammals, the nematode *Caenorhabditis elegans*, and yeast, FIT proteins are required for proper budding of LDs. Yeast FIT mutants display blocked LD budding, whereas FIT mutants of *C. elegans* exhibit decreased LD number and size, leading to lethality (Choudhary *et al.*, 2015). Other proteins with membrane-deforming activities but as not yet confirmed impact on LD

budding from the ER are the protein complex Arf1/COPI, which was shown to be sufficient to bud off nano-LDs from larger LDs in *Drosophila melanogaster* cells *in vitro* (Wilfling *et al.*, 2014). FIT proteins as well as oleosins (plant counterparts of animal caveolins) have also been suggested to play a role in LD budding in plants (Frandsen *et al.*, 2001; Cai *et al.*, 2017; Table1).

On completion of LD biogenesis, the LDs should not only bud off the ER membrane but also be released to the cytosol. Interestingly, in fungi it is still unclear whether LDs indeed bud off from the ER; at least in the budding yeast *S. cerevisiae* this does not seem to occur (Jacquier *et al.*, 2011). A recent *in vitro* study by Ben M'barek *et al.* (2017) has revealed a major impact of phospholipids and surface tension upon LD budding, when the phospholipid composition regulates the membrane surface tension. However, the budding LDs still need to be released into the cytosol rather than into the ER lumen. Although regulation of this directionality remains largely elusive, a recent study has established that oleosins have a key role in cytosolic directional release of ER-budding LDs in plants (Huang and Huang, 2017; Table 1).

Importantly, beside classic ER-derived LDs, plants have an additional type of lipoprotein particles derived from and localized on the thylakoid membrane of chloroplasts and known as plastoglobuli (PGs). We introduce PGs here because of potential involvement of autophagy in their turnover. However, due to space limitation, we do not describe the PG biogenesis process and instead refer readers to the relevant literature (Austin *et al.*, 2006; Rottet, *et al.*, 2015).

The role of autophagy in lipid deposition

The role of autophagy in the differentiation of lipid-storing cells in animals

Besides the housekeeping recycling purpose, autophagy can also re-model cellular contents during cell differentiation (Mizushima and Levine, 2010). Animals, in contrast to plants, have a specialized fat-storing tissue composed of terminally differentiated cells called adipocytes. The volume of adipocyte cells is almost entirely occupied by a single large LD, while the cytoplasm is greatly reduced. Thus, there is a requirement for massive cytoplasmic remodelling during the differentiation of these cells from mesenchymal (adult bone marrow) stem cells (Fig. 1). It has been shown that adipocyte differentiation correlates with enhanced autophagic flux (Baerga *et al.*, 2009; Zhang *et al.*, 2009). Accordingly, knockout of either *ATG5* or *ATG7* results in dramatic suppression of adipocyte differentiation (Baerga *et al.*, 2009; Zhang *et al.*, 2009) and a decrease in TAG accumulation in pre-adipocytes (Singh *et al.*, 2009*b*). *In vivo* studies have also revealed early neonatal death of *atg5* or *atg7* knockout mice, associated with decreased amino acid levels, reduced white adipose tissue, and smaller adipocytes containing multilocular LDs instead of a single large LD (Kuma *et al.*, 2004; Zhang *et al.*, 2009). These characteristics are more typical for brown than white fat tissue, which has been confirmed by detection of brown fat tissue-specific enzymes within the white fat tissue of the mutant mice (Singh *et al.*, 2009*b*; Zhang *et al.*, 2009). Apart from being the main remodeller of the pre-adipocyte cells, autophagy also seems to exert its effect on adipocyte differentiation through stabilization of the peroxisome proliferator-activated receptor (PPARγ2), a central transcription factor of adipogenesis. This autophagy-mediated stabilization of PPARγ2 is achieved by hindering its proteosomal degradation (Zhang *et al.*, 2013).

During stress, free FAs are remobilized from adipose tissue to accumulate in the liver as LDs. Apart from a growing body of evidence implicating autophagy in adipocyte differentiation, autophagy might also play a role in the accumulation of LDs in hepatocytes (liver cells; Fig.1), although the results thus far are contradictory. Indeed, knockout of *ATG7* in hepatocytes in two different laboratories led to contrasting results, namely suppression (Shibata *et al.*, 2009) versus stimulation (Singh *et al.*, 2009*a*) of LD formation, and thus TAG accumulation in mice hepatocytes after starvation. The two laboratories used the same mice lines, but the mice differed in age by ~70 d, which could partly explain the contradictory results. Furthermore, *ATG7* has been suggested to play different roles in the response to starvation and normal feeding (Mizushima and Levine, 2010). Both Shibata *et al.* (2009) and Singh *et al.* (2009*a*), however, observed ATG8 (LC3 in animals) localization to LDs in hepatocytes under starvation conditions. A recent study in yeast further supports the role of ATG8 in the formation of LDs, however uncoupled from the rest of the autophagy machinery (Maeda *et al.*, 2017). The authors report a reduction of LD size in the *atg8* mutant and, accordingly, formation of enlarged LDs and increased TAG content upon overexpression of ATG8.

The role of autophagy in the differentiation of lipid-storing cells in plants

Plants can accumulate large amounts of TAGs within LDs in specialized cells, such as cells of the endosperm and embryonic organs (cotyledons and hypocotyl; Chapman and Ohlrogge, 2012). The role of autophagy in the differentiation of these cells and/or formation of LDs remains unexplored. Yet, some indirect evidence comes from a study by Kurusu *et al.* (2014) who examined the role of autophagy in male reproductive development in rice, *Oryza sativa* (Fig. 1). The tapetum, the innermost layer of the anther, provides nutrients and lipid components to the developing microspore. In *Brassica* species the tapetal cells harbour specific vesicle- and LD-containing organelles, tapetosomes. Monocots such as rice do not have tapetosomes but display LDs within the tapetal cells (Hsieh and Huang, 2007). The autophagy-deficient knockout rice mutant *Osatg7* displayed the absence of LDs in tapetal cells, reduced TAG content in pollen grains, and complete sporophytic male sterility (Kurusu *et al.*, 2014). In addition, *Osatg7* plants had incomplete degradation of the tapetal cells by programmed cell death (PCD), the process known to play an important role in pollen development and fertility (Fig. 1; Ku *et al.*, 2003; Li *et al.*, 2006). Therefore, autophagy might in this case be required not only for the formation of tapetal LDs but also for the activation or execution

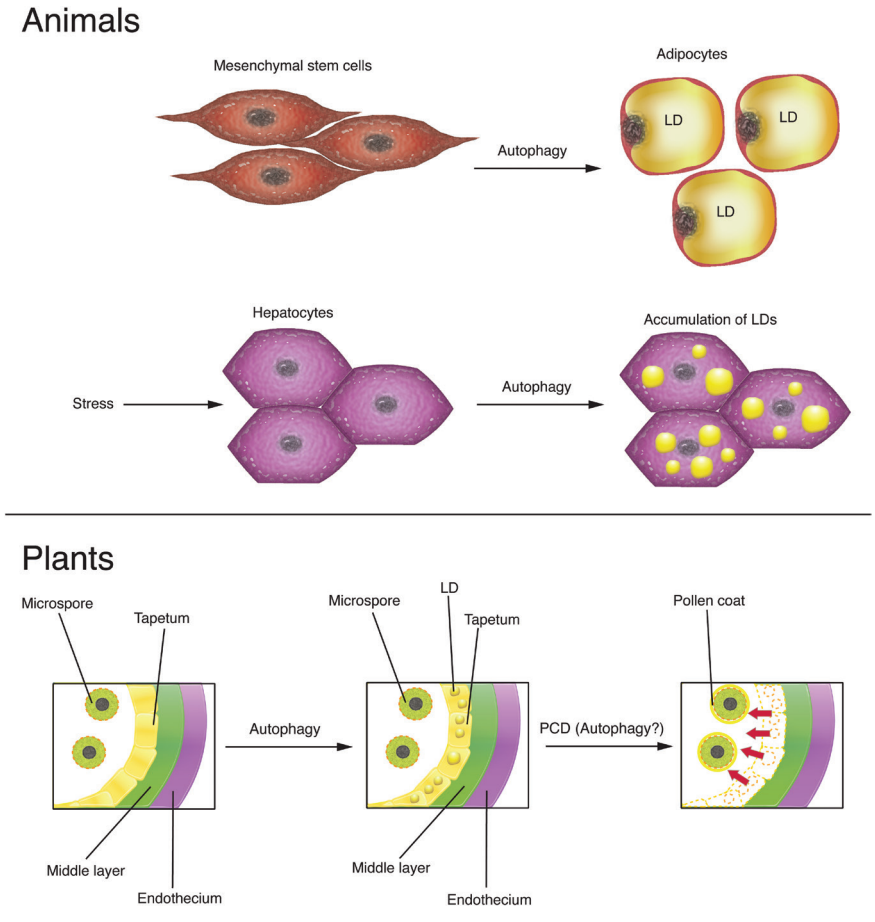

Fig. 1. The role of autophagy in lipid deposition In animals, the differentiation of mesenchymal stem cells into adipocytes involves autophagy-dependent cell remodelling, whereas hepatocytes (liver cells) subjected to starvation activate autophagy to accumulate LDs. In rice plants, autophagy confers accumulation of LDs within tapetal cells and might also be required for the degeneration of the tapetum by PCD, leading to the remobilization of lipids from tapetal LDs to form the pollen coat (red arrows).

of the developmentally regulated PCD (Minina *et al.*, 2014). Kurusu *et al.* (2014) have also revealed that autophagy deficiency affects plant lipid metabolism by showing impaired phosphatidylcholine editing and lipid desaturation in *Osatg7* mutants, which can be an additional factor causing pollen sterility. Importantly, the Arabidopsis *atg6* mutant is also male-sterile due to a failure in pollen germination (Fujiki, *et al.*, 2007), but, since the other *atg* mutants are fertile in Arabidopsis (Yoshimoto, 2012), one can assume that the Atg6-mediated effect on pollen development is independent of autophagy.

Further evidence for the potential role of autophagy in the formation of LDs in plants comes from the recent study of the unicellular algae *Chlamydomonas reinhardtii* (Couso *et al.*, 2018). Cells deprived of nitrogen or phosphate accumulated large numbers of LDs, an effect abolished by the application of the vacuolar ATPase inhibitor concanamycin A that blocks autophagic flux. The authors hypothesize that the autophagic turnover of cellular material under nutrient stress is required for TAG biosynthesis and the formation of LDs (Couso *et al.*, 2018).

LD catabolism

LD catabolism in plants

Plant LDs serve as transient FA storage necessary for membrane building or generation of energy, primarily during seed germination. In the cotyledons from oil-rich seeds, FAs are degraded via β-oxidation in a specialized type of peroxisomes

named glyoxysomes. These organelles are metabolically distinct from peroxisomes due to the presence of two enzymes unique to the glyoxylate cycle: malate synthase and isocitrate lyase. Glyoxysomes perform β-oxidation during seed germination and senescence (Nishimura *et al.*, 1993), whereas other specialized and unspecialized peroxisomes carry out β-oxidation during other developmental stages (reviewed in Beevers, 1979). While most plants harbour most of their LDs in the seeds, all necessary enzymes for TAG synthesis, however, exist in leaves (Chapman and Ohlrogge, 2012) and the oil content in seeds versus leaves varies among different plant families (Lersten *et al.*, 2006). Yet, the major wave of LD degradation takes place in the cotyledons upon seed germination to provide the seedling with energy for growth before the photosynthetic machinery is established.

There are several lipases found to be involved in LD lipolysis, with sugar dependent protein1 (SDP1; Eastmond, 2006) and SDP1-LIKE (SDP1L; Kelly *et al.*, 2011) being the major enzymes executing TAG breakdown (Fig. 2). Together, they are responsible for >95% of the initial step of LD degradation in Arabidopsis seedlings (Kelly *et al.*, 2011). SDP1 and SDP1L are patatin-like TAG lipases carrying out the initial hydrolysis of TAGs to free FAs and glycerol. After the initial hydrolysis, the FAs are subjected to β-oxidation in glyoxysomes or peroxisomes. The transport of FAs into the peroxisome/glyoxysome is mediated by an ABC transporter which was identified in three independent screens and thus independently named *PEROXISOMAL ABC TRANSPORTER 1* (*PXA1*; Zolman *et al.*, 2001), *PEROXISOME DEFICIENT 3* (*PED3*; Hayashi *et al.*, 2002), and *COMATOSE* (*CTS*; Footitt *et al.*, 2002). β-Oxidation in the glyoxysome is initiated by an esterification of FAs to acyl-CoAs by LACSs, and proceeds in four-step cycles which are repeated until the initial acyl-CoA molecule is oxidized into a two-carbon-long acetyl-CoA (Shockey *et al.*, 2002). The acetyl-CoAs from the β-oxidation can be further converted to four-carbon carbohydrates via the glyoxylate cycle, also operating in the glyoxysomes. In cotyledons and senescing leaves, the carbohydrates are then exported from the glyoxysomes to the cytosol and mitochondria as substrates for gluconeogenesis, sucrose synthesis, and subsequent ATP production (Fig.2).

TAG degradation by SDP1 and SDP1L also yields, besides FAs, free glycerol. Free glycerol has long been known to be converted to sucrose in the germinated seedlings (Beevers, 1956). However, the pathway responsible for this conversion remained elusive until Eastmond (2004) made a

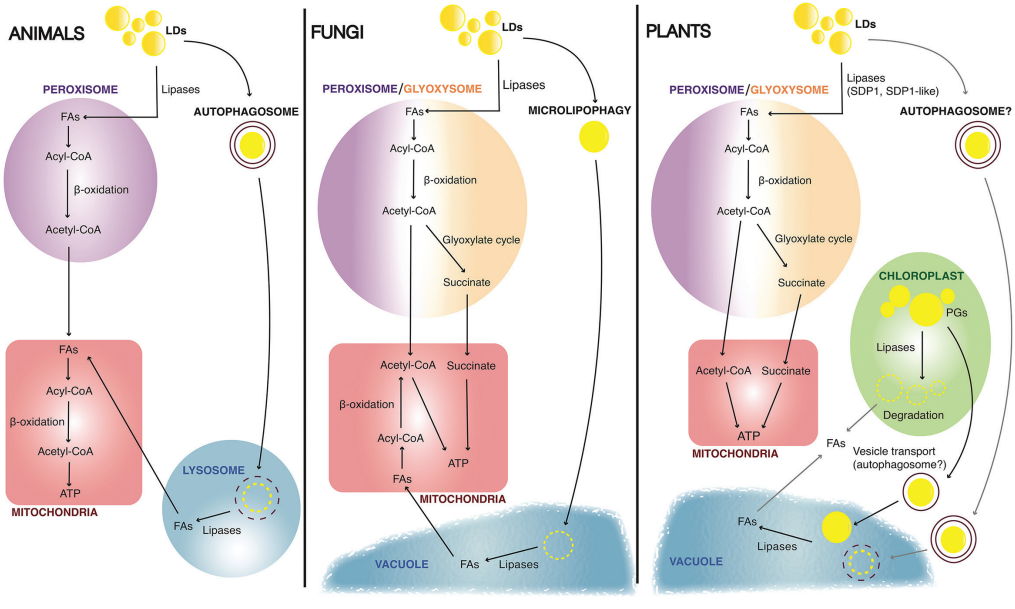

Fig. 2. Cross-kingdom comparison of LD degradation pathways. Animals, apart from cytosolic lipolysis and subsequent β-oxidation of free fatty acids (FAs) in peroxisomes and mitochondria, have evolved an LD degradation pathway through macroautophagy (autophagy), called lipophagy. The LDs are engulfed by autophagosomes and delivered to the lysosome for degradation to release free FAs. Fungi feature an alternative autophagy-like process of LD degradation called microlipophagy, whereupon LDs are directly engulfed by the vacuole. The resulting free FAs are, as in animal systems, transferred to the mitochondria for β-oxidation. Plants differ from animal and fungal systems by harbouring different types of lipid bodies, with ER-derived LDs and plastid-derived plastoglobules (PGs) being the best characterized types. LDs and PGs take different degradation pathways. While LDs undergo cytosolic lipolysis carried out by SDP1 and SDP1-like lipases, PGs have been shown to be transferred to the vacuole, presumably by autophagosomes or via microlipophagy. Whether autophagy participates in the degradation of ER-derived LDs in plants thus remains elusive. β-Oxidation of free FAs in plants takes place in peroxisomes and glyoxysomes. Peroxisomes in fungi also harbour the glyoxylate cycle, and older literature refers to these organelles as glyoxysomes. Black arrows indicate known pathways, whereas grey arrows (in the part of the figure dedicated to plants) indicate hypothetical pathways.

screen of glycerol-insensitive mutants and found that glycerol is converted to glycerol-3-phosphate and subsequently to dihydroxyacetone phosphate (DHAP) catalysed by glycerol-3-phosphate dehydrogenase. DHAP then proceeds through gluconeogenesis.

Role of autophagy in LD catabolism in animals and fungi

The process of autophagy-mediated selective degradation of LDs termed lipophagy represents a pivotal mechanism of lipid turnover in animal and fungal cells (Ward *et al.*, 2016; Zechner *et al.*, 2017). Lipid degradation by lipophagy can be executed via macro- or microlipophagy. During macrolipophagy, the phagophore either engulfs small LDs or sequesters portions of larger LDs. The autophagosomes deliver the LDs to the lysosome or vacuole where they are degraded to release free FAs, which can be transported to the mitochondria for β-oxidation and production of ATP (Fig.2). Macrolipophagy is well studied in animals, whereas the mechanism of direct engulfment of LDs by the vacuole or lysosome (i.e. microlipophagy) has not received much attention. Microlipophagy might, however, have an important function in, for example, hepatic lipophagy (Schulze *et al.*, 2017). In contrast to animals, microlipophagy constitutes the main LD degradation pathway in fungi and is especially well studied in budding yeast *S. cerevisiae* (van Zutphen *et al.*, 2014; Fig. 2).

The role of lipophagy differs between different cell types, from fast degradation of large quantities of lipids in liver cells during fasting (Ward *et al.*, 2016) to the regulation of protein levels by increased concentrations of endogenous free FAs in neurons (Kaushik *et al.*, 2011). Lipophagy was first discovered by Singh *et al.* (2009*a*) in mice. The authors showed that pharmacological inhibition of autophagy by 3-methyladenine increased the TAG content in hepatocytes *in vitro*. Further analysis revealed increased TAG levels and both increased size and number of LDs in embryonic fibroblasts from *atg5* knockout mice and *in vitro* cultured *ATG5* knockdown hepatocyte cells (Singh *et al.*, 2009*a*).

Even though *S. cerevisiae* harbours TAG lipases in the cytosol, LDs are frequently found within the vacuole (van Zutphen *et al.*, 2014). Also when lacking these TAG lipases, yeast cells sustain growth for >12 d under starvation conditions by instead degrading LDs via microlipophagy (van Zutphen *et al.*, 2014). The authors found that yeast microlipophagy required Atg1 and lipase Atg15. LDs in *atg1* mutant cells remained in the cytosol where their degradation was instead executed by cytosolic lipases, whereas *ATG15*-deficient cells accumulated LDs in the vacuole without subsequent degradation, leading to a shortage of TAG degradation products (van Zutphen *et al.*, 2014). Seo *et al.* (2017) further confirmed microlipophagy-mediated LD degradation in yeast under acute glucose starvation, and identified additional Atg proteins regulating this process. Interestingly, Atg14, known to be dispensable for other types of autophagy, was found to be essential for microlipophagy. Under starvation, Atg14 translocates from ER exit sites to the vacuolar membrane in an AMP-activated protein kinase (AMPK)-dependent manner, and in this way was suggested to initiate microlipophagy (Seo *et al.*, 2017). To date, we recognize lipophagy as an environmentally controlled process, whose activity varies depending on nutritional status. Yet, the lipophagy pathway itself is regulated by multiple factors, which have just started to be unravelled (Zechner *et al.*, 2017). Membrane trafficking plays a pivotal role in the inter-organelle communication and correct movement of cargo (e.g. lipids and proteins). For most types of cargo, the inter-organelle transport is mediated by membrane-bound vesicles coated with a range of proteins depending on the sending and recipient organelle. Vesicular transport requires an intact cytoskeleton, mostly the microtubules but also the actin filaments (DePina and Langford, 1999). The cargo destination is recognized by specific proteins on the vesicle surface, for example the well-conserved family of Rab GTPases, which upon finding the target membrane tether the vesicle to the membrane. Other proteins such as soluble *N*-ethylamide-sensitive factor attachment protein receptors (SNAREs) execute fusion of the target membrane with the vesicle, an event immediately preceding cargo unloading. Do membrane trafficking proteins play a role in lipophagy?

Four Rab proteins (Rab7, Rab10, Rab18, and Rab32) have been repeatedly found to be linked to turnover of LDs or, specifically, to autophagic degradation of LDs. Rab7 has been shown to be an important factor for normal progression of the autophagosome maturation and fusion with lysosomes (Gutierrez *et al.*, 2004), and simultaneously a conserved component of the LD membrane (Martin *et al.*, 2005). Schroeder *et al.* (2015) revealed that Rab7 is highly activated in hepatocytes upon starvation and that its depletion impedes the docking of LDs to autophagosomes, multivesicular bodies, and lysosomes, leading to attenuation of lipophagy. In *S. cerevisiae*, Rab7-like (or Ypt7p) has been shown to regulate membrane trafficking between the vacuole and LDs (Bouchez *et al.*, 2015).

Rab10 as another key player of lipophagy. Knockdown of Rab10 in hepatocytes led to a significant increase in LD content, thus linking Rab10 and LD breakdown (Z. Li *et al.*, 2016). Rab10 associates with nascent LC3-positive phagophores, triggering the assembly of a trimeric protein complex containing Rab10, endocytic adaptor EH domain binding protein 1 (EHBP1), and the ATPase EH domain containing 2 (EHD2). This complex was suggested to target selectively the autophagic machinery to LDs, regulate autophagic membrane extension, and facilitate the engulfment of LDs by lipophagy (Z. Li *et al.*, 2016). Rab (also called Ypt proteins in yeast) 4, 5, 7, and 11 have also been detected in an LD proteome of the oleaginous yeast *Rhodosporidium toruloides*, and ascribed a role in mediating the interactions between LDs and other organelles (Zhu *et al.*, 2015).

Rab18 has thus far been solely found to localize on the LD membrane in adipocytes and other cell types (Ozeki *et al.*, 2005; Martin *et al.*, 2005). Loss of Rab18 function causes Warburg Micro syndrome in humans, an autosomal recessive genetic disorder effecting brain development. Mouse Rab18-deficient embryonic fibroblasts develop more and larger LDs, suggesting Rab18 to have a role in LD homeostasis (Liegel *et al.*, 2013). Further research is, however, required to elucidate whether Rab18 acts via lipophagy or lipolysis.

Finally, Rab32 expression is greatly elevated in the fat body of *Drosophila* (Wang *et al.*, 2012). Instead of localizing to LDs, Rab32 was found on ring-like structures (autolysosomes) positive for lysosomal marker and LC3. *Drosophila* Rab32 loss-of-function mutants exhibited reduced size and number of LDs in larval adipose tissue (Wang *et al.*, 2012), the phenotype recently confirmed in mammalian hepatocytes (Q. Li *et al.*, 2016) and opposite to the LD phenotype caused by deficiency of the other three above-described Rabs. Wang *et al.* (2012) suggest that Rab32 does not directly contribute to LD degradation in *Drosophila*, but might rather take part in regulating autophagy.

The canonical cytosolic lipolysis in mammals is executed by adipose triglyceride lipase (ATGL), whose activity plays a direct role in TAG breakdown and also facilitates the subsequent channelling of FAs to oxidative pathways (Wu *et al.*, 2012). Investigation of the possible crosstalks between cytosolic lipolysis and autophagy has revealed several connections. For example, depletion of Rab32 has been found to induce lipolysis through indirectly enhancing ATGL expression (Q Li *et al.*, 2016). Also, chaperone-mediated autophagy degrades the LD-associated proteins PLIN2 and 3, facilitating association of ATGL and lipophagy-related proteins with the LDs (Kaushik and Cuervo, 2015). Another recent study has shown that ATGL can promote lipophagy in liver through the well-known autophagy regulator sirtuin1, suggesting that this crosstalk between lipolysis and lipophagy is a bona fide pathway responsible for LD catabolism in the liver (Sathyanarayan *et al.*, 2017).

SNARE proteins are structurally divided into Q-SNAREs and R-SNAREs, according to conserved amino acid residues. Generally R-SNAREs are vesicle associated (v-SNAREs) and Q-SNAREs are target membrane associated (t-SNAREs). The fusion of a vesicle and target membrane is mediated by intermolecular interaction between complementary v-SNAREs and t-SNAREs which forms the SNARE complex (for a review, see Jahn and Scheller, 2006). In yeast autophagy, several SNARE proteins are necessary for fusion between the autophagosome and the vacuole. In animals, an autophagosomal SNARE Syntaxin 17 (Stx17) has been shown to mediate the autophagosome–lysosome fusion by interaction with two other SNAREs, SNAP-29 and VAMP8 (Itakura, *et al.*, 2012). The SNAREs SNAP23, Syntaxin-5, and VAMP4 are all present on LDs where they facilitate LD–LD fusion (Boström *et al.*, 2007). It remains to be investigated, however, whether these or any other SNAREs target autophagosomes to LDs.

Is there a role for autophagy in LD catabolism in plants?

Extensive experimental evidence of autophagy-mediated LD degradation in animals and fungi opens up the question of why lipophagy has not also been found to be an instrument of LD degradation in plants. Thus far, autophagic degradation of LDs and/or PGs has been demonstrated in the algal systems, *Auxenochlorella protothecoides* (Zhao *et al.*, 2014) and *Micrasterias denticulate* (Schwartz *et al.*, 2017). *Auxenochlorella protothecoides* is a microalga which can grow both autotrophically and heterotrophically. The transition between the two growth modes requires major cell remodelling. The authors investigated the role of autophagy during the transition from heterotrophic to autotrophic growth and revealed a direct sequestering of the LDs by the vacuole in a microlipophagy-like process (Zhao *et al.*, 2014). In *M. denticulate*, PGs were evenly distributed in the chloroplasts of control cells, whereas upon carbon starvation the PGs were translocated to the cytoplasm where they were engulfed by autophagosome-like structures (Schwarz *et al.*, 2017).

Indeed, increased release of PGs from chloroplasts to the cytoplasm (Guiamet *et al.*, 1999; Ghosh *et al.*, 2001; Krupinska, 2007) with subsequent accumulation and degradation in the vacuole (Inada *et al.*, 1998; Guiamet *et al.*, 1999; Liu, 2016) are cellular hallmarks of plant senescence. Kurusu *et al.* (2014) have also observed LDs in the vacuoles of tapetal cells in wild-type rice. Whether vacuolar localization of PGs and tapetal LDs is caused by canonical, ATG-dependent autophagy is unknown.

Avin-Wittenberg *et al.* (2015) investigated the metabolome of Arabidopsis *atg5* and *atg7* mutant seedlings grown under limited carbon conditions and found increased content of most TAG species. Further studies are required to link these observations with the mobilization of LDs in autophagy-deficient seedlings. As described earlier in this review, the Rab and SNARE protein families play important roles as autophagy or lipophagy regulators in animal systems. Although there is a new evidence for the involvement of Rab and SNARE proteins in the regulation of plant autophagy (Surpin *et al.*, 2003; Kwon *et al.*, 2010), there are no reports yet linking these proteins to plant LDs. Another potential implication of autophagy in plant lipid catabolism might be related to pexophagy (Farmer *et al.*, 2013; Kim *et al.*, 2013; Shibata *et al.*, 2013; Yoshimoto *et al.*, 2014), an autophagic process ensuring quality control of peroxisomes, which among other processes perform β-oxidation of FAs in plants (Fig. 2). It has not, however, been resolved whether pexophagy could affect the β-oxidation. Arabidopsis *atg2* mutants (Shibata *et al.*, 2013) as well as both *atg5* and *atg7* mutants (Kim *et al.*, 2013) displayed no effect on β-oxidation compared with wild-type plants, albeit that the levels of TAGs or LDs in the plants were not examined. More research encompassing other *ATG* genes, as well as assessing LD formation and the TAG level, is needed to address the role of pexophagy in lipid catabolism.

Future perspectives

Autophagy plays fundamental role in the turnover of lipid reserves in animals, whereas its implication in plant lipid metabolism remains largely obscure. Arabidopsis *atg* mutant seeds germinate normally without a carbon source, albeit that seedlings display slightly delayed growth and increased accumulation of TAGs (Avin-Wittenberg *et al.*, 2015). Clearly, these preliminary data are exciting and call for further investigation into the status of LDs and TAGs upon early post-embryonic development of autophagy-deficient plants.

Another vital line of research with great importance for the understanding of the evolution of autophagy-mediated LD catabolism is related to the participation of membrane trafficking proteins such as SNAREs and Rabs in the targeting of LDs and the plastid-specific type PGs to the plant lytic vacuoles. Better understanding of the mechanistic connection between autophagy and the turnover of plant lipid reserves will in the long run be translated into practical methods for improving accumulation and mobilization of plant oils.

Acknowledgements

We thank Volkmar Passoth for stimulating discussions about yeast lipid biogenesis and degradation. Research in our laboratory is supported by grants from the Swedish Foundation for Strategic Research, Trees and Crops for the Future Research Programme, the Swedish Research Council (VR), Knut and Alice Wallenberg Foundation, Olle Engkvist Foundation, and Carl Tryggers Foundation. Writing this review article was promoted by the COST (European Cooperation in Science and Technology)-Action Transautophagy (CA15138).

References

Adeyo O, Horn PJ, Lee S, Binns DD, Chandrahas A, Chapman KD, Goodman JM. 2011. The yeast lipin orthologue Pah1p is important for biogenesis of lipid droplets. Journal of Cell Biology **192,** 1043–1055.

Austin JR 2nd, Frost E, Vidi PA, Kessler F, Staehelin LA. 2006. Plastoglobules are lipoprotein subcompartments of the chloroplast that are permanently coupled to thylakoid membranes and contain biosynthetic enzymes. The Plant Cell **18,** 1693–1703.

Avin-Wittenberg T, Bajdzienko K, Wittenberg G, Alseekh S, Tohge T, Bock R, Giavalisco P, Fernie AR. 2015. Global analysis of the role of autophagy in cellular metabolism and energy homeostasis in Arabidopsis seedlings under carbon starvation. The Plant Cell **27,** 306–322.

Baerga R, Zhang Y, Chen P-H, Goldman S, Jin S. 2009. Targeted deletion of autophagy-related 5 (atg5) impairs adipogenesis in a cellular model and in mice. Autophagy **5,** 1118–1130.

Barrat J-L, Hansen J-P. 2003. Basic concepts for simple and complex liquids. Cambridge: Cambridge University Press.

Beevers H. 1956. Utilization of glycerol in the tissues of the castor bean seedling. Plant Physiology **31,** 440–445.

Beevers H. 1979. Microbodies in higher plants. Annual Review of Plant Physiology **30,** 159–193.

Beller M, Bulankina AV, Hsiao H-H, Urlaub H, Jäckle H, Kühnlein RP. 2010. PERILIPIN-dependent control of lipid droplet structure and fat storage in Drosophila. Cell Metabolism **12,** 521–532.

Ben M'barek K, Ajjaji D, Chorlay A, Vanni S, Forêt L, Thiam AR. 2017. ER membrane phospholipids and surface tension control cellular lipid droplet formation. Developmental Cell **41,** 591–604.

Blouin CM, Le Lay S, Eberl A, *et al*. 2010. Lipid droplet analysis in caveolin-deficient adipocytes: alterations in surface phospholipid composition and maturation defects. Journal of Lipid Research **51,** 945–956.

Boström P, Andersson L, Rutberg M, *et al*. 2007. SNARE proteins mediate fusion between cytosolic lipid droplets and are implicated in insulin sensitivity. Nature Cell Biology **9,** 1286–1293.

Bouchez I, Pouteaux M, Canonge M, Genet M, Chardot T, Guillot A, Froissard M. 2015. Regulation of lipid droplet dynamics in *Saccharomyces cerevisiae* depends on the Rab7-like Ypt7p, HOPS complex and V1-ATPase. Biology Open **4,** 764–75

Bulankina AV, Deggerich A, Wenzel D, Mutenda K, Wittmann JG, Rudolph MG, Burger KN, Höning S. 2009. TIP47 functions in the biogenesis of lipid droplets. Journal of Cell Biology **185,** 641–655.

Cai Y, Goodman JM, Pyc M, Mullen RT, Dyer JM, Chapman KD. 2015. Arabidopsis SEIPIN proteins modulate triacylglycerol accumulation and influence lipid droplet proliferation. The Plant Cell **27,** 2616–2636.

Cai Y, McClinchie E, Price A, *et al*. 2017. Mouse fat storage-inducing transmembrane protein 2 (FIT2) promotes lipid droplet accumulation in plants. Plant Biotechnology Journal **15,** 824–836.

Cartwright BR, Binns DD, Hilton CL, Han S, Gao Q, Goodman JM. 2015. Seipin performs dissectible functions in promoting lipid droplet biogenesis and regulating droplet morphology. Molecular Biology of the Cell **26,** 726–739.

Chapman KD, Ohlrogge JB. 2012. Compartmentation of triacylglycerol accumulation in plants. Journal of Biological Chemistry **287,** 2288–2294.

Choudhary V, Ojha N, Golden A, Prinz WA. 2015. A conserved family of proteins facilitates nascent lipid droplet budding from the ER. Journal of Cell Biology **211,** 261–271.

Couso I, Perez-Perez ME, Martinez-Force E, Kim H-S, He, Y, Umen JG, Crespo JL. 2018. Autophagic flux is required for the synthesis of triacylglycerols and ribosomal protein turnover in *Chlamydomonas*. Journal of Experimental Botany **69**, 1355–1367).

DePina AS, Langford GM. 1999. Vesicle transport: the role of actin filaments and myosin motors. Microscopy Research and Technique **47,** 93–106.

Ducharme NA, Bickel PE. 2008. Lipid droplets in lipogenesis and lipolysis. Endocrinology **149,** 942–949.

Eastmond PJ. 2004. Glycerol-insensitive Arabidopsis mutants: gli1 seedlings lack glycerol kinase, accumulate glycerol and are more resistant to abiotic stress. The Plant Journal **37,** 617–625.

Eastmond PJ. 2006. SUGAR-DEPENDENT1 encodes a patatin domain triacylglycerol lipase that initiates storage oil breakdown in germinating Arabidopsis seeds. The Plant Cell **18,** 665–675.

Fan Y, Ortiz-Urquiza A, Garrett T, Pei Y, Keyhani NO. 2015. Involvement of a caleosin in lipid storage, spore dispersal, and virulence in the entomopathogenic filamentous fungus, *Beauveria bassiana.* Environmental Microbiology **17,** 4600–4614.

Farmer LM, Rinaldi MA, Young PG, Danan CH, Burkhart SE, Bartel B. 2013. Disrupting autophagy restores peroxisome function to an Arabidopsis lon2 mutant and reveals a role for the LON2 protease in peroxisomal matrix protein degradation. The Plant Cell **25,** 4085–4100.

Fei W, Shui G, Gaeta B, Du X, Kuerschner L, Li P, Brown AJ, Wenk MR, Parton RG, Yang H. 2008. Fld1p, a functional homologue of human seipin, regulates the size of lipid droplets in yeast. Journal of Cell Biology **180,** 473–482.

Feng Y, He D, Yao Z, Klionsky DJ. 2014. The machinery of macroautophagy. Cell Research **24,** 24–41.

Footitt S, Slocombe SP, Larner V, Kurup S, Wu Y, Larson T, Graham I, Baker A, Holdsworth M. 2002. Control of germination and lipid mobilization by COMATOSE, the Arabidopsis homologue of human ALDP. EMBO Journal **21,** 2912–2922.

Frandsen GI, Mundy J, Tzen JT. 2001. Oil bodies and their associated proteins, oleosin and caleosin. Physiologia Plantarum **112,** 301–307.

Fujiki Y, Yoshimoto K, Ohsumi Y. 2007. An Arabidopsis homolog of yeast ATG6/VPS30 is essential for pollen germination. Plant Physiology **143,** 1132–1139.

Fujimoto Y, Itabe H, Kinoshita T, *et al*. 2007. Involvement of ACSL in local synthesis of neutral lipids in cytoplasmic lipid droplets in human hepatocyte HuH7. Journal of Lipid Research **48,** 1280–1292.

Gao Q, Binns DD, Kinch LN, Grishin NV, Ortiz N, Chen X, Goodman JM. 2017. Pet10p is a yeast perilipin that stabilizes lipid droplets and promotes their assembly. Journal of Cell Biology **216,** 3199–3217.

Ghosh S, Mahoney SR, Penterman JN, Peirson D, Dumbroff EB. 2001. Ultrastructural and biochemical changes in chloroplasts during *Brassica napus* senescence. Plant Physiology and Biochemistry **39,** 777–784.

Gong J, Sun Z, Wu L, *et al*. 2011. Fsp27 promotes lipid droplet growth by lipid exchange and transfer at lipid droplet contact sites. Journal of Cell Biology **195,** 953–963.

Gross DA, Zhan C, Silver DL. 2011. Direct binding of triglyceride to fat storage-inducing transmembrane proteins 1 and 2 is important for lipid droplet formation. Proceedings of the National Academy of Sciences, USA **108,** 19581–19586.

Guiamet JJ, Pichersky E, Nooden LD. 1999. Mass exodus from senescing soybean chloroplasts. Plant and Cell Physiology **40,** 986–992.

Gutierrez MG, Munafó DB, Berón W, Colombo MI. 2004. Rab7 is required for the normal progression of the autophagic pathway in mammalian cells. Journal of Cell Science **117,** 2687–2697.

Hayashi M, Nito K, Takei-Hoshi R, Yagi M, Kondo M, Suenaga A, Yamaya T, Nishimura M. 2002. Ped3p is a peroxisomal ATP-binding cassette transporter that might supply substrates for fatty acid beta-oxidation. Plant and Cell Physiology **43,** 1–11.

Hsieh K, Huang AH. 2007. Tapetosomes in *Brassica tapetum* accumulate endoplasmic reticulum-derived flavonoids and alkanes for delivery to the pollen surface. The Plant Cell **19,** 582–596.

Huang CY, Huang AHC. 2017. Motifs in oleosin target the cytosolic side of endoplasmic reticulum and budding lipid droplet. Plant Physiology **174,** 2248–2260.

Inada N, Sakai A, Kuroiwa H, Kuroiwa T. 1998. Three-dimensional analysis of the senescence program in rice (*Oryza sativa* L.) coleoptiles. Planta **206,** 585–597.

Itabe H, Yamaguchi T, Nimura S, Sasabe N. 2017. Perilipins: a diversity of intracellular lipid droplet proteins. Lipids in Health and Disease **16,** 83.

Itakura E, Kishi-Itakura C, Mizushima N. 2012. The hairpin-type tail-anchored SNARE syntaxin 17 targets to autophagosomes for fusion with endosomes/lysosomes. Cell **151,** 1256–1269.

Jacquier N, Choudhary V, Mari M, Toulmay A, Reggiori F, Schneiter R. 2011. Lipid droplets are functionally connected to the endoplasmic reticulum in *Saccharomyces cerevisiae*. Journal of Cell Science **124,** 2424–2437.

Jahn R, Scheller RH. 2006. SNAREs—engines for membrane fusion. Nature Reviews Molecular Cell Biology **7,** 631–643.

Jolivet P, Roux E, d'Andrea S, Davanture M, Negroni L, Zivy M, Chardot T. 2004. Protein composition of oil bodies in *Arabidopsis thaliana* ecotype WS. Plant Physiology and Biochemistry **42,** 501–509.

Kadereit B, Kumar P, Wang W-J, Miranda D, Snapp EL, Severina N, Torregroza I, Evans T, Silver DL. 2008. Evolutionarily conserved gene family important for fat storage. Proceedings of the National Academy of Sciences, USA **105,** 94–99.

Kassan A, Herms A, Fernández-Vidal A, *et al*. 2013. Acyl-CoA synthetase 3 promotes lipid droplet biogenesis in ER microdomains. Journal of Cell Biology **203,** 985–1001.

Kaushik S, Cuervo AM. 2015. Degradation of lipid droplet-associated proteins by chaperone-mediated autophagy facilitates lipolysis. Nature Cell Biology **17,** 759–770.

Kaushik S, Rodriguez-Navarro JA, Arias E, Kiffin R, Sahu S, Schwartz GJ, Cuervo AM, Singh R. 2011. Autophagy in hypothalamic AgRP neurons regulates food intake and energy balance. Cell Metabolism **14,** 173–183.

Kelly AA, Quettier AL, Shaw E, Eastmond PJ. 2011. Seed storage oil mobilization is important but not essential for germination or seedling establishment in Arabidopsis. Plant Physiology **157,** 866–875.

Kim J, Lee H, Lee HN, Kim SH, Shin KD, Chung T. 2013. Autophagy-related proteins are required for degradation of peroxisomes in Arabidopsis hypocotyls during seedling growth. The Plant Cell **25,** 4956–4966.

Kimmel AR, Brasaemle DL, McAndrews-Hill M, Sztalryd C, Londos C. 2010. Adoption of PERILIPIN as a unifying nomenclature for the mammalian PAT-family of intracellular lipid storage droplet proteins. Journal of Lipid Research **51,** 468–471.

Krupinska K. 2007. Fate and activities of plastids during leaf senescence. Dordrecht: Springer, 433–449.

Ku S, Yoon H, Suh HS, Chung YY. 2003. Male-sterility of thermosensitive genic male-sterile rice is associated with premature programmed cell death of the tapetum. Planta **217,** 559–565.

Kuma A, Hatano M, Matsui M, Yamamoto A, Nakaya H, Yoshimori T, Ohsumi Y, Tokuhisa T, Mizushima N. 2004. The role of autophagy during the early neonatal starvation period. Nature **432,** 1032–1036.

Kurusu T, Koyano T, Hanamata S, *et al*. 2014. OsATG7 is required for autophagy-dependent lipid metabolism in rice postmeiotic anther development. Autophagy **10,** 878–888.

Kwon SI, Cho HJ, Jung JH, Yoshimoto K, Shirasu K, Park OK. 2010. The Rab GTPase RabG3b functions in autophagy and contributes to tracheary element differentiation in Arabidopsis. The Plant Journal **64,** 151–164.

Lersten NR, Czlapinski AR, Curtis JD, Freckmann R, Horner HT. 2006. Oil bodies in leaf mesophyll cells of angiosperms: overview and a selected survey. American Journal of Botany **93,** 1731–1739.

Li N, Zhang DS, Liu HS, *et al*. 2006. The rice tapetum degeneration retardation gene is required for tapetum degradation and anther development. The Plant Cell **18,** 2999–3014.

Li Q, Wang J, Wan Y, Chen D. 2016. Depletion of Rab32 decreases intracellular lipid accumulation and induces lipolysis through enhancing ATGL expression in hepatocytes. Biochemical and Biophysical Research Communications **471,** 492–496.

Li Z, Schulze RJ, Weller SG, *et al*. 2016. A novel Rab10–EHBP1–EHD2 complex essential for the autophagic engulfment of lipid droplets. Science Advances **2,** e1601470.

Liegel RP, Handley MT, Ronchetti A, *et al*. 2013. Loss-of-function mutations in TBC1D20 cause cataracts and male infertility in blind sterile mice and Warburg micro syndrome in humans. American Journal of Human Genetics **93,** 1001–1014.

Liu K, Czaja MJ. 2013. Regulation of lipid stores and metabolism by lipophagy. Cell Death and Differentiation **20,** 3–11.

Liu L. 2016. Ultramicroscopy reveals that senescence induces in-situ and vacuolar degradation of plastoglobules in aging watermelon leaves. Micron **80,** 135–144.

Maeda Y, Oku M, Sakai Y. 2017. Autophagy-independent function of Atg8 in lipid droplet dynamics in yeast. Journal of Biochemistry **161,** 339–348.

Martin S, Driessen K, Nixon SJ, Zerial M, Parton RG. 2005. Regulated localization of Rab18 to lipid droplets: effects of lipolytic stimulation and inhibition of lipid droplet catabolism. Journal of Biological Chemistry **280,** 42325–42335.

Minina EA, Bozhkov PV, Hofius D. 2014. Autophagy as initiator or executioner of cell death. Trends in Plant Science **19,** 692–697.

Mizushima N, Komatsu M. 2011. Autophagy: renovation of cells and tissues. Cell **147,** 728–741.

Mizushima N, Levine B. 2010. Autophagy in mammalian development and differentiation. Nature Cell Biology **12,** 823–830.

Moir RD, Gross DA, Silver DL, Willis IM, Engelke D. 2012. SCS3 and YFT2 link transcription of phospholipid biosynthetic genes to ER stress and the UPR. PLoS Genetics **8,** e1002890.

Murphy DJ. 2001. The biogenesis and functions of lipid bodies in animals, plants and microorganisms. Progress in Lipid Research **40,** 325–438.

Nishimura M, Takeuchi Y, De Bellis L, Hara-Nishimura I. 1993. Leaf peroxisomes are directly transformed to glyoxysomes during senescence of pumpkin cotyledons. Protoplasma **175,** 131–137.

Ohsumi Y. 2014. Historical landmarks of autophagy research. Cell Research **24,** 9–23.

Ozeki S, Cheng J, Tauchi-Sato K, Hatano N, Taniguchi H, Fujimoto T. 2005. Rab18 localizes to lipid droplets and induces their close apposition to the endoplasmic reticulum-derived membrane. Journal of Cell Science **118,** 2601–2611.

Robenek H, Hofnagel O, Buers I, Robenek MJ, Troyer D, Severs NJ. 2006. Adipophilin-enriched domains in the ER membrane are sites of lipid droplet biogenesis. Journal of Cell Science **119,** 4215–4224.

Rottet S, Besagni C, Kessler F. 2015. The role of plastoglobules in thylakoid lipid remodeling during plant development. Biochimica et Biophysica Acta **1847,** 889–899.

Salo VT, Belevich I, Li S, *et al*. 2016. Seipin regulates ER–lipid droplet contacts and cargo delivery. EMBO Journal **35,** 2699–2716.

Sathyanarayan A, Mashek MT, Mashek DG. 2017. ATGL promotes autophagy/lipophagy via SIRT1 to control hepatic lipid droplet catabolism. Cell Reports **19,** 1–9.

Schmid K, Ohlrogge J. 2002. Lipid metabolism in plants. In: Vance DE, Vance JE, eds. Biochemistry of lipids, lipoproteins and membranes, 4th edn. Amsterdam: Elsevier, 93–106.

Schroeder B, Schulze RJ, Weller SG, Sletten AC, Casey CA, McNiven MA. 2015. The small GTPase Rab7 as a central regulator of hepatocellular lipophagy. Hepatology **61,** 1896–1907.

Schulze RJ, Drižytė K, Casey CA, McNiven MA. 2017. Hepatic lipophagy: new insights into autophagic catabolism of lipid droplets in the liver. Hepatology Communications **1,** 359–369.

Schwarz V, Andosch A, Geretschläger A, Affenzeller M, Lütz-Meindl U. 2017. Carbon starvation induces lipid degradation via autophagy in the model alga Micrasterias. Journal of Plant Physiology **208,** 115–127.

Sembongi H, Miranda M, Han GS, Fakas S, Grimsey N, Vendrell J, Carman GM, Siniossoglou S. 2013. Distinct roles of the phosphatidate phosphatases lipin 1 and 2 during adipogenesis and lipid droplet biogenesis in 3T3-L1 cells. Journal of Biological Chemistry **288,** 34502–34513.

Seo AY, Lau P-W, Feliciano D, Sengupta P, Le Gros MA, Cinquin B, Larabell CA, Lippincott-Schwartz J. 2017. AMPK and vacuole-associated Atg14p orchestrate μ-lipophagy for energy production and long-term survival under glucose starvation. eLife **6,** e21690.

Shen Y, Xie J, Liu RD, Ni XF, Wang XH, Li ZX, Zhang M. 2014. Genomic analysis and expression investigation of caleosin gene family in Arabidopsis. Biochemical and Biophysical Research Communications **448,** 365–371.

Shibata M, Oikawa K, Yoshimoto K, *et al*. 2013. Highly oxidized peroxisomes are selectively degraded via autophagy in Arabidopsis. The Plant Cell **25,** 4967–4983.

Shibata M, Yoshimura K, Furuya N, *et al*. 2009. The MAP1–LC3 conjugation system is involved in lipid droplet formation. Biochemical and Biophysical Research Communications **382,** 419–423.

Shockey JM, Fulda MS, Browse JA. 2002. Arabidopsis contains nine long-chain acyl-coenzyme A synthetase genes that participate in fatty acid and glycerolipid metabolism. Plant Physiology **129,** 1710–1722.

Singh R, Kaushik S, Wang Y, Xiang Y, Novak I, Komatsu M, Tanaka K, Cuervo AM, Czaja MJ. 2009*a*. Autophagy regulates lipid metabolism. Nature **458,** 1131–1135.

Singh R, Xiang Y, Wang Y, *et al*. 2009*b*. Autophagy regulates adipose mass and differentiation in mice. Journal of Clinical Investigation **119,** 3329–3339.

Surpin M, Zheng H, Morita MT, *et al*. 2003. The VTI family of SNARE proteins is necessary for plant viability and mediates different protein transport pathways. The Plant Cell **15,** 2885–2899.

Szymanski KM, Binns D, Bartz R, Grishin NV, Li W-P, Agarwal AK, Garg A, Anderson RGW, Goodman JM. 2007. The lipodystrophy protein seipin is found at endoplasmic reticulum lipid droplet junctions and is important for droplet morphology. Proceedings of the National Academy of Sciences, USA **104,** 20890–20895.

Thiam AR, Farese RV Jr, Walther TC. 2013. The biophysics and cell biology of lipid droplets. Nature Reviews Molecular Cell Biology **14,** 775–786.

Thiam AR, Forêt L. 2016. The physics of lipid droplet nucleation, growth and budding. Biochimica et Biophysica Acta **1861,** 715–722.

van Zutphen T, Todde V, de Boer R, Kreim M, Hofbauer HF, Wolinski H, Veenhuis M, van der Klei IJ, Kohlwein SD. 2014. Lipid droplet autophagy in the yeast *Saccharomyces cerevisiae*. Molecular Biology of the Cell **25,** 290–301.

Wang C, Liu Z, Huang X. 2012. Rab32 is important for autophagy and lipid storage in Drosophila. PLoS One **7,** e32086.

Ward C, Martinez-Lopez N, Otten EG, Carroll B, Maetzel D, Singh R, Sarkar S, Korolchuk VI. 2016. Autophagy, lipophagy and lysosomal lipid storage disorders. Biochimica et Biophysica Acta **1861,** 269–284.

Wilfling F, Thiam AR, Olarte MJ, *et al*. 2014. Arf1/COPI machinery acts directly on lipid droplets and enables their connection to the ER for protein targeting. eLife **3,** e01607.

Wu JW, Wang SP, Casavant S, Moreau A, Yang GS, Mitchell GA. 2012. Fasting energy homeostasis in mice with adipose deficiency of desnutrin/adipose triglyceride lipase. Endocrinology **153,** 2198–2207.

Yang H, Galea A, Sytnyk V, Crossley M. 2012. Controlling the size of lipid droplets: lipid and protein factors. Current Opinion in Cell Biology **24,** 509–516.

Yoshimoto K. 2012. Beginning to understand autophagy, an intracellular self-degradation system in plants. Plant and Cell Physiology **53,** 1355–1365.

Yoshimoto K, Shibata M, Kondo M, Oikawa K, Sato M, Toyooka K, Shirasu K, Nishimura M, Ohsumi Y. 2014. Organ-specific quality control of plant peroxisomes is mediated by autophagy. Journal of Cell Science **127,** 1161–1168.

Zechner R, Madeo F, Kratky D. 2017. Cytosolic lipolysis and lipophagy: two sides of the same coin. Nature Reviews. Molecular Cell Biology **18,** 671–684.

Zhang Y, Goldman S, Baerga R, Zhao Y, Komatsu M, Jin S. 2009. Adipose-specific deletion of autophagy-related gene 7 (atg7) in mice reveals a role in adipogenesis. Proceedings of the National Academy of Sciences, USA **106,** 19860–19865.

Zhang C, He Y, Okutsu M, Ong LC, Jin Y, Zheng L, Chow P, Yu S, Zhang M, Yan Z. 2013. Autophagy is involved in adipogenic differentiation by repressesing proteasome-dependent PPARγ2 degradation. American Journal of Physiology **305,** E530–E539.

Zhao L, Dai J, Wu Q. 2014. Autophagy-like processes are involved in lipid droplet degradation in *Auxenochlorella protothecoides* during the heterotrophy–autotrophy transition. Frontiers in Plant Science **5,** 400.

Zhao L, Katavic V, Li F, Haughn GW, Kunst L. 2010. Insertional mutant analysis reveals that long-chain acyl-CoA synthetase 1 (LACS1), but not LACS8, functionally overlaps with LACS9 in Arabidopsis seed oil biosynthesis. The Plant Journal **64,** 1048–1058.

Zhu Z, Ding Y, Gong Z, *et al*. 2015. Dynamics of the lipid droplet proteome of the Oleaginous yeast *Rhodosporidium toruloides*. Eukaryotic Cell **14,** 252–264.

Zolman BK, Silva ID, Bartel B. 2001. The Arabidopsis pxa1 mutant is defective in an ATP-binding cassette transporter-like protein required for peroxisomal fatty acid beta-oxidation. Plant Physiology **127,** 1266–1278.

IV

Article

SOURCE DATA | TRANSPARENT PROCESS | OPEN ACCESS

THE EMBO JOURNAL

Tudor staphylococcal nuclease is a docking platform for stress granule components and is essential for SnRK1 activation in *Arabidopsis*

Emilio Gutierrez-Beltran[1,2,*], Pernilla H Elander[3], Kerstin Dalman[3], Guy W Dayhoff II[4], Panagiotis N Moschou[5,6,7], Vladimir N Uversky[8,9], Jose L Crespo[1] & Peter V Bozhkov[3,**]

Abstract

Tudor staphylococcal nuclease (TSN; also known as Tudor-SN, p100, or SND1) is a multifunctional, evolutionarily conserved regulator of gene expression, exhibiting cytoprotective activity in animals and plants and oncogenic activity in mammals. During stress, TSN stably associates with stress granules (SGs), in a poorly understood process. Here, we show that in the model plant *Arabidopsis thaliana*, TSN is an intrinsically disordered protein (IDP) acting as a scaffold for a large pool of other IDPs, enriched for conserved stress granule components as well as novel or plant-specific SG-localized proteins. While approximately 30% of TSN interactors are recruited to stress granules de novo upon stress perception, 70% form a protein–protein interaction network present before the onset of stress. Finally, we demonstrate that TSN and stress granule formation promote heat-induced activation of the evolutionarily conserved energy-sensing SNF1-related protein kinase 1 (SnRK1), the plant orthologue of mammalian AMP-activated protein kinase (AMPK). Our results establish TSN as a docking platform for stress granule proteins, with an important role in stress signalling.

Keywords heat stress; intrinsically disordered regions; SnRK1/SNF1/AMPK; stress granules; tudor staphylococcal nuclease

Subject Categories Plant Biology; Proteomics; RNA Biology

DOI 10.15252/embj.2020105043 | Received 18 March 2020 | Revised 23 June 2021 | Accepted 1 July 2021 | Published online 21 July 2021

The EMBO Journal (2021) 40: e105043

Introduction

Upon stress perception, eukaryotic cells compartmentalize specific mRNA molecules stalled in translation initiation into a type of evolutionary conserved membrane-less organelles called stress granules (SGs) (Thomas *et al*, 2011; Protter & Parker, 2016). In these biomolecular condensates, mRNA molecules are stored, degraded, or kept silent to prevent energy expenditure on the production of useless, surplus, or even harmful proteins under stress conditions. Recent research in yeast *Saccharomyces cerevisiae* and animal models established the molecular composition of SGs. SGs typically contain translationally arrested mRNAs, small ribosomal subunits, various translation initiation factors (eIF), poly(A)-binding protein (PAB), and a variety of RNA-binding proteins (RBPs) and non-RNA-binding proteins (Buchan & Parker, 2009). SGs play a major role in translational repression by sequestering, stabilizing and storing mRNA molecules, as well as by indirectly modulating signalling pathways (Protter & Parker, 2016; Mahboubi & Stochaj, 2017). Accordingly, SGs have a pro-survival function during stress and relate to cancer and human disease (Wolozin, 2012; Anderson *et al*, 2015; Wolozin & Ivanov, 2019).

Apart from components of SGs, proteomic and genetic screens in yeast and animal models have identified proteins modulating SG assembly, which is a highly coordinated process driven by the collective interactions of a core protein–RNA network (Ohn *et al*, 2008; Buchan *et al*, 2011; Martinez *et al*, 2013; Jain *et al*, 2016; Yang *et al*, 2020). A recent model for the assembly of mammalian and yeast SGs encompasses two major steps: first the formation of a dense stable SG core by a liquid–liquid phase separation (LLPS) followed by accumulation of proteins into a peripheral shell (Jain *et al*, 2016; Markmiller *et al*, 2018). Although the molecular

1 Instituto de Bioquímica Vegetal y Fotosíntesis, Consejo Superior de Investigaciones Científicas (CSIC)-Universidad de Sevilla, Sevilla, Spain
2 Departamento de Bioquímica Vegetal y Biología Molecular, Facultad de Biología, Universidad de Sevilla, Sevilla, Spain
3 Department of Molecular Sciences, Uppsala BioCenter, Swedish University of Agricultural Sciences and Linnean Center for Plant Biology, Uppsala, Sweden
4 Department of Chemistry, College of Art and Sciences, University of South Florida, Tampa, FL, USA
5 Institute of Molecular Biology and Biotechnology, Foundation for Research and Technology - Hellas, Heraklion, Greece
6 Department of Plant Biology, Uppsala BioCenter, Swedish University of Agricultural Sciences and Linnean Center for Plant Biology, Uppsala, Sweden
7 Department of Biology, University of Crete, Heraklion, Greece
8 Department of Molecular Medicine and USF Health Byrd Alzheimer's Research Institute, Morsani College of Medicine, University of South Florida, Tampa, FL, USA
9 Institute for Biological Instrumentation of the Russian Academy of Sciences, Federal Research Center "Pushchino Scientific Center for Biological Research of the Russian Academy of Sciences", Pushchino, Russia
*Corresponding author. Tel: +34 954489595; E-mail: egutierrez@us.es
**Corresponding author. Tel: +46 18673228; E-mail: peter.bozhkov@slu.se

© 2021 The Authors. Published under the terms of the CC BY 4.0 license

mechanisms underlying SG assembly remain currently unclear, all of the proposed models converge on the idea that SG assembly is driven by a combination of homotypic and heterotypic interactions involving intrinsically disordered regions (IDRs) (Guillen-Boixet *et al*, 2020; Schmit *et al*, 2021). Several lines of evidence also suggest that the dynamics of SGs are controlled, at least in part, by SG remodellers, that include ATP-dependent complexes or ubiquitin-related proteins (Seguin *et al*, 2014; Jain *et al*, 2016; Marmor-Kollet *et al*, 2020).

In plants, little is known about the molecular composition and function of SGs as well as their assembly and cross-talk with other signalling pathways. Previous studies in *Arabidopsis thaliana* (*Arabidopsis*) revealed formation of SGs under heat, hypoxia and salt stress (Sorenson & Bailey-Serres, 2014; Yan *et al*, 2014; Gutierrez-Beltran *et al*, 2015b) and both proteome and metabolome compositions of heat-induced SGs (Kosmacz *et al*, 2019). To date, a few protein components of plant SGs have been functionally characterized and most of them have direct homologues in yeast and/or mammalian SG proteomes. These include RNA-binding protein 47 (RBP47), Oligouridylate Binding Protein 1 (UBP1) and Tudor Staphylococcal Nuclease (TSN) (Sorenson & Bailey-Serres, 2014; Gutierrez-Beltran *et al*, 2015b; Kosmacz *et al*, 2018). Two recent lines of evidence suggest that TSN might be important for assembly and/or function of SGs. First, TSN localizes in SGs in such distant lineages as protozoa, animals and plants (Zhu *et al*, 2013; Yan *et al*, 2014; Gao *et al*, 2015; Gutierrez-Beltran *et al*, 2015b; Cazares-Apatiga *et al*, 2017). Second, TSN interacts with proteins constituting the core of SGs, such as PAB1, eIF4E and eIF5A in different organisms including mammalian and *Bombyx mori* cells (Weissbach & Scadden, 2012; Zhu *et al*, 2013; Gao *et al*, 2014).

The domain architecture of TSN is conserved in all studied organisms and includes a tandem repeat of four Staphylococcal Nuclease (SN) domains at the N terminus followed by a Tudor domain and a partial SN domain at the C terminus (Abe *et al*, 2003; Gutierrez-Beltran *et al*, 2016). TSN is known to be critically involved in the regulation of virtually all pathways of gene expression, ranging from transcription to RNA silencing (Gutierrez-Beltran *et al*, 2016; Chou *et al*, 2017). For example, *Arabidopsis* TSN1 and TSN2, two functionally redundant TSN homologues, have been described to play two antagonistic roles in RNA metabolism during stress (Gutierrez-Beltran *et al*, 2015a). Yet, the cellular level of TSN protein itself should be carefully regulated. While its depletion triggers cell death (Sundström *et al*, 2009; Gutierrez-Beltran *et al*, 2016; Cui *et al*, 2018), increased expression of TSN is closely associated with various types of cancer, adding it to a shortlist of most potent oncogenes and attractive targets for anti-cancer therapy (Jariwala *et al*, 2017; Yu *et al*, 2017).

In yeast and mammals, the universal molecular components of SGs co-exist with other, cell type- and stress stimuli-specific proteins, suggesting that SGs might play additional, yet unexplored, roles during stress. For example, SG formation in both yeast and human cells mediates target of rapamycin (TOR) signalling under stress by sequestering both TOR complex (TORC1) and downstream kinases (Takahara & Maeda, 2012; Wippich *et al*, 2013). By contrast, sequestration of the pleiotropic adaptor protein Receptor For Activated C Kinase 1 (RACK1) in SGs inhibits the stress-induced activation of the c-Jun N-terminal kinases (JNK) cascade that triggers apoptotic death (Arimoto *et al*, 2008). In yet another scenario, sequestration of the coiled-coil containing Rho-associated protein kinase 1 (ROCK1) into SGs promotes cell survival by abolishing JNK-mediated cell death (Tsai & Wei, 2010). In summary, SG formation can alter signalling pathways by protein sequestration during stress conditions, but whether such a mode of regulation exists in plants remains elusive.

Here, we isolated TSN-interacting proteins from *Arabidopsis* plants subjected to heat and salt stress, and further combined microscopy, reverse genetics and bioinformatics to advance our understanding of the regulation and molecular function of SGs in plants. We show that TSN engages its highly disordered N-terminal region in providing a platform for docking homologues of key components of yeast and mammalian SGs, as well as novel or plant-specific SG-localized proteins. TSN forms a large disorder-enriched protein–protein interaction network under non-stress conditions, that is poised to enable rapid SG assembly in response to stress. Finally, our data demonstrate that TSN and formation of SGs confer heat-induced activation of the catalytic α-subunit (SnRK1α) of SnRK1 heterotrimeric complex, thus linking TSN and SGs to the energy status of the plant cells.

Results

Generation and characterization of *Arabidopsis* TAPa-expressing lines

As a first step to investigate the role of TSN in SGs, we used TSN2, one of the two *Arabidopsis* TSN isoforms, as bait for alternative tandem affinity purification (TAPa; Fig EV1A) (Rubio *et al*, 2005). TSN2 and green fluorescent protein (GFP; negative control) were tagged at their C-termini with TAPa epitope containing two copies of the immunoglobulin-binding domain of protein A from *Staphylococcus aureus*, a human rhinovirus 3 protease cleavage site, a 6-histidine repeat and 9-Myc epitopes (Figs 1A and EV1A). The resulting TSN2-TAPa and GFP-TAPa vectors were introduced into *Arabidopsis* Columbia (Col) background. Two lines per construct showing readily detectable expression by immunoblot were selected for further studies (Fig EV1B).

To verify whether the presence of TAPa epitope could affect intracellular localization and functionality of TSN protein, we performed two additional experiments. First, the immunostaining of root cells from 5-day-old seedlings using α-Myc revealed that similar to native TSN (Yan *et al*, 2014; Gutierrez-Beltran *et al*, 2015b), TSN2-TAPa displayed diffuse cytoplasmic localization under no stress (NS) conditions but redistributed to cytoplasmic foci following heat stress (HS) (Fig 1B). In contrast, GFP-TAPa remained cytoplasmic regardless of conditions (Fig 1B). Co-localization analysis of the TSN2-TAPa and SG marker eIF4E confirmed that the HS-induced TSN2-TAPa foci are SGs (Fig EV1C). Second, expression of *TSN2-TAPa* in *tsn1 tsn2* seedlings complemented previously reported root cell death phenotype under HS caused by TSN deficiency (Fig EV1D) (Gutierrez-Beltran *et al*, 2015b). Heat stress induction in these experiments was confirmed by expression analysis of *HSP101* and *HSF*, two HS marker genes (Pecinka *et al*, 2010) (Appendix Fig S1). Collectively, these data demonstrate that C-terminally TAPa-tagged TSN retains localization and function of its native counterpart when expressed in *Arabidopsis* and therefore can be used as a bait for the isolation of TSN-interacting proteins.

 © 2021 The Authors

Isolation of TSN2-interacting proteins

Since previously we identified TSN2 as a robust marker of SGs induced by HS (Gutierrez-Beltran *et al*, 2015b), we initially analysed TSN2 interactomes isolated from fully expanded leaves of 18-day-old plants growing under NS conditions (23°C) or subjected to HS (39°C for 60 min). To examine the efficiency of purifying TSN2-TAPa and GFP-TAPa proteins from the corresponding transgenic

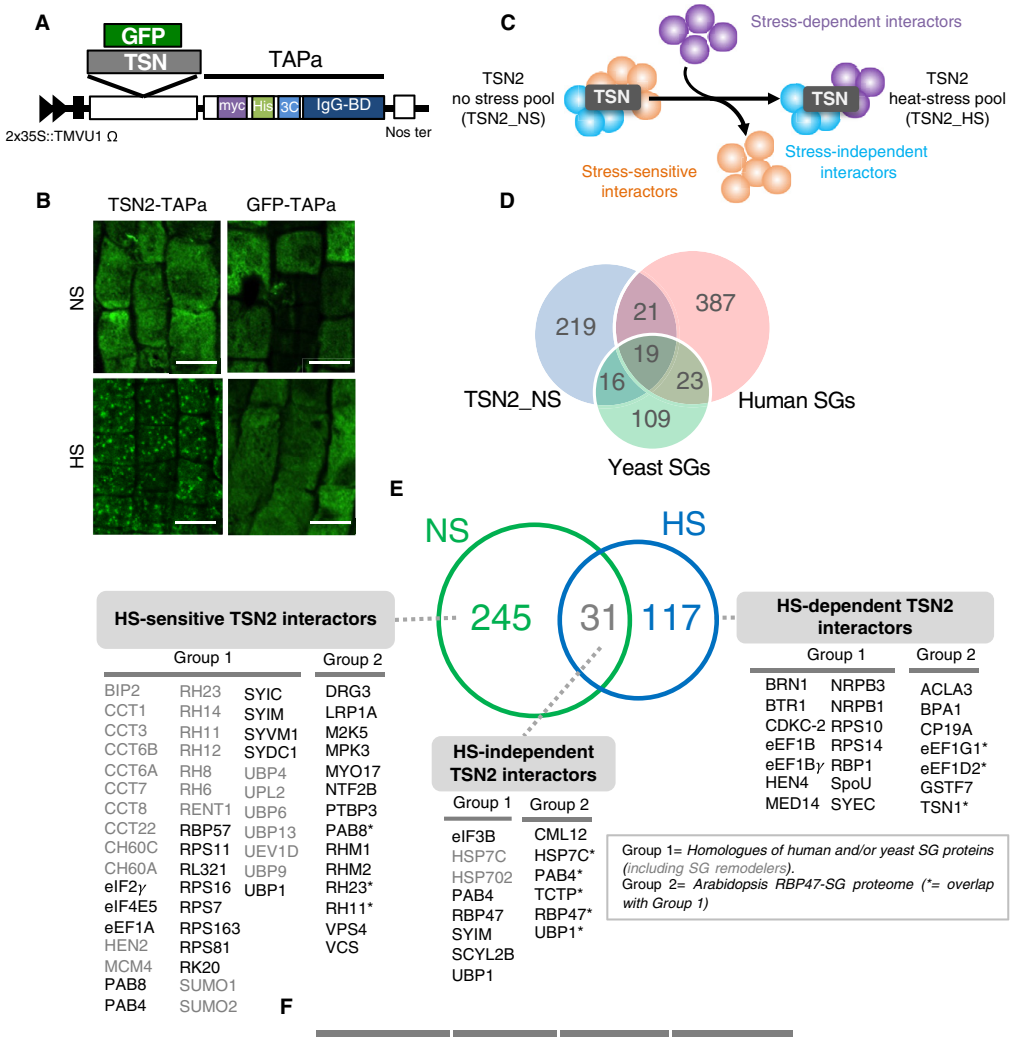

F

	RBPs	Prion-like domain	ATPase activity
TSN2_NS (277)	153 (55%)	22 (7.9%)	27 (9.7%)
TSN2_HS (149)	79 (55%)	12 (8.0%)	6 (4.0%)
Yeast SGs (159)	39 (24%)	23 (14.5%)	24 (15.0%)
Human SGs (411)	224 (55%)	32 (7.8%)	37 (9.0%)

Figure 1.

© 2021 The Authors

Figure 1. Tandem affinity purification and characterization of the *Arabidopsis* TSN2-interacting proteins.

A Schematic illustration of the expression cassette in TAPa vector. The vector allows translational fusion of TSN or GFP at their C termini to the TAPa tag. The expression is driven by two copies of the cauliflower mosaic virus 35S promoter (2 × 35S) and a tobacco mosaic virus (TMV) U1 X translational enhancer. The TAPa tag consists of two copies of the protein A IgG-binding domain (IgG-BD), an eight amino acid sequence corresponding to the 3C protease cleavage site (3C), a 6-histidine stretch (His), and nine repeats of the Myc epitope (myc). A Nos terminator (Nos ter) sequence is located downstream of each expression cassette.

B Immunolocalization of TSN2-TAPa and GFP-TAPa fusion proteins in root cells of 5-day-old seedlings. The seedlings were grown under no stress (NS) conditions (23°C) or incubated for 40 min at 39°C (HS) and then immunostained with α-Myc. Scale bars = 10 μm.

C Schematic representation of three classes of TSN-interacting proteins, i.e. stress-dependent, stress-sensitive and stress-independent interactors, identified upon the comparison of TSN2_NS and TSN2_HS protein pools.

D Venn diagram showing the comparison of TSN2_NS interactome with human and yeast SG proteomes (Jain *et al*, 2016).

E Venn diagram showing the comparison between TSN2_NS and TSN2_HS protein pools. TSN2-interacting proteins are divided into three classes: HS-sensitive, HS-independent and HS-dependent. Within each class, the proteins are further classified into two groups. Group 1 contains known human or yeast SG proteins (Jain *et al*, 2016), including SG remodellers (marked in grey colour), whereas group 2 represents components of recently isolated *Arabidopsis* RBP47-SG proteome (Kosmacz *et al*, 2019). The full lists of TSN2-interacting proteins, including previously uncharacterized and potentially novel SG components not belonging to either group 1 or group 2, are provided in Dataset EV1.

F Frequency of RBPs and proteins with prion-like domains or ATPase activity found in TSN2_NS and TSN2_HS protein pools in comparison with yeast and human SG proteomes (Jain *et al*, 2016).

plants, we performed TAPa approach (Fig EV1A) on a small scale using 10-day-old seedlings. Immunoblot analysis with α-Myc confirmed that both TAPa-tagged proteins could be efficiently purified (Fig EV1E).

Mass spectrometry-based label-free quantitative proteomics analysis yielded 2,535 hits across all samples. The relative abundance of proteins was determined using MaxQuant intensity-based absolute quantification (iBAQ), which reports summed intensity values of the identified peptides divided by the number of theoretical peptides (Tyanova *et al*, 2016; Esgleas *et al*, 2020). In order to identify specific interactors of TSN2, we filtered the results using a two-step procedure. First, we selected proteins specifically enriched in either TSN2_NS or TSN2_HS pools compared with the GFP pool. Thereafter, proteins were filtered based on subcellular localization according to the *Arabidopsis* subcellular database SUBA version 4 (Hooper *et al*, 2017), excluding proteins localized to chloroplasts. As a result, we obtained 277 and 149 proteins representing presumptively physiologically relevant interactomes of TSN2 under NS and HS settings, respectively (TSN2_NS and TSN2_HS pools; Dataset EV1).

TSN forms a network of SG protein–protein interactions before the onset of stress

The comparison of TSN2_NS and TSN2_HS protein pools enabled classification of TSN interactors into one of the three classes (Fig 1C): (i) stress-independent interactors, which always associate with TSN regardless of conditions; (ii) stress-dependent interactors, which associate with TSN only under HS; and (iii) stress-sensitive interactors, whose association with TSN is lost during HS.

Although SGs are microscopically visible only under stress conditions (Jain *et al*, 2016), analysis of eggNOG orthologs (Huerta-Cepas *et al*, 2019) revealed that ~20% of proteins from both TSN2_NS and TSN2_HS pools are known components of human or yeast SGs [Fig 1D and E (group 1) and Fig EV2A; Dataset EV2] (Jain *et al*, 2016). Furthermore, the *in silico* analysis showed a significant degree of similarity in the functional distribution of composite proteins between TSN2_NS and TSN2_HS pools and both yeast and human SG proteomes. All of them were enriched in RNA-binding proteins (RBPs), proteins with predicted prion-like domains and proteins with ATPase activity (Fig 1F, Dataset EV2). Apart from the overlaps between TSN2_NS and TSN2_HS pools and yeast and human SG proteomes, 7.5% (21 hits) and 10.7% (16 hits) proteins from TSN2_NS or TSN2_HS pools, respectively, were shared with the recently published *Arabidopsis* SG proteome [RBP47-SG proteome; Fig 1E (group 2) and Fig EV2B; Dataset EV2] isolated from heat-stressed (30 min at 42°C) seedlings expressing GFP-RBP47 (Kosmacz *et al*, 2019). However, larger parts, i.e. 77% (214 proteins) and 79% (118 proteins) of TSN2_NS and TSN_HS protein pools, respectively, were not shared with either yeast, human or *Arabidopsis* RBP47-SG proteomes (Dataset EV2), representing ample resource for finding novel or plant-specific SG components.

Interestingly, 89% (245/277) of hits from the TSN2_NS pool were absent in the TSN2_HS pool, thus constituting the HS-sensitive part of the TSN2 interactome (Fig 1C and E). A significant part of the HS-sensitive pool was represented by the homologues of yeast or human SG remodellers (Fig 1E, proteins marked in grey colour), including protein chaperones [e.g. cpn60 chaperonin proteins (CCTs) or heat shock proteins, such as CH60s and BIP2], multiple RNA and DNA helicases (e.g. RH, MCM and RENT1) or ubiquitin-related proteins (e.g. SUMO1, SUMO2, UPLs or UBPs). The remaining, smaller part of the TSN2_NS pool (11%, 31/277 proteins) was shared with the TSN2_HS pool and represented HS-independent TSN2 interactors (Fig 1C and E). The latter class of proteins included UBP1, RBP47, PAB4 and TCTP, among others. Lastly, 78% (117/149) proteins from the TSN2_HS pool, including several RBPs (HEN4 or BRN1), individual subunits of eEF1 elongation factor (eEF1B and eEF1Bγ), or DNA-directed RNA polymerase II subunits (NRPB1 and NRPB3), were absent from the TSN2_NS pool, representing HS-dependent TSN2 interactors (Fig 1C and E).

We additionally retrieved publicly available direct protein–protein interaction (PPI) data for all proteins found in our proteomic studies. Both TSN2_NS and TSN2_HS protein pools formed a dense network of protein–protein interactions, comprising 239 and 120 nodes and 1,059 and 177 edges, respectively (Appendix Fig S2). In this context, the average number of interactions per protein for these two pools was 8.86 ($P < 1 \times 10^{-16}$) and 2.95 ($P = 7.5 \times 10^{-07}$), respectively. Together with our findings that known SG remodellers interact with TSN in *Arabidopsis* cells in the absence of stress (Fig 1E), these new results pointed to a pre-existing steady-state network of protein–protein interactions as a basal mechanism during SG formation, where TSN could act as a protein assembly platform.

 © 2021 The Authors

TSN is a scaffold protein for SG components

Stress granules are constituted by a dynamic shell and a more stable core (Jain *et al*, 2016). Core proteins have been suggested to act as a scaffold for other SG components (Guillen-Boixet *et al*, 2020; Schmit *et al*, 2021). In a previous study, we observed that TSN did not exchange between the cytoplasm and SG foci upon a fluorescence recovery after photobleaching (FRAP) analysis, suggesting its role as a scaffold protein (Gutierrez-Beltran *et al*, 2015b).

Deletion of scaffold-like molecules is known to have a strong effect on the composition of membrane-less organelles (Espinosa *et al*, 2020; Xing *et al*, 2020). With this in mind and in order to gain a better insight into presumably scaffolding role of TSN in SGs, we investigated the effect of TSN deficiency on the interactome of another plant SG marker protein, RBP47 (Weber *et al*, 2008; Kosmacz *et al*, 2019). For this, we immunoprecipitated GFP-RBP47-bound protein complexes from fully expanded leaves of 18-day-old WT and double *tsn1 tsn2* knockout plants growing under NS conditions (23°C) or subjected to HS (39°C for 60 min) (Appendix Fig S3). In these experiments, we used free GFP-expressing plants as control and followed the same label-free quantitative proteomics procedure as described above for the TSN2-TAPa experiments. Notably, TSN2 was identified in both RBP47_NS and RBP47_HS protein pools (Dataset EV3).

We discovered that in the absence of stress, deletion of TSN resulted in more than 10-fold increase in the RBP47 interactome size accompanied by complete renewal of its protein composition (Fig 2A and B; Dataset EV3). Although TSN deficiency did not significantly affect the size of the RBP47 interactome under HS conditions, it induced almost complete renewal of the protein pool (Fig 2A and B; Dataset EV3). Apart from that, comparison of RBP47 interactomes and TSN2 interactomes revealed ˜11% (31 proteins) overlap in the protein composition between the TSN2_NS pool and RBP47_NS pool isolated from *tsn1 tsn2* plants (Fig 2B). Furthermore, 11 out of 31 shared proteins are homologous to the yeast ATP-driven remodelling complexes [Sheet RBP47_NS (*tsn1 tsn2*), Dataset EV3]. Taken together, these data demonstrate massive reorganization of the RBP47 interactome induced by TSN deficiency, providing evidence for the role of TSN as a scaffold during SG formation.

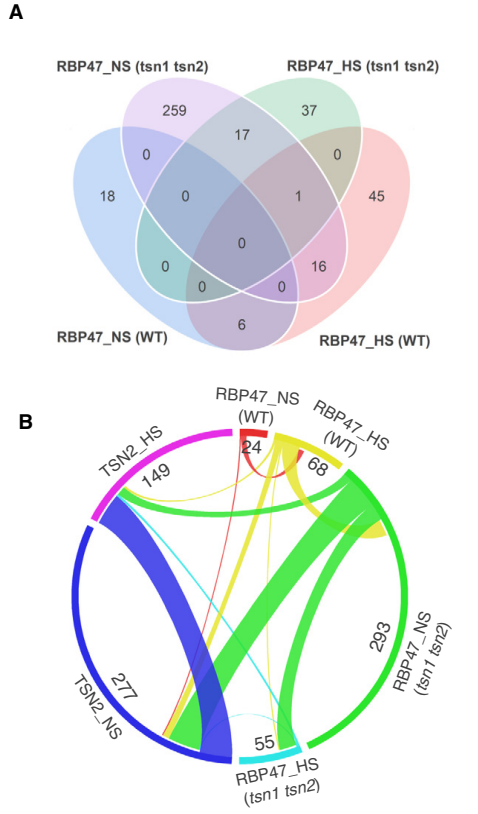

Figure 2. TSN deficiency promotes a massive reorganization of the RBP47 interactome.

A Venn diagram showing the comparison between RBP47_NS and RBP47_HS protein pools isolated from WT and *tsn1 tsn2* plants.

B Circos plot showing the comparison between four RBP47 interactomes and two TSN2 interactomes.

TSN-interacting proteins co-localize with TSN2 in cytoplasmic foci

To ascertain the SG localization of TSN2-interacting proteins identified by mass spectroscopy, we selected 16 of the most interesting proteins (Fig 3A). These included homologues of well-known yeast and animal SG-associated proteins (eIF4E5, PAB4 and the ribosomal subunit RPS11) and hypothetical plant-specific SG components with a role in fundamental eukaryotic pathways (e.g. SKP1, MCA-Ia, TCTP and both SnRK1α1 and SnRK1α2 isoforms). First, we performed co-localization studies to investigate whether selected TSN-interacting proteins were translocated to TSN2 foci under stress. To this end, protoplasts were isolated from *Nicotiana benthamiana* (*N. benthamiana)* leaves co-transformed with RFP-TSN2 and individual GFP-TSN-interacting proteins. Co-transformation of the cytoplasmic protein GFP-ADH2 or the SG marker GFP-UBP1 with RFP-TSN2 was used as a negative and positive control, respectively (Fig 3B and C). The degree of co-localization was calculated using pixel correlation analysis (Fig 3C) (French *et al*, 2008). As shown in Figs 3B and C, and EV3; Appendix Fig S4, all selected proteins co-localized with TSN2 in punctate foci upon HS.

Next, to elucidate whether these proteins are associated with TSN2 in the heat-induced SGs, we performed bimolecular fluorescence complementation (BiFC) analyses in *N. benthamiana* leaf cells or protoplasts co-transformed with cYFP-TSN2 and individual nYFP-TSN-interacting proteins. Fluorescence complementation was observed in 10 out of 16 shortlisted TSN-interacting proteins. The YFP signal exhibited diffuse cytoplasmic localization under control conditions (23°C; Appendix Fig S5) and redistributed to punctate foci upon HS (Fig 3D).

© 2021 The Authors

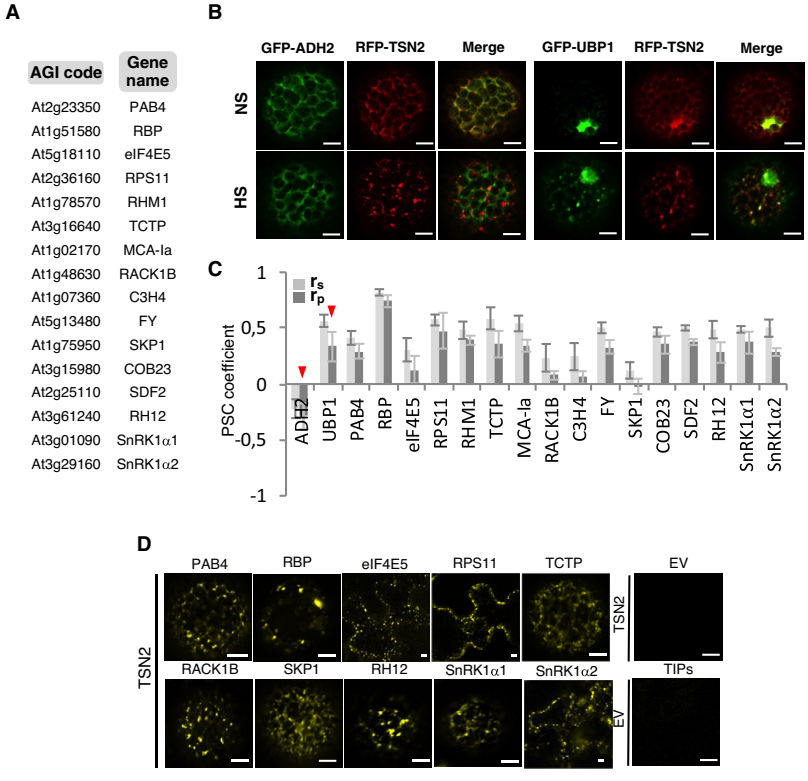

Figure 3. TSN2 and its interactors are localized in heat-induced SGs.

A A list of TSN-interacting proteins selected for the co-localization analysis.

B Co-localization of RFP-TSN2 (red) with GFP-ADH2 (negative control) and GFP-UBP1 (positive control) in *N. benthamiana* protoplasts incubated under 23°C (NS) or at 39°C for 40 min (HS). Scale bars = 5 μm.

C Pearson and Spearman coefficients (r_p and r_s, respectively) of co-localization (PSC) of RFP-TSN2 with individual GFP-tagged TSN-interacting proteins listed in *A* and with both negative and positive control proteins (denoted by red arrowheads) under HS. Data represent means ± SD of at least five replicate measurements from three independent experiments.

D BiFC between cYFP-TSN2 and nYFP-TSN-interacting proteins in *N. benthamiana* leaf cells or protoplasts after HS (39°C for 40 min). BiFC analysis of cYFP-TSN2 and nYFP-TSN-interacting proteins (TIPs) with empty vectors (EV) encoding nYFP and cYFP, respectively, was used as a negative control. Only one representative example of BiFC between cYFP and nYFP-TIP is shown. Scale bars = 5 μm.

To further corroborate the association of TSN with novel plant SG components *in planta*, translationally controlled tumour protein (TCTP) and an uncharacterized RNA-binding protein (RBP) were selected. TCTP was previously observed in both nuclei and cytoplasm (Betsch *et al*, 2017). GFP-tagged RBP and TCTP proteins relocalized to cytoplasmic foci under HS in *Arabidopsis* root tip cells (Fig EV4A). The SG identity of the RBP and TCTP foci was validated by co-localization analysis with the SG marker eIF4E (Fig EV4B) (Gutierrez-Beltran *et al*, 2015b). Subsequently, a Förster resonance energy transfer (FRET) assay in heat-stressed *N. benthamiana* leaves confirmed that TSN2 interacted with TCTP and RBP (Fig EV4C). Finally, TSN co-immunoprecipitated with both TCTP and RBP but not with GFP (negative control) in *Arabidopsis* protein extracts, confirming the *in vivo* protein–protein interaction (Fig EV4D). Taken together, these findings further reinforce the view that TSN plays a scaffolding role in recruiting a wide range of proteins to SGs.

TSN associates with SG proteins via the highly disordered N-terminal region

Studies in mammalian and yeast cells have suggested that SGs are multicomponent viscous liquid droplets formed in the cytoplasm by LLPS (Kroschwald *et al*, 2015; Protter & Parker, 2016). Although the molecular details underlying intracellular LLPS are largely obscure, recent evidence suggests that IDRs mediate this process (Posey *et al*,

 © 2021 The Authors

2018; Alberti *et al*, 2019; Yang *et al*, 2020). In this context, we estimated the predicted enrichment of IDRs and propensity of proteins for LLPS for both TSN2_NS and TSN2_HS interactomes as compared to GFP-TAPa control protein pools using IUPred and PSPredictor algorithms, respectively (preprint: Sun *et al*, 2019; Erdos & Dosztanyi, 2020). The analysis revealed significant enhancement of IDR frequency (Fig 4A) and propensity for LLPS (Fig 4B) in both TSN interactomes in agreement with the scaffolding role of TSN in the formation of phase-separated granules.

In mammalian cells, IDRs of G3BP or hnRNPA1 regulate SG assembly via LLPS (Molliex *et al*, 2015; Guillen-Boixet *et al*, 2020; Yang *et al*, 2020). Considering this fact as well as that TSN was shown to modulate the integrity of SGs in *Arabidopsis* (Gutierrez-Beltran *et al*, 2015b), we evaluated the per-residue intrinsically disordered propensities of TSN2 itself by six commonly used predictors, including PONDR-VLXT, PONDR-VL3, PONDR-VSL2, IUpred_short, IUpred_long and PONDR-FIT (Meng *et al*, 2015). Figure 4C shows that TSN2 is expected to have 11 disordered regions if averaged for six predictors (score above 0.5). Thus, the SN region (tandem repeat of four N-terminally located SN domains) of TNS2 is predicted to be highly disordered, whereas the Tudor domain is predicted to be one of the most ordered parts of the protein. This observation was confirmed using the D^2P^2 database providing information about the predicted disorder and selected disorder-related functions (Appendix Fig S6A) (Oates *et al*, 2013). Notably, similar results were obtained for the TSN1 protein isoform which is functionally redundant with TSN2 (Appendix Fig S6A and B) (dit Frey *et al*, 2010).

To investigate whether it is the highly disordered part of TSN which is required for interaction with SG components, we compared the association of the SN region, the Tudor region (composed of the Tudor domain and the fifth, partial SN domain; Fig 4C) and full-length TSN (as a control) with four different TSN-interacting proteins in heat-stressed *N. benthamiana* leaves using BiFC (Fig 4D). The experiment revealed reconstitution of fluorescent signal with all four TSN interactors in case of both full-length TSN2 and SN region, whereas none of the interactors could form a complex with Tudor region (Fig 4D). Furthermore, expression of either full-length TSN2 or SN region yielded identical, punctate BiFC localization pattern. Taken together, these results prompted us to hypothesize that TSN protein could recruit SG components via IDRs, promoting rapid coalescence of microscopically visible SGs upon stress exposure.

Arabidopsis SG-associated proteins are common targets of both TSN1 and TSN2 isoforms

TSN1 and TSN2 proteins were suggested to be redundant in conferring *Arabidopsis* stress tolerance (dit Frey *et al*, 2010; Gutierrez-Beltran *et al*, 2015b). To investigate whether this redundancy is conserved at the SG level, we isolated the TSN1 interactome from unstressed plants using the same TAPa procedure as described above for TSN2 (Fig EV1A, B and E). As a result, we obtained the TSN1_NS pool enriched in 215 proteins (Dataset EV1). Out of these, 110 (51%) were TSN1-specific, whereas the remaining fraction (105 proteins, 49%) represented common interactors of TSN1 and TSN2, reflecting their functional redundancy (Fig 5A). Notably, the pool of common interactors of TSN1 and TSN2 was enriched in homologues of human and/or yeast SG proteins, such as PAB4, small ribosomal subunits, RNA or DNA helicases or CCT proteins (group 1, Fig 5A). In addition, the common TSN1 and TSN2 interactors included many recently identified members of *Arabidopsis* RBP47-SG proteome (group 2, Fig 5A) (Kosmacz *et al*, 2019), as well as novel plant SG components (group 3, Fig 5A) verified in the current study through either BiFC analysis or co-localization or by using both methods (Figs 3, EV3 and EV4).

To corroborate the proteomics results, we chose DEAD-box ATP-dependent RNA helicase 12 (RH12), as a common interactor of TSN1 and TSN2. RH12 is a nucleocytoplasmic protein associated with SGs under stress (Chantarachot *et al*, 2020). First, we confirmed the molecular interaction between two isoforms of TSN and RH12 by co-immunoprecipitation in cell extracts from *Agrobacterium*-infiltrated *N. benthamiana* leaves. RH12 co-immunoprecipitated with both TSN1 and TSN2 but not with GFP (Fig 5B). Second, we produced *Arabidopsis* lines stably expressing GFP-RH12 under its native promoter and observed re-localization of the fusion protein to heat-induced SGs in root tip cells (Fig 5C and Appendix Fig S7). Taken together, these data are consistent with TSN1 and TSN2 as functionally redundant in providing a scaffold platform for the recruitment of a wide range of plant SG components.

Identification of a salt stress-induced TSN2 interactome

TSN2 localizes to SGs under salt stress (Yan *et al*, 2014). To investigate the differences between salt stress- and HS-induced TSN interactomes as a proxy for SG proteome variability under different types of stresses, we purified TSN2-interacting proteins from salt-treated *Arabidopsis* plants using our standard TAPa purification procedure. The resulting TSN2_NaCl protein pool was much (9.3–17 times) smaller than both TSN2_NS and TSN2_HS pools, and contained only 16 protein hits (Dataset EV1), 5 and 7 of which were shared with TSN2_NS and TSN2_HS pools, respectively (Fig 6A). Apart from the presence of well-defined mammalian and/or yeast SG proteins, such as HSP70, all three protein pools contained RBP47. To corroborate this result, we performed co-immunoprecipitation of native TSN using protein extracts prepared from GFP-RBP47-expressing *Arabidopsis* seedlings exposed to heat (60 min at 39°C) or salt (60 min, 200 mM NaCl) stress. TSN co-immunoprecipated with GFP-RBP47 under both stresses, as well as in the absence of stress (Fig 6B), suggesting that RBP47 is a constitutive interactor of TSN that might be recruited to SGs under various types of stresses.

Since we have found that TSN exhibits stress type-dependent variation in both size and composition of its interactome (Fig 6A; Dataset EV1), we then addressed SG recruitment of TSN-interacting proteins to SGs in a stress-type-specific manner using confocal microscopy. To this end, we examined the localization of RBP47 (present in all three TSN2 interactomes), as well as UBP1, TCTP and SnRK1α2 (all present in both TSN_NS and TSN_HS pools but absent in TSN2_NaCl pool) in root tip cells of 5-day-old *Arabidopsis* seedlings expressing GFP-tagged fusions of these proteins. Analysis revealed that while RBP47 and UBP1 were localized to both HS- and salt-induced cytoplasmic puncta, TCTP and SnRK1α2 showed punctate localization only under HS (Fig 6C). These data point to heterogeneity of SG composition in plants and additionally demonstrate that some SG resident proteins might not associate with TSN in SGs (e.g. UBP1 absent in the TSN2_NaCl protein pool).

© 2021 The Authors

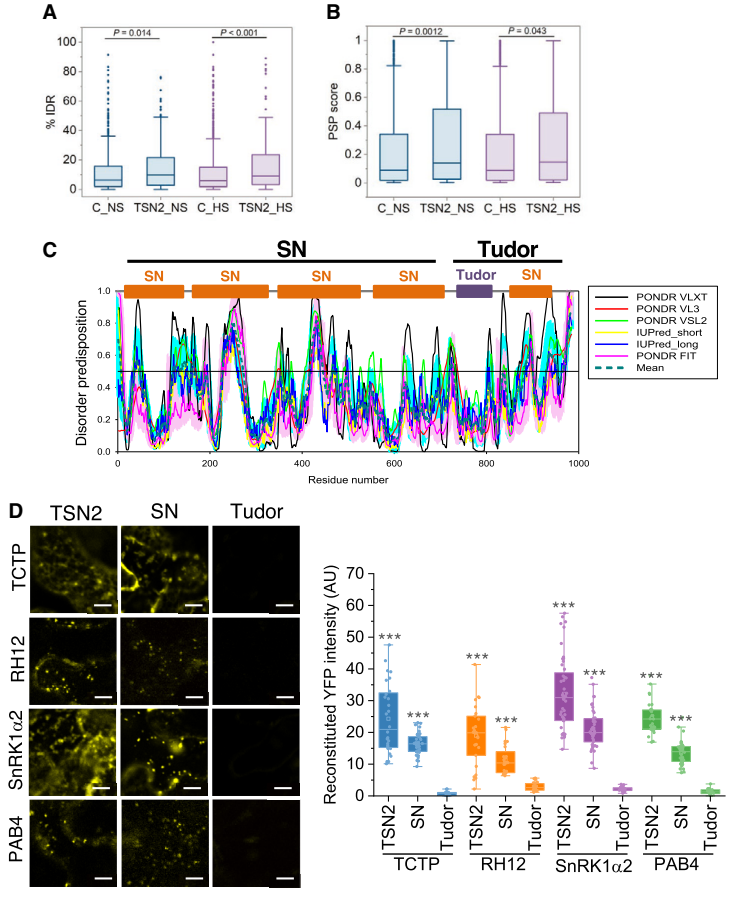

Figure 4. The highly disordered region of TSN2 is required for interaction with SG proteins.

A, B % IDR (A) and propensity for LLPS (B) in TSN2_NS and TSN2_HS interactomes versus corresponding GFP-TAPa controls (C_NS and C-HS) using IUPred and PSPredictor algorithms, respectively. Upper and lower quartiles, medians and extreme points are shown. The number of protein sequences included to the analyses was 566, 277, 995 and 149 for C_NS, TSN2_NS, C_HS and TSN2_HS, respectively. *P* values denote statistically significant differences for comparisons to controls (two-tailed *t*-test).

C Disorder profiles of TSN2 generated by PONDR-VLXT, PONDR-VL3, PONDR-VSL2, IUPred-short, IUPred-long and PONDR-FIT and a consensus disorder profile (based on mean values of six predictors). SN, staphylococcal nuclease region composed of four N-terminally situated SN domains. C-terminally situated Tudor region is composed of the domain of the same name and a partial SN domain.

D BiFC between cYFP-TSN2 (full-length), cYFP-SN or cYFP-Tudor and nYFP-TSN-interacting proteins in *N. benthamiana* protoplasts after HS (39°C for 40 min). Scale bars = 10 μm. Boxplots show quantification of the reconstituted YFP signal. AU, arbitrary units. Upper and lower box boundaries represent the first and third quantiles, respectively, horizontal lines mark the median, and whiskers mark the highest and lowest values. Three independent experiments, each containing seven individual measurements, were performed. ***$P < 0.001$ versus Tudor (one-way ANOVA).

TSN interacts with and mediates assembly of SnRK1α in heat SGs

The evolutionary conserved subfamily of yeast sucrose nonfermenting-1 protein kinase (SNF1)/mammalian AMP-activated protein kinase (AMPK)/plant SNF1-related kinase 1 (SnRK1) plays a central role in metabolic responses to declined energy levels in response to nutritional and environmental stresses (Broeckx *et al*, 2016). These kinases typically function as a heterotrimeric complex composed of two regulatory subunits, β and γ, and an α-catalytic subunit. In *Arabidopsis*, the α-catalytic subunit of SnRK1 is encoded

 © 2021 The Authors

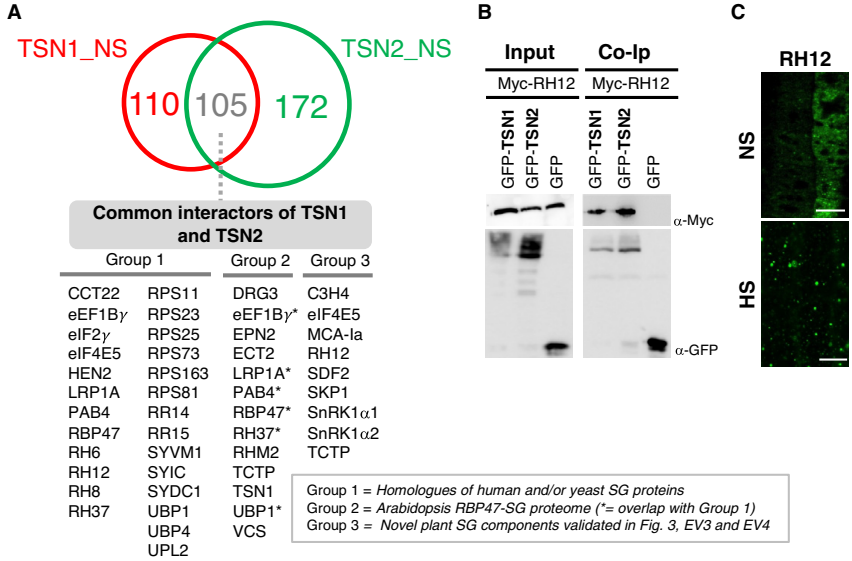

Figure 5. Interactomes of *Arabidopsis* TSN1 and TSN2 largely overlap.

A Venn diagram showing the overlap between TSN1 and TSN2 interactomes isolated by TAPa from *Arabidopsis* plants grown under NS conditions. Common interactors of TSN1 and TSN2 are classified into three groups: (i) homologues of human and/or yeast SG proteins, (ii) proteins constituting recently isolated *Arabidopsis* RBP47-SG proteome (Kosmacz *et al*, 2019) and (iii) novel plant SG components validated in Figs 3, EV3 and EV4. The full lists of TSN1- and TSN2-interacting proteins, including as yet uncharacterized and potentially novel SG components not belonging to any of the three groups, are provided in Dataset EV1.

B Co-immunoprecipitation (Co-Ip) of the two TSN isoforms and RH12 in protein extracts prepared from *N. benthamiana* leaves agro-infiltrated with GFP-TSN1 or GFP-TSN2 and Myc-RH12. Free GFP was used as a negative control. Input and Co-Ip fractions were analysed by immunoblotting using α-Myc and α-GFP.

C Localization of RH12 in root cells of 5-day-old *Arabidopsis* seedlings expressing GFP-RH12 under control of the native promoter. The seedlings were grown under 23°C (NS) or incubated at 39°C for 60 min (HS). Scale bars = 10 μm.

Source data are available online for this figure.

by two functionally redundant genes, *SnRK1α1* and *SnRK1α2* (Baena-Gonzalez *et al*, 2007). We found that SnRK1α1 and SnRK1α2 (also known as KIN10 and KIN11, respectively) are TSN-interacting proteins re-localized to SGs upon HS (Figs 3, 4D and 6C). To dissect the functional relevance of TSN binding and SG localization of SnRK1α1 and SnRK1α2 proteins, we first corroborated the interaction with TSN2 using two different approaches. First, we performed co-immunoprecipitation of native TSN from protein extracts prepared from heat-stressed *Arabidopsis* plants expressing GFP-SnRK1α1 and GFP-SnRK1α2. We found that native TSN co-immunoprecipitated with both GFP-SnRK1α1 and GFP-SnRK1α2 but not with free GFP, which was used as a negative control (Fig 7A). In addition, co-immunoprecipitation analysis confirmed our proteomics data suggesting that SnRK1α is bound to TSN also in the absence of stress (Fig 7B). Second, a FRET assay demonstrated that TSN2 directly interacts with both SnRK1α1 and SnRK1α2 in *N. benthamiana* leaves under HS (Fig 7C).

To explore the molecular link between SnRK1α and TSN2, we first examined the potential localization of SnRK1 in the root tip cells of heat-stressed WT and TSN-deficient (*tsn1 tsn2*) plants. As shown in Fig 7D, TSN is dispensible for localization of either GFP-SnRK1α1 or GFP-SnRK1α2 to cytoplasmic foci. However, we observed a significant decrease in the number of SnRK1α foci and a simultaneous increase in their size in *tsn1 tsn2* compared with WT plants (Fig 7E and F). The HS induction in WT and *tsn1 tsn2* plants was confirmed by expression analysis of *HSP101* and *HSF* (Appendix Fig S1). We conclude that TSN takes part in the assembly of SnRK1α isoforms in *Arabidopsis* heat SGs.

Stress granules are dynamic structures where many proteins move continuously (Mahboubi & Stochaj, 2017). To investigate the role of TSN in the SnRK1α dynamics, we measured SnRK1α mobility within heat-induced SGs in the root tip cells of WT and *tsn1 tsn2* plants using FRAP. While SnRK1α2 revealed a lack of any fluorescent signal recovery in a TSN-independent manner, TSN deficiency led to a significant decrease in both signal recovery rate and proportion of the initial signal recovery of SnRK1α1 (Figs 7G and H, and EV5A). Thus, we conclude that TSN is required for full mobility of the SnRK1α1 isoform.

Catalytic and regulatory domains of SnRK1α1 exhibit differential behaviour in SGs

To investigate the role of N-terminal catalytic and C-terminal regulatory domains of SnRK1α1 (hereafter designated as SnRK1α1^{CD} and

© 2021 The Authors

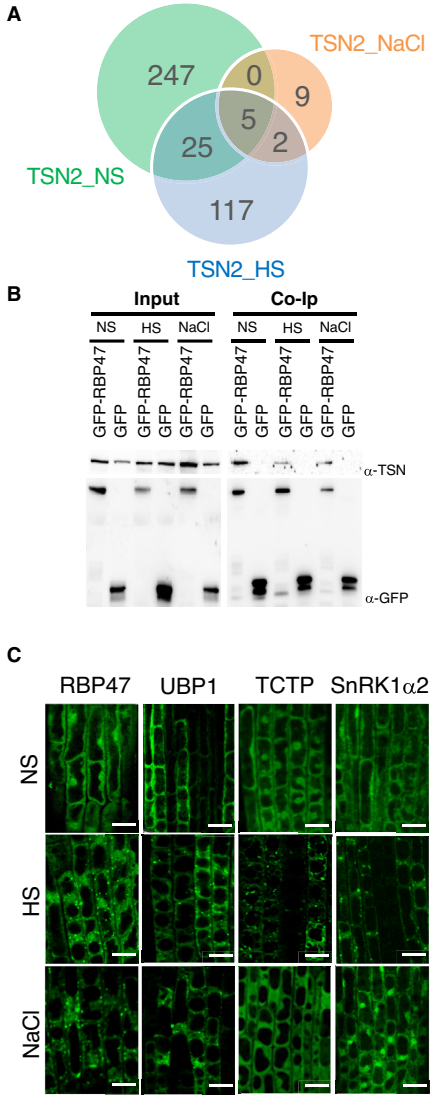

Figure 6. Identification of *Arabidopsis* salt-induced TSN2 interactome.

A Venn diagram showing a comparison between TSN2_NS, TSN2_HS and TSN2_NaCl protein pools.

B Co-immunoprecipitation (Co-Ip) of TSN and RBP47 in protein extracts prepared from 10-day-old *Arabidopsis* seedlings expressing *Pro35S:GFP-RBP47* and grown under no stress (NS), HS (39°C for 60 min) or salt (NaCl) stress (150 mM NaCl for 60 min) conditions. The GFP-expressing line was used as a negative control. Endogenous TSN (107 kD) was detected in total fractions (Input) and fractions co-immunoprecipitated (Co-Ip) with RBP47 but not with free GFP in all three conditions. Input and Co-Ip fractions were analysed by immunoblotting using α-TSN and α-GFP.

C Localization of GFP-tagged proteins in root cells of 5-day-old *Arabidopsis* seedlings expressing *Pro35S:GFP-RBP47*, *Pro35S:GFP-UBP1*, *Pro35S:GFP-TCTP* and *ProUBQ:GFP-SnRK1α2*. The seedlings were grown under 23°C (NS), incubated at 39°C for 60 min (HS) or treated with 200 mM NaCl at 23°C for 60 min (NaCl). Scale bars = 10 μm.

Source data are available online for this figure.

SnRK1α1RD, respectively; Fig 7I) in SGs, we monitored the localization of their GFP-tagged variants and SG marker RFP-RBP47 in *N. benthamiana* protoplasts. Under control conditions (NS), both SnRK1α1^{CD} and SnRK1α1RD domains were localized in the cytoplasm and nucleus, similar to the full-length SnRK1α1 (Fig EV5B). After exposure to HS (40 min at 39°C), SnRK1α1 and SnRK1α1^{CD} became associated with RBP47 foci, whereas SnRK1α1RD remained mostly in the cytoplasm (Fig 7J). Notably, re-localization of both SnRK1α1 and RBP47 to cytoplasmic puncta during HS was strongly suppressed by the addition of cycloheximide (CHX), which is known to prevent the formation of SGs in yeast, mammalian and plant cells by reducing the pool of free RNA (Fig 7J) (Gutierrez-Beltran *et al*, 2015b; Jain *et al*, 2016; Saad *et al*, 2017). Punctate and predominantly diffused cytoplasmic localization patterns of the catalytic and the regulatory domains of SnRK1α1, respectively, were also observed in root tip cells from 5-day-old *Arabidopsis* WT seedlings expressing GFP-SnRK1α1^{CD} or GFP-SnRK1α1RD and exposed to HS (Fig EV5C), and was confirmed by foci quantification (Fig EV5D). Furthermore, in a kinetic analysis the number of SnRK1α1RD foci in *N. benthamiana* protoplasts was higher at 20 min than at 40 min of HS (Fig EV5E). Collectively, these results indicate that regulatory and catalytic domains may have different roles in targeting SnRK1α1 to the heat SGs.

TSN and SGs confer heat-induced activation of SnRK1

To link SG localization of SnRK1α1 with its heat-dependent regulation, we initially investigated whether HS affects SnRK1 kinase activity *in vivo*. To this end, we subjected 10-day-old WT *Arabidopsis* seedlings to 39°C for 0, 20, 40 and 60 min and then assessed SnRK1α T175 phosphorylation by immunoblotting using α-phospho-AMPK Thr175 (α-pT175), which recognizes phosphorylated forms of both SnRK1α1 (upper band 61.2 kD) and SnRK1α2 (lower band 58.7 kD) (Rodrigues *et al*, 2013; Nukarinen *et al*, 2016). In a control test, we confirmed the α-pT175 affinity efficiency using ABA treatment which is known to induce SnRK1α T175 phosphorylation (Appendix Fig S8) (Jossier *et al*, 2009). Time-course analysis of the level of SnRK1α T175 phosphorylation under HS demonstrated that the two SnRK1α isoforms were rapidly activated by stress (Fig 8A). Yet, the levels of unphosphorylated SnRK1α and TSN remained constant during HS (Fig 8A). To verify whether heat-induced activation of SnRK1α depends on the formation of SGs, the seedlings were treated with CHX and then subjected to HS. CHX treatment abrogated heat-induced phosphorylation of SnRK1α T175 (Fig 8B). To correlate heat-induced activation of the SnRK1α isoforms with their targeting to SGs, we carried out a time-course analysis of SnRK1α localization in root tip cells of 5-day-old seedlings expressing GFP-SnRK1α1 or GFP-SnRK1α2. This analysis revealed that both SnRK1α isoforms become visibly associated with SGs after 40 min of HS and that the number of GFP-SnRK1α foci further increases by 60 min

 © 2021 The Authors

(Fig 8C and D), perfectly matching the kinetics of SnRK1α T175 phosphorylation (Fig 8A). These results establish a link between the formation of heat SGs and activation of SnRK1α.

To investigate whether TSN is involved in the regulation of the SnRK1α kinase activity, we evaluated the level of SnRK1α T175 phosphorylation in *tsn1 tsn2* seedlings under HS. Similar to the CHX treatment, TSN deficiency prevented heat-induced phosphorylation of SnRK1α T175 (Fig 8E). This effect was reverted by complementation of the *tsn1 tsn2* mutant with *TSN2* (Fig 8F). Thus, we hypothesized that TSN might be a positive upstream regulator of the SnRK1-dependent stress signalling pathway. Next, we performed RT–qPCR analysis of the *DARK INDUCIBLE 2* (*DIN2; At3g60140*) and *DIN6 (At3g47340)*, two target genes of the SnRK1-dependent signalling pathway (Baena-Gonzalez *et al*, 2007; Rodrigues *et al*, 2013; Belda-Palazon *et al*, 2020), in 10-day-old WT and *tsn1 tsn2* seedlings. Given the lethality of the double *snrk1α1 snrk1α2* knockout, we employed a partial loss-of-function mutant *snrk1α1*$^{-/-}$ *snrk1α2*$^{-/+}$ as a control (Belda-Palazon *et al*, 2020). Heat stress

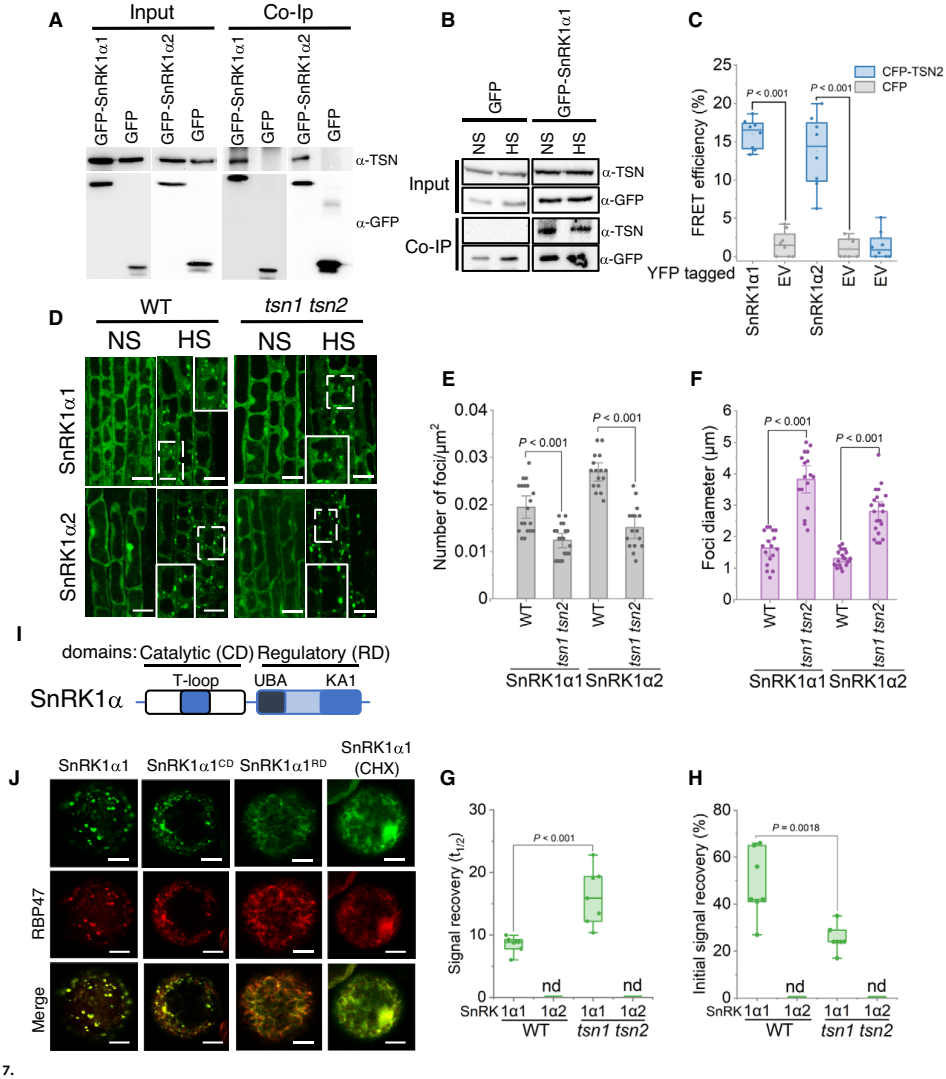

Figure 7.

© 2021 The Authors

Figure 7. TSN interacts with and mediates the assembly of SnRK1α in heat SGs.

A Co-immunoprecipitation of TSN and SnRK1α1 and SnRK1α2 in protein extracts prepared from 10-day-old *Arabidopsis* seedlings expressing *ProUBQ:GFP-SnRK1α1* or *ProUBQ:GFP-SnRK1α2* and exposed to HS (39°C for 60 min). The GFP-expressing line was used as a negative control. Endogenous TSN was detected in the total fractions (Input) and in the fractions co-immunoprecipitated (Co-Ip) with SnRK1α1 or SnRK1α2 but not with free GFP. Input and Co-Ip fractions were analysed by immunoblotting using α-TSN and α-GFP.

B Co-immunoprecipitation of TSN and SnRK1α1 in protein extracts prepared from 10-day-old *Arabidopsis* seedlings expressing *ProUBQ:GFP-SnRK1α1* and grown under NS (23°C) conditions or subjected to HS (39°C for 60 min). Endogenous TSN was detected in the total fractions (Input) and in the fractions co-immunoprecipitated (Co-Ip) with SnRK1α1 under both NS and HS conditions. Input and Co-Ip fractions were analysed by immunoblotting using α-TSN and α-GFP.

C FRET assay of the indicated protein combinations using CFP-YFP pair in *N. benthamiana* leaves under HS (39°C for 40 min). EV, empty vector (negative control). Upper and lower box boundaries represent the first and third quantiles, respectively; horizontal lines mark the median of at least eight replicate measurements, and whiskers mark the highest and lowest values. The experiment was repeated three times with similar results. *P* values denote statistically significant differences for comparisons to plants expressing EV (two-tailed *t*-test).

D Localization of GFP-SnRK1α1 and GFP-SnRK1α2 in root cells of 5-day-old *Arabidopsis* WT and *tsn1 tsn2* seedlings grown under 23°C (NS) or incubated at 39°C for 60 min (HS). Insets show enlarged areas inside dashed rectangles. Scale bars = 10 μm.

E, F Number (E) and size (F) of SnRK1α1- and SnRK1α2-foci in root tip cells of WT and *tsn1 tsn2* seedling expressing *ProUBQ:GFP-SnRK1α1* or *ProUBQ:GFP-SnRK1α2*, respectively, after HS (60 min at 39°C). Data represent means ± SD of at least 16 replicate measurements from three independent experiments. *P* values denote statistically significant differences for comparisons to WT plants (two-tailed *t*-test).

G, H Signal recovery rate ($t_{1/2}$; G) and proportion of the initial signal recovered (%; H) of GFP-tagged isoforms of SnRK1α in root tip cells of WT and *tsn1 tsn2* seedlings expressing *ProUBQ:GFP-SnRK1α1* and *ProUBQ:GFP-SnRK1α2* after HS (60 min at 39°C). nd, not detected. Upper and lower box boundaries represent the first and third quantiles, respectively; horizontal lines mark the median of at least seven replicate measurements, and whiskers mark the highest and lowest values. The experiment was repeated three times with similar results. *P* values denote statistically significant differences for comparisons to WT plants (two-tailed *t*-test).

I Schematic diagram of SnRK1α protein structure showing catalytic (CD) and regulatory (RD) domains. The CD includes the phosphorylated T-loop region. RD includes both kinase-associated 1 (KA1) and ubiquitin-associated (UBA) subdomains.

J Co-localization of GFP-SnRK1α1, GFP-SnRK1α1^{CD} or GFP-SnRK1α1RD with RFP-RBP47 in *N. benthamiana* protoplasts subjected to HS (40 min at 39°C). For co-localization analysis under NS conditions see Fig EV5B. For CHX treatment, protoplasts were incubated with 200 ng/μl CHX for 30 min at 23°C before HS. GFP and RFP fusion proteins were expressed under the control of the UBQ and 35S promoter, respectively. Scale bars = 5 μm.

Source data are available online for this figure.

induction in WT and mutants was confirmed by increased expression of *HSP101* and *HSF* (Appendix Fig S1). We found that while in WT, the expression of *DIN2* and *DIN6* was markedly enhanced by HS, this effect was abrogated by CHX treatment or deficiency of either SnRK1α (*snrk1α1*$^{-/-}$ *snrk1α2*$^{-/+}$) or TSN (*tsn1 tsn2*) (Fig 8G). Accordingly, complementation of *tsn1 tsn2* mutant with *TSN2* WT allele partly rescued the HS-dependent increase in expression of *DIN2* and *DIN6* (Fig 8G). Our data demonstrate that TSN is essential for SnRK1-dependent signalling under HS.

Discussion

One of the earliest, evolutionarily conserved events upon stress perception in eukaryotic cells is the assembly of cytoplasmic SGs which provide a mechanism for cell survival (Thomas *et al*, 2011; Mahboubi & Stochaj, 2017). Understanding the molecular composition and regulation of SGs is a rapidly growing field, but most of the research so far has utilized animal or yeast systems.

The scaffold-client model has been used to explain the composition heterogeneity of membrane-less organelles, such as SGs, in mammalian and yeast cells (Banani *et al*, 2016; Schmit *et al*, 2021). In this model, the assembly of granules is regulated by the valency, concentration and molar ratio of scaffold molecules. In accordance with this model, deletion of the scaffold-like molecules perturbs the molecular composition of membrane-less organelles (Espinosa *et al*, 2020; Xing *et al*, 2020). While scaffolds are defined as components essential for the structural integrity of the membrane-less organelles, clients are not necessary for the integrity but are recruited through interactions with scaffolds. Multiple lines of evidence suggest also that IDRs of scaffold proteins contribute to the assembly of the membrane-less organelles including SGs (Gilks *et al*, 2004; Yang *et al*, 2020; Fomicheva & Ross, 2021).

We have previously shown that TSN is stably associated with *Arabidopsis* SGs and that its deletion affects the structural integrity of SGs, the observations leading us to assume scaffolding role for TSN (Gutierrez-Beltran *et al*, 2015b). In agreement with the proposed role, here we present experimental evidence that TSN deficiency strongly affects the composition of the SG proteome (Fig 2). These results, together with the finding that the N-terminal tandem repeat of four SN domains is an ID-reach region recruiting TSN to SGs and participating in protein–protein interaction make it reasonable to envisage the role of the SN domains of TSN as a docking platform maintaining a pre-existing state of SGs in plant cells.

It has been recently postulated that SG assembly in yeast and mammalian cells is a highly regulated multi-step process controlled by numerous proteins collectively known as SG remodellers, and in particular by ATP-dependent remodelling complexes (Jain *et al*, 2016; Protter & Parker, 2016). Thus, ATP-dependent events mediated by ATPases, such as movement of mRNPs to sites of SG formation by motor proteins or remodelling of mRNPs to load required components, could be imperative for promoting SG assembly. In this context, the interaction of the CCT ATPase complex with SG components and activity of the DEAD-box helicase 1 (Ded1) are both crucial for the proper assembly of SGs in yeast cells (Hilliker *et al*, 2011; Jain *et al*, 2016). In addition to ATP-dependent remodellers, ubiquitin-related proteins including ubiquitin-like SUMO ligases, ubiquitin-protein ligases (UPL) and proteases (UBP) have been shown to control the assembly of mammalian and yeast SGs (Xie *et al*, 2018; Keiten-Schmitz *et al*, 2020; Marmor-Kollet *et al*, 2020). Considering that enrichment of the TSN interactome for SG remodellers, including CCT proteins, SUMO ligases, ubiquitin-related proteins and DEAD-box RNA/DNA helicases, occurs in the absence of stress stimulus (Fig 1E), we hypothesize that interaction between these proteins and TSN is necessary for the early steps of SG assembly in plants. Once stress

 © 2021 The Authors

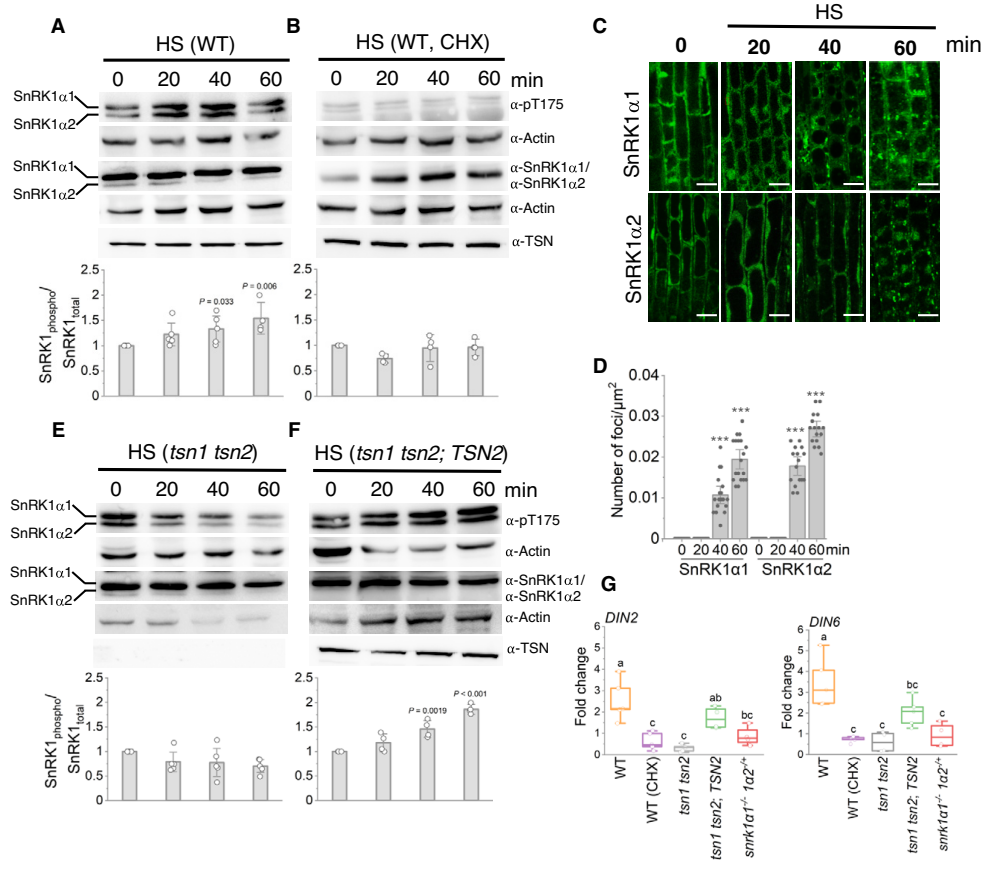

Figure 8. TSN and SGs confer heat-induced activation of SnRK1.

A, B Immunoblot analysis with indicated antibodies of protein extracts prepared from root tips of 10-day-old *Arabidopsis* WT heat-stressed seedlings (39°C) 0, 20, 40 and 60 min after the onset of HS. For CHX treatment in B, the seedlings were pre-treated with 200 ng/μl CHX for 30 min before HS. The charts show SnRK1 activity, expressed as the ratio of phosphorylated to total SnRK1 protein. The data represent mean ratios of integrated band intensities (for both isoforms) normalized to 0 min ± SD from at least four different experiments. *P* values denote statistically significant differences for comparisons to 0 min (two-tailed *t*-test).

C Localization of GFP-SnRK1α1 and GFP-SnRK1α2 in root cells of 5-day-old *Arabidopsis* WT seedlings incubated at 39°C and imaged at the indicated time points. Scale bars = 10 μm.

D Quantification of GFP-SnRK1α1 and GFP-SnRK1α2 foci in the experiment shown in C. Data represent means ± SD of at least 16 replicate measurements. The experiment was repeated three times with similar results. ***$P < 0.05$ (two-tailed *t*-test).

E, F Immunoblot analysis with indicated antibodies of protein extracts prepared from root tips of 10-day-old *Arabidopsis tsn1 tsn2* (E) *or tsn1 tsn2* expressing *ProTSN2:GFP-TSN2* (F) heat-stressed seedlings (39°C) 0, 20, 40 and 60 min after the onset of HS. The charts show SnRK1 activity, expressed as the ratio of phosphorylated to total SnRK1 protein. The data represent mean ratios of integrated band intensities (for both isoforms) normalized to 0 min ± SD from at least four different experiments. *P* values denote statistically significant differences for comparisons to 0 min (two-tailed *t*-test).

G Expression levels of *DIN2* and *DIN6* in *Arabidopsis* WT, *tsn1 tsn2*, *tsn1 tsn2;TSN2* and *snrk1α1*$^{-/-}$ *snrk1α2*$^{-/+}$ 10-day-old heat-stressed seedlings relative to unstressed controls. For CHX treatment, the WT seedlings were pre-treated with 200 ng/μl CHX for 30 min before HS. Upper and lower box boundaries represent the first and third quantiles, respectively. Horizontal lines mark the median of five replicate measurements, and whiskers mark the highest and lowest values. Means with different letters are significantly different at $P < 0.05$ (one-way ANOVA).

Source data are available online for this figure.

© 2021 The Authors

stimulus is perceived, the SG remodellers might detach from TSN and aid in SG shell assembly.

Our present study has identified more than 400 TSN interactors, most of which (~77%) are previously unknown candidates for SG components. While this provides a broad resource for functional studies, one should however keep in mind a caveat of detecting non-specific binders by expressing a bait protein under strong promoter (Van Leene *et al*, 2015; Xing *et al*, 2016) and therefore the need for further validation of a particular TSN interactor.

The composition of the SG proteome in animal and yeast cells displays highly variable characteristics influenced by the type of stress or cell type (Markmiller *et al*, 2018). In agreement, we found profound variation in the repertoire of TSN-interacting proteins isolated under different types of stress (Fig 6). One of the most enriched categories of SG-associated proteins is RBPs regulating RNA transport, silencing, translation and degradation (Wolozin & Apicco, 2015). Likewise, RBPs accounted for 55% of TSN2_HS and TSN2_NS interactomes (Fig 1F), providing a further mechanistic explanation for the previously established role of TSN in mRNA stabilization and degradation (Gutierrez-Beltran *et al*, 2015a).

The current predominant model for SG assembly rests on LLPS driven by multivalent interactions through IDRs (Molliex *et al*, 2015; Rayman *et al*, 2018; Kuechler *et al*, 2020). Our data further demonstrate that TSN interactomes under NS and HS conditions are significantly enriched in IDRs (Fig 4A) and proteins with a propensity for LLPS (Fig 4B). Lastly, TSN itself is highly disordered, with the most ID found within tandem of four N-terminally situated SN domains (Fig 4C). This part of TSN confers its interaction with partner proteins, SG localization and cytoprotective property in both mammalian and plant cells (Fig 4D; Gao *et al*, 2015; Gutierrez-Beltran *et al*, 2015b). Taken together, our results demonstrate that the function of IDRs in SG condensation is conserved in plants.

It is well known that numerous stress- and nutrient-signalling pathways converge on SGs (Kedersha *et al*, 2013; Mahboubi & Stochaj, 2017). Our study has established the two-component catalytic subunit of the *Arabidopsis* SnRK1 complex as a TSN interactor. The SnRK1 complex is considered a central regulator of the plant transcriptome in response to darkness and other stress signals (Baena-Gonzalez *et al*, 2007). Recent work showed that overexpression of the catalytic domain of the SnRK1α1 kinase in *Arabidopsis* protoplasts was sufficient to promote SnRK1 signalling (Ramon *et al*, 2019). Here, we show that SG localization of SnRK1α1^{CD} and full-length SnRK1α isoforms coincides with increase in SnRK1α kinase activity (Figs 8 and EV5C and D) pointing to the possibility that targeting to SGs could provide a mechanism for increasing enzyme concentration via condensation to ensure enhanced SnRK1 signalling during stress exposure (Alberti *et al*, 2019; Lyon *et al*, 2021). Furthermore, TSN appears to mediate SnRK1α condensation as its deletion decreased the number and increased the size of the cytoplasmic SnRK1α puncta in the heat-stressed cells (Fig 7E and F). Interestingly, the regulatory domain of SnRK1α1 (SnRK1α1RD) revealed a faster association with SGs than SnRK1α1^{CD} upon HS (Figs EV5E and 7J). Given that the SnRK1α1RD is responsible for binding the β and γ regulatory SnRK1 subunits (Kleinow *et al*, 2000) and that SnRK1β2 was shown to control SnRK1α1 localization (Ramon *et al*, 2019), it is tempting to speculate that localization of SnRK1α1 in SG is controlled by interaction with SnRK1 β and γ subunits through its regulatory domain.

SnRK1 and its yeast and mammalian orthologues SNF1 and AMPK, respectively, have been extensively studied as one of the key regulators of target of rapamycin (TOR) (Shaw, 2009; Van Leene *et al*, 2019). In plants, SnRK1 and TOR proteins play central and antagonistic roles as integrators of transcriptional networks in stress and energy signalling (Baena-Gonzalez *et al*, 2007; Belda-Palazon *et al*, 2020). Whereas SnRK1 signalling is activated during stress and energy limitation, TOR promotes growth and biosynthetic processes in response to nutrients and energy availability (Baena-Gonzalez & Hanson, 2017; Carroll & Dunlop, 2017; Van Leene *et al*, 2019). Although it has been demonstrated that the mammalian orthologue (AMPK) is a *bona fide* SG component involved in the regulation of SG biogenesis (Mahboubi *et al*, 2015), there is no evidence connecting SnRK1 activation and SGs. Here, we demonstrate that the formation of SGs and the presence of TSN are both necessary for activation of SnRK1 signalling in response to HS (Fig 8).

It has been shown that mammalian mTOR is translocated to SGs under stress, leading to its inactivation (Heberle *et al*, 2015). While there is no evidence so far that TOR is a component of plant SGs, inhibition of TOR kinase activity in plants by nutritional or cold stress has been reported (Xiong *et al*, 2013; Wang *et al*, 2017). We thus speculate that SGs and their integral constituent protein TSN might regulate the SnRK1-TOR signalling module; however, further work is required to decipher the mechanistic details and physiological roles of this regulation.

In conclusion, our study has two important implications. First, despite recent advances in understanding SGs in mammals and budding yeast, our insights into plant SGs are still very limited. Our work provides a broad resource of SG-related protein interactions and functional data that should promote plant SG research. Second, there is growing evidence linking SGs, AMPK and TSN with cancer and other human diseases. Our work suggests a new mechanism of stress-induced AMPK/SNF1/SnRK1 activation engaging both TSN and formation of SGs. It remains to be seen whether a similar mechanism is conserved in mammals and could thus be used in medical interventions.

Materials and Methods

Plant material and growth conditions

The *tsn1 tsn2* double mutant for *TSN1* (At5g07350) and *TSN2* (At5g61780), in the Landsberg erecta (Ler; line CSHL_ET12646) and Columbia (Col; line SALK_143497) backgrounds, respectively, was isolated as shown previously (Gutierrez-Beltran *et al*, 2015b). The mutant was back-crossed five times with Col plants to generate an isogenic pair. Finally, both *tsn1 tsn2* mutant and wild-type (WT) plants were selected from F5. The *snrk1α1*$^{-/-}$ *snrk1α2*$^{-/+}$ mutant was previously described (Ramon *et al*, 2019). *snrk1α1*$^{-/-}$ *snrk1α2*$^{-/+}$ plants were preselected on BASTA-containing medium. Plants were grown on soil or half-strength Murashige and Skoog (MS) medium (Sigma-Aldrich) containing 0.5% sugar and 0.8% agar under long-day conditions (16-h light/8-h dark) at 23°C (NS conditions). For visualization of SGs, 5-day-old seedlings expressing GFP fusion proteins were grown on vertical plates containing half-strength MS medium and incubated for 60 min on a thermoblock at 39°C (HS conditions) or on plates containing 200 mM NaCl (salt stress).

 © 2021 The Authors

Plasmid construction

All oligonucleotide primers and constructs used in this study are described in Appendix Tables S1 and S2, respectively. All plasmids and constructs were verified by sequencing using the M13 forward and reverse primers. *TSN1*, *TSN2* and *GFP* were amplified by PCR and resulting cDNA sequences were introduced into pC-TAPa (C-terminal TAPa fusion) to generate *Pro35S:TSN1-TAPa*, *Pro35S:TSN2-TAPa* and *Pro35S:GFP-TAPa*, respectively (Rubio *et al*, 2005). *RH12* cDNA and promoter (2 kb) were amplified and cloned into pGWB4 vector using HiFi DNA assembly cloning kit (NEB biolabs) to generate *ProH12:RH12-GFP*. *TCTP*, *UBP1* and *RBP47* cDNAs were amplified and cloned into pMDC43 vector to generate *Pro35S:GFP-TCTP*, *Pro35S:GFP-UBP1* and *Pro35S:GFP-RBP47*, respectively. *SnRK1α1*, *SnRK1α1CD*, *SnRK1α1RD* and *SnRK1α2* cDNAs were amplified and cloned into pUBC-GFP-Dest vector to generate *ProUBQ:SnRK1α1-GFP* (including variants) and *ProUBQ:SnRK1α2*, respectively (Grefen *et al*, 2010).

cDNA clones of TSN-interacting proteins in the Gateway compatible vector pENTR223 were obtained from the ABRC stock centre (Yamada *et al*, 2003). For expression of N-terminal GFP and RFP fusions under the control of 35S promoter, cDNAs encoding *TSN2* and TSN-interacting proteins were introduced into the destination vectors pMDC43 and pGWB655, respectively (Curtis & Grossniklaus, 2003). For the BiFC assay, cDNAs for *TSN2*, TSN-interacting proteins, and *SN* and *Tudor* regions were cloned into pSITE-BiFC destination vectors (Martin *et al*, 2009). For FRET experiments, cDNAs for TSN2 and TSN-interacting proteins were introduced into pGWB642 (YFP) and pGWB645 (CFP) destination vectors (Nakamura *et al*, 2010).

Tandem affinity purification

Fully expanded leaves from *Arabidopsis* Col transgenic plants expressing TSN-TAPa and GFP-TAPa and grown for 18 days in 18:6 light/dark conditions at 23°C (NS), 39°C for 60 min (HS) and 200 mM NaCl for 5 h (NaCl) were harvested (15 g, fresh weight) and ground in liquid N_2 in 2 volumes of extraction buffer (50 mM Tris–HCl pH 7.5, 150 mM NaCl, 10% glycerol, 0.1% Nonidet P-40 and 1× protease inhibitor cocktail; Sigma-Aldrich) and centrifuged for 12,000 *g* for 10 min at 4°C. Supernatants were collected and filtered through two layers of Miracloth (Calbiochem). Plant extracts were incubated with 700 µl IgG beads (Amersham Biosciences) for 4–5 h at 4°C with gentle rotation. After centrifugation at 250 *g* for 3 min at 4°C, the IgG beads were recovered and washed three times with 10 ml of washing buffer (50 mM Tris–HCl, pH 7.5, 150 mM NaCl, 10% glycerol and 0.1% Nonidet P-40) and once with 5 ml of cleavage buffer (50 mM Tris–HCl, pH 7.5, 150 mM NaCl, 10% glycerol, Nonidet P-40 and 1 mM DTT). Elution from the IgG beads was performed by incubation with 15 µl (40 units) of PreScission protease (Amersham Biosciences) in 5 ml of cleavage buffer at 4°C with gentle rotation. Supernatants were recovered after centrifugation at 250 *g* for 3 min at 4°C and stored at 4°C. The IgG beads were washed with 5 ml of washing buffer, centrifuged again and the eluates pooled. The pooled eluates were transferred together with 1.2 ml of Ni-NTA resin (Qiagen, Valencia, CA, USA) into a 15-ml Falcon tube and incubated for 2 h at 4°C with gentle rotation. After centrifugation at 250 *g* for 3 min at 4°C, the Ni-NTA resin was washed three times with 10 ml washing buffer. Finally, elution was performed using 4 ml of imidazole-containing buffer (50 mM Tris–HCl pH 7.5, 150 mM NaCl, 10% glycerol, 0.1% Nonidet P-40, 200 mM imidazole). All the steps in the purification procedure were carried out at 4°C. For each large-scale TAPa purification, three TAPa plant samples (15 g, fresh weight each) were processed in parallel as described above. Final eluates were pooled together, proteins were precipitated using TCA/acetone extraction, and 100 µg of protein was digested according to the FASP method (Wisniewski *et al*, 2009). Two biological replicates were performed for isolating TSN interactomes from unstressed and stressed plants, respectively.

Liquid chromatography and mass spectrometry analysis for TAPa procedure

Peptides were analysed using EASYnano-LC 1000 on a Q Exactive Plus Orbitrap mass spectrometer (Thermo Scientific). Peptides were separated on a pre-column 75 µm × 2 cm, nanoViper, C18, 3 µm, 100 Å (Acclaim PepMap 100) and analytical column 50 µm × 15 cm, nanoViper, C18, 2 µm, 100 Å (Acclaim PepMap RSLC) at a flow rate of 200 nl/min. Water and ACN, both containing 0.1% formic acid, were used as solvents A and B, respectively. The gradient was started and kept at 0–35% B for 0–220 min, ramped to 35–45% B over 10 min and kept at 45–90% B for another 10 min. The mass spectrometer was operated in the data-dependent mode (DDA) to automatically switch between full-scan MS and MS/MS acquisition. We acquired survey full-scan MS spectra from 200 to 1,800 m/z in the Orbitrap with a resolution of R = 70,000 at m/z 100. For data-dependent analysis, the top 10 most abundant ions were analysed by MS/MS, while +1 ions were excluded, with a normalized collision energy of 32%.

RBP47 immunoprecipitation

Fully expanded leaves from *Arabidopsis* Col and *tsn1 tsn2* transgenic plants (1 g) expressing GFP-RBP47 and GFP and grown for 18 days in 18:6 light/dark conditions at 23°C (NS) and 39°C for 60 min (HS) were harvested (15 g, fresh weight) and ground in liquid N_2 in 2 volumes of extraction buffer (50 mM Tris–HCl pH 7.5, 150 mM NaCl, 0.1% Nonidet P-40 and 1× protease inhibitor cocktail; Sigma-Aldrich) and centrifuged for 10,000 *g* for 15 min at 4°C. Immunoprecipitation was performed with mMACS Epitope Tag Protein Isolation Kits (Miltenyi Biotec). The supernatants were mixed with magnetic beads conjugated to α-GFP (Miltenyi Biotec) and then incubated for 60 min at 4°C. The mixtures were applied to m-Columns (Miltenyi Biotec) in a magnetic field to capture the magnetic antigen–antibody complex. After extensive washing with extraction buffer (four times, 500 µl each) and 50 mM NH_4HCO_3 (four times, 500 µl each), immunoaffinity complexes were eluted by removing the column from the magnet and adding 200 µl of NH_4HCO_3. Two biological replicates were performed for isolating RBP47 interactomes.

Liquid chromatography and mass spectrometry analysis for GFP-RBP47 immunoprecipitation

After immunoprecipitation, the peptides were digested on-beads. To this end, 0.2 µg trypsin was added to each sample before overnight incubation at 37°C. The samples were then desalted with stage tip,

© 2021 The Authors

dried under vacuum and analysed by LC-MS using Nano LC-MS/MS (Dionex Ultimate 3000 RLSC nano System, Thermo Fisher) interfaced with Eclipse (Thermo Fisher). Samples were loaded onto a fused silica trap column Acclaim PepMap 100, 75 μm × 2 cm (Thermo Fisher). After washing for 5 min at 5 μl/min with 0.1% TFA, the trap column was brought in-line with an analytical column (Nanoease MZ peptide BEH C18, 130A, 1.7 μm, 75 μm × 250 mm; Waters) for LC-MS/MS. Peptides were fractionated at 300 nL/min using a segmented linear-gradient 4–15% of buffer B in buffer A over 30 min (A: 0.2% formic acid and B: 0.16% formic acid, 80% acetonitrile), and then 15%-25%, 25%-50% and 50–90% over 40, 44 and 44 min, respectively. Buffer B then returned at 4% for 5 min for the next run.

The scan sequence began with an MS1 spectrum [Orbitrap analysis, resolution 120,000, scan range from *m/z* 375–1,500, automatic gain control (AGC) target 1E6, maximum injection time 100 ms]. The top duty cycle (3 s) scheme and dynamic exclusion of 60 s were used for the selection of parent ions of 2–7 charges for MS/MS. Parent masses were isolated in the quadrupole with an isolation window of 1.2 *m/z*, AGC target 1E5, and fragmented with higher-energy collisional dissociation with a normalized collision energy of 30%. The fragments were scanned in Orbitrap with 15,000 resolution. The MS/MS scan range was determined by the charge state of the parent ion, with a lower limit set at 110 amu.

Mass spectrometry data analysis

The raw data from TAPa and on-bead-digestion were processed using MaxQuant software (version 1.6.10.43) (Tyanova *et al*, 2016) and searched against an TAIR11 protein database. The following modifications were selected for the search: carbamidomethyl (C; fixed), acetyl (N-term; variable) and oxidation (M; variable). For both the full-scan MS spectra (MS1) and the MS/MS spectra (MS2), the mass error tolerances were set to 20 ppm. Trypsin was selected as a protease with a maximum of two miscleavages. For protein identification, a minimum of one unique peptide with a peptide length of at least seven amino acids and a false discovery rate below 0.01 was required. The match between runs function was enabled, and a time window of one min was set. Label-free quantification was selected using iBAQ (calculated as the sum of the intensities of the identified peptides divided by the number of observable peptides of a protein) (Schwanhausser *et al*, 2011).

The proteinGroups.txt file, an output of MaxQuant, was further analysed using Perseus 1.16.10.43 (Tyanova *et al*, 2016). The iBAQ values were normalized to summed total iBAQ value of all proteins of that sample and $\log_2$ transformed. After filtering out the protein groups with no valid Quan value, the missing values were replaced with a random normal distribution of small values. The non-paired two-tailed *t*-test (Tusher *et al*, 2001) was used to calculate significant differences between the two samples. Identified proteins were considered as interaction partners if their MaxQuant iBAQ values displayed a > 1.5- or 2-fold change enrichment and $P < 0.05$ (*t*-test) when compared to the control. Furthermore, at least two unique peptides were required per protein group.

Protoplast and plant transformation

Protoplasts were isolated from leaves of 15- to 20-day-old *N. benthamiana* transiently expressing the corresponding fluorescent proteins, as described previously (Wu *et al*, 2009). The cell walls were digested by incubation in enzymatic solution containing 1% (w/v) Cellulose R-10, 0.25% (w/v) Macerozyme R-10, 20 mM MES-HOK pH 5.7, 400 mM Mannitol, 10 mM $CaCl_2$, 20 mM KCl, 0.1% (w/v) Bovine serum albumin (BSA) for 60 min. Protoplasts were separated from debris by centrifugation (100 *g*, 3 min, 4°C), washed two times with ice-cold W5 buffer (154 mM NaCl, 125 mM $CaCl_2$, 5 mM KCl and 2 mM MES-KOH pH 5.7) and resuspended in ice-cold W5 buffer at a density of 2.5×10^5 protoplasts/ml. The protoplast suspension was incubated for 15 min on ice before HS at 39°C.

Arabidopsis Col plants were transformed as described previously (Clough & Bent, 1998) using *Agrobacterium tumefaciens* (Agrobacterium) strain GV3101. In Figs 5–8, plants from the T2 and T3 generations were used. Transgenic plants were confirmed by genotyping. For transient expression in *N. benthamiana* mesophyll cells, *Agrobacterium* strain GV3101 was transformed with the appropriate binary vectors by electroporation as described previously (Gutierrez-Beltran *et al*, 2017). Positive clones were grown in Luria-Bertani until reaching OD_{600} = 0.4 and were pelleted after centrifugation at 3,000 *g* for 10 min. Cells were resuspended in MM (10 mM MES, pH 5.7, 10 mM $MgCl_2$ supplemented with 0.2 mM acetosyringone) until OD_{600} = 0.4, incubated at room temperature for 2 h and infiltrated in *N. benthamiana* leaves using a 1 ml hypodermic syringe. Leaves were analysed after 48 h using a Zeiss 780 confocal microscope with the 40× water-immersion objective. The excitation/emission wavelength was 480/508 nm for GFP and 561/610 nm for RFP.

Bimolecular fluorescence complementation (BiFC)

For BiFC assays, *Agrobacterium* strains GV3101 carrying *cYFP-TSN2 cYFP-SN or cYFP-Tudor* and the corresponding *nYFP-TSN-interacting proteins* were co-infiltrated into *N. benthamiana* leaves (OD_{600} = 0.3). Fluorescence images were obtained 48 h after infiltration using a Leica TCS Sp2/DMRE confocal microscope, with an excitation wavelength of 514 nm. Transient expression of proteins in *N. benthamiana* leaves via agroinfiltration was performed as previously described (Gutierrez-Beltran *et al*, 2017).

Immunocytochemistry and imaging

For immunocytochemistry, roots of 5-day-old *Arabidopsis* seedlings were fixed for 60 min at room temperature with 4% (w/v) paraformaldehyde in 50 mM PIPES, pH 6.8, 5 mM EGTA, 2 mM $MgCl_2$ and 0.4% Triton X-100. The fixative was washed away with phosphate-buffered saline buffer supplemented with Tween-20 (PBST), and cells were treated for 8 min at room temperature with a solution of 2% (w/v), driselase (Sigma-Aldrich) in 0.4 M mannitol, 5 mM EGTA, 15 mM MES pH 5.0, 1 mM PMSF, 10 μg/ml leupeptin and 10 μg/ml pepstatin A. Thereafter, roots were washed twice, 10 min each, in PBST and then in 1% (w/v) BSA in PBST for 30 min before overnight incubation with a primary antibody (rabbit α-eIF4E diluted 1:500 or rabbit/mouse α-Myc diluted 1:500). The specimens were then washed three times for 90 min in PBST and incubated overnight with the corresponding secondary antibody [goat α-rabbit/mouse fluorescein isothiocyanate (FITC)/rhodamine conjugate] diluted 1:200. After washing in PBST, the specimens were mounted in Vectashield mounting medium (Vector Laboratories).

 © 2021 The Authors

Staining with FDA and SYTOX Orange (both from Molecular Probes, Invitrogen) was performed on 5-day-old *Arabidopsis* seedlings. FDA and SYTOX Orange were added to final concentrations of 250 nM and 2 mg/ml, respectively, in water. After 10 min of incubation in the dark, the samples were washed twice with half-strength liquid MS medium supplemented with 1% (w/v) sucrose, pH 5.7, and observed immediately. For the CHX treatment, the protoplast suspension or seedling roots were incubated with 200 ng/μ1 drug for 30 min and then heat-stressed at 39°C.

Förster resonance energy transfer (FRET)

The assay was performed as described previously (Moschou *et al*, 2013). FRET was performed using Zeiss 780 laser scanning confocal microscope and a plan-apochromat 20×/0.8 M27 objective. FRET acceptor photobleaching mode of Zeiss 780 ZEN software was used, with the following parameters: acquisition of 10 pre-bleach images, one bleach scan and 80 post-bleach scans. Bleaching was performed using 488, 514 and 561-nm laser lines at 100% transmittance and 40 iterations. Pre- and post-bleach scans were at minimum possible laser power (0.8% transmittance) for the 458 nm or 514 nm (4.7%) and 5% for 561 nm; 512 × 512 8-bit pixel format; pinhole of 181 μm and zoom factor of 2.0. Fluorescence intensity was measured in the ROIs corresponding to the bleached region. One ROI was measured outside the bleached region to serve as the background. The background values were subtracted from the fluorescence recovery values, and the resulting values were normalized by the first post-bleach time point. Three pre-bleach and three post-bleach intensities were averaged and used for calculations using the formula $FRET_{eff} = (D_{post}\text{-}D_{pre})/D_{post}$, where D is intensity in arbitrary units.

Fluorescence recovery after photobleaching (FRAP)

The assay was performed as described previously (Moschou *et al*, 2013). Five-day-old seedlings were grown on sterile plates containing half-strength MS with 1% (w/v) sucrose. For HS treatment, plates were incubated for 60 min on a thermoblock at 39°C. GFP fluorescence was detected using a water-corrected 403 objective. During analyses, the FRAP mode of Zeiss 780 ZEN software was set up for the acquisition of one pre-bleach image, one bleach scan and 40 post-bleach scans. In FRAP of SGs, the width of the bleached region was 2 mm. The following settings were used for f photobleaching: 10–20 iterations, 10–60 s per frame and 75% transmittance with the 458- to 561-nm laser lines of the argon laser. Prebleach and post-bleach scans were at the minimum possible laser power (1.4 to 20% transmittance) for 488 or 561 nm and at 0% for all other laser lines, 512 × 512 pixel format and zoom factor of 5.1. Analyses of fluorescence intensities during FRAP were performed in regions of interest corresponding to the size of the bleached region. One region of interest was measured outside the bleached region to serve as the background. The background values were subtracted from the fluorescence recovery values, and the resulting values were normalized by the first post-bleach time point. Initial signal recovery (%) = $100 \times (I_{\text{final,post-bleach}} - I_{\text{initial,post-bleach}})/(I_{\text{prebleach}} - I_{\text{initial,post-bleach}})$, where I is the normalized signal intensity (relative to the background intensity). Values were corrected for the artificial loss of fluorescence using values from the neighbouring cells. At least ten cells from different roots were analysed for each FRAP experiment.

Protein extraction and immunoblotting

Two hundred milligrams of leaf material were mixed with 350 μl of extraction buffer (100 mM Tris–HCl, pH 7.5, 150 mM NaCl, 0.1% Nonidet P-40 and 1× Protease inhibitor cocktail (Sigma, P599) and centrifuged for 15 min at 14,000 *g*. 4× Laemmli sample buffer was added to 100 μl supernatant and boiled for 5 min. Equal amounts of supernatant were loaded on 10% poly-acrylamide gels and blotted on a polyvinylidene difluoride (PVDF) membrane. α-Myc and α-rabbit horseradish peroxidase conjugates (Amersham, GE Healthcare) were used at dilutions 1:1,000 and 1:5,000, respectively. The reaction was developed for 1 min using a Luminata Crescendo Millipore immunoblotting detection system (Millipore, WBLUR0500).

For detection of the phosphorylated forms of SnRK1α proteins, 10-day-old seedlings were collected and ground in liquid nitrogen and the proteins were extracted using the following extraction buffer: 25 mM Tris–HCl pH 7.8, 75 mM NaCl, 15 mM EGTA, 10 mM $MgCl_2$, 10 mM B-glycerophosphate, 15 mM 4-Nitrophenylphosphate bis, 1 mM DTT, 1 mM NaF, 0.5 mM Na_3VO_4, 0.5 mM PMSF, 1% Protease inhibitor cocktail (Sigma, P599) and 0.1% Tween-20. The protein extracts were centrifuged at 14,000 *g* and 4°C for 10 min and supernatants transferred to a new tube. The protein concentration was measured using Bradford Dye Reagent (Bio-Rad); equal amounts (15 μg) of total protein for each sample were separated by SDS–PAGE (10% acrylamide gel) and transferred to a PVDF membrane (Bio-Rad). The membrane was blocked in TBST buffer containing 5% (w/v) BSA and incubated with primary antibody and secondary antibody. Antibodies used for immunoblotting were as follows: α–Phospho-AMPKα (Thr175) (α-pT175) (dilution 1:1,000, Cell Signaling Technology), α-Kin10 (dilution 1:1,000, Agrisera), α-Kin11 (dilution 1:1,000, Agrisera), α-TSN [dilution 1:1,000, (Sundström *et al*, 2009)] and α-Actin (dilution 1:10,000, Agrisera).

Co-immunoprecipitation (Co-Ip)

Total proteins were extracted from 10-day-old seedlings with no-salt lysis buffer [50 mM Tris, pH 8.0, 0.1% Nonidet P-40 and 1% Protease inhibitor cocktail (Sigma)] at a fresh weight:buffer volume ratio of 1 g:2 ml. After centrifugation at 6,000 *g* and 4°C for 5 min, 20 μl of α-GFP microbeads (Miltenyi Biotec) were added to the resultant supernatant and incubated for 1 h at 4°C on a rotating wheel. Subsequent washing and elution steps were performed according to the manufacturer (μMACS GFP Isolation Kit; Miltenyi Biotec). Immunoblot analysis was done essentially as described above, and immunoprecipitates from transgenic lines expressing free GFP were used as controls. GFP-TSN-interacting proteins and native TSN were detected by mouse α-GFP (monoclonal antibody JL-8; Clontech) and mouse α-TSN (Sundström *et al*, 2009) at final dilutions of 1:1,000 and 1:5,000, respectively.

Image analysis

The image analysis was done using ImageJ v1.41 (NIH) software (http://rsb.info.nih.gov/ij/index.html). For co-localization analyses, we calculated the linear Pearson (rp) and nonlinear Spearman's

© 2021 The Authors

rank (rs) correlation coefficient (PSC) for the pixels representing the fluorescence signals in both channels (French *et al*, 2008). Levels of co-localization can range from +1 to −1 for positive and negative correlations, respectively.

Quantitative RT–PCR

Total RNA was isolated with RNA plant kit (Bioline) from 10-day-old *Arabidopsis* seedlings grown on liquid MS medium with or without HS (60 min at 39°C). First-strand cDNA was generated using the iScript cDNA Synthesis kit (Bio-Rad) in a 20-µl reaction mixture containing 1 µg of total RNA. The PCR mixtures were performed in a final volume of 18 µl using the SsoAdvanced Universal SYBR Green Supermix (Bio-Rad). The data were normalized to *UBQ10* expression, a constitutively expressed gene that is used as an internal control in *Arabidopsis* (Ramon *et al*, 2019; Belda-Palazon *et al*, 2020; Chantarachot *et al*, 2020). Relative expression levels were determined as described previously (de la Torre *et al*, 2013).

Bioinformatics

In silico analysis of subcellular protein localization was performed using SUBA4 (Hooper *et al*, 2017). Prion-like domains were identified using PLAAC (Lancaster *et al*, 2014), with the minimum length for prion domains Lcore = 60, organism background *Arabidopsis*, and the parameter $\alpha = 1$. The RNA-binding proteins were predicted by the RNApred tool (Kumar *et al*, 2011). The prediction approach was based on amino acid composition, and the threshold for the support vector machine (SVM) was 0.5. To retrieve protein–protein interaction data, we used STRING database (V10) (Szklarczyk *et al*, 2015). Only physical protein–protein interactions were considered. Per-residue disorder content was evaluated by PONDR predictors, including PONDR-FIT (Xue *et al*, 2010) and PONDR-VSL2 (Peng *et al*, 2005). The intrinsic disorder propensities of TSN were evaluated according to the previously described method (Santamaria *et al*, 2017; Uversky, 2017). Disorder evaluations together with disorder-related functional information were retrieved from the D_2P_2 database (http://d2p2.pro/) (Oates *et al*, 2013). Intrinsically disordered regions were predicted using Iupred2A (Erdos & Dosztanyi, 2020). LLPS predisposition was evaluated using the PSPredictor tool (preprint: Sun *et al*, 2019). The image analysis was done using ImageJ version 1.52 software (http://rsb.info.nih.gov/ij/index.html). SGs were scored as positive when they had a minimum size of 0.5 µm. SG counting was performed manually with the Cell Counter plugin of ImageJ (http://rsbweb.nih.gov/ij/ plugins/cell-counter.html).

Data availability

The mass spectrometry data from this publication have been deposited to the JPOST repository. For TSN and RBP47 interactomes, the dataset identifiers are JPST000766 (https://repository.jpostdb.org/entry/JPST000766) and JPST001103 (https://repository.jpostdb.org/entry/JPST001103), respectively.

Expanded View for this article is available online.

Acknowledgements
We thank Filip Rolland (Katholieke Universiteit Leuven) for providing *snrk1α1*$^{-/-}$ *snrk1α2*$^{-/+}$ mutant, Tsuyoshi Nakagawa (Shimane University) for providing Gateway binary vectors, Elena Baena-Gonzalez (Instituto Gulbenkian de Ciência, Portugal) for providing *SnRK1α1* cDNA and critical discussion and Glenn Hicks (University of California, Riverside) for critical reading of the manuscript. This work was supported by the European Commission (MSCA-IF-ReSGulating- 702473), the Ministerio de Economía y Competitividad (Juan de la Cierva-Incorporacion, IJCI-2016-30763) and University of Seville (VIPPIT-2020-IV.4 and -I.5) to E.G.-B, by the Ministerio de Economía y Competitividad (PGC2018-099048-B-100) to J.L.C., by grants from Knut and Alice Wallenberg Foundation (2018.0026), the Swedish Research Council VR (2019-04250_VR), the Swedish Foundation for Strategic Research (RBP14-0037), and by Crops for the Future Research Programme to P.V.B.

Author contributions
Conceptualization, EG-B and PVB; Methodology, EG-B, PNM, VNU, JLC, and PVB; Investigation, EG-B, PHE, GWDII, and VNU; Writing—original and revised manuscripts, EG-B and PVB; Writing—review and editing, EG-B, KD, PNM, VNU, JLC, and PVB; Funding Acquisition, EG-B, JLC, and PVB.

Conflict of interest
The authors declare that they have no conflict of interest.

References

Abe S, Sakai M, Yagi K, Hagino T, Ochi K, Shibata K, Davies E (2003) A Tudor protein with multiple SNc domains from pea seedlings: cellular localization, partial characterization, sequence analysis, and phylogenetic relationships. *J Exp Bot* 54: 971 – 983

Alberti S, Gladfelter A, Mittag T (2019) Considerations and challenges in studying liquid-liquid phase separation and biomolecular condensates. *Cell* 176: 419 – 434

Anderson P, Kedersha N, Ivanov P (2015) Stress granules, P-bodies and cancer. *BBA-Gene Regul Mech* 1849: 861 – 870

Arimoto K, Fukuda H, Imajoh-Ohmi S, Saito H, Takekawa M (2008) Formation of stress granules inhibits apoptosis by suppressing stress-responsive MAPK pathways. *Nat Cell Biol* 10: 1324 – 1332

Baena-Gonzalez E, Hanson J (2017) Shaping plant development through the SnRK1-TOR metabolic regulators. *Curr Opin Plant Biol* 35: 152 – 157

Baena-Gonzalez E, Rolland F, Thevelein JM, Sheen J (2007) A central integrator of transcription networks in plant stress and energy signalling. *Nature* 448: 938 – 942

Banani SF, Rice AM, Peeples WB, Lin Y, Jain S, Parker R, Rosen MK (2016) Compositional control of phase-separated cellular bodies. *Cell* 166: 651 – 663

Belda-Palazon B, Adamo M, Valerio C, Ferreira LJ, Confraria A, Reis-Barata D, Rodrigues A, Meyer C, Rodriguez PL, Baena-Gonzalez E (2020) A dual function of SnRK2 kinases in the regulation of SnRK1 and plant growth. *Nat Plants* 6: 1345 – 1353

Betsch L, Savarin J, Bendahmane M, Szecsi J (2017) Roles of the translationally controlled tumor protein (TCTP) in plant development. *Results Probl Cell Differ* 64: 149 – 172

Broeckx T, Hulsmans S, Rolland F (2016) The plant energy sensor: evolutionary conservation and divergence of SnRK1 structure, regulation, and function. *J Exp Bot* 67: 6215 – 6252

Buchan JR, Parker R (2009) Eukaryotic stress granules: the ins and outs of translation. *Mol Cell* 36: 932 – 941

 © 2021 The Authors

Buchan JR, Yoon JH, Parker R (2011) Stress-specific composition, assembly and kinetics of stress granules in Saccharomyces cerevisiae. *J Cell Sci* 124: 228 – 239

Carroll B, Dunlop EA (2017) The lysosome: a crucial hub for AMPK and mTORC1 signalling. *Biochem J* 474: 1453 – 1466

Cazares-Apatiga J, Medina-Gomez C, Chavez-Munguia B, Calixto-Galvez M, Orozco E, Vazquez-Calzada C, Martinez-Higuera A, Rodriguez MA (2017) The tudor staphylococcal nuclease protein of entamoeba histolytica participates in transcription regulation and stress response. *Front Cell Infect Microbiol* 7: 52

Chantarachot T, Sorenson RS, Hummel M, Ke H, Kettenburg AT, Chen D, Aiyetiwa K, Dehesh K, Eulgem T, Sieburth LE *et al* (2020) DHH1/DDX6-like RNA helicases maintain ephemeral half-lives of stress-response mRNAs. *Nat Plants* 6: 675 – 685

Chou HL, Tian L, Kumamaru T, Hamada S, Okita TW (2017) Multifunctional RNA Binding protein OsTudor-SN in storage protein mRNA transport and localization. *Plant Physiol* 175: 1608 – 1623

Clough SJ, Bent AF (1998) Floral dip: a simplified method for Agrobacterium-mediated transformation of *Arabidopsis thaliana*. *Plant J* 16: 735 – 743

Cui X, Zhao C, Yao X, Qian B, Su C, Ren Y, Yao Z, Gao X, Yang J (2018) SND1 acts as an anti-apoptotic factor via regulating the expression of lncRNA UCA1 in hepatocellular carcinoma. *RNA Biol* 15: 1364 – 1375

Curtis MD, Grossniklaus U (2003) A gateway cloning vector set for high-throughput functional analysis of genes in planta. *Plant Physiol* 133: 462 – 469

Ditfrey NF, Muller P, Jammes F, Kizis D, Leung J, Perrot-Rechenmann C, Bianchi MW (2010) The RNA binding protein Tudor-SN is essential for stress tolerance and stabilizes levels of stress-responsive mRNAs encoding secreted proteins in *Arabidopsis*. *Plant Cell* 22: 1575 – 1591

Erdos G, Dosztanyi Z (2020) Analyzing protein disorder with IUPred2A. *Curr Protoc Bioinformatics* 70: e99

Esgleas M, Falk S, Forné I, Thiry M, Najas S, Zhang S, Mas-Sanchez A, Geerlof A, Niessing D, Wang Z *et al* (2020) Trnp1 organizes diverse nuclear membrane-less compartments in neural stem cells. *EMBO J* 39: e103373

Espinosa JR, Joseph JA, Sanchez-Burgos I, Garaizar A, Frenkel D, Collepardo-Guevara R (2020) Liquid network connectivity regulates the stability and composition of biomolecular condensates with many components. *Proc Natl Acad Sci USA* 117: 13238 – 13247

Fomicheva A, Ross ED (2021) From prions to stress granules: defining the compositional features of prion-like domains that promote different types of assemblies. *Int J Mol Sci* 22: 1 – 19.

French AP, Mills S, Swarup R, Bennett MJ, Pridmore TP (2008) Colocalization of fluorescent markers in confocal microscope images of plant cells. *Nat Protoc* 3: 619 – 628

Gao X, Fu X, Song J, Zhang Y, Cui X, Su C, Ge L, Shao J, Xin L, Saarikettu J *et al* (2015) Poly(A)(+) mRNA-binding protein Tudor-SN regulates stress granules aggregation dynamics. *FEBS J* 282: 874 – 890

Gao X, Shi X, Fu X, Ge L, Zhang Y, Su C, Yang X, Silvennoinen O, Yao Z, He J *et al* (2014) Human tudor staphylococcal nuclease (Tudor-SN) protein modulates the kinetics of AGTR1-3'UTR granule formation. *FEBS Lett* 588: 2154 – 2161

Gilks N, Kedersha N, Ayodele M, Shen L, Stoecklin G, Dember LM, Anderson P (2004) Stress granule assembly is mediated by prion-like aggregation of TIA-1. *Mol Biol Cell* 15: 5383 – 5398

Grefen C, Donald N, Hashimoto K, Kudla J, Schumacher K, Blatt MR (2010) A ubiquitin-10 promoter-based vector set for fluorescent protein tagging facilitates temporal stability and native protein distribution in transient and stable expression studies. *Plant J* 64: 355 – 365

Guillén-Boixet J, Kopach A, Holehouse AS, Wittmann S, Jahnel M, Schlüßler R, Kim K, Trussina IREA, Wang J, Mateju D *et al* (2020) RNA-induced conformational switching and clustering of G3BP drive stress granule assembly by condensation. *Cell* 181: 346 – 361.e17

Gutierrez-Beltran E, Bozhkov PV, Moschou PN (2015a) Tudor Staphylococcal Nuclease plays two antagonistic roles in RNA metabolism under stress. *Plant Signal Behav* 10: e1071005

Gutierrez-Beltran E, Denisenko TV, Zhivotovsky B, Bozhkov PV (2016) Tudor staphylococcal nuclease: biochemistry and functions. *Cell Death Differ* 23: 1739 – 1748

Gutierrez-Beltran E, Moschou PN, Smertenko AP, Bozhkov PV (2015b) Tudor staphylococcal nuclease links formation of stress granules and processing bodies with mRNA catabolism in *Arabidopsis*. *Plant Cell* 27: 926 – 943

Gutierrez-Beltran E, Personat JM, de la Torre F, Del Pozo O (2017) A universal stress protein involved in oxidative stress is a phosphorylation target for protein kinase CIPK6. *Plant Physiol* 173: 836 – 852

Heberle AM, Prentzell MT, van Eunen K, Bakker BM, Grellscheid SN, Thedieck K (2015) Molecular mechanisms of mTOR regulation by stress. *Mol Cell Oncol* 2: e970489

Hilliker A, Gao Z, Jankowsky E, Parker R (2011) The DEAD-box protein Ded1 modulates translation by the formation and resolution of an eIF4F-mRNA complex. *Mol Cell* 43: 962 – 972

Hooper CM, Castleden IR, Tanz SK, Aryamanesh N, Millar AH (2017) SUBA4: the interactive data analysis centre for *Arabidopsis* subcellular protein locations. *Nucleic Acids Res* 45: D1064 – D1074

Huerta-Cepas J, Szklarczyk D, Heller D, Hernandez-Plaza A, Forslund SK, Cook H, Mende DR, Letunic I, Rattei T, Jensen LJ *et al* (2019) eggNOG 5.0: a hierarchical, functionally and phylogenetically annotated orthology resource based on 5090 organisms and 2502 viruses. *Nucleic Acids Res* 47: D309 – D314

Jain S, Wheeler JR, Walters RW, Agrawal A, Barsic A, Parker R (2016) ATPase-modulated stress granules contain a diverse proteome and substructure. *Cell* 164: 487 – 498

Jariwala N, Rajasekaran D, Mendoza RG, Shen X-N, Siddiq A, Akiel MA, Robertson CL, Subler MA, Windle JJ, Fisher PB *et al* (2017) Oncogenic role of SND1 in development and progression of hepatocellular carcinoma. *Cancer Res* 77: 3306 – 3316

Jossier M, Bouly JP, Meimoun P, Arjmand A, Lessard P, Hawley S, Grahame Hardie D, Thomas M (2009) SnRK1 (SNF1-related kinase 1) has a central role in sugar and ABA signalling in *Arabidopsis thaliana*. *Plant J* 59: 316 – 328

Kedersha N, Ivanov P, Anderson P (2013) Stress granules and cell signaling: more than just a passing phase? *Trends Biochem Sci* 38: 494 – 506

Keiten-Schmitz J, Wagner K, Piller T, Kaulich M, Alberti S, Muller S (2020) The nuclear SUMO-targeted ubiquitin quality control network regulates the dynamics of cytoplasmic stress granules. *Mol Cell* 79: 54 – 67 e57

Kleinow T, Bhalerao R, Breuer F, Umeda M, Salchert K, Koncz C (2000) Functional identification of an *Arabidopsis* snf4 ortholog by screening for heterologous multicopy suppressors of snf4 deficiency in yeast. *Plant J* 23: 115 – 122

Kosmacz M, Gorka M, Schmidt S, Luzarowski M, Moreno JC, Szlachetko J, Leniak E, Sokolowska EM, Sofroni K, Schnittger A *et al* (2019) Protein and metabolite composition of *Arabidopsis* stress granules. *New Phytol* 222: 1420 – 1433

Kosmacz M, Luzarowski M, Kerber O, Leniak E, Gutierrez-Beltran E, Moreno Beltran JC, Gorka M, Szlachetko J, Veyel D, Graf A *et al* (2018) Interaction of 2',3'-cAMP with Rbp47b Plays a role in stress granule formation. *Plant Physiol* 177: 411 – 421

© 2021 The Authors

Kroschwald S, Maharana S, Mateju D, Malinovska L, Nuske E, Poser I, Richter D, Alberti S (2015) Promiscuous interactions and protein disaggregases determine the material state of stress-inducible RNP granules. *Elife* 4: e06807

Kuechler ER, Budzynska PM, Bernardini JP, Gsponer J, Mayor T (2020) Distinct features of stress granule proteins predict localization in membraneless organelles. *J Mol Biol* 432: 2349 – 2368

Kumar M, Gromiha MM, Raghava GP (2011) SVM based prediction of RNA-binding proteins using binding residues and evolutionary information. *J Mol Recognit* 24: 303 – 313

Lancaster AK, Nutter-Upham A, Lindquist S, King OD (2014) PLAAC: a web and command-line application to identify proteins with prion-like amino acid composition. *Bioinformatics* 30: 2501 – 2502

Lyon AS, Peeples WB, Rosen MK (2021) A framework for understanding the functions of biomolecular condensates across scales. *Nat Rev Mol Cell Biol* 22: 215 – 235

Mahboubi H, Barise R, Stochaj U (2015) 5'-AMP-activated protein kinase alpha regulates stress granule biogenesis. *Biochem Biophys Acta* 1853: 1725 – 1737

Mahboubi H, Stochaj U (2017) Cytoplasmic stress granules: dynamic modulators of cell signaling and disease. *Biochem Biophys Acta* 1863: 884 – 895

Markmiller S, Soltanieh S, Server KL, Mak R, Jin W, Fang MY, Luo E-C, Krach F, Yang D, Sen A *et al* (2018) Context-dependent and disease-specific diversity in protein interactions within stress granules. *Cell* 172: 590 – 604.e13

Marmor-Kollet H, Siany A, Kedersha N, Knafo N, Rivkin N, Danino YM, Moens TG, Olender T, Sheban D, Cohen N *et al* (2020) Spatiotemporal proteomic analysis of stress granule disassembly using APEX reveals regulation by SUMOylation and links to ALS pathogenesis. *Mol Cell* 80: 876 – 891 e876

Martin K, Kopperud K, Chakrabarty R, Banerjee R, Brooks R, Goodin MM (2009) Transient expression in *Nicotiana benthamiana* fluorescent marker lines provides enhanced definition of protein localization, movement and interactions in planta. *Plant J* 59: 150 – 162

Martínez JP, Pérez-Vilaró G, Muthukumar Y, Scheller N, Hirsch T, Diestel R, Steinmetz H, Jansen R, Frank R, Sasse F *et al* (2013) Screening of small molecules affecting mammalian P-body assembly uncovers links with diverse intracellular processes and organelle physiology. *RNA Biol* 10: 1661 – 1669

Meng F, Na I, Kurgan L, Uversky VN (2015) Compartmentalization and functionality of nuclear disorder: intrinsic disorder and protein-protein interactions in intra-nuclear compartments. *Int J Mol Sci* 17: 24

Molliex A, Temirov J, Lee J, Coughlin M, Kanagaraj AP, Kim HJ, Mittag T, Taylor JP (2015) Phase separation by low complexity domains promotes stress granule assembly and drives pathological fibrillization. *Cell* 163: 123 – 133

Moschou PN, Smertenko AP, Minina EA, Fukada K, Savenkov EI, Robert S, Hussey PJ, Bozhkov PV (2013) The caspase-related protease separase (extra spindle poles) regulates cell polarity and cytokinesis in *Arabidopsis*. *Plant Cell* 25: 2171 – 2186

Nakamura S, Mano S, Tanaka Y, Ohnishi M, Nakamori C, Araki M, Niwa T, Nishimura M, Kaminaka H, Nakagawa T *et al* (2010) Gateway binary vectors with the bialaphos resistance gene, bar, as a selection marker for plant transformation. *Biosci Biotechnol Biochem* 74: 1315 – 1319

Nukarinen E, Nägele T, Pedrotti L, Wurzinger B, Mair A, Landgraf R, Börnke F, Hanson J, Teige M, Baena-Gonzalez E *et al* (2016) Quantitative phosphoproteomics reveals the role of the AMPK plant ortholog SnRK1 as a metabolic master regulator under energy deprivation. *Sci Rep* 6: 31697

Oates ME, Romero P, Ishida T, Ghalwash M, Mizianty MJ, Xue B, Dosztanyi Z, Uversky VN, Obradovic Z, Kurgan L *et al* (2013) D(2)P(2): database of disordered protein predictions. *Nucleic Acids Res* 41: D508 – 516

Ohn T, Kedersha N, Hickman T, Tisdale S, Anderson P (2008) A functional RNAi screen links O-GlcNAc modification of ribosomal proteins to stress granule and processing body assembly. *Nat Cell Biol* 10: 1224 – 1231

Pecinka A, Dinh HQ, Baubec T, Rosa M, Lettner N, Mittelsten Scheid O (2010) Epigenetic regulation of repetitive elements is attenuated by prolonged heat stress in *Arabidopsis*. *Plant Cell* 22: 3118 – 3129

Peng K, Vucetic S, Radivojac P, Brown CJ, Dunker AK, Obradovic Z (2005) Optimizing long intrinsic disorder predictors with protein evolutionary information. *J Bioinform Comput Biol* 3: 35 – 60

Posey AE, Holehouse AS, Pappu RV (2018) Phase separation of intrinsically disordered proteins. *Methods Enzymol* 611: 1 – 30

Protter DS, Parker R (2016) Principles and properties of stress granules. *Trends Cell Biol* 26: 668 – 679

Ramon M, Dang TVT, Broeckx T, Hulsmans S, Crepin N, Sheen J, Rolland F (2019) Default activation and nuclear translocation of the plant cellular energy sensor SnRK1 regulate metabolic stress responses and development. *Plant Cell* 31: 1614 – 1632

Rayman JB, Karl KA, Kandel ER (2018) TIA-1 Self-multimerization, phase separation, and recruitment into stress granules are dynamically regulated by Zn(2). *Cell Rep* 22: 59 – 71

Rodrigues A, Adamo M, Crozet P, Margalha L, Confraria A, Martinho C, Elias A, Rabissi A, Lumbreras V, Gonzalez-Guzman M *et al* (2013) ABI1 and PP2CA phosphatases are negative regulators of Snf1-related protein kinase1 signaling in *Arabidopsis*. *Plant Cell* 25: 3871 – 3884

Rubio V, Shen Y, Saijo Y, Liu Y, Gusmaroli G, Dinesh-Kumar SP, Deng XW (2005) An alternative tandem affinity purification strategy applied to *Arabidopsis* protein complex isolation. *Plant J* 41: 767 – 778

Saad S, Cereghetti G, Feng Y, Picotti P, Peter M, Dechant R (2017) Reversible protein aggregation is a protective mechanism to ensure cell cycle restart after stress. *Nat Cell Biol* 19: 1202 – 1213

Santamaria N, Alhothali M, Alfonso MH, Breydo L, Uversky VN (2017) Intrinsic disorder in proteins involved in amyotrophic lateral sclerosis. *Cell Mol Life Sci* 74: 1297 – 1318

Schmit JD, Feric M, Dundr M (2021) How hierarchical interactions make membraneless organelles tick like clockwork. *Trends Biochem Sci* 46: 525 – 534

Schwanhausser B, Busse D, Li N, Dittmar G, Schuchhardt J, Wolf J, Chen W, Selbach M (2011) Global quantification of mammalian gene expression control. *Nature* 473: 337 – 342

Seguin SJ, Morelli FF, Vinet J, Amore D, De Biasi S, Poletti A, Rubinsztein DC, Carra S (2014) Inhibition of autophagy, lysosome and VCP function impairs stress granule assembly. *Cell Death Differ* 21: 1838 – 1851

Shaw RJ (2009) LKB1 and AMP-activated protein kinase control of mTOR signalling and growth. *Acta Physiol* 196: 65 – 80

Sorenson R, Bailey-Serres J (2014) Selective mRNA sequestration by oligouridylate-binding proTEIN 1 contributes to translational control during hypoxia in *Arabidopsis*. *Proc Natl Acad Sci USA* 111: 2373 – 2378

Sun T, Li Q, Xu Y, Zhang Z, Lai L, Pei J (2019) Prediction of liquid-liquid phase separation proteins using machine learning. *bioRxiv* https://doi.org/10.1101/842336 [PREPRINT]

Sundström JF, Vaculova A, Smertenko AP, Savenkov EI, Golovko A, Minina E, Tiwari BS, Rodriguez-Nieto S, Zamyatnin AA, Välineva T *et al* (2009) Tudor staphylococcal nuclease is an evolutionarily conserved component of the programmed cell death degradome. *Nat Cell Biol* 11: 1347 – 1354

 © 2021 The Authors

Szklarczyk D, Franceschini A, Wyder S, Forslund K, Heller D, Huerta-Cepas J, Simonovic M, Roth A, Santos A, Tsafou KP *et al* (2015) STRING v10: protein-protein interaction networks, integrated over the tree of life. *Nucleic Acids Res* 43: D447 – 452

Takahara T, Maeda T (2012) Transient sequestration of TORC1 into stress granules during heat stress. *Mol Cell* 47: 242 – 252

Thomas MG, Loschi M, Desbats MA, Boccaccio GL (2011) RNA granules: the good, the bad and the ugly. *Cell Signal* 23: 324 – 334

de la Torre F, Gutierrez-Beltran E, Pareja-Jaime Y, Chakravarthy S, Martin GB, del Pozo O (2013) The tomato calcium sensor Cbl10 and its interacting protein kinase Cipk6 define a signaling pathway in plant immunity. *Plant Cell* 25: 2748 – 2764

Tsai NP, Wei LN (2010) RhoA/ROCK1 signaling regulates stress granule formation and apoptosis. *Cell Signal* 22: 668 – 675

Tusher VG, Tibshirani R, Chu G (2001) Significance analysis of microarrays applied to the ionizing radiation response. *Proc Natl Acad Sci USA* 98: 5116 – 5121

Tyanova S, Temu T, Cox J (2016) The MaxQuant computational platform for mass spectrometry-based shotgun proteomics. *Nat Protoc* 11: 2301 – 2319

Uversky VN (2017) How to predict disorder in a protein of interest. *Methods Mol Biol* 1484: 137 – 158

Van Leene J, Eeckhout D, Cannoot B, De Winne N, Persiau G, Van De Slijke E, Vercruysse L, Dedecker M, Verkest A, Vandepoele K *et al* (2015) An improved toolbox to unravel the plant cellular machinery by tandem affinity purification of *Arabidopsis* protein complexes. *Nat Protoc* 10: 169 – 187

Van Leene J, Han C, Gadeyne A, Eeckhout D, Matthijs C, Cannoot B, De Winne N, Persiau G, Van De Slijke E, Van de Cotte B *et al* (2019) Capturing the phosphorylation and protein interaction landscape of the plant TOR kinase. *Nat Plants* 5: 316 – 327

Wang L, Li H, Zhao C, Li S, Kong L, Wu W, Kong W, Liu Y, Wei Y, Zhu JK *et al* (2017) The inhibition of protein translation mediated by AtGCN1 is essential for cold tolerance in *Arabidopsis thaliana*. *Plant Cell Environ* 40: 56 – 68

Weber C, Nover L, Fauth M (2008) Plant stress granules and mRNA processing bodies are distinct from heat stress granules. *Plant J* 56: 517 – 530

Weissbach R, Scadden AD (2012) Tudor-SN and ADAR1 are components of cytoplasmic stress granules. *RNA* 18: 462 – 471

Wippich F, Bodenmiller B, Trajkovska MG, Wanka S, Aebersold R, Pelkmans L (2013) Dual specificity kinase DYRK3 couples stress granule condensation/dissolution to mTORC1 signaling. *Cell* 152: 791 – 805

Wisniewski JR, Zougman A, Nagaraj N, Mann M (2009) Universal sample preparation method for proteome analysis. *Nat Methods* 6: 359 – 362

Wolozin B (2012) Regulated protein aggregation: stress granules and neurodegeneration. *Mol Neurodegener* 7: 56

Wolozin B, Apicco D (2015) RNA binding proteins and the genesis of neurodegenerative diseases. *Adv Exp Med Biol* 822: 11 – 15

Wolozin B, Ivanov P (2019) Stress granules and neurodegeneration. *Nat Rev Neurosci* 20: 649 – 666

Wu FH, Shen SC, Lee LY, Lee SH, Chan MT, Lin CS (2009) Tape-*Arabidopsis* Sandwich - a simpler *Arabidopsis* protoplast isolation method. *Plant Methods* 5: 16

Xie X, Matsumoto S, Endo A, Fukushima T, Kawahara H, Saeki Y, Komada M (2018) Deubiquitylases USP5 and USP13 are recruited to and regulate heat-induced stress granules through their deubiquitylating activities. *J Cell Sci* 131: 1 – 11

Xing S, Wallmeroth N, Berendzen KW, Grefen C (2016) Techniques for the analysis of protein-protein interactions in vivo. *Plant Physiol* 171: 727 – 758

Xing W, Muhlrad D, Parker R, Rosen MK (2020) A quantitative inventory of yeast P body proteins reveals principles of composition and specificity. *Elife* 9: 1 – 25

Xiong Y, McCormack M, Li L, Hall Q, Xiang C, Sheen J (2013) Glucose-TOR signalling reprograms the transcriptome and activates meristems. *Nature* 496: 181 – 186

Xue B, Dunbrack RL, Williams RW, Dunker AK, Uversky VN (2010) PONDR-FIT: a meta-predictor of intrinsically disordered amino acids. *Biochem Biophys Acta* 1804: 996 – 1010

Yamada K, Lim J, Dale JM, Chen H, Shinn P, Palm CJ, Southwick AM, Wu HC, Kim C, Nguyen M *et al* (2003) Empirical analysis of transcriptional activity in the *Arabidopsis* genome. *Science* 302: 842 – 846

Yan C, Yan Z, Wang Y, Yan X, Han Y (2014) Tudor-SN, a component of stress granules, regulates growth under salt stress by modulating GA20ox3 mRNA levels in *Arabidopsis*. *J Exp Botany* 65: 5933 – 5944

Yang P, Mathieu C, Kolaitis R-M, Zhang P, Messing J, Yurtsever U, Yang Z, Wu J, Li Y, Pan Q *et al* (2020) G3BP1 is a tunable switch that triggers phase separation to assemble stress granules. *Cell* 181: 325 – 345.e28

Yu L, Di Y, Xin L, Ren Y, Liu X, Sun X, Zhang W, Yao Z, Yang J (2017) SND1 acts as a novel gene transcription activator recognizing the conserved Motif domains of Smad promoters, inducing TGFbeta1 response and breast cancer metastasis. *Oncogene* 36: 3903 – 3914

Zhu L, Tatsuke T, Mon H, Li Z, Xu J, Lee JM, Kusakabe T (2013) Characterization of Tudor-sn-containing granules in the silkworm, *Bombyx mori*. *Insect Biochem Mol Biol* 43: 664 – 674

License: This is an open access article under the terms of the Creative Commons Attribution License, which permits use, distribution and reproduction in any medium, provided the original work is properly cited.

Acta Universitatis Agriculturae Sueciae

Doctoral Thesis No. 2022:60

To ensure food security in times of extreme weather events due to climate change and global warming we need to develop stress-resilient plants. In order to do so, an enhanced understanding of plant stress is essential. In this thesis two plant subcellular mechanisms fundamental to plant stress response, autophagy and stress granules, have been studied. The findings presented provide important addition to our knowledge of plant stress resilience.

Pernilla Helena Elander received her graduate education at the Department of Molecular Sciences at SLU, Uppsala, the University where she also received her B.Sc in Biology and M.Sc in Genetic and Molecular Plant Biology. She is also a proud soldier of the Swedish Armed Forces.

Acta Universitatis Agriculturae Sueciae presents doctoral theses from the Swedish University of Agricultural Sciences (SLU).

SLU generates knowledge for the sustainable use of biological natural resources. Research, education, extension, as well as environmental monitoring and assessment are used to achieve this goal.

ISSN 1652-6880
ISBN (print version) 978-91-7760-995-7
ISBN (electronic version) 978-91-7760-996-4